Détoxification des eaux usées urbaines par photocatalyse solaire

Faouzi Achouri

THESE EN COTUTELLE

Présentée en vue d'obtenir le grade de :

DOCTEUR DE

L'Université de Lorraine et de L'Université de Carthage

Discipline:

« Génie des Produits et des Procédés » - « Sciences Biologiques »

Par

Faouzi Achouri

Détoxification Des Eaux Usées Urbaines Par Photocatalyse Solaire

Soutenue le 18 juillet 2016

Membres du Jury

Rapporteurs :

- **Mme Marie-Pierre Fontaine-Aupart,** Directrice de Recherches CNRS, Orsay (France)
- **Mr Mongi Seffen**, Professeur, Université de Sousse (Tunisie)

Examinateurs :

- **Mme Halima Alem-Marchand**, Maître de Conférences, Université de Lorraine (France)
- **Mme Latifa Bousselmi**, Professeur, CERTE, Université de Carthage (Tunisie)
- **Mr Ahmed Landoulsi**, Professeur, Université de Carthage (Tunisie)

Directeurs de Thèse :

- **Mr Raphaël Schneider,** Professeur, Université de Lorraine (France)
- **Mr Serge Corbel,** Chargé de Recherches CNRS (France)
- **Mr Ahmed Ghrabi,** Professeur, CERTE, Université de Carthage (Tunisie)

Dédicace

Je dédie ce modeste travail à mon cher père ***Lazher****, ma chère mère* ***Mbarka****, pour leur irremplaçable et inconditionnel soutien, pour leur dévouement et leurs sacrifices. Ils ont été présents pour écarter mes doutes, soigner mes blessures et partager mes joies. Que dieu les recompense par le paradis éternel.*

A mon cher frère le professeur ***Mohamed Sghaier****, mon leader et exemple, qui est toujours présent avec ces conseils et soutiens,*

A ma chérie ***Feten*** *qui a vécu avec moi tous les moments durant mon parcours universitaire, elle me soutient et m'encourage toujours. Que dieu nous conserve et nous réunit dans cette vie et au paradis éternel.*

A mes ***chers frères*** *et* ***chères soeurs*** *pour leurs soutiens inébranlables*

Dans tous les moments. Que Dieu bénisse notre union et vous garde pour moi.

A mes fidèles amis ***Riadh Akrmi****,* ***Ali Gadouari****,* ***Ramzi Marouani****,* ***Themer Herchi****,* ***Anis Ajouli*** *pour leurs soutiens, leur joie et leur beauté.*

A tous mes amis qui sont toujours avec moi, ils me supportent infiniment à tous moment.

Je prie mon grand Dieu de me faciliter le chemin pour que je puisse

Contribuer, par un travail sincère et utile à l'humanité.

Remerciements

Tout d'abord, je tiens à exprimer ma profonde reconnaissance à mon directeur de thèse, Monsieur ***Raphael Schneider****, Professeur à l'université de lorraine pour son encadrement tout au long de ma thèse, pour ses idées pertinentes, ses conseils, sa sympathie, le temps accordé ainsi que pour son aide lors des manipulations, la rédaction des articles et la correction de cette thèse.*

Aussi je voudrais exprimer mes vifs remerciements à mon co-encadreur Monsieur ***Serge Corbel****, HDR au CNRS, pour sa sympathie, sa qualité humaine, ainsi que pour ses conseils et son aide précieuse durant la rédaction de la thèse.*

J'adresse mes sincéres remerciements à mon directeur de thèse Monsieur ***Ahmed Ghrabi****, Professeur et Directeur du Centre de Recherches et Technologies des Eaux (****CERTE****) pour m'avoir accueilli au sein de son équipe du laboratoire « Eaux usées et environnement », pour sa confiance, son intérêt, son temps et tout le support scientifique nécessaire à ce travail.*

J'adresse mes chaleureux remerciements à Monsieurs ***Christophe Merlin****, et à Madame* ***Laurence Mathieu****, Maîtres de conférences au laboratoire* ***LCPME****, Pôle de l'eau, pour m'avoir accueilli au sein de leur équipe durant les stages effectués à Nancy, ainsi que pour leur aide, leur patience et leurs conseils pertinents.*

Mes vifs remerciements vont à Madame ***Latifa Bousselmi****, Professeur et Directrice du laboratoire 'Eaux Usées et Environnemet' (****CERTE****), pour sa contribution scientifique à l'élaboration de ce sujet de thèse, pour son aide et ses conseils.*

Egalement je voudrais remercier Mademoiselle ***Myriam BenSaid,*** *Maître assistante (CERTE) pour son aide précieuse durant la manipulation et la rédaction des publications scientifiques, sa gentillesse et ses conseils pertinents.*

Un grand remerciement aussi à toute l'équipe du ***LRGP*** *et* ***LCPME*** *à Nancy,*

*Tous les membres du laboratoire « Eaux Usées et Environnement » au (****CERTE****) Tunis, ainsi que tous ceux qui ont contribué à la réalisation de cette thèse.*

Je remercie encore tous mes collègues au ***LRGP*** *(Nancy) ainsi que mes collègues du* ***CERTE*** *pour les bons moments que nous avons passés ensemble.*

Sommaire

Liste des abréviations

λ_{em}: Longueur d'onde d'émission (nm)

μ_t *:* Adsorption coefficient.

$^1O_2$: Oxygène singulet

A: the retention of viability and cultivability rate in the contact with disinfectant agent.

ADN: Acide désoxyribonucléique

AHA: Acide haloacétique

AHL: Acylhomoserine lactone

ARN: Acide ribonucléique

AT: Acide téichoïque

C: the disinfectant concentration with

CB: Bande de Conduction

Ce : concentration à l'équilibre du polluant (mmol/L).

CFU: colony forming unit

CoA: Coenzyme A

Cr : Coefficient de réactivation

CV: Bande de valence

C-W: Chick-Watson

d: catalytic concentration (g/L)

DST: Disodium terephthalate

E. coli: Escherichia coli

e^-/h^+ : Eléctron/ Trou

EDS: Energy Dispersive X-ray Spectrometer

E_{gap}: Energie gap

ENR: Entités Nitrées réactives

EROs: Espèces réactives de l'oxygène

eV: Eléctron Volt

FAO: Formes activées de l'oxygène

FMC: Cytomtrie en flux

$HO^{\bullet}$: Radical hydroxyle

$HO_2^{\bullet}$: Radical hydroperoxyle

k: Constante cinétique de dégradation (µmol/L/min).

K : Constante d'adsorption du substrat (L/mmol).

$k_{(d,QUV)}$: global photocatalytic inactivation coefficient

k: disinfection kinetic constant

k_d: the disinfection kinetic constant related separately to the catalytic actio

kJ: kilo joule

k_{QUV} : disinfection kinetic constant related to solar UV effects

LB: Lysogenic Broth

LPS: Lipopolysaccharide

m: empirical parameter that controls the deflection of the inactivation rate

M_a: Active bacteria responsible for production and maturation of biofilm

M_a: Active bacteria

M_b: Total biomass of the biofilm as it continues to grow for the control test

M_d: Defective bacteria.

M_d: Inactive bacteria no longer involved in the construction of biofilm;

MDA: Malondialdehyde

M_r: part of resuscitate bacteria.

N/N_0: the reduction in the bacterial concentration

N: Number of viable and cultivable bacteria remaining after exposure to experimental conditions

n: threshold level of series-event model

N_0: Number of the initial viable bacteria

NBT: Nitroblue tetrazolium

N_C,: Number of CFUs after the first contact with solar UV radiation

N_d: Initial number of CFUs in the dark condition

NRs : Nanorods

ɵ: Taux de recouvrement de la surface du catalyseur par le substrat.

$O_2^{-\bullet}$: Anion superoxyde

OMS: Organisation Mondiale de Santé

ONPG: β- D- galactopyranoside

P. aeruginosa : Pseudomonas aeruginosa

PI: Propidium iodure

PIE: Point isoélectrique

PL: Photoluminescence

POA : Procédés d'Oxydation Avancée

PZC: Point zéro Charge

QS: Quorum Sensing

Q_{UV}: accumulated UV energy (KJ/L)

Q_{UV}: accumulated UV energy (KJ/L)

RCS: Entités halogénées réactives

RO•: radical alkoxyle

ROO•: radical peroxyde

ROOH: Hydroperoxyde organique

S. Typhi: *Salmonella enterica* Typhi

SA: Salicylic acid

SDS-PAGE: Sodium Dodecylsulfate Polyacrylamide Gel Electrophoresis

SODIS: Désinfection solaire.

SPD: Sous-Produits de Désinfection

t: time (min)

TEM: Transmission electron microscopy

THM: Trihalométhane

Trp: Tryptophan

UV: Ultraviolet

V: vitesse de la réaction (µmol/L/min).

XPS: X-ray photoelectron spectroscopy

XRD: X-ray diffraction

γ: error estimation due to the putative presence of cells aggregation.

μ: biofilm growth rate; and C_t is the disinfectant concentration (UV-A/TiO_2)

Liste des figures

Liste des tableaux

Introduction générale

De nos jours, la vie sur terre est menacée par divers problèmes, dont la pénurie et la pollution de l'eau. En effet, l'accroissement de la population et les fortes activités industrielles, urbaines et agricoles combinées à la rareté de l'eau qui toucheles pays méditerranéens, sont les causes principales à ces problèmes. Ces problèmes provoquent une pression sur les réserves d'eau naturelles (barrages, lacs, rivières, mers, …) et provoquent un déséquilibre affectant l'harmonie entre l'être humain et son milieu naturel. Auparavant, les déchets étaient issus directement de matières naturelles ou en rapport avec les activités des êtres vivants, ils s'inséraient dans les cycles naturels et se dégradaient facilement par voie biologique, ou par des processus d'oxydoréduction naturels (autoépuration naturelle). Actuellement, ce n'est plus le cas. Les micropolluants de l'eau dépassent largement sa capacité d'autoépuration et, par conséquent, l'eau polluée devient le principal vecteur de maladies dans le monde. Selon l'OMS [1], la pollution se place devant la malnutrition comme responsable de maladies mortelles. Le manque d'accès à une eau potable, l'absence d'un assainissement adéquatet lemanque d'hygiène, sont des facteurs qui contribuent aux décès de 1,5 million de personnesannuellement affectées par des maladies diarrhéiques. En conséquence, et pour faire face à ces problèmes, l'utilisation et la gestion des eaux se posent avec acuité pour beaucoup de pays.

La mise au point de méthodes efficaces de traitement et d'approvisionnement en eau et en services d'assainissement ont fait l'objet d'un nombre considérable d'études et de travaux de recherche.

Les techniques classiques de traitement des eaux, comme les méthodes physiques (adsorption, filtration, coagulation, floculation, …), chimiques (chloration, ozonation, oxydation classique…) et biologiques (boue activée, …), se sont avérées insuffisantes et présentent des limites (coût élevé, présence de sous-produits plus nocifs, inefficacité pour l'élimination des microorganismes pathogènes, …).

En plein essor, ces dernières décennies, la photocatalyseest une technique de traitement assez efficace, se positionne comme une alternative aux techniques classiques. Elle a l'avantage d'être relativement peu coûteuse et est basée sur l'utilisation d'un matériau semi-conducteur

et d'une source d'énergie inépuisable, à savoir la lumière solaire. Cette technique très intéressante a reçu beaucoup d'attentions ces dernières années. Le mécanisme de la photocatalyse est complexe et comprend l'adsorption du polluant à la surface du catalyseur et des réactions d'oxydoréduction sous l'effet de la lumière.

Dans nos travaux de recherche, nous nous sommes intéressés au traitement des eaux usées par photocatalyse solaire. L'objectif principal est orienté vers l'optimisation de cette technique d'oxydation pour la dépollution des eaux usées urbaines. Pour étudier les performances de cette technologie nous avons orienté nos travaux vers : (1) l'étude et le développement de nouveaux semi-conducteurs, (2) des tests de dégradation photocalytique sur des polluants chimiques modèles (Orange II et acide salicylique), et (3) l'application de la photocatalyse dans la désinfection des eaux usées (utilisation des bactéries modèles).

Le présent mémoire est structuré en trois parties :

La première partie est dédiée à une étude bibliographique ; elle concerne, d'une part les généralités sur la pollution de l'eau et les causes principales mettant en lumière les problématiques à résoudre et d'autre part, les techniques de traitement utilisées et les résultats obtenus dans la littérature.

La deuxième partie traite de la synthèse de nouveaux nanomatériaux à base de ZnO et leur application pour la dégradation photocatalytique des polluants chimiques et microbiologiques ; elle comprend trois chapitres :

Le chapitre 1 présente la synthèse d'hétérostructures ZnO/Fe_2O_3 par simple hydrolyse de $FeCl_3$ en présence de ZnO pour l'amélioration de la production des espèces réactives oxygène (EROs) qui permettent la dégradation photocatalytique d'un polluant modèle, l'acide salicylique. Le photocatalyseur a été immobilisé dans un microréacteur.

Le chapitre 2 est consacré au dopage de nanobâtonnets ZnO avec Mn^{2+} par voie solvothermale en vue de l'amélioration de la dégradation photocatalytique du colorant Orange II en réacteur ouvert sous irradiation solaire.

Le chapitre 3 se focalise sur la synthèse de nanobâtonnets ZnO par voie solvothermale en vue de la dégradation photocatalytique de l'Orange II et l'étude du mécanisme d'inactivation

d'une souche bactérienne *Escherichia coli* MG 1655 avec le catalyseur immobilisé ou dispersé sous irradiation solaire.

La troisième partie permet de mieux comprendre les mécanismes d'inactivation photocatalytique de souches bactériennes en utilisant un autre semiconducteur commercial, TiO_2 P25, pour générer les EROs, Cette partiese subdivise en deux chapitres :

Le chapitre 1 est consacré au suivi de la cinétique d'inactivation photocatalytique de différentes souches bactériennes de référence (*Escherichia coli, Pseudomonas aeruginosa* et *Salmonella enterica* Typhi) avec TiO_2 immobilisé et sous irradiation solaire. Pour les bactéries étudiées, la comparaison de différents paramètres cinétiques (k, A) déterminés à travers les modèles de Chick-Watson et le modèle series d'évènement sont analysés et discutés.

Le chapitre 2 illustre l'impact de la photocatalyse sous irradiation UV sur l'inactivation et l'atténuation des caractères de virulence d'une souche de référence *Pseudomonas aeruginosa (*ATCC 4114).

La dernière partie est une conclusion générale et permet d'ouvrir des perspectives afin d'améliorer la technique de photocatalyse. Cette partie décrit notamment les solutions envisagées afin d'augmenter l'efficacité des catalyseurs dans le domaine du visible. Cela ne peut se faire qu'avec une meilleure compréhension du mécanisme d'action sur les polluants récalcitrants, y compris les microorganismes pathogènes, ainsi que par une bonne optimisation des paramètres opérationnels pour passer à l'application industrielle.

PARTIE I : Etude Bibliographique

Etude Bibliographique

Introduction

La pollution de l'eau survient lorsque des matières sont déversées dans l'eau et que celles-ci en dégradent sa qualité. Ainsi, la pollution de l'eau peut résulter d'une dégradation physique, chimique, biologique ou bactériologique, provoquée par l'homme et ses activités. Elle perturbe les conditions de la vie de la flore et de la faune aquatiques; elle compromet les utilisations de l'eau et l'équilibre du milieu naturel. La pollution hydrique est provoquée par le rejet d'eau salie par les activités domestiques (lavages et nettoyages divers, évacuation des urines et matières fécales, ...) mais également par les rejets dus aux activités industrielles et agricoles.

I. Pollution hydrique

I.1 Principales sources de contamination des eaux

Il y a pricipalement deux sources de pollution des eaux. La première comprend les usines, les installations de traitement des eaux usées, et les systèmes de fosses septiques. La seconde a des origines plus complexes car on ne peut pas les localiser à un emplacement particulier. Elles incluent les écoulements de sédiments, engrais, produits chimiques, déchets d'animaux de ferme, champs, chantiers et mines. L'enfouissement des déchets doit également être considéré comme une source de pollution si ces déchets sont au contact d'effluents aqueux.

Les contaminants de l'eau affectent les principales réserves d'eau (nappes phréatiques, barrages, lacs, fleuves, rivières et mers). Ceci engendre la création d'un déséquilibre affectant l'harmonie entre l'être humain et son milieu naturel. Les eaux naturelles possèdent un pouvoir auto-épurateur grâce à l'activité biologique de sa faune et sa flore, tant que la quantité de polluants apportés reste raisonnable et inférieure à sa capacité d'autoépuration. En revanche, si des quantités importantes de micropolluants toxiques se retrouvent dans l'eau et dépassent sa capacité d'autoépuration, il y a une accumulation de substances dangereuses conduisant à l'altération de ses qualités physico-chimiques et biologiques.

En général, ce sont les eaux des usines qui sont à l'origine des difficultés les plus importantes [2]. D'autres sources, comme les eaux usées provenant des industries du papier ou du textile ont un impact visuel important du fait de leur coloration [3]. Il est prouvé que les effluents papetiers contiennent des substances eutrophisantes (azote et phosphore sous différentes formes) qui apportent un surcroît de matières organiques aux milieux aquatiques, et qui les déstabilisent en favorisant l'accroissement des végétaux (algues) au détriment des autres espèces habitant ces milieux [4,2].

I.2 La composition des eaux usées

La composition des eaux usées est extrêmement variable en fonction de leur origine (industrielle, domestique, …). Ces eaux peuvent contenir de nombreuses substances, sous forme solide en suspension ou dissoute, ainsi que de nombreux micro-organismes. En fonction de leurs caractéristiques physiques, chimiques, biologiques et du danger sanitaire qu'elles représentent, ces substances peuvent être classées en quatre groupes : les micro-organismes, les matières en suspension, les éléments traces minéraux ou organiques, et les substances nutritives.

Dans ce travail, nous nous sommes notamment intéressés à la qualité bactériologique des eaux usées et aux bactéries pathogènes qui peuvent présenter un risque sanitaire. Une étude du paramètre dose/réponse a été menée afin d'optimiser l'étape de traitement par photocatalyse hétérogène.

I.3 Pollution bactérienne

I.3.1 Définition des bactéries

Les bactéries sont des êtres vivants microscopiques procaryotes donc dépourvus de noyau. Il s'agit d'organismes unicellulaires de taille comprise entre 0,2 et 5 µm, ubiquitaires dans tous les milieux. Actuellement, il existe des milliers d'espèces différentes de bactéries qui sont classées en différents taxons. Cette taxonomie est fondée sur des caractères morphologiques, biochimiques, antigéniques, génétiques et/ou moléculaires [5].

I.3.2 Structure des bactéries

La structure des bactéries comporte une membrane cytoplasmique constituée de deux feuillets phospholipidiques contenant des protéines, qui délimite le cytoplasme où baignent le ribosome, le matériel génétique ainsi que les substances de réserve. D'autres composants comme les plasmides (molécules d'ADN) interviennent dans la résistance des bactéries contre les antibiotiques ou les facteurs de virulence [6].

La paroi cellulaire constitue une couche externe rigide responsable de la forme des cellules et assurant l'intégrité de la bactérie, la protégeant ainsi contre les variations des paramètres physiques et chimiques [7].

Le peptidoglycane est la molécule fondamentale existante dans toutes les parois bactériennes. Ce réseau est composé de chaînes de glycanes reliées entre elles par des chaînons peptidiques. Selon les conditions environnementales, certaines bactéries ont du s'adapter et la structure a subi des évolutions. Par exemple, certaines bactéries secrètent des polymères organiques, appelés capsules, qui constituent une couche externe par rapport à la paroi. Paroi et capsule forment l'enveloppe d'une bactérie

I.3.3 Classification des bactéries

Les bactéries diffèrent les unes des autres par leur morphologie, leur rôle biochimique, leur mode de vie, leur fonction dans un écosystème et de nombreux autres facteurs, ce qui entraine différentes possibilités de leur classification.

I.3.3.1 Classification selon la forme

La forme des cellules bactériennes varie d'une espèce à l'autre (**Figure 1**) [8]. Certaines sont courtes, pratiquement sphériques (cocci ou coques) et d'autres sont allongées (bacilles).

Les bacilles sont essentiellement des cylindres à extrémités hémisphériques (*Bacterium, Clostridium*). D'autres bactéries sont des cellules à extrémités fines, pointues (formes en fuseau) ou au contraire planes (bacilles dits « à bouts carrés»). Certains corps bacillaires sont incurvés ou spiralés (*Vibrio, Campylobacter*). Habituellement, les cellules d'une espèce bactérienne donnée partagent une même forme. Cependant pour certaines espèces, la forme varie d'une cellule à l'autre, parfois de façon très marquée. On parle alors de *pleiomorphisme.* Dans l'environnement, les bactéries peuvent s'associer en amas de cellules

qui sont caractéristiques chacune d'une espèce donnée [8], ces groupements sont essentiellement induits par le processus de division bactérienne.

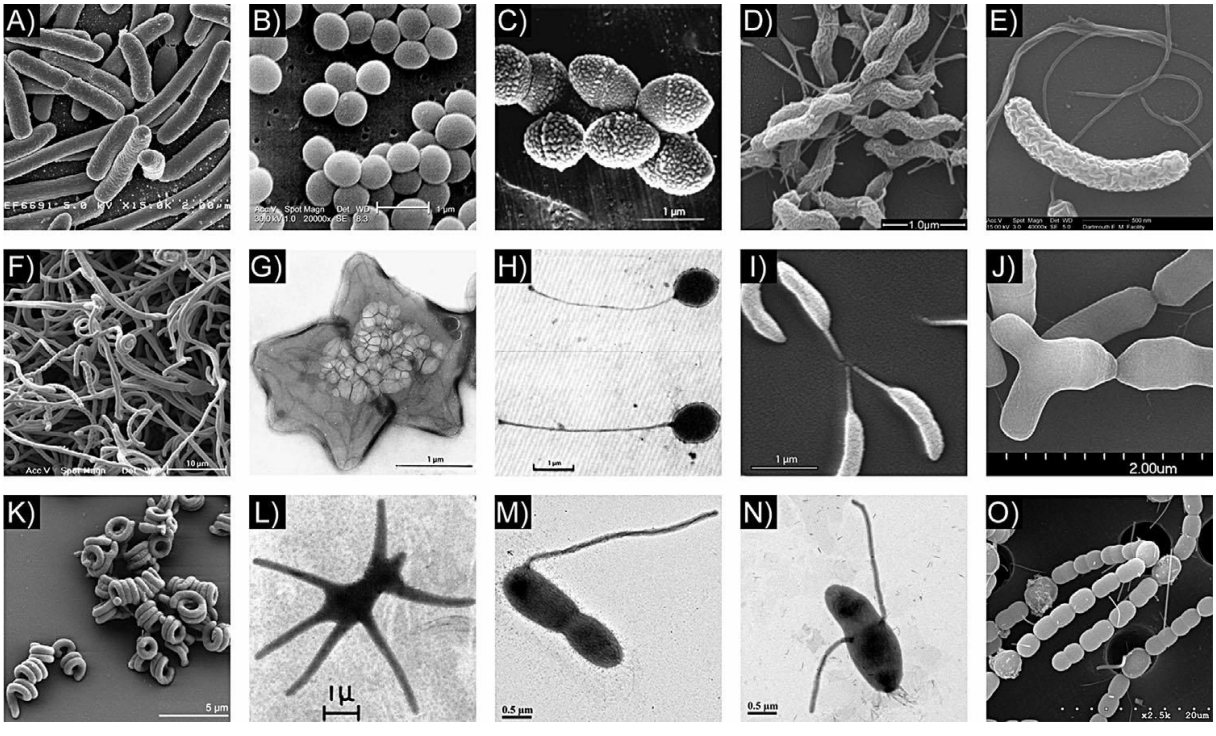

Figure 1: Différentes formes des bactéries [8]

A : forme batonnet, *Escherichia coli*, **B**: Sphère, *Staphylococcus aureus* **C**: Ovococcoide, *Streptococcus pneumoniae*. **D**: Spirale, *Campylobacter jejuni*. **E**: Croissant, *Vibrio cholerae*. **F**: filaments ramifiés, *Streptomyces Coelicolor*. **G**: étoile, *Stella vacuolata*. **H**: pétiolée, *Planctomyces maris*. **I**: petiole et croissant, *Caulobacter crescentus*. **J**: Bifide / forme Y, *Bifidobacterium breve*. **K**: bobine, *Spirosoma linguale*. **L**: Multi-pétiole, *Ancalomicrobium adetum*. **M**: pétiolée, *Asticcacaulis excentricus*. **N**: pétiolée, *Asticcacaulis biprosthecum*. **O**: Chaîne et hétèrocystes, *Anabaena variabilis*.

I.3.3.2 Classification selon la structure de la paroi bactérienne

La paroi est l'enveloppe externe de la cellule bactérienne. Son rôle consiste à protéger les bactéries contre les agents extérieurs et à maintenir une pression intracellulaire très élevée (10 à 20 atmosphères). La paroi résiste à cette pression grâce à sa rigidité et à sa résistance physique qui sont dues à une substance complexe, le peptidoglycane. Le peptidoglycane (ou

mucopeptide ou muréine) est un polymère composé de chaînes linéaires de D-glucosamine N-acétyl et d'acide N-Acétylmuramique reliés par des liaisons osidiques.

C'est une structure complexe possédant deux caractéristiques : i) une structure en réseau qui confère à la bactérie sa rigidité et sa résistance mécanique. ii) la présence d'acide N-acétyl muramique spécifique des bactéries [9].

On peut distinguer deux groupes principaux de bactéries en se basant sur l'organisation du peptidoglycane de la paroi. Les bactéries à Gram positif et les bactéries à Gram négatif (**Figure 2**).

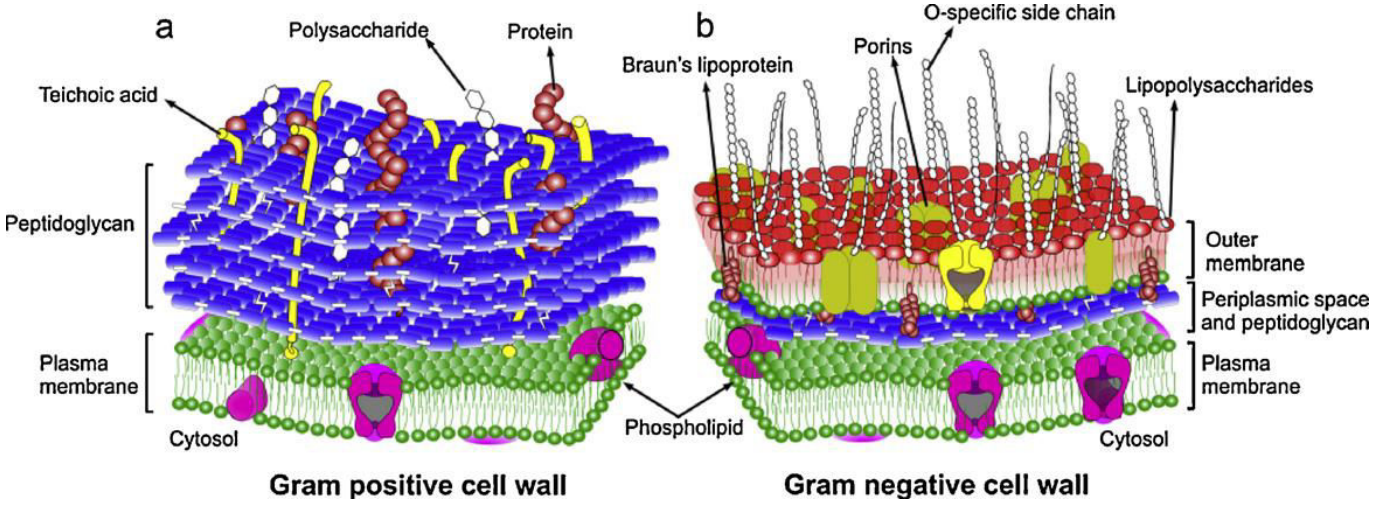

Figure 2 : Différence entre la paroi d'une bactérie gram-négative et gram-positive [9]

I.3.3.2.1 Les bactéries Gram positif

La paroi se présente sous forme d'une couche homogène de peptidoglycane, d'acides téichoïques (20 à 80 nm d'épaisseur) qui sont des polymères de glycérol ou de ribitol et de phosphates ancrés, la plupart du temps, dans la membrane cytoplasmique par une partie glucolipidique [10]. Ces chaînes traversent le peptidoglycane et forment des structures chargées négativement à la surface bactérienne. Les acides téichoïques (AT), une autre classe majeure de constituants de la paroi cellulaire des bactéries Gram-positives, jouent un rôle

important dans la morphogenèse des cellules (élongation cellulaire, division cellulaire) [9]. Les acides lipotéichoïques sont à leur tour fixés à travers leur partie lipidique dans la membrane cytoplasmique et s'étendent dans la paroi. Ils jouent le même rôle que les acides teicoïques, mais interviennent aussi dans l'adhérence aux cellules et ils ont un faible effet toxique. Chez de nombreuses bactéries Gram positif, l'épaisseur de la couche de peptidoglycane représente à peu près 80% de la paroi cellulaire. Le reste (10 à 20%) est formé d'acides téchoïques et de quantités mineures de lipides, de protéines et de lipopolysaccharides.

I.3.3.2.2 Les bactéries Gram négatif

Dans ce type de bactéries, la paroi est une couche mince de peptidoglycane (1 à 3 nm) entourée par une membrane externe d'environ 6 à 18 nm d'épaisseur, composée de lipopolysaccharides (50%), de phospholipides (35%) et de lipoprotéines (15%); elle sert d'interface entre la cellule et son environnement, de même qu'elle contrôle le passage des substances solubles et externes vers la membrane cytoplasmique. C'est à son niveau que se trouvent les sites récepteurs de certains bactériophages. Cette membrane externe est traversée par des porines qui sont des trimères protéiques constituants des pores rendant cette structure perméable à de petites molécules hydrophiles [10].

I.3.3.3 Classification selon la température de croissance

La température est un facteur limitant dans la croissance et la survie bactérienne. C'est pour cela que le monde bactérien peut se subdiviser en trois groupes selon la température de croissance [11] :

- Les bactéries **mésophiles** (*Escherichia coli*) croissent à des températures moyennes comprises entre 20 et 40° C.
- Les bactéries **psychrophiles** ont une température optimale de croissance aux alentours de 0°C. Ces bactéries sont largement répandues dans l'environnement (*Pseudomonas, Acinetobacter).*
- Les bactéries **thermophiles** sont des bactéries qui supportent des températures supérieures à 45°C et 80 °C.
- Les bactéries **hyperthermophiles** ont un optimum de croissance au delà de 80°C Certaines bactéries (*Pyrodictum occultum*) peuvent croitre dans des sources chaudes océaniques à des températures proches de 250°C et à des pressions voisines de 260 atmosphères.

I.3.4 Risques sanitaires microbiologiques

Les risques microbiologiques d'origine hydrique proviennent de l'existence de microorganismes pathogènes dans l'eau comme les bactéries (*E coli, Salmonella, Pseudomenas*, …), les virus (hépatite A), et les protozoaires (*Toxoplasma, Cryptosporidium*) [12]. Ces microorganismes peuvent présenter des risques pour la santé humaine. Bien que les microorganismes soient ubiquitaires, colonisant différents endroits (sol, eau, air, …), une faible proportion est pathogène. En outre, plusieurs types de microorganismes vivent en symbiose avec l'homme alors que d'autres peuvent être utilisés pour la production de pains et de fromages ainsi que pour la production de vaccins et d'antibiotiques [13]. Les maladies d'origine hydrique constituent la première cause de mortalité dans le monde devant la malnutrition. Ces problèmes sont associés à l'absence d'eau de bonne qualité. En effet 1,2 milliard de personnes manquent d'accès à l'eau potable, 2,6 milliards ne bénéficient pas ou peu d'un assainissement des eaux et des millions de personnes meurent chaque année, dont 3900 enfants par jour à cause de maladies transmises par l'intermédiaire de l'eau insalubre ou des excréments humains [14].

Selon l'OMS, en 2008, 88% des cas de diarrhée dans le monde étaient attribués à une eau non potable entrainant la mort de plus de 1,5 millions de personnes par an, dont la plupart sont des enfants [1]. Dans les pays sous-développés, chaque année environ 3 millions de personnes meurent de maladies liées à l'eau dont la majorité sont des enfants de moins de 5 ans, suivis par les femmes et les populations pauvres qui n'ont pas accès à l'eau propre et à un assainissement approprié [15]. La pénurie en eau salubre touche principalement les pays en voie de développement mais les maladies d'origine hydriques demeurent répandues dans le monde entier. De plus, les eaux brutes peuvent véhiculer de nombreux types de microorganismes, dont certains peuvent être pathogènes et d'autres saprophytes. En effet, le seuil d'infection (nombre de germes nécessaires à l'induction d'une infection) dépend du type de microorganismes mis en jeu. Cependant, des millions de bactéries sont nécessaires pour induire le choléra ou la fièvre typhoïde; par contre l'ingestion d'un à dix virus peuvent, dans certains cas, provoquer une maladie [16]. Les eaux usées sont habituellement un mélange de nature domestique, industrielle et pluviale. L'eau usée industrielle contient souvent des concentrations élevées en métaux, métalloïdes et composés volatils ou semi-volatils, alors que l'eau usée domestique est plus nocive en raison de sa charge en microorganismes pathogènes [17]. Par exemple, les salmonelles prédominent dans les eaux usées avec des concentrations

variant entre 10^2 et 10^4 dans 100 ml [1], et sont responsables des fièvres typhoïdes et paratyphoïdes et des gastro-entérites [18]. Il existe aussi d'autres types de maladies, telle que la pneumonie, provoquée par des *streptocoques* et des *pseudomonas*. Certaines infections bactériennes (ex: intoxications alimentaires) se contractent par ingestion de nourriture ou d'eau contaminée avec des bactéries cutanées, nasales ou fécales telles que le *Shigella*, la *campylobactérie* et les *salmonelles*. Le **tableau I.1** ci-dessous regroupe les principaux types de microorganismes pathogènes présentant des risques sur la santé humaine.

Tableau I.1 : Principaux microorganismes pathogènes rencontrées dans les eaux usées urbaines. [18]

Microorganismes pathogènes	**Exemple**	**Maladies engendrées**
Bactéries	-*Salmonella spp* -*Shigella spp* -*Vibrio cholerae* -*E coli* (souches pathogènes) -*Campylobacter spp* -*Yersinia enterocolitica* -*Leptospira*	Fièvre typhoïde, salmonellose Dysenterie bactérienne Choléra Diarrhées Camylobactériose Gastroentérite aiguë Leptospirose
Virus	-Poliovirus -Entérovirus -Virus de l'hépatite A -Norwalk -Rotavirus	Poliomyélite méningite Méningite Hépatite Gastroentérites Gastroentérites et dysenterie
Protozoaires parasites	-*Giadia spp* -*Cryptosporidium spp* -*Entamoeba spp*	Giardiase Cryptosporidiose Dysenterie amibienne
Vers parasites	-Vers plats ou plathelminthes (*Taenia spp, Schistosoma haematobium*, *S mansoni, Fasciola hepatica*). -Vers ronds ou Némathelminthes (*Ascaris spp, Trichuris trichiura, Necator americanus, Ankylostoma duodenale)*	Parasitisme

L'eau représente une source de vie, mais cette substance vitale peut se transformer en un vecteur de propagation de différentes maladies d'origine hydrique. La désinfection de l'eau est considérée comme une étape primordiale ayant pour but de minimiser tout risque d'infection par des microorganismes pathogènes et d'empêcher la diffusion de maladies.

II. Procédés de dépollution des eaux

Pour résoudre le problème de pollution de l'eau et atteindre les normes soulignées par la réglementation, il est important de mettre en place des techniques et des procédés de traitement prometteurs et variés et qui sont généralement classés en trois types: physiques, chimiques et biologiques.

II.1 Procédés physiques

Le charbon actif est le meilleur candidat pour le piégeage de nombreux composés en raison de sa grande surface spécifique (de 750 à 1500 m^2/g) [19]. Il est largement utilisé dans le traitement de l'air et dans la dépollution de l'eau, en particulier, pour traiter les polluants organiques et inorganiques [20,21]. Des études ont aussi montré qu'il est possible de piéger des ions métalliques tels que le cuivre, le zinc, le cadmium ou le chrome [22,23]. Ce traitement présente deux principales limites : (i) d'une part, les polluants ne sont pas dégradés mais concentrés sur le charbon actif qui doit être traité ultérieurement pour être régénéré, et (ii) d'autre part, le coût du charbon actif est relativement élevé.

Les techniques membranaires permettent la séparation de particules, de molécules ou d'ions entre deux phases. La membrane est constituée d'une couche mince (de dix à quelques centaines de microns) d'une matière permettant l'arrêt ou le passage sélectif de substances sous l'action d'une force motrice de transfert. Cette force peut provenir de la convection ou de la diffusion des molécules induites par un gradient de champ électrique, de concentration, de pression ou encore de température [24]. La coagulation et la filtration servent principalement à éliminer les matières en suspension. Les matières colloïdales sont coagulées par un apport de sels minéraux de fer ou d'aluminium puis éliminées sous formes de flocs. Le choix et la performance des coagulants ont fait l'objet d'un grand nombre de travaux de recherche destinés à améliorer le rendement d'élimination des composés organiques [25,26]. Ensuite, la précipitation des espèces chimiques en solution se fait par l'ajout d'un agent chimique qui les rend insolubles, puis elles sont récupérées par filtration.

II.2 Procédés chimiques

Ces procédés peuvent être classés en plusieurs catégories (chloration, ozonation,…). D'autres procédés plus innovants font appel à la lumière (procédés d'oxydation avancée) qui seront détaillés plus loin.

II.2.1 Utilisation du chlore

La chloration est une méthode utilisée fréquemment dans la désinfection des eaux. Cette technologie à base de chlore a longtemps été utilisée comme procédé de désinfection de l'eau potable et également pour le traitement tertiaire des effluents d'eaux usées. Cependant, cette dernière est en train de soulever de plus en plus de questions en raison de récentes études sur la formation des produits potentiellement dangereux comme les chloro-organiques issus de la désinfection [27]. Ces composés sont formés par réaction du chlore avec les matières organiques naturelles dans l'eau et comprennent les trihalométhanes (THM) et les acides haloacétiques (AHA). Le contrôle des sous-produits issu de la désinfection est devenu insistant [28-31]. Les scientifiques ont mis en évidence les effets nocifs sur la santé de ces sous-produits halogénés sur les animaux et les humains [32]. Une autre préoccupation de la désinfection traditionnelle est que certains organismes ont tendance à développer une résistance au chlore ou nécessitent des doses supérieures à la normale pour l'inactivation complète [33, 34]. De ce fait, le chlore est remplacé progressivement par un oxydant plus puissant, à savoir l'ozone, qui s'avère être plus efficace contre les microorganismes.

II.2.2 Utilisation de l'ozone

En raison de sa forte capacité d'oxydation et donc de son potentiel de désinfection, l'ozone a reçu beaucoup d'attention dans les technologies de traitement de l'eau. Malgré les avantages de l'ozone, cette méthode présente des inconvénients qui limitent son application dans le traitement de l'eau. D'une part, l'ozonation reste une technique limitée aux grandes unités de production d'eau potable en raison de son coût plus élevé que la chloration. D'autre part, l'ozone est très instable, il doit être produit sur site, ce qui nécessite des compétences techniques supplémentaires. L'ozone est connu pour être un oxydant puissant, mais il réagit lentement avec certains composés organiques tels que les composés aromatiques inactivés. Dans de nombreux cas, il n'est pas assez puissant pour permettre l'oxydation complète des composés organiques, par exemple des matières organiques naturelles (NOM), ce qui conduit à la formation de la matière organique biodégradable (acides carboxyliques, composés

carbonylés) [35]. En outre, les réactions entre l'ozone et des composés organiques induisent la formation de sous-produits dangereux pour les êtres humains [36].

II.3 Procédés biologiques

Ces procédés sont particulièrement utilisés pour le traitement des eaux usées urbaines et sont basés sur l'utilisation de microorganismes pour la conversion des contaminants organiques en composés moins toxiques (minéralisation en dioxyde de carbone, eau et sels inorganiques dans des bioréacteurs spécifiques). Plusieurs travaux décrivent le traitement biologique des eaux contaminées par divers polluants chimiques comme les perchlorates [25], les bromates [26] et les hydrocarbures aromatiques polycycliques [37]. Ces procédés présentent des inconvénients comme l'apport d'énergie supplémentaire et le pompage de l'eau à traiter.

De plus, ces procédés ne sont généralement pas applicables à des fortes concentrations de polluants de grande toxicité ou de très faible biodégradabilité.

Pour ces raisons de nouveaux procédés d'oxydation avancés sont constamment recherchés comme alternatives à ces procédés traditionnels.

II. 4 Les Procédés d'Oxydation Avancée (POA)

II.4.1 Généralités

Les Procédés d'Oxydation d'Avancée (POA) sont apparus ces dernières décennies comme étant des méthodes efficaces pour le traitement des polluants récalcitrants de diverses natures (**tableau II-1**). Parmi eux, « la photocatalyse hétérogène» a montré son utilité pour la dégradation d'un grand panel de composés tels que les insecticides [38], les composés azotés [39], les pesticides [40], les colorants [41],... De plus, la photocatalyse peut être utilisée pour désinfecter l'eau de microorganismes comme les bactéries, les protozoaires, les champignons et les virus [42, 43].

Les POA présentent plusieurs avantages:

- Ils permettent la transformation des polluants récalcitrants en produits biodégradables traités par la suite par des méthodes de traitements biologiques moins coûteux.
- Ils assurent une minéralisation complète de la majorité des polluants en CO_2 et H_2O.
- Ils consomment moins d'énergie que d'autres méthodes telle que l´incinération.

- Ils évitent l´emploi de désinfectants et d'oxydants comme le chlore dont les résidus peuvent avoir des effets néfastes sur la santé.

Les PAO sont basés sur la production d'espèces oxydantes très réactives de l'oxygène (ERO_S) tels que le radical hydroxyle ($^{\cdot}OH$) ou l'anion superoxyde ($O_2^{-\cdot}$). La formation de ces radicaux peut être induite par une activation de nature variée comme présenté dans le tableau ci-dessous

Tableau II. 1 : Différents types de procédés d'oxydation avancée [44]

Procédés non-photochimiques	**Procédés photochimiques**
Oxydation électrochimique	Photolyse de l´eau (UV / H_2O)
Electro-Fenton	Photolyse du peroxyde d'hydrogène (UV / H_2O_2)
Sonolyse	Photolyse à l'ozone (UV / O_3)
Radiolyse	UV / H_2O_2 / O_3
Peroxonation (O_3 / H_2O_2)	Photocatalyse hétérogène
Procédé de Fenton (Fe^{2+} / H_2O_2)	Photo-Fenton (Fe^{2+} / H_2O_2 / UV)

Dans notre travail, nous nous sommes principalement intéressés à la photocatalyse hétérogène qui est basée sur des réactions d'oxydo-réduction pour la production des radicaux libres très réactifs pour la dégradation des polluants.

II.4.2 Photocatalyse hétérogène

La photocatalyse hétérogène est en plein essor ces dernières années et beaucoup de travaux sont publiés dans ce domaine. Au cours des 30 dernières années, une augmentation remarquable du nombre de publications décrivant la désinfection photocatalytique a été observée (Figure 3) [45]. Ce procédé permet la production d'EROs hautement réactives à température et pression ambiante (le radical hydroxyl $^{\cdot}OH$ est le plus puissant) [14].

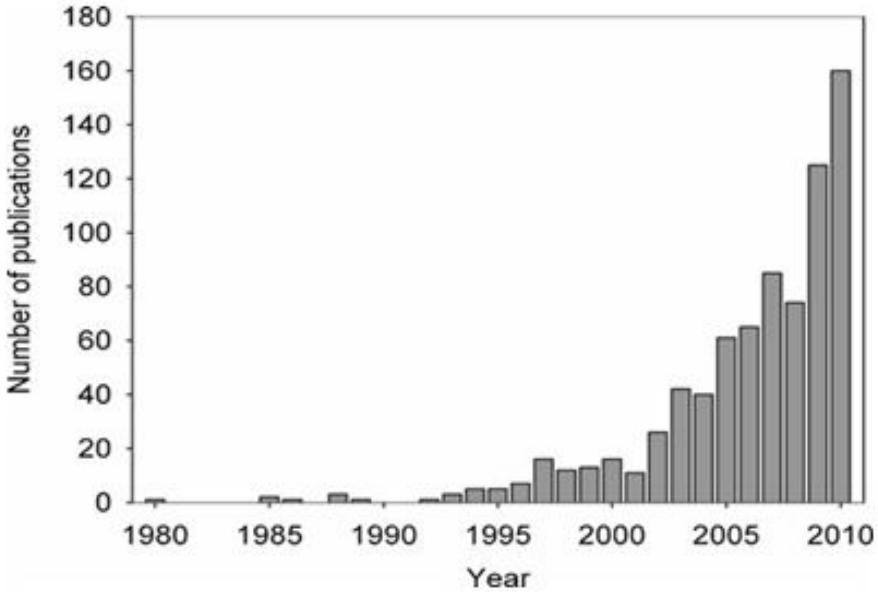

Figure 3: Nombre de publications sur la désinfection photocatalytique [45]

II.4.2.1 Principe

La photocatalyse hétérogène est un processus catalytique basé sur l'excitation d'un semi-conducteur par un rayonnement lumineux assurant la photo-dégradation d'un polluant par des réactions d'oxydation localisées à la surface du semi-conducteur. Le processus photocatalytique peut être résumé en cinq étapes indépendantes [46] :

- Transfert du ou des réactifs de la phase fluide vers la surface du catalyseur.
- Adsorption du réactif.
- Réactions d'oxydation de la phase adsorbée.
- Désorption des produits.
- Transfert de ces produits de la surface du catalyseur vers la phase fluide.

L'absorption d'un photon par un semi-conducteur (par exemple le dioxyde de titane TiO_2), après irradiation avec une source lumineuse dont l'énergie des photons est supérieure ou égale à la différence d'énergie entre les bandes de valence et de conduction du semi-conducteur,induit le passage d'un électron de la bande de valence à la bande de conduction (noté e^-_{BC}), laissant un trou dans la bande de valence (noté h^+_{VB}) (**figure 4**)

$$TiO_2 + h\nu \rightarrow e^-_{CB} + h^+_{VB} \qquad (1)$$

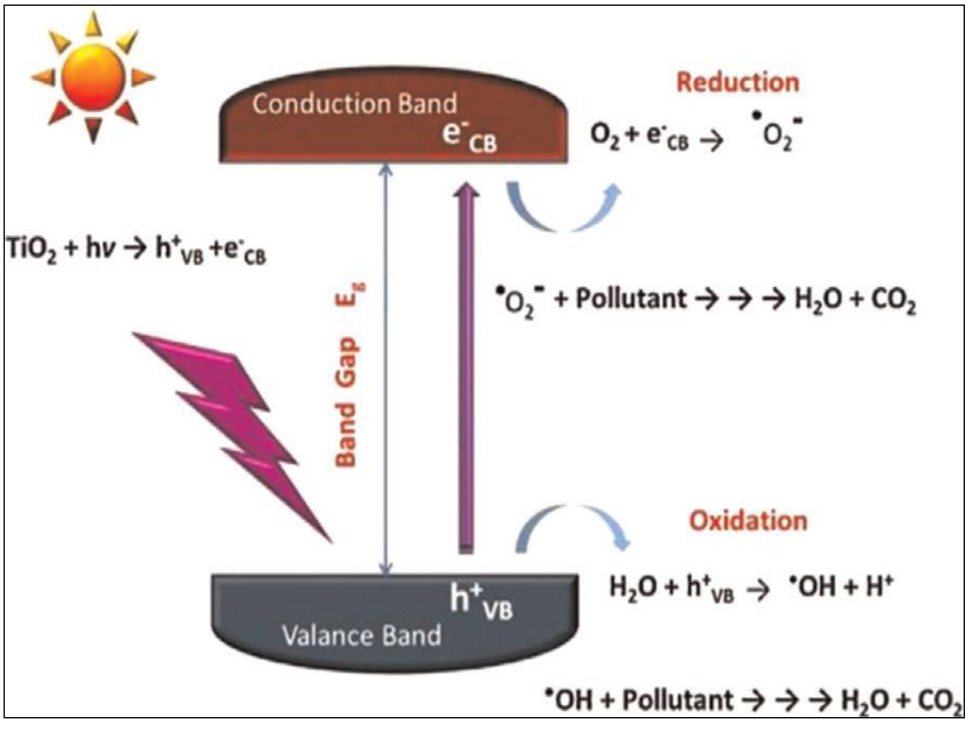

Figure 4 : Schéma réactionnel de la photocatalyse hétérogène [46]

Les entités formées peuvent ensuite se recombiner, être piégées, ou réagir à la surface du catalyseur, soit avec un accepteur d'électrons, soit avec un donneur d'électrons. Ainsi, des radicaux hydroxyles sont formés à la surface du catalyseur par oxydation des molécules d'eau adsorbées, des ions hydroxydes ou des groupements titanols (Ti-OH) de surface. Les radicaux superoxydes et perhydroxyles sont également formés par les réactions entre les électrons et l'oxygène adsorbé. Les principales réactions mises en jeu sont les suivantes [47]:

$$TiO_2 \Rightarrow TiO_2^* (e_{cb}^- + h_{vb}^+) \qquad E_{bg} = 3.2\ eV$$

$$(e_{cb}^- + h_{vb}^+) \Rightarrow e_{cb}^- + h_{vb}^+$$

Réactions e_{cb}^-

$$O_2 + e_{cb}^- \Rightarrow O_2^{\bullet -}$$

$$O_2 + 2\, e_{cb}^- + 2H^+ \Rightarrow H_2O_2$$

$$O_2^{\bullet -} + H_2O_2 \Rightarrow HO^\bullet + OH^- + O_2$$

$$O_2^{\bullet -} + H^+ \Rightarrow {}^\bullet OOH$$

$$H_2O_2 + e_{cb}^- \Rightarrow HO^\bullet + OH\ aq^-$$

$$H_2O_2 + h\upsilon \Rightarrow 2\ HO^\bullet$$

Réaction de h_{vb}^+

$$H_2O + h_{vb}^+ \Rightarrow HO^\bullet + H\ aq^+$$

$$OH^- + h_{vb+} \Rightarrow HO^\bullet$$

Les trous de la bande de valence jouent le rôle d'un oxydant puissant tandis que les électrons de la bande de conduction se comportent comme des réducteurs [48] et participent à la formation des radicaux dans le milieu. Les trous peuvent réagir avec des ions hydroxydes ou des molécules d'eau pour former les radicaux hydroxyles, alors que les électrons de la bande de conduction sont captés par des molécules d'oxygène pour générer des radicaux $O_2^{\bullet -}$ ou du peroxyde d'hydrogène en présence de protons. Les espèces radicalaires ainsi formées jouent

un rôle essentiel dans l'oxydation des substrats en solution [49]. Les espèces oxydantes les plus réactives sont h^+_{BV} et ·OH.

L'oxygène singulet $^1O_2$ est une autre forme d'EROs correspond à l'état excité de l'oxygène, il peut être formé durant le processus de photo-oxydation [50]. Sa demi-vie dans l'état excité est longue (10^{-6}-10^{-5} secondes) comparée aux autres EROs. $^1O_2$ est aussi généré durant certains processus naturels de peroxydation des lipides [51] ou encore par la réaction de l'anion superoxyde ($O_2^{\cdot -}$) avec le peroxyde d'hydrogène (H_2O_2) *via* la réaction d'Haber-Weiss [52]:

$$H_2O_2 + O_2^{\cdot -} \Rightarrow OH^- + {}^{\cdot}OH + {}^1O_2$$

La dégradation des composés dépend d'un certain nombre de paramètres comme la nature du semi-conducteur et sa concentration dans la solution, la porosité des particules, la concentration dans le milieu des donneurs et des accepteurs d'électrons (en particulier la concentration en oxygène dissous, anions et cations), l'intensité du rayonnement, le pH de la solution, et la température.

II.4. 3 Les nanomatériaux semi-conducteurs

Les matériaux nanostructurés ont connu un essor considérable au cours des dernières années en raison de leurs propriétés particulières par rapport aux matériaux massifs. La préparation de ces matériaux met en jeu des procédés assurant la structuration de la matière afin d'obtenir des nanoparticules dont la taille est généralement de dimension inférieure à 100 nm.

Les propriétés des nanoparticules sont liées à leur taille, leur composition, leur structure cristalline et leur surface, caractéristiques qui vont dépendre du procédé de synthèse. Lorsque la taille diminue, la surface spécifique augmente, et le nombre d'atomes en surface devient plus important. Cela a pour conséquence une modification des propriétés optiques, électriques, magnétiques, physiques (diminution de la température de fusion), catalytiques (réactivité accrue) du matériau nano-particulaire par comparaison au même matériau à l'échelle microscopique. Le **tableau II.2** résume quelques données sur l'importance des nanomatériaux produits à l'échelle mondiale.

Tableau II.2 : Estimation de la production mondiale actuelle pour différentes catégories de nanomatériaux [53].

Application	Matériau / dispositif	Production estimée (t/an)		
		Présent	2005-2010	2011-2020
Applications structurales	Céramiques, catalyseurs, composites, revêtements, films fins, poudres, métaux	10	10^3	10^4-10^5
Produits de soin pour la peau	Oxydes métalliques (dioxyde de titane, oxyde de zinc, oxyde de fer)	10^3	10^3	10^3 ou moins
ICT	Nanotubes simple feuillet, nanoélectronique, matériaux opto-électroniques (dioxyde de titane, oxyde de zinc, oxyde de fer), OLEDs	10	10^2	10^3 ou plus
Biotechnologies	Nanocapsules, envoi ciblé de médicaments, compatibilité biologique, quantum dots, composites, biodétecteurs	moins de 1	1	10
Instruments, détecteurs, caractérisation	MEMS, NEMS, SPM, lithographie dip pen, outils d'écriture directe (direct write tools)	10	10^2	10^2-10^3
Environnementale	Nanofiltration, membranes	10	10^2	10^3-10^4

Les nanomatériaux sont largement utilisés à court, moyen et long terme dans plusieurs secteurs industriels et font partie de notre quotidien. Ils constituent d'excellents catalyseurs, adsorbants, capteurs en raison de leur grande surface spécifique et de leur forte réactivité. Plus récemment, plusieurs nanomatériaux naturels et artificiels se sont avérés avoir de fortes propriétés antimicrobiennes comme le chitosane [54], l'argent (Ag) [55], et photocatalytiques comme le dioxyde de titane (TiO_2) [43]. Au contraire des désinfectants chimiques classiques, ces nanomatériaux antimicrobiens ne sont pas des oxydants forts et sont relativement inertes dans l'eau. Par conséquent, ils ne produisent pas de sous-produits de désinfection nocifs. S'ils sont correctement intégrés dans les processus de traitement, ils ont le potentiel de remplacer ou d'améliorer les méthodes traditionnelles de désinfection.

II.4.3.1 Dioxyde de titane (TiO_2)

Le dioxyde de titane (TiO_2) est le matériau le plus fréquemment utilisé dans les applications photocatalytiques en raison de son faible coût, sa stabilité, sa non toxicité, et de son inertie chimique et biologique [56]. TiO_2 est un matériau important dans un large éventail d'applications commerciales, en tant que pigment dans certaines formulations telles que les peintures [57], les dentifrices et les crèmes solaires [58,59] en raison de sa couleur blanche.Il

est également utilisé dans diverses applications telles que le fractionnement de l'eau [60], l'auto-nettoyage [61], la stérilisation [62], les matériaux antibuée [63], la lithographie [64], la dégradation de composés organiques [65], et la prévention de la corrosion des métaux [66].

Le dioxyde de titane existe dans la nature sous trois formes cristallines différentes, à savoir anatase, brookite et rutile (**figure 5**), cette dernière étant la plus abondante et la plus stable du point de vue thermodynamique [44]. Cependant, l'anatase est la plus photo-active des trois formes en raison de sa plus grande mobilité des porteurs de charge et du plus grand nombre de groupes hydroxyles en surface. En effet, les propriétés physico-chimiques du dioxyde de titane différent selon la nature de la phase, mais aussi de la structure cristalline [67].

Les différences de structure induisent des différences de propriétés entre les deux formes. Ainsi, la phase rutile n'absorbe pas bien l'oxygène, ne piège pas bien des électrons, d'où un nombre de recombinaisons électron-trou plus important [68].

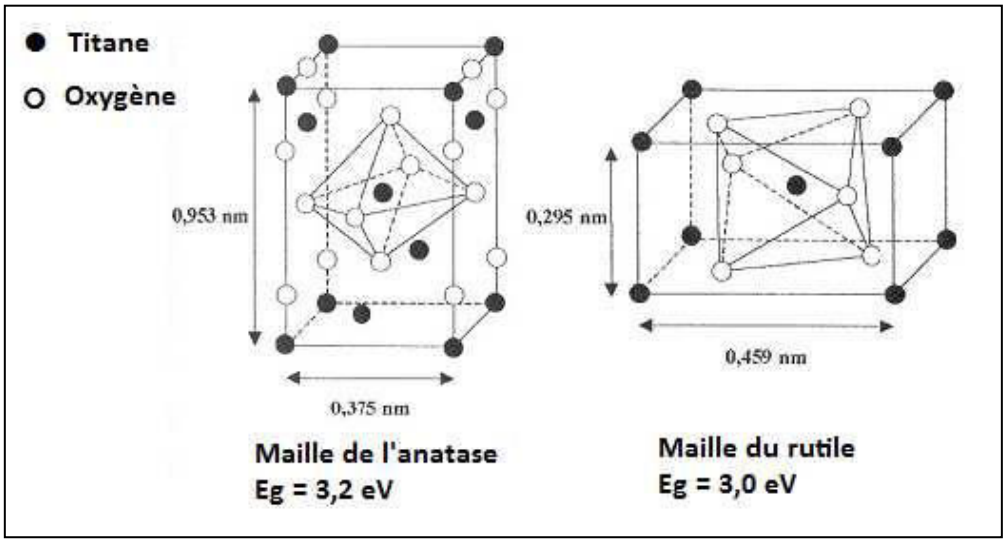

Figure 5 : Schéma de la maille cristalline de TiO_2 sous ses formes anatase et rutile [44]

II.4.3.2 Oxyde de zinc (ZnO)

L'oxyde de zinc est un matériau semi-conducteur de type II-VI étudié depuis le 20^{ième} siècle, avec une large bande interdite (3.3 eV) et une grande énergie de liaison d'exciton (60 meV) à température ambiante. ZnO est attractif pour ses larges applications potentielles comme la luminescence [69], la photo-détection [70], les cellules solaires [71], les capteurs de gaz [72],

la médecine [73] et la photocatalyse pour la dégradation et l'élimination des polluants environnementaux [74,75]. D'autres propriétés, telles que sa conductivité thermique élevée, sa capacité thermique et son point de fusion élevé ont fait de ZnO un bon candidat pour l'industrie céramique [76, 77]. ZnO peut être synthétisé sous forme nanométrique avec des morphologies diverses telles que des points, des tiges, des fils, des ceintures, des ressorts, des arcs, des hélices et des prismes. Pour la photocatalyse, ZnO a également été considéré comme une alternative à TiO_2 en raison d'un band-gap similaire, de sa photosensibilité élevée, de sa stabilité chimique élevée, d'une faible toxicité et de son faible coût. D'après Özgür et al. [78], ZnO peut exister dans trois structures cristallines, wurtzite, zinc blende et rocksalt (**figure 6**).

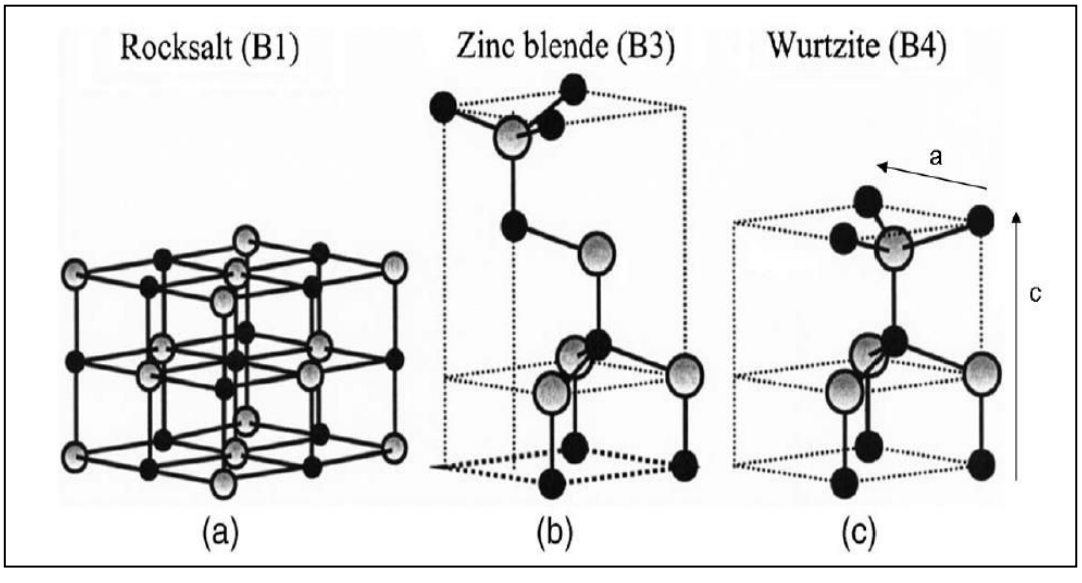

Figure 6 : Structure cristallines de ZnO en phase a) NaCl ; b) Zinc blende ; et c) Wurtzite [78]

II.4.3.3 Synthèses d'oxydes photocatalytiquement actifs

Les voies de synthèse des nanomatériaux sont extrêmement variées. Deux méthodes essentielles sont utilisées : la méthode ascendante (*bottom-up*) et la méthode descendante (*top-down*) [79]. Pour la méthode *bottom-up*, les nanoparticules sont construites « atome par atome » ou « molécule par molécule » (hydrolyse ou condensation d'alkoxydes). Dans la voie *top-down*, une grande structure est progressivement subdivisée, afin d'obtenir des dimensions nanométriques par des procédés mécaniques sévères, chocs violents et fortes déformations par broyage. L'avantage de l'approche ascendante réside dans la production d'une plus grande diversité d'architectures avec un meilleur contrôle de l'état nanométrique (tailles et

distributions granulométriques relativement monodisperses, positionnement des molécules, homogénéité des produits). Le principal avantage de la méthode descendante réside dans la capacité de production plus importante mais le contrôle de l'état nanométrique est plus délicat.

Diverses méthodes ont été consacrées à la synthèse de nanostructures de ZnO, comme le transport en phase vapeur, le dépôt chimique en phase vapeur, le dépôt par pulvérisation via pyrolyse, les procédés micro-ondes assistée par voie chimique, les synthèses hydrothermale ou solvothermale ainsi que des procédés chimiques par voie humide [80-84].

La synthèse d'oxyde de titane nanoparticulaire, en couches minces, sous forme nanoporeuse peut être réalisée via diverses méthodes comme le broyage mécanique [85], la pyrolyse laser [86], la méthode sol-gel [87], les méthodes hydrothermale et solvothermale. Toutes ces méthodes permettent d'obtenir des nanoparticules de faible distribution en taille et de cristallinité contrôlée. En ajustant les conditions expérimentales [88], des nano-fils, des nanotubes ou des nano-bâtonnets peuvent être synthétisés par les méthodes précédemment mentionnées ou par des procédés d'électrodéposition et d'oxydation directe du titane [89].

II.4. 3.4 Dopage des semiconducteurs.

TiO_2 et ZnO sont des bons matériaux semi-conducteurs pour les applications photocatalytiques en raison de leur stabilité environnementale et de leur faible coût par rapport à d'autres oxydes métalliques nanométriques. Leur inconvénient majeur est qu'ils absorbent seulement dans la région UV en raison de leur grande largeur de bande interdite de 3,2 eV et 3,37, respectivement pour TiO_2 et ZnO. Comme le montre la **figure 7**, seul 4 à 5% du spectre solaire se situe dans la gamme des UV [90]. Par conséquent, l'utilisation efficace de l'énergie solaire reste encore un défi avec ces matériaux pour la photocatalyse.

De plus, le processus de recombinaison rapide des électrons et des trous limite l'efficacité photocatalytique.

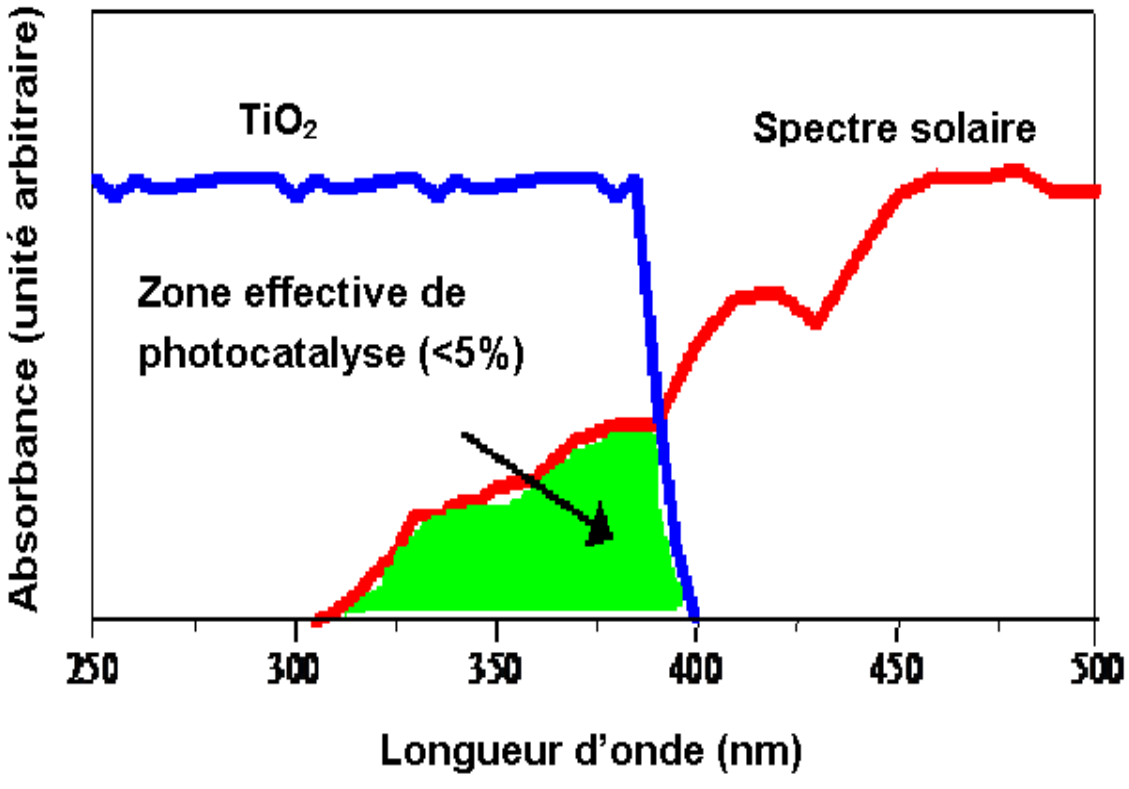

Figure 7 : Comparaison du spectre solaire et du spectre d'absorption du TiO_2 [90]

De nombreux travaux sont orientés vers l'élargissement de la gamme spectrale d'absorption des semi-conducteurs tels que TiO_2 et ZnO vers le domaine visible, ce qui permettrait l'utilisation plus efficace du rayonnement solaire comme source d'irradiation. En effet, l'activité photocatalytique peut être optimisée en modifiant les propriétés physico-chimiques des matériaux semi-conducteurs. Ceci est possible en les dopant avec d'autres éléments ou en les combinant avec d'autres matériaux (création d'hétérojonctions). Le dopage consiste à l'incorporation intentionnelle d'impuretés dans la maille cristalline d'un semi-conducteur pour ajuster ou moduler ses propriétés optiques et chimiques [91].

Différentes méthodes de dopage ont été étudiées dans la littérature (**figure 8**). Ce procédé est efficace pour la réduction de la largeur de la bande interdite et l'extension de la plage d'absorbance à la région visible et améliore la séparation de la paire électron-trou et, par conséquent, permet d'améliorer l'activité photocatalytique [92]. Le dopage de ZnO avec d'autres matériaux, par exemple $CaFe_2O_4$ [93], avec des métaux de transition tels que Sc, Ti,

V, Cr, Mn, Fe, Co, Ni, et Cu a été décrit [94]. Des études ont montré que le couplage de TiO_2 avec CdS (Eg=2,4 eV), ZnO (Eg=3,3 eV) ou SiC (Eg= 3 eV) permettait d'améliorer l'activité photocatalytique de 1,5 à 4 fois par rapport à TiO_2 lors de la dégradation du phénol ou de l'oxydation de la méthyléthylcétone [95, 96, 97].

En outre, l'analyse optique des spectres d'absorption ont montré que CdS-TiO_2 pouvait absorber les photons de longueurs d'onde allant jusqu'à 520 nm.

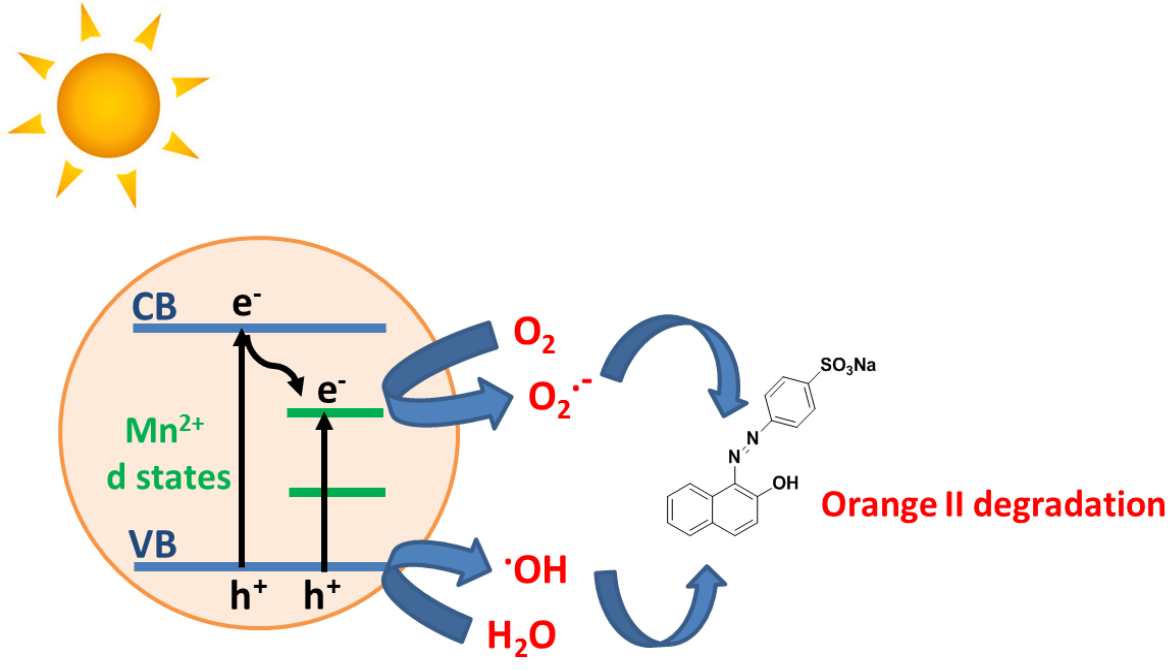

Figure 8 : Représentation schématique de la production de radicaux $OH^{\cdot}$ et $O_2^{\cdot -}$ par le nanocomposite ZnO dopé Mn [92]

D'autres types de dopage anionique et cationique sont utilisés encore pour contrôler les propriétés du dioxyde de titane et améliorer les performances du photocatalyseur. L'ajout des éléments dopants à TiO_2 et/ou ZnO ont comme résultats la formation de nouveaux niveaux énergétiques dans la bande interdite de ces matériaux [98,99], la création de sites de piégeage de porteurs de charge [100], la réduction du « band-gap » [101] et l'amélioration de la surface spécifique [102].

II.4.4 Les espèces réactives de l'oxygène

Dans le monde vivant et à l'état physiologique normal, les formes activées de l'oxygène (FAO) sont produites à partir du métabolisme aérobie. Ces formes sont classées en trois grands groupes : les espèces réactives oxygénées (EROs), les entités nitrées réactives (ENR) et les entités halogénées réactives (RCS) [103]. Ces FAO sont des radicaux libres qui présentent des atomes ou des molécules portant, pour la plupart d'entre elles, un électron non apparié; ce sont des molécules à réactivité très forte du fait de la tendance de cet électron à se rapparier pour se stabiliser, déstabilisant ainsi d'autres molécules. Les molécules ainsi transformées deviennent à leur tour d'autres radicaux libres et amorcent alors une réaction en chaîne. La production de ces radicaux a plusieurs origines comme la chaîne respiratoire, les systèmes enzymatiques, les métaux, ou les rayonnements (gamma, X, et UV). Dans notre étude, nous nous sommes intéressés aux espèces réactives oxygénées (ERO_S) générées par une réaction photocatalytique. Les principales espèces réactives de l'oxygène sont :

- Le radical hydroxyle (HO•),
- Le radical peroxyde (ROO•),
- Le radical alkoxyle (RO•),
- Le peroxyde d'hydrogène (H_2O_2),
- L'hydroperoxyde organique (ROOH),
- L'oxygène singulet ($^1O_2$),
- Le radical superoxyde ($O_2^{\bullet-}$).

II.4.4.1 Production de radicaux hydroxyles

Un radical hydroxyle (HO•) est une molécule composée d'un atome d'oxygène et d'hydrogène possédant un électron non apparié (électron célibataire) sur son orbital externe. Il a une durée de vie très courte (~10^{-8} seconde) dans un milieu à pH neutre. Son potentiel normal d'oxydoréduction est de 2,7 V par rapport à l'électrode normale à hydrogène, ce qui le place parmi les oxydants les plus forts en milieu aqueux (**tableau II.3**). De plus, il présente des critères de non sélectivité vis-à-vis les polluants organiques et inorganiques. Il n'induit pas de pollution secondaire, n'est pas toxique ni corrosif pour les équipements [104].

Tableau II.3 : Potentiels standard de différents oxydants utilisés [104]

Réaction redox	E° (V/ENH) (pH= 0)
$XeF + e^- \rightarrow Xe + F^-$	3,4
$2\ OF_2(g) + 4\ H^+ + 4\ e^- \rightarrow O_2(g) + 4\ HF$	3,29
$HO^\bullet + H^+ + e^- \rightarrow H_2O$	**2,7**
$HO^\bullet + e^- \rightarrow HO^-$	**2,33**
$O_3 + 2\ H^+ + 2\ e^- \rightarrow O_2 + H_2O$	2,07
$HClO_2 + 3\ H^+ + 4\ e^- \rightarrow Cl^- + H_2O$	1,57
$MnO_4^- + 8\ H^+ + 5\ e^- \rightarrow Mn^{2+} + 4\ H_2O$	1,51
$HO_2^\bullet + H^+ + 2\ e^- \rightarrow H_2O_2$	1,44
$Cl_2 + 2\ e^- \rightarrow 2\ Cl^-$	1,36
$O_2 + 4\ H^+ + 4\ e^- \rightarrow 2\ H_2O$	1,23

Ce tableau résume les potentiels de réduction des oxydants utilisés en milieux aqueux. Le radical hydroxyle est l'espèce qui a le pouvoir oxydant le plus élevé des oxydants chimiques utilisés en milieu aqueux, c'est l'espèce chimique la plus oxydante, après le fluor (E° = 3,05 V/ESH à 25 °C). Les autres espèces telles que XeF et OF_2 ont une réactivité plus grande que le radical hydroxyle, mais ne sont pas utilisés pour la dépollution de l'eau en raison de leur extrême réactivité, de leur nocivité sous formes réduites et de leur aptitude à former des trihalométhanes cancérigènes avec les matériaux organiques.

II.4.4.2 Mode d'action des radicaux hydroxyles sur les polluants

D'après Buxton *et al* [105], les radicaux hydroxyles agissent sur les polluants de différentes manières qui peuvent être résumées comme suit :

- Arrachement d'atome d'hydrogène (déshydrogénation).
- Les radicaux hydroxyles peuvent oxyder les composés organiques par élimination d'atomes d'hydrogène sur des chaînes hydrocarbonées saturées, sur lesquelles des sites radicalaires sont crés et où l'oxygène pourra ensuite réagir. Ce processus induit la rupture homolytique d'une liaison C-H:

$$RH + {}^{\bullet}OH \rightarrow R^{\bullet} + H_2O$$

Par la suite le radical peroxyde $ROO^{\bullet}$ est obtenu par réaction entre le radical $R^{\bullet}$ ainsi formé et l'oxygène moléculaire pour amorcer une séquence de réactions de dégradations oxydantes conduisant à la minéralisation du composé RH :

$$R^{\bullet} + O_2 \rightarrow ROO^{\bullet}$$

$$ROO^{\bullet} + n\ ({}^{\bullet}OH/O_2) \rightarrow x\ CO_2 + y\ H_2O$$

- Addition électrophile sur des liaisons non saturées (hydroxylation)

Les radicaux hydroxyles s'additionnent sur les liaisons insaturées des composés aromatiques, des alcènes et des alcynes après attaque des régions de forte densité électronique:

$$ArX + {}^{\bullet}OH \rightarrow HOArX^{\bullet}$$

$$HOArX^{\bullet} + n\ (O_2/\ {}^{\bullet}OH) \rightarrow HX + x\ CO_2 + y\ H_2O$$

- Transfert d'électrons (oxydo-réduction)

Le phénomène d'oxydation induit l'ionisation de la molécule. Cependant ces réactions d'oxydo-réduction génèrent des radicaux organiques, qui par addition de dioxygène donneront des radicaux peroxyles, initiant en retour des réactions en chaîne de dégradation oxydative pour conduire à la minéralisation du composé de départ :

$$RX + {}^{\bullet}OH \rightarrow RX^{\bullet+} + OH^{-}$$

$$RX^{\bullet+} + n\ (O_2/\ {}^{\bullet}OH) \rightarrow HX + x\ CO_2 + y\ H_2O$$

II.4.5 Paramètres influençant la photocatalyse hétérogène

II.4.5.1 Effet du pH

Le pH de la solution aqueuse affecte de manière significative la surface du catalyseur, y compris la charge des particules, la taille des agrégats éventuellement formés, et par conséquent la position des bandes de conduction et de valence [14]. Le rendement des procédés photocatalytiques dépend fortement du pH de la solution réactionnelle et du comportement amphotère de TiO_2. La charge de surface de TiO_2 varie avec le pH de la solution : on définit ainsi le pH pour lequel la charge de surface d'un catalyseur est nulle,

c'est le point zéro Charge, (pH_{pzc}) ou point isoélectrique (PIE). Pour TiO_2 Degussa P25, ce pH_{pzc} est compris entre 6 et 6,5. La surface de TiO_2 est chargée positivement ($TiOH_2^+$) dans des solutions acides, ce qui favorise l'adsorption des anions par attraction électrostatique, alors qu'à pH > 6,5, elle est chargée négativement (TiO^-), ce qui induit l'attraction des cations [106].

$$TiOH_2^+ \quad TiOH + H^+ \rightarrow \qquad pH < \; pH_{pzc} = 6.5 \quad (1)$$

$$TiOH \quad TiO^- + H^+ \rightarrow \qquad pH > \; pH_{pzc} = 6.5 \quad (2)$$

Les constantes d'équilibre de ces réactions ont été déterminées par Kormann *et al* [107], pK ($TiOH_2^+$) = 2.4 et pK (TiOH) = 8. La nature des espèces présentes en fonction du pH est la suivante :

$$3 < pH < 10 \quad TiOH_2^+ \geq 80\% \qquad (3)$$

$$pH > 10 \quad TiO^- \geq 20\% \qquad (4)$$

$$pH < 3 \quad TiOH_2^+ \geq 20\% \qquad (5)$$

Lorsque le pH est proche du pH_{pzc}, le catalyseur possède autant de charges positives que négatives, cela entraine le phénomène d'agrégation et la formation de clusters de TiO_2 est favorisée [108]. Il en résulte une baisse de l'efficacité photocatalytique à pH 7 car les clusters limitent la transmission et l'absorption de la lumière. La taille des agrégats formés par des particules de TiO_2 est également affectée par le pH, elle vaut environ 300 nm pour un pH éloigné de 7 mais augmente de 2 à 4 µm lorsque la dispersion atteint le pH_{pzc} [14].

Dans de nombreux cas, pendant la réaction, une multitude de produits intermédiaires sont produits et peuvent se comporter différemment en fonction du pH de la solution [14]. Herrmann *et al* [109] ont montré qu'une élévation de pH (> 10) induit une augmentation de l'efficacité photocatalytique car plus de radicaux $OH^{\bullet}$ sont formés.

$$OH^- + h^+ \rightarrow OH^{\cdot} \qquad (6)$$

L'effet du pH sur la dégradation photocatalytique avec TiO_2 de différents colorants (rouge Congo, orange G (OG), bleue de méthylène (BM) a été étudié par Guillard *et al* [110].

Ils ont noté que la dégradation du BM est favorisée à pH élevé, où il se présente sous sa forme cationique, ce qui favorise son adsorption par TiO_2 chargé négativement. Par contre, la charge négative de l'Orange G défavorise son adsorption à pH élevé.

De même, plusieurs auteurs ont montré l'effet du pH sur la dégradation photocatalytique des composés azotés [111], des acides aminés [112], et des bactéries [113]. Une meilleure oxydation photocatalytique de l'éthanol à pH acide plutôt qu'à pH alcalin ou neutre a été montrée par Norzita et al. [114].

II.4.5.2 Effet de la température

De nombreuses études ont été menées sur la dépendance de la réaction photocatalytique à l'égard de la température de réaction [115]. En raison de l'activation photonique, les systèmes photocatalytiques ne nécessitent pas de chauffage et fonctionnent à la température ambiante. La véritable énergie d'activation est égale à zéro, alors que l'énergie d'activation apparente est souvent très faible (quelques kJ/ mol) dans la plage de températures moyennes (entre 20 et 80 °C) [14]. La diminution de la température favorise l'adsorption qui est un phénomène spontanément exothermique. Au contraire, quand la température augmente au-dessus de 80°C, l'adsorption exothermique des polluants est défavorisée [48]. Pour la photodésinfection utilisant le photocatalyseur TiO_2, l'élévation de la température de réaction augmente la vitesse d'inactivation de micro-organismes [116]. La température de croissance des bactéries est aussi un facteur important pour des tests de décontamination [113], ceci peut être lié à la variation de la composition membranaire qui dépend de la température [117]. À ce jour, il n'y a aucune étude exhaustive menée pour comparer l'effet de TiO_2 sur la photo-désinfection en fonction du type de micro-organisme et pour une température de fonctionnement donnée [48]. L'absence de chauffage est énergétiquement favorable pour des réactions photocatalytiques en milieux aqueux et, en particulier, pour la purification photocatalytique de l'eau. La température n'affecte que très peu la cinétique de dégradation, ce qui permet de travailler à température ambiante (optimum entre 20°C et 80°C), et ainsi de faire des économies d'energie importantes.

II.4.5.3 Effet de la concentration en catalyseur

La concentration optimale en catalyseur dépend des conditions expérimentales et de la géométrie du photoréacteur. La vitesse de dégradation photocatalytique est liée à la charge catalytique jusqu'à une valeur limite. Si le photocatalyseur est déposé sur une surface, le seuil

de dépôt pour le TiO_2 est d'environ 1,3 mg/cm² [49]. Ould-Mame *et al* (2000) ont trouvé une valeur très similaire dans le cas de la dégradation photocatalytique de l'acide salicylique [118]. Plusieurs travaux [119-122] considèrent une concentration optimale de TiO_2 en suspension de 1 mg/mL pour l'inactivation bactérienne. En revanche, il existe un certain nombre d'études dont les résultats sont très différents, mais de manière générale, le rayonnement incident et la géométrie du réacteur sont essentiels dans la détermination de la concentration optimale de catalyseur [14]. Plus la charge en catalyseur est importante et plus l'inactivation photocatalytique est rapide et meilleure (**figure 9**). Selon les conditions opératoires, lorsque la concentration du photocatalyseur atteint une valeur limite, la solution devient opaque et un effet d'écran apparaît, empêchant ainsi la pénétration de la lumière au centre du réacteur, ce qui affecte le rendement photocatalytique de la réaction [123].

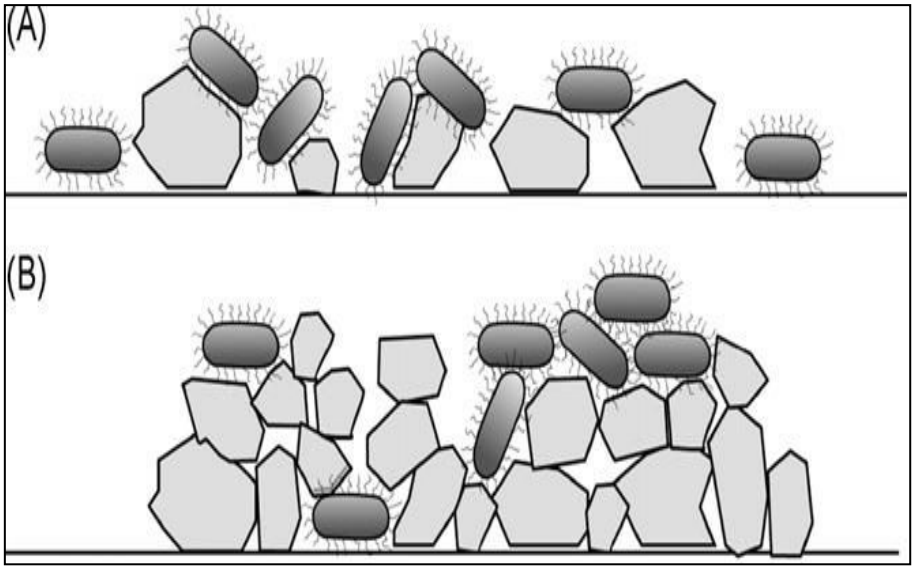

Figure 9 : Représentation schématique illustrant le contact entre les bactéries et TiO_2 lors du processus d'inactivation photocatalytique. A) faible taux de charge de TiO_2 : un contact optimal entre les cellules et TiO_2, une bonne transmission de la lumière et un meilleur taux d'inactivation. B) Charge forte en TiO_2 : mauvais contact entre les cellules et TiO_2, baisse de transmission de la lumière ainsi qu'un faible taux d'inactivation bactérienne. [123]

II.4.5.4 Effet de l'intensité lumineuse

L'intensité lumineuse est un facteur crucial dans la dégradation photocatalytique. Il est très important que le réacteur soit bien éclairé. En fait, une bonne illumination de la surface du catalyseur favorise l'augmentation du taux de paires électron-trou formées. La vitesse de la

réaction de dégradation photocatalytique d'un polluant est proportionnelle à l'intensité d'irradiation jusqu'à une valeur approximative de 25 mW/cm^2 à partir de laquelle la vitesse devient proportionnelle à la racine carrée de l'intensité lumineuse [48].

II.4.5.5 Effet de la structure cristalline du photocatalyseur

Le rendement photocatalytique d'un photocatalyseur est lié étroitement à sa structure cristalline. TiO_2 se présente sous trois formes cristallines (anatase, rutile et brookite) dont les principales sont l'anatase et le rutile. ZnO existe sous trois formes dont la forme wurtzite est la plus active en photocatalyse. Des études comparatives de l'activité photocatalytique de l'anatase et du rutile ont montré que la vitesse de recombinaison des paires e^-/h^+ est plus élevée pour le rutile que pour l'anatase [124], ce qui défavorise la formation des radicaux et altère la dégradation des polluants. Généralement, on considère que l'anatase est la forme photoactive, alors que le rutile est celle présentant une faible activité photocatalytique. Le mélange d'anatase (80%) et de rutile (20%), présent dans le photocatalyseur commercial sous le nom de Degussa P25, donne la meilleure activité photocatalytique [115]. La combinaison entre ces deux formes cristallines assure ainsi une meilleure activité que l'anatase seule [125].

II.4.5.6 Effet de la surface spécifique et la taille des particules

En plus de la structure cristallographique, il existe d'autres paramètres jouant un rôle primordial dans la réaction photocatalytique : la surface spécifique et la taille des particules qui est inversement proportionnelle à la surface spécifique du catalyseur. Il est généralement admis que la diminution de la taille engendre une augmentation de l'activité photocatalytique [126]. Ceci s'explique par l'augmentation de la surface spécifique et, par conséquent, du nombre de sites actifs au sein du catalyseur. Des auteurs ont montré qu'il existe une taille idéale pour la dégradation photocatalytique des polluants organiques. Par exemple, Shah *et al* [127] ont trouvé lors de la photodégradation du 2-chlorophénol sous UV, une taille optimum de l'anatase à 17 nm en faisant varier la taille de l'anatase dans TiO_2 entre 12 et 23 nm.

II.4.5.7 Effet de l'oxygène dissous et des accepteurs d'électrons.

Un problème pratique lors de l'utilisation du TiO_2 en tant que photocatalyseur est la perte d'énergie lors de la recombinaison électron-trou qui se traduit par une faible efficacité de dégradation des polluants. Dans la réaction photocatalytique hétérogène, l'oxygène

moléculaire (de l'air) agit comme un accepteur d'électrons et diminue la recombinaison électron trou en favorisant la formation de l'anion superoxyde ($O_2^{\cdot-}$) [128].

Des expériences ont montré que lorsque tout l'oxygène est consommé, le processus photocatalytique s'arrête [129]. Une approche visant à prévenir la recombinaison électron-trou consiste à rajouter des accepteurs d'électrons dans la réaction. La présence de certains accepteurs d'électrons (oxydants), tels que H_2O_2, $S_2O_8^{2-}$ et BrO_3^- peuvent servir de pièges à électrons pour empêcher la recombinaison et améliorer l'efficacité de la photodégradation.

II.4.5.8 Effet de la concentration initiale en polluant

Généralement, le rendement de dégradation photocatalytique diminue avec l'augmentation de la concentration initiale du polluant. Une forte concentration initiale en polluant induit une concentration plus élevée du polluant adsorbé à la surface, ce qui diminue le rendement de la dégradation. Ceci peut s'expliquer par une diminution de la pénétration des photons à la surface (effet d'écran). L'influence de la concentration initiale est importante du point de vue cinétique de la réaction et de la conception du photoréacteur [130]. Lorsque la concentration initiale en polluant augmente, la probabilité que des radicaux $HO^{\bullet}$ réagissent avec les molécules de polluant augmente également. Cependant, quand les sites actifs à la surface du catalyseur ont été remplacés et/ou recouverts par des molécules de polluant, la génération de radicaux $HO^{\bullet}$ est réduite, car il y a moins de sites actifs disponibles pour la production de radicaux $HO^{\bullet}$ [131]. La cinétique de dégradation photocatalytique d'un polluant peut être décrite par le modèle de Langmuir-Hinshelwood [117]. Ce modèle permet d'évaluer la vitesse de dégradation d'un polluant organique à différentes concentrations. Utilisé d'abord pour caractériser des réactions hétérogènes en phase gazeuse [132], il a été ensuite utilisé par Ollis [133] pour décrire des réactions liquide-solide.

Les hypothèses sur lesquelles est fondé ce modèle sont les suivantes :

- A l'équilibre, le nombre de sites d'adsorption est fixe.
- Une seule molécule de substrat est adsorbée par site d'adsorption (adsorption en monocouche).
- L'énergie d'adsorption est identique pour tous les sites d'adsorption et indépendante du taux de recouvrement de la surface.
- L'adsorption est rapide par rapport aux réactions secondaires du substrat en solution.

- Seules les molécules adsorbées à la surface du catalyseur réagissent.

A partir de ces hypothèses, la vitesse de dégradation photocatalytique (V) est proportionnelle au taux de recouvrement (θ) de la surface du catalyseur par le polluant, c'est-à-dire à la quantité de substrat adsorbé à la surface de catalyseur [134] (**figure 10**). L'expression de la vitesse dans un réacteur fermé (batch) est donnée par l'équation suivante :

$$V = -\frac{dC}{dt} = k\theta = k\frac{\varphi_e}{\varphi_{max}} \quad (1)$$

La quantité de substrat adsorbé à l'équilibre Qe dépend de la concentration en solution à l'équilibre Ce :

$$\varphi_e = \frac{K.\varphi_{max}.C_e}{1 + K.C_e} \quad (2)$$

Le taux de recouvrement Θ s'écrit:

$$\theta = \frac{K.C_e}{1 + K.C_e} = \frac{\varphi_e}{\varphi_{max}} \quad (3)$$

L'expression de la vitesse de Langmuir-Hinshelwood s'écrit donc:

$$V = \frac{k.K.C_e}{1 + K.C_e} (4)$$

où :

V : vitesse de la réaction (µmol/L/min).

ɵ: taux de recouvrement de la surface du catalyseur par le substrat.

k : constante cinétique de dégradation (µmol/L/min).

K : constante d'adsorption du substrat (L/mmol).

Ce : concentration à l'équilibre du polluant (mmol/L).

Pour de faibles concentrations en polluants, le produit (K.Ce) devient négligeable devant 1 (K.Ce << 1), la vitesse de réaction devient directement proportionnelle à la concentration de polluant. La cinétique de réaction peut alors être considérée du premier ordre par rapport à la concentration du polluant et l'équation devient :

$$V = k.'C_e = k.K.C_e \quad (5)$$

Pour de grandes concentrations en polluants, K.Ce >> 1, la vitesse de réaction tend vers la constante k, elle est maximale et d'ordre zéro [135].

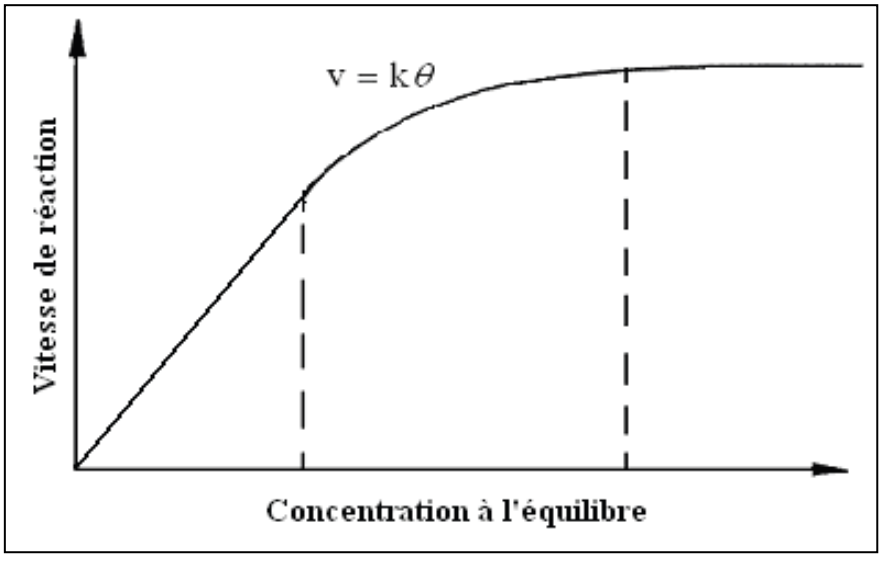

Figure 10 : Variation de la vitesse de réaction en fonction de la concentration en polluant à l'équilibre [133].

II.4.5.9 Effet ionique

La présence d'anions tels que Cl^-, NO_3^-, HCO_3^-, ClO_4^-, SO_4^{2-}, HPO_4^{2-}et PO_4^{3-} et de cations tels que Na^+, K^+, Ca^{2+}, Cu^{2+} , Mn^{2+}, $Mg^{2+,}$ $Ni^{2+,}$ Fe^{2+}, Zn^{2+} et Al^{3+} est inévitable dans les stations de traitement des eaux usées ou industrielles. L'application du traitement photocatalytique dans ces stations nécessite la compréhension des effets de ces ions et cations qui peuvent affecter fortement l'efficacité photocatalytique en raison de leur adsorption compétitive sur le catalyseur et de leur capacité à piéger les EROs [136].

Lors de l'inactivation photocatalytique d'*E. coli K12* par TiO_2, Rincón et *al.* [115] ont étudié l'effet de l'ajout de substances organiques et inorganiques à la suspension aqueuse *d'E. coli* et ont trouvé que l'ajout de certains ions inorganiques (0,2 mmol/L) comme HCO_3^-, HPO_4^{2-}, Cl^-, NO_3^- et SO_4^{2-} diminuait le taux d'inactivation (compétition avec *E. coli* et les radicaux oxydants issus de ces anions et/ou blocage des sites actifs sur le catalyseur TiO_2).

III. Inactivation bactérienne par photocatalyse

III.1 Introduction

L'utilisation de semi-conducteurs en tant que matériaux antibactériens a été largement décrite dans la littérature. En 1985, Matsunaga *et al* [121] sont parmi les pionniers qui ont étudié l'inactivation photocatalytique des bactéries en utilisant TiO_2 combiné avec le platine (TiO_2/Pt) comme photocatalyseur pour l'inactivation des cellules microbiennes dans l'eau (*E. coli, Lactobacillus, Acidophilus,…*).

En 2006, Paspaltsis *et al* [137] ont montré que la photocatalyse est capable de détruire une large gamme d'organismes comprenant des bactéries Gram-négatives et Gram-positives, ainsi que les endospores, les champignons, les algues, les protozoaires et les virus. Il a été également démontré que le TiO_2 est capable d'inactiver les prions. Herrera *et al* [138] ont également testé sur des eaux urbaines résiduaires pour inactiver totalement des coliformes et *Streptococcus faecalis* par photocatalyse TiO_2 sous lampes UV et lumière solaire.

La résistance à la désinfection peut varier en fonction du type de microorganisme, même au sein de différentes souches de la même espèce. De manière générale, on peut dire que les microorganismes qui forment des spores sont plus résistants à la désinfection que ceux qui ne le font pas, même s'ils appartiennent au même type.

III.2 Epuration de l'eau par la lumière solaire

En 1877, la lumière solaire naturelle a été décrite pour la première fois comme agent désinfectant agissant sur les micro-organismes [139]. Au cours de ces dernières années, les travaux ont porté sur l'exposition des récipients transparents à la lumière solaire contenant des volumes d'eau réduite (1,5 L). L'irradiation des réservoirs peut durer jusqu'à 8h. Cette méthode simple, communément connue sous le nom SODIS (désinfection solaire de l'eau) s'est montrée efficace pour une grande variété d'agents pathogènes [140]. En 1990, Acra *et al* [141] ont mentionné que l'eau peut être épurée par le rayonnement solaire à grande échelle à

travers des systèmes à flux continu. Cependant, l'application de la technique SODIS en utilisant la lumière solaire naturelle ou artificielle est largement étudiée pour l'inactivation d'un grand panel de bactéries (*E. coli, Enterococcus faecalis, Shigella dysenteriae, Cryptosporidium, Salmonella typhi, Pseudomonas sp.*) [142, 143].

En 1998, McGuigan *et al* [143] ont étudié l'effet optique et thermique de la lumière solaire sur l'inactivation d'*E. coli*. Ils ont suggéré que l'effet de la température était important seulement au-delà de 45°C. La lumière UV-A (320 - 400 nm) et visible est la principale cause de l'inactivation d'*E. coli* car le rayonnement UV-B (280-320 nm) est filtré par la bouteille en polyéthylène (PET). L'effet des UV-B et les UV-A est la conséquence de l'absorption par les composants cellulaires appelés chromophores intracellulaires [144, 145]. Parmi ceux-ci, le L-tryptophane est le plus connu. Après irradiation, il produit des photo-produits toxiques inhibant la recombinaison des mutants de *Salmonella typhimurium* et d'*E. coli* [146, 147].

La désinfection solaire (SODIS) s'est avérée une technique prometteuse, peu coûteuse et intéressante en termes d'application dans les pays en voie de développement afin d'améliorer la qualité de l'eau. Mais, son efficacité est limitée par la fluctuation quotidienne et saisonnière de l'intensité du soleil, ce qui peut nécessiter un prolongement du temps d'exposition [148]. De plus, la réactivation des bactéries après traitement de l'eau est un paramètre dont il faut tenir compte [149], du fait de l'existence de certains germes résistants à la lumière solaire et à la charge de l'eau qui peut entraver la pénétration de la lumière [150].

Pour résoudre ces problèmes et augmenter l'efficacité du procédé (SODIS), quelques solutions sont proposées via l'utilisation d'additifs oxydants tels que H_2O_2 et/ou O_3, ainsi que des catalyseurs TiO_2, Fe_2O_3, ZnO, SiO_2, ...

Cependant, la résistance des microorganismes au rayonnement solaire a été étudiée par plusieurs auteurs et peut varier suivant leur type [151]. *E. coli* est souvent choisi comme référence des bactéries coliformes entériques dans de nombreuses études (**figure 11**). Cette bactérie est largement reconnue comme étant une cible «facile» pour la désinfection, car elle est relativement simple à inactiver par le rayonnement solaire ainsi que l'illustre un certain nombre d'articles [150,152].

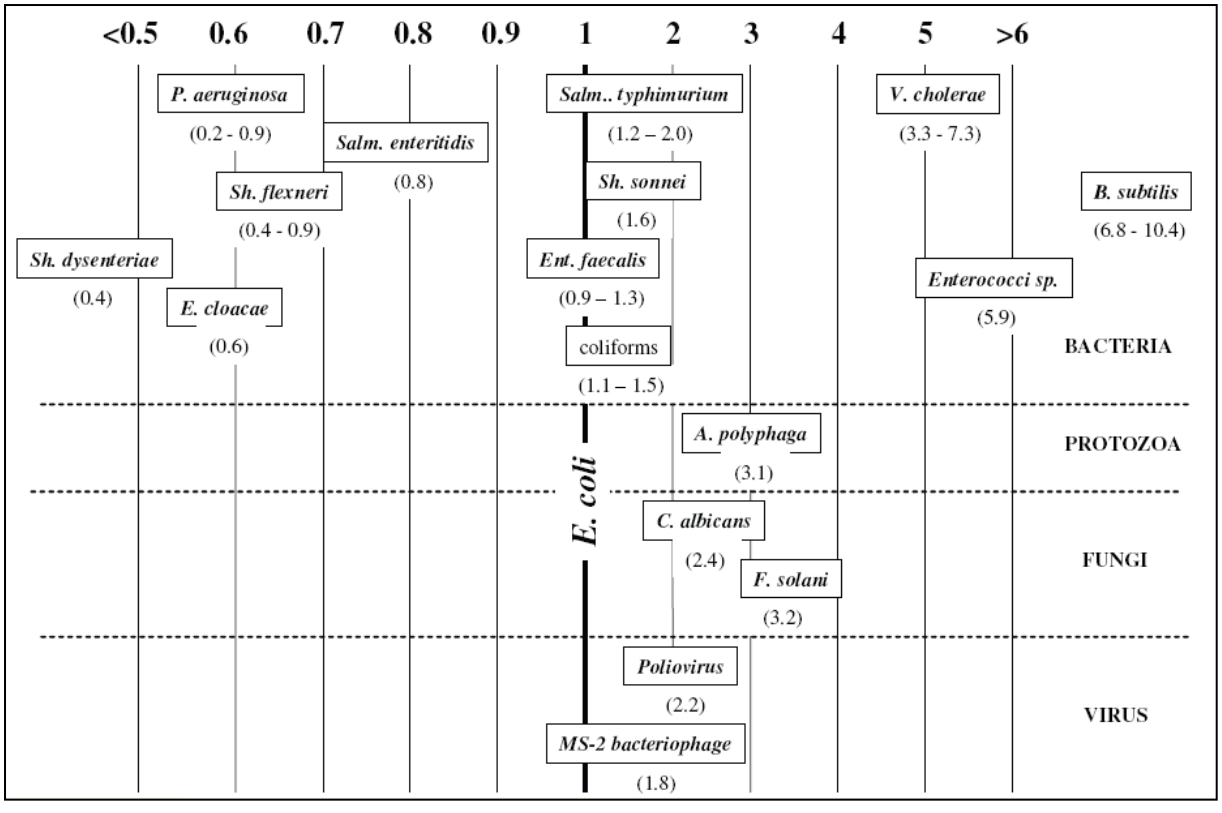

Figure 11 : Résistance au rayonnement solaire de plusieurs microorganismes *(E. coli* est la référence) [150].

III.3 Interactions entre les bactéries et les nanoparticules

Le contact entre les bactéries et les nanoparticules telles que TiO_2 et ZnO est considéré selon de nombreuses recherches comme le point clé de l'inactivation bactérienne. En effet, ces nanoparticules interagissent avec les cellules microbiennes à travers différents mécanismes. Les mécanismes antimicrobiens majeurs rapportés dans la littérature sont résumés dans la **figure 12.**

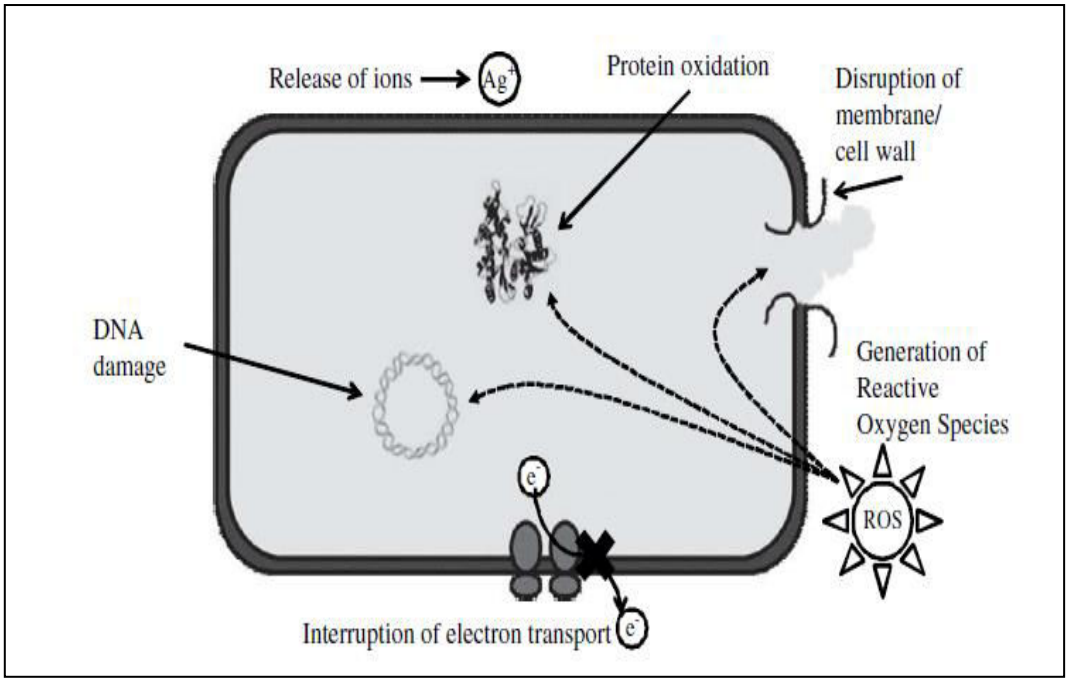

Figure 12 : Mécanismes de l'activité antimicrobienne exercée par les nanomatériaux [56].

Les nanoparticules peuvent interagir directement avec les cellules microbiennes, par exemple, en interrompant le transfert d'électrons transmembranaires. Ils peuvent perturber et pénétrer l'enveloppe cellulaire pour oxyder des composants cellulaires ou encore produire des produits secondaires qui causent des dommages cellulaires (par exemple, les espèces réactives de l'oxygène (ERO_S) ou des ions de métaux lourds dissous).

L'attachement de nanoparticules à la surface bactérienne se fait soit à travers les forces électrostatiques (forces de Van der Waals) ou via des interactions ligand-récepteur sachant que le potentiel zêta de ZnO suspendu avec *E. coli* à pH = 7 est d'environ 24 mV [153]. Le potentiel de surface d'*E. coli* est de -7.2 mV (surface d'*E. coli* chargée négativement en raison des polysaccharides et des lipopolysaccharides [154]. Cependant, des auteurs affirment que l'interaction de ZnO avec *E. coli* est favorisée par des forces électrostatiques qui engendrent la rupture de la paroi cellulaire, induisant ainsi l'internalisation des nanoparticules dans la cellule bactérienne et, par conséquent, la modification de la morphologie et la fuite du contenu intracellulaire [155]. Gogniat *et al* ont aussi montré que l'adsorption des bactéries à la surface de nanoparticules de TiO_2 favorise des modifications de perméabilité membranaire même à l'obscurité, ce qui induit une augmentation des dommages cellulaires lors du traitement

photocatalytique [156]. Les dommages oxydatifs commencent tout d'abord par le contact entre la paroi bactérienne et la particule du TiO_2 (**figure 13**). Les cellules souffrent de lésions de la paroi cellulaire bien qu'encore viables. De fait, l'action photocatalytique augmente progressivement la perméabilité cellulaire et, par conséquent, l'écoulement libre des composants intracellulaires, ce qui permet un accès plus facile des particules du TiO_2 et la photo-oxydation des éléments intracellulaires et finit par accélérer la mort cellulaire [157].

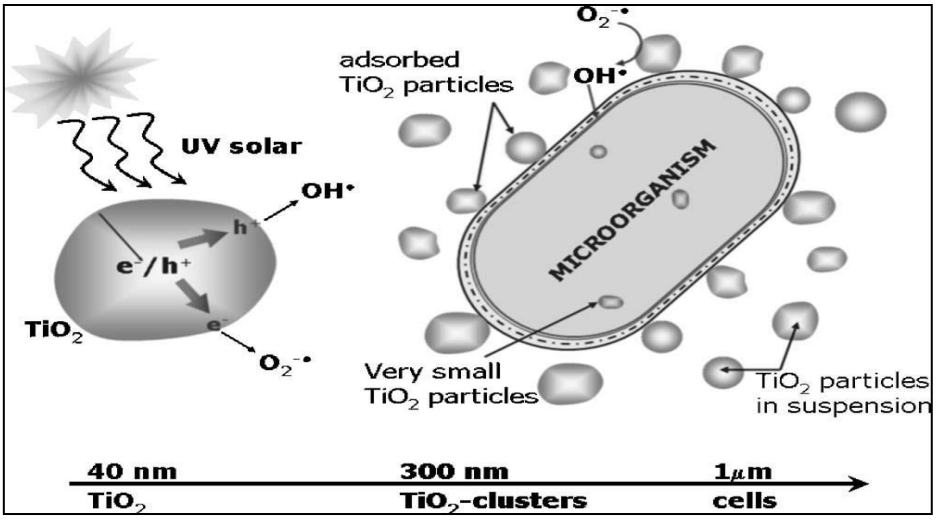

Figure 13 : Illustration schématique du procédé photocatalytique solaire pour l'inactivation des bactéries en présence d'une suspension aqueuse de TiO_2 [157].

Des travaux publiés par Sunada *et al* en 2003 [158] ont trouvé des résultats similaires à ceux rapportés par Huang *et al* (2000). Ils suggèrent que la réaction de photo-destruction est initiée par décomposition partielle de la membrane externe, suivie de la désorganisation de la membrane cytoplasmique conduisant à la mort cellulaire.

III.4 Effet des EROs sur les bactéries.

Les nanoparticules de TiO_2 et ZnO présentent un effet bactéricide qui s'accentue lors de l'irradiation [159]. Plusieurs travaux de recherches ont montré que l'inactivation bactérienne par photocatalyse est due essentiellement aux EROs (•OH, $O_2^{\bullet-}$, H_2O_2) générés lors de l'irradiation d'un semiconducteur par un rayonnement lumineux approprié [14, 159,160, 161]. Parmi ces EROs, les radicaux hydroxyles sont responsables en grande partie del'effet bactéricide photocatalytique. Ils sont impliqués dans l'inactivation des kystes de *Cryptosporidium parvum*, bien que d'autres EROs ont également contribuées à cet effet [160].

Une autre étude a montré que l'inactivation du phage *Lactobacillus* PL1 par des films minces de TiO_2 en suspension dans un liquide a été induite par un dommage initial à la protéine de la capside par •OH, suivie par des dommages à l'ADN du phage à l'intérieur des particules [162]. Huang *et al* (2008) et Brayner *et al* (2006) ont constaté l'existence d'inclusions riches en zinc à l'intérieur de bactéries lors du contact avec des nanoparticules de ZnO. Cela pourrait être attribué à une dissolution des nanoparticules, puis à l'internalisation et à la précipitation des ions Zn^{2+} dans les bactéries [163, 164].

Les radicaux •OH ont une durée de vie très courte de l'ordre de la nanoseconde (10^{-9} s) et ne peuvent probablement pas diffuser au-delà de 1 µm à partir de la surface du TiO_2. En présence de la matière organique, Kikuchi *et al* (1997) ont montré que l'inactivation d'*E. coli* a encore lieu, même lorsque les bactéries ont été séparées de la surface de TiO_2 par une membrane poreuse de 50 µm d'épaisseur [165]. Cet effet est attribué au peroxyde d'hydrogène H_2O_2 qui serait impliqué dans la mort cellulaire grâce à l'absence de charge électrique qui lui permet de passer à l'intérieur de la cellule contrairement aux radicaux hydroxyles qui ne peuvent pas diffuser comme l'illustre la **figure 14**.

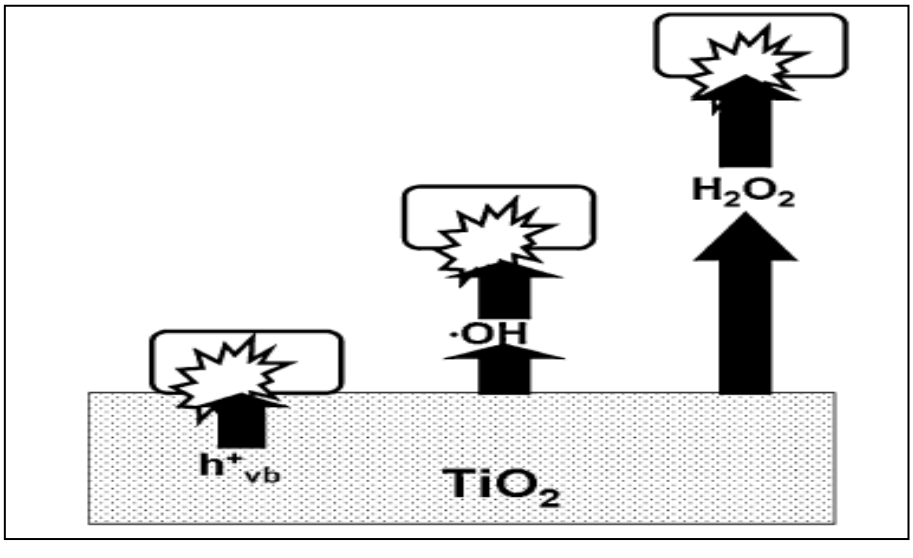

Figure 14 : Rôle des ERO_s dans la destruction photocatalytique des bactéries et effet de la distance d'action : •OH agit à proximité de la surface de TiO_2 alors que H_2O_2 a la capacité de diffuser et d'agir à distance [45].

III.5 Mécanisme d'action des EROs sur les bactéries

Les premiers travaux sur ce sujet sont présentés par Matsunaga *et al* qui ont démontré la photooxydation du coenzyme A (CoA) chez les bactéries *Lactobacillus acidophilus* et *Escherichia coli* et chez la levure *Saccharomyces cerevisiae* dans les suspensions de TiO_2 irradié [121]. La diminution de CoA dans ces cellules a provoqué une altération de leur activité métabolique, ce qui conduit à la mort cellulaire. D'autres études ont également confirmé cette observation. Saito *et al* [119] ont montré que l'inactivation photocatalytique de *Streptococcus sobrinus* engendre des ruptures au niveau de la membrane cellulaire, ce qui se traduit par un relargage intracellulaire des ions K^+ provoquant la perte de viabilité. Le mécanisme d'action anti-bactérien proposé est résumé sur la **figure 15**. Il est prouvé que lors de l'activation d'un semi-conducteur avec la lumière, un électron passe de la bande de valence vers la bande de conduction fournissant un trou positif dans la bande de valence. Les EROs générés tels que $O_2^{\bullet-}$, $^1O_2$, $^\bullet OH$, H_2O_2 et $^\bullet HO_2$ induisent la mort des bactéries [166].

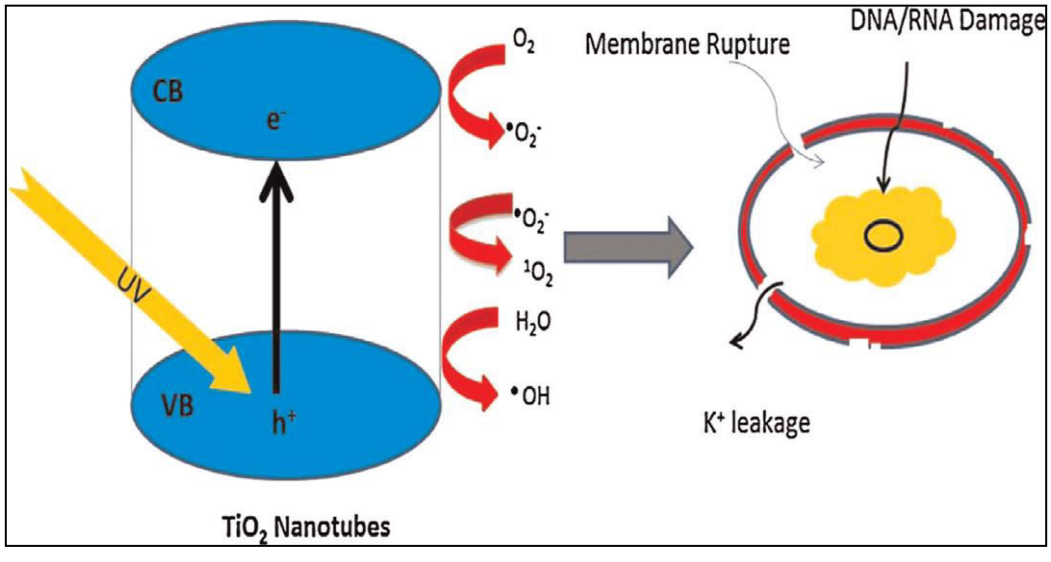

Figure 15 : Mécanisme d'action photocatalytique sur les bactéries [166].

Un autre processus d'inactivation d'*E. coli* sur TiO_2 en film est illustré par la figure 16. En effet, la première réaction est une décomposition partielle de la membrane externe par les espèces réactives produites par photocatalyse à l'aide de TiO_2 [167].

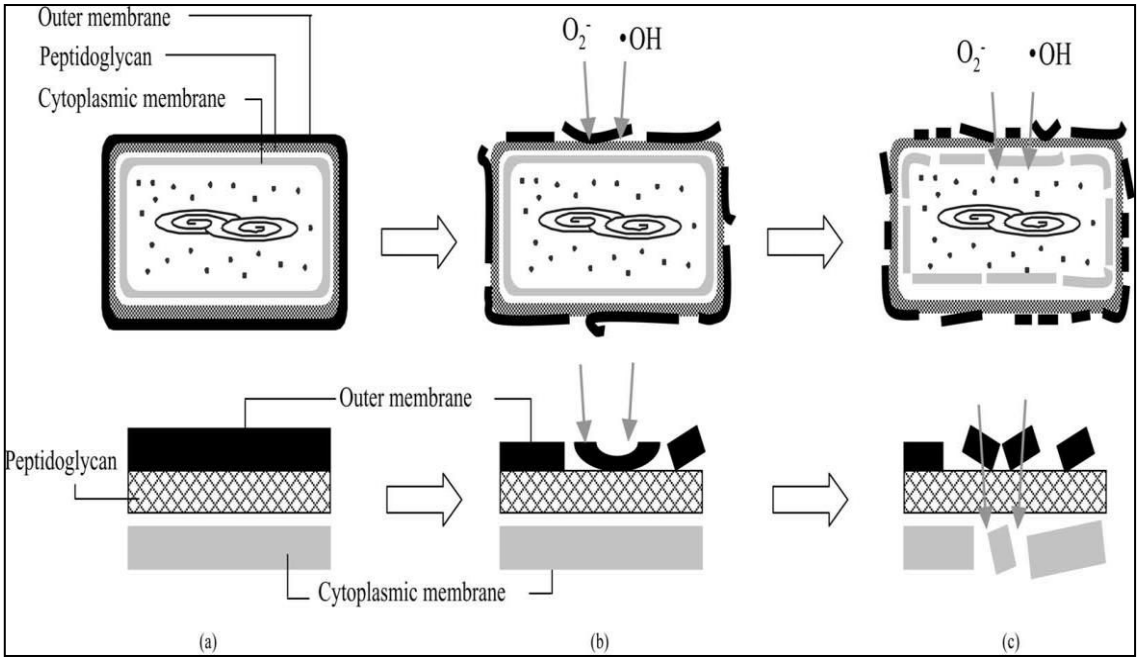

Figure 16 : Mécanisme d'action des ERO_s sur la cellule bactérienne [167].

Durant ce mécanisme, la décomposition partielle de la membrane modifie sa perméabilité aux espèces réactives. En conséquence, le changement de perméabilité de la membrane externe permet aux espèces réactives d'oxygène d'accéder facilement à la membrane cytoplasmique. Ainsi, la membrane cytoplasmique est attaquée par ces espèces réactives, ce qui conduit à la peroxydation des lipides membranaires.

Un éclaircissement plus profond de ce mécanisme a été présenté par Sunada *et al* [167] qui ont prouvé la destruction photocatalytique d'une endotoxine, une composante intégrale de la membrane externe d'*Escherichia coli*. Dans une autre étude, Jacoby *et al* ont mentionné la production de malondialdehyde (MDA) indiquant la peroxydation des lipides membranaires durant le traitement d'*E coli* par TiO_2/UV_A [168]. Les troubles structuraux et fonctionnels de la membrane cytoplasmique en raison de la peroxydation des lipides conduisent à la perte de la viabilité cellulaire et la mort cellulaire. En outre, la mesure de la peroxydation lipidique induite par photocatalyse avec TiO_2 est en accord avec plusieurs autres résultats [169, 170,171].

La formation des produits de la peroxydation, tels que les aldéhydes, les cétones et les acides carboxyliques, a été détectée en parallèle de la disparition de la paroi cellulaire, des

constituants des membranes et des produits d'oxydation sous l'effet de la photocatalyse avec TiO_2 sur les polysaccharides, les chaînes lipidiques et les polypeptides [172]. La perturbation de la perméabilité membranairepar photocatalyse induit la libération de petites molécules comme l'ortho-nitrophénol β-D-galactopyranoside (ONPG) suivie des constituants de grands poids comme le β-galactosidase [63].

Les EROs induisent des dommages sur le matériel génétique (ADN et ARN) par le relargage des ARN et des protéines dans le milieu extracellulaire [123]. Les EROs endommagent l'ADN et l'ARN et favorisent la formation de dimères de pyrimidines, altèrent la conformation tridimensionnelle de l'ADN et affectent par la suite le processus de réplication cellulaire induisant par conséquence l'inactivation puis la mort cellulaire [173].

IV. Conclusion

La photocatalyse hétérogène est un processus catalytique basé sur l'excitation d'un semi-conducteur par un rayonnement lumineux assurant la photodégradation d'un polluant par des réactions d'oxydation à la surface d'un semiconducteur. Au cours des trente dernières années, beaucoup de travaux de recherche ont été publiés se rapportant à l'application de la photocatalyse pour le traitement des eaux. Ce procédé assure la production d'espèces réactives de l'oxygène hautement réactives à la température et la pression ambiante. Plusieurs semiconducteurs ont été testés. Le dioxyde de titane (TiO_2) est le matériau le plus fréquemment utilisé en raison de son faible coût, sa stabilité, et sa non toxicité. L'oxyde de zinc est également étudié et s'est également montré attractif pour ses larges applications potentielles dans la dégradation et l'élimination des polluants.

La désinfection solaire utilisant un semi-conducteur est souvent présentée comme une technique prometteuse pour améliorer la qualité de l'eau. Le contact entre les bactéries et les nanoparticules telles que TiO_2 et ZnO est considéré selon de nombreuses recherches comme le point clé de l'inactivation bactérienne. En effet, ces nanoparticules interagissent avec les cellules microbiennes à travers différents mécanismes.

Suite à cette synthèse bibliographique et en se basant sur les travaux publiés, notre contribution développée dans les différentes parties du présent mémoire sera focalisée (1) sur la synthèse de nouveaux catalyseurs capables d'absorber dans le domaine visible et (2) sur l'étude de la dégradation de quelques polluants modèles organiques et biologiques.

V. Références bibliographiques

[1] Qadir M, Michelins D, Raschid-Sally L, McCornick P.G, Drechsel P, Bahri A, Minhas P.S. The challenges of wastewater irrigation in developing countries. *Agr. Water. Manage*. 97 (2010) 561–568

[2] Ali M. Evolution of Concrete Skyscrapers: from Ingalls to Jin mao. *Electronic Journal of Structural Engineering*. 1 (2001) 2-14.

[3] Bousselmi L, Ghozzi K, Mhenni F, Pichat P, Zayani G. Etude de la Cinétique de Dégradation photocatalytique du Colorant Commercial Azoïque (JauneCibacron FN-2R). *Proceedings of International Symposium on Environmental Pollution Control and Waste Management*. (2002) 838-845.

[4] Rana T, Gupta S, kumar D, Sharma S, Rana M, Rathore V.S, Preira B.M.J. Toxic effects of pulp and paper-mill effluents on male reproductive organs and some systemic parameters in rats. *Environ. Toxicol. Pharmacol*. 18 (2004) 1–7

[5] Brenner D.J, Staley J.T, Kriej N, Bergey's. *Manual of Systematic Bacteriology*. 1 (2001)

[6] Oluwafemi S, Obayori, Lateef B.S, Degradation of polycyclic aromatic hydrocarbons: Role of plasmids. *Sci. Res. Essays.* 5 (2010) 4093-4106

[7] http://campus.cerimes.fr/microbiologie/enseignement/microbiologie_4/site/html/cours.pdf

[8] ifsi-gouriet_doc.pdf

[9] Tripathi P, Beaussart A, Rolain A, Lebeer S, Vanderleyden J, Hols P and Dufrêne Y. Towards a nanoscale view of lactic acid bacteria. *Micron.* 43 (2012) 1323-1330.

[10] Jean Pelmont. Bactéries et environnement, Adaptations physiologique, presses université de Grenoble. livre. (1993) 6-83

[11] www.ebiologie.fr › Cours › Microbiologie

[12] Hartemann P. Contamination des eaux en milieu professionnel. *EMC-Toxicologie Pathologie.*1 (2004) 63–78.

[13] Rivet L. Les biotechnologies en Belgique. *Courrier hebdomadaire du CRISP* 5/1984 (n° 1030) 1-29

[14] Malato S, Fernandez-Ibanez P, Maldonado M.I, Blanco J, Gernjak W. Decontamination and disinfection of water by solar photocatalysis: Recent overview and trends. *Catal. Today.* 147 (2009) 1–59.

[15] Moles J. Eau de distribution, désinfection. In : *Les techniques de l'ingénieur* (2007) W 5500.

[16] World Bank. Environmental Health and child Survival Epidemiology, Economics Experience.World Bank, Washington DC.USA, 2008, p 210.

[17] Rapport sur la qualité de l'eau et de l'assainissement en France, 2003.

[18] Jimenez B, Chavez A. Chlorine disinfection of advanced primary effluent for reuse in irrigation in Mexico. AWWA water reuses conf. Proc. Jan 30-Feb. 2, 2000. San Antonio, Texas.

[19] http://www.who.int/fr/.

[20] Gergova K, Galushko A, Petrov N, Minkova V. Investigation of the porous structure of activated carbons prepared by pyrolysis of agricultural by-products in a stream of water vapor. *Carbon*. 30 (1992) 721-727.

[21] Jayson G.G, Lawless T.A and Fairhurst D. The adsorption of organic and inorganic phosphates onto a new activated carbon adsorbent. *J. Colloid. Interf. Sci*. 86 (1982) 397-410.

[22] Utrera-Hidalgo E, Moreno-Castilla C, Rivera-Utrilla J, Ferro-Garcia M. and Carrasco-Marin F. Activated carbon columns as adsorbents of gallic acid from aqueous solutions: Effect of the presence of different electrolytes. *Carbon*. 30

(1992) 107-111.

[23] Ferro-García M.A, Rivera-Utrilla J, Rodríguez-Gordillo J, and Bautista-Toledo I. Adsorption of zinc, cadmium, and copper on activated carbons obtained from agricultural by-products. *Carbon*. 26 (1988) 363–373.

[24] Strelko V, Malik D. Characterization and metal sorptive properties of oxidized active carbon. *J. Colloid. Interf. Sci*. 250 (2002) 213–220.

[25] Min B, Evans P.J, Chu A.K, Logan B.E. Perchlorate removal in sand and plastic media bioreactors. *Water. Res*. 38 (2004) 47–60.

[26] Butler R, Ehrenberg S, Godley A.R, Lake R, Lytton L, Cartmell E. Remediation of bromate-contaminated groundwater in an exsitu fixed-film bioreactor. *Sci. Total. Environ*. 366, (2006) 12–20.

[27] Sadiq R, Rodriguez M.J. Disinfection by-products (DBPs) in drinking water and the predictive models for their occurrence: a review. *Sci .Total. Environ*. 321 (2004) 21-46

[28] Dalrymple O.K, Stefanakos E, Trotz M.A, Yogi G.D. A review of the mechanisms and modeling of photocatalytic disinfection. *App. Catal. B: Environ*. 98 (2010) 27–38

[29] Gallard H, VonGunten U. Chlorination of Natural Organic Matter: Kinetics of Chlorination and of THM Formation. *Water. Res.*36 (2002) 65-74.

[30] Arora H, LeChevallier M.W, Dixon K.L. DBP occurrence survey. *J.Am. Wat. Wor Ass.* 89 (1997) 60 –68.

[31] Chen W. J, and Weisel C.P. Halogenated DBP concentrations in a distribution system. *J. Am. Wat. Wor. Ass*. 90 (1998) 151-163.

[32] Franceschi. M, Girou A, Carro-Diaz A.M, Maurette M.T, Puech-Costes E. Optimisation of the coagulation–flocculation process of raw water by optimal design method. *Water. Res*. 36 (2002) 3561–3572.

[33] Rice E.W, Hoff J.C, Schaefer F.W. 3rd Inactivation of Giardia Cysts by Chlorine. *Appl. Environ. Microbiol*. 43 (1982) 250–251.

[34] Walter Q.B, Joan B.R. Drinking water treatment processes for removal of Cryptosporidium and Giardia. *Veter. Parasit.* 126 (2004) 219–234.

[35] Barbara K.H, Maria Z, Jacek N. Catalytic ozonation and methods of enhancing molecular ozone reactions in water treatment. *Appl. Catal. B: Environ.* 46 (2003) 639–669.

[36] Huang W.J, Fang G.C., Wang C.C. The determination and fate of disinfection by-products from ozonation of polluted raw water. *Sci. Total. Environ*. 345 (2005) 261-272.

[37] Guieysse B, Bernhoft I, Andersson B.E, Henrysson T, Olsson S, Mattiasson B, Degradation of acenaphthene, phenanthrene and pyrene in a packed-bed biofilm reactor. *Appl. Microbiol. Biotechnol*. 54 (2000) 826–831.

[38] Topalov A, Molnár G.D, Abramovic B, Korom S, Pericin D, Photocatalytic removal of the insecticide fenitrothion from water sensitized with TiO_2. *J. Photochem. Photobiol. A.* 160 (2003) 195-201.

[39] Low G.K.C, McEvoy S.R, Matthews R.W. Formation of nitrate and ammonium ions in titanium dioxide mediated photocatalytic degradation of organic compounds containing nitrogen atoms. *Environ. Sci .Technol.* 25 (1991) 460-467.

[40] Herrmann J.M, Guillard C, Arguello M, Agüera A, Tejedor A, Piedra L, Fernández A A, Photocatalytic degradation of pesticide pirimiphos-methyl: Determination of the reaction pathway and identification of intermediate products by various analytical methods. *Catal. Today*.54 (1999) 353-367.

[41] Karkmaz M, Puzenat E, Guillard C, Herrmann J.M. Photocatalytic degradation of the alimentary azo dye amaranth: Mineralization of the azo group to nitrogen. *Appl. Catal.B: Environ*. 51 (2004) 183-194.

[42] Bekbölet M, Araz C.V. Inactivation of *Escherichia coli* by photocatalytic oxidation. *Chemosphere*. 32 (1996) 959-96.

[43] Sichel C, Cara M, Tello J, Blanco J, Fernández I. P. Solar photocatalytic disinfection of agricultural pathogenic fungi: *Fusarium species. Appl. Catal. B: Environ*. 74 (2007) 152-160.

[44] Haddou M. Degradation de derives de l'acide benzoique par les procédés

d'oxydation avancee en phase homogene et heterogene: procedes Fenton, photo-

Fenton et photocatalyse, these a l'Universite Toulouse III - Paul Sabatier, Thèse, 2010.

[45] Foster H.A, Ditta I.B, Varghese S, Steele A. Photocatalytic disinfection using titanium dioxide: spectrum and mechanism of antimicrobial activity. *Appl. Microb. Biotech*. 90 (2011) 1847–1868.

[46] Herrmann J.M. Heterogeneous photocatalysis: fundamentals and applications to the removal of various types of aqueous pollutants. *Catal. Today.* 53 (1999) 115-129.

[47] Swagata B, Dionysios D.D, Suresh C.P. Self-cleaning applications of TiO_2 by photo-induced hydrophilicity and photocatalysis. *Appl. Catal. B: Environ*. 396 (2015) 176–177.

[48] Meng N.C, Bo J, Christopher W.K.C, Chris. S. Recent developments in photocatalytic water treatment technology: A review. *Water. Res*. 44 (2010) 2997-3027.

[49] Wen S, Zhao J, Sheng G, Fu J, Peng P. Photocatalytic reactions of phenanthrene at TiO_2/water interfaces. *Chemosphere*. 46 (2002) 871-877

[50] Foote C. S, Shook F. C, Abakerli R. B. Characterization of singlet oxygen. *Methods. Enzymol*. 105 (1984) 36-47.

[51] Thom S. R, Elbuken M. E. Oxygen-dependent antagonism of lipid peroxidation. *Free. Radic.Biol. Med*.10 (1991) 413-26.

[52] Koppenol W. H. The Haber-Weiss cycle.70 years later. *Redox. Rep*. 6 (2001) 229-34

[53] Afsset – Les nanomatériaux : effets sur la santé de l'homme et sur l'environnement – Juillet (2006).

[54] Qilin Li, Shaily M, Delina Y. L, Lena B, Michael V.L, Dong L, Pedro J.J.A. Antimicrobial nanomaterials for water disinfection and microbial control: Potential applications and implications. *Water. Res*. 42 (2008) 4591 – 4602.

[55] Ansari M.A ,Khan H.M , Khan A.A , Malik A , Sultan A , Shahid M , Shujatullah F, Azam A . Evaluation of antibacterial activity of silver nanoparticles against MSSA and MRSA on isolates from skin infections. *Biol. Med*. 3 (2011) 141-146.

[56] Mills A, Lee S. A web-based overview of semiconductor photochemistry-based current commercial applications. *J. Photochem. Photobiol. A*.152 (2002)233–247.

[57] Allen N.S, Edge M, Ortega A, Sandoval G, Liauw C.M, Verran J, Stratton J, McIntyre R. B. Degradation and stabilisation of polymers and coatings: nano versus pigmentary titania particles. *Polym. Degrad. Stab*. 85 (2004) 927-946

[58] Buchalska M, Kras G, Oszajca M, Łasocha W, Macyk W. Singlet oxygen generation in the presence of titanium dioxide materials used as sunscreens in suntan lotions. *J. Photochem. Photobiol. A*. 213 (2010) 158-163

[59] Weir A, Westerhoff P, Fabricius L, Hristovski K, Von G.N.Titanium dioxide nanoparticles in food and personal care products. *Environ. Sci. Technol*. 46 (2012) 2242-50.

[60] Khan S.U.M, Al-Shahry M, Ingler W.B. Efficient photochemical water splitting by a chemically modified n-TiO_2. *Science*. 297 (2002) 2243-5.

[61] Zhang L, Mohamed H.H, Dillert R, Bahnemann D. Kinetics and mechanisms of charge transfer processes in photocatalytic systems: A review. *J. Photochem. Photobiol. C* .13 (2012) 263.

[62] Mills A, Hepburn J, Hazafy D, O'Rourke C, Krysa J, Baudys M, Zlamal M, Bartkova H, Hill C.E, Winn K.R, Simonsen M.E, Søgaard E.G, Pillai S.C, Leyland N. S, Fagan R, Neumann F, Lampe C, Graumann T. *J. Photochem. Photobiol. A*. 272 (2013) 18-20.

[63] Banerjee S, Dionysiou D.D, Pillai S.C. New Insights into the Mechanism of Visible Light Photocatalysis. *Appl. Catal. B : Environ*. 396 (2015) 176–177

[64] MacFarlane J.W, Jenkinson H.F, Scott T.B. Sterilization of micro- · organisms on jet spray formed titanium dioxide surfaces. *Appl. Catal. B: Environ*. 106 (2011) 181-185.

[65] Hashimoto K, Irie H, Fujishima A. TiO_2 Photocatalysis: A Historical Overview and Future Prospects. *Jpn. J. Appl. Phys*. 44 (2005) 8269- 8285.

[66] Zsilák Z, Szabó-Bárdos E., Fónagy O, Horváth O, Horváth K, Hajós P. Degradation of benzenesulfonate by heterogeneous photocatalysis combined with ozonation. *Catal. Today*. 230 (2014) 55-60.

[67] Ohko Y, Saitoh S, Tatsuma T, Fujishima A. Photoelectrochemical anticorrosion and self-cleaning effects of a TiO_2 coating for type 304 stainless steel. *J. Electrochem. Soc*. 148 (2001) B24-B28.

[68] Tatsuma T, Saitoh S, Ohko Y, Fujishima A. TiO_2-WO_3 Photoelectrochemical anticorrosion system with an energy storage ability. *Chem. Mater*. 13 (2001) 2838-2842.

[69] Pelaez M, Nolan N.T, Pillai S.C, Seery M.K, Falaras P, Kontos A.G, Dunlop P.S. M, Hamilton J.W.J, Byrne J.A, O'Shea K, Entezari M.H, Dionysiou D. D. A review on the visible light active titanium dioxide photocatalysts for environmental applications. *Appl. Catal. B: Environ*. 125 (2012) 331-349.

[70] Lewis N.S, Rosenbluth M.L. Photocatalysis fundamentals and applications, Serpone Pelizetti N., E. éds. *Wiley Interscience* : New York, (1989). p. 99

[71] Ali G.M, Chakrabarti P. ZnO-based interdigitated MSM and MISIM ultraviolet

photodetectors. *J. Phys. D: Appl. Phys*. 43 (2010) 415103–415110.

[72] Kaur M, Chauhan S.V.S, Sinha S, Bharti M, Mohan R, Gupta S.K, Yakhmi J.V. Application of aligned ZnO nanowires/nanobelts as a room temperature NO gas sensor. *J. Nanosci. Nanotechno*. 9 (2009) 5293–5297.

[73] Premanathan M, Karthikeyan K, Jeyasubramanian K, Manivannan G. Selective toxicity of ZnO nanoparticles toward Gram-positive bacteria and cancer cells by apoptosis through lipid peroxidation. *Nanomedicine: NBM*. 7 (2011) 184–192.

[74] Law M, Greene L.E, Johnson J.C, Saykally R, Yang P. Nanowire dye-sensitized solar cells. *Nature. Mater*. 4 (2005) 455–459.

[75] Zeng J.H, Jin B.B, Wang Y.F. Facet enhanced photocatalytic effect with uniform single-crystalline zinc oxide nanodisks. *Chem. Phys. Lett*. 472 (2009) 90–95.

[76] Degen A. Kosec M. Effect of pH and impurities on the surface charge of zinc oxide in aqueous solution. *J. Eur. Ceram. Soc*. 20 (2000) 667- 673

[77] Yamabi S, Imai H. Growth conditions for wurtzite zinc oxide films in aqueous solutions. *J. Mater. Chem.* 12 (2002) 3773-3778.

[78] Özgür Ü, Alivov Y.I, Liu C, Teke A, Reshchikov M. A, Doğan, S, Avrutin V. Cho S.J, Morkoç H. A comprehensive review of ZnO materials and devices. *J. Appl. Phys*. 98 (2005).

[79] Afsset. Les nanomatériaux: Effets sur la santé de l'homme et sur l'environnement. (2006) p.221.

[80] Jeong J. S, Lee J. Y, Cho J. H, Lee C. J, An S. J, Yi G. Gronsky C. Growth behaviour of well-aligned ZnO nanowires on a Si substrate at low temperature and their optical properties. *Nanotechnology*. 16 (2005) 2455-2461.

[81] Wang Z.L. Zinc oxide nanostructures: growth, properties and applications. *J. Phys: Condens. Matter*.16 (2004) R829-R858.

[82] Kuo C.L, Kuo T.J, Huang M.H. Hydrothermal synthesis of ZnO microspheres and hexagonal microrods with sheetlike and platelike nanostructures. *J. Phys. Chem.*

B. 109 (2005) 20115-21.

[83] Irzh A, Perkas N, Gedanken A. Microwave-Assisted Coating of PMMA beads by silver nanoparticles. *Langmuir*. 23 (2007) 9891-9897.

[84] Xiaosheng T, Eugene S.G.C, Ling L, Jun D, Junmin X. Synthesis of ZnO nanoparticles with tunable emission colors and their cell labeling applications. *J. Mater. Chem*. 22 (2010) 3383-3388.

[85] Anuradha T.V, Ranganathan S. Nanocrystalline TiO_2 by three different synthetic approaches: A comparison. *Bull. Mater. Sci*. 30 (2007) 263-269,

[86] Casey J.D, Haggerty.J.S. Laser-induced vapour-phase synthesis of titanium dioxide. *J. Mater. Sci*. 22 (1987) 4307-4312.

[87] Moritz T, Reiss J, Diesner K, Su D, Chemseddine A. Nanostructured Crystalline TiO_2 through Growth Control and Stabilization of Intermediate Structural Building Units. *J. Phys. Chem. B*. 101 (1997) 8052-8053.

[88] Cassaignon S, Koelsch M, Jolivet J.P. Selective synthesis of brookite, anatase and rutile nanoparticles: thermolysis of $TiCl_4$ in aqueous nitric acid. *J. Mater. Sci*. 42 (2007) 6689-6695.

[89] Jiang L.C, Zhang W.D. Electrodeposition of TiO_2 Nanoparticles on Multiwalled Carbon Nanotube Arrays for Hydrogen Peroxide Sensing. *Electroanalysis.* 21(2009) 988-993.

[90] Torck B. catalyse acido-basique. *Technique de l'ingenieur*. (1992) J1200.

[91] Norris D.J, Efros A.L, Erwin S.C, Doped nanocrystals. *Science.* 319 (2008) 1776-1779.

[92] Achouri F., Corbel S., Balan L., Mozet K., Girot E., Medjahdi G., Ben Said M., Ghrabi A., Schneider R. Porous Mn-doped ZnO nanoparticles for enhanced solar and visible light photocatalysis. *Mater. Des*. 101 (2016) 309–316.

[93] Shifu C, Wei Z, Sujuan Z, Wei L. Preparation, characterization and activity evaluation of p–n junction photocatalyst p-$CaFe_2O_4$/n-ZnO. *Chem. Eng. J*. 148 (2009) 263–269.

[94] Lokesh R.N, Balakrishnan L , Jeganathan K, Layek S, Verma H.C, Gopalakrishnan N. Role of surface functionalization in ZnO:Fe nanostructures. *Mat. Sci. Eng. B.* 183 (2014) 39–46.

[95] Keller V, Garin F. Photocatalytic behavior of a new composite ternary system: WO_3/SiC TiO_2. Effect of the coupling of semiconductors and oxides in photocatalytic oxidation of methylethylketone in the gas phase. *Catal. Comm*. 4 (2003) 377-383.

[96] Liao S, Donggen H, Yu D, Su Y, Yuan G. Preparation and characterization of ZnO/TiO_2, SO_4/ZnO/TiO_2 photocatalyst and their photocatalysis. *J. Photochem. Photobiol. A.* 168 (2004) 1-13.

[97] Serpone E, Maruthamuthu P, Pichat P, Pelizetti E, Hidaka H. Exploiting the interparticle electron transfer process in the photocatalysed oxidation of phenol, 2-chlorophenol and pentachlorophenol: chemical evidence for electron and hole transfer between coupled semi-conductors. *J. Photochem. Photobiol. A*. 85(1995) 247-255.

[98] Kudo A, Miseki Y: Heterogeneous Photocatalyst Materials For Water Splitting. *Chem. Soc. Rev*. 38 (2008) 253-278.

[99] Burns A, Li W, Baker C, Shah S.I. Sol-Gel Synthesis and Characterization of Neodymium-Ion Doped Nanostructured Titania Thin Films. *Mater. Res. Soc .Symp. Proc*. 703 (2002) 5.2.1-5.2.6.

[100] Umebayashi T, Yamaki T, ItohH, Asai K. Band gap narrowing of titanium dioxide by sulfur doping. *App. Phys. Lett*. 81 (2002) 454-456.

[101] Sharma S.D, Singh D, Saini K, Kant C, Sharma V, Jain S.C, Sharma C.P. Sol-gel derived super-hydriphilic nickel doped TiO_2 film as an active photocatalyst. *Appl. Catal. A*. 314 (2006) 40-46.

[102] Legrini O, Oliveros E, Braun A.M. Photochemical processes for water treatment. *Chem. Rev.* 93 (1993) 671-698.

[103] Alexandre O. Mécanisme et spécificité structurale des Méthionine sulfoxyde réductases (Msr) de *Neisseria meningitidis* et rôle du métal dans les MsrB, thèse, (2005).

[104] Buxton G. V, Greenstock C. L, Helman W. P, Ross, A. B. Critical review of rate constant for reactions of hydrated electrons, hydrogen atoms and hydroxyl radicals (HO• /O•-) in aqueous solution. *J. Phys. Chem.* 17 (1988) 613-759.

[105] Weimin X, Geissen S.U. Separation of titanium dioxide from photocatalytically treated water by cross-flow microfiltration. *Water. Res*. 35 (2001) 1256-1262.

[106] Kormann C, Bahnemann D, Hofmann M.R. Photocatalysis of chloroform and other organic molecules in aqueous TiO_2 suspensions. *Environ. Sci. technol*. 25 (1991) 494-500.

[107] Bravo A, Garcia J, Domenech X, Peral J. Some aspects of the photocatalytic oxidation of ammonium ion by titanium dioxide. *J. Chem. Res.* 9 (1993) 376-377

[108] Herrmann J.M, Guillard C, Pichat P. Heterogeneous photocatalysis: an emerging technology for water treatment. *Catal. Today*. 17 (1993) 7-20.

[109] Guillard C, Lachheb H, Houas A, Ksibi M, Elaloui E, Herrmann J.M. Influence of chemical structure of dyes, of pH and of inorganic salts on their photocatalytic degradation by TiO_2 comparison of the efficiency of powder and supported TiO_2. *J. Photochem. Photobiol. A.* 158 (2003) 27-36.

[110] Zhu X, Castleberry S.R, Nanny M.A, Butler E.C. Effects of pH and Catalyst Concentration on Photocatalytic Oxidation of Aqueous Ammonia and Nitrite in Titanium Dioxide Suspensions. *Environ. Sci. Tech*. 39 (2005) 3784-3791.

[111] Elsellami L, Vocanson F, Dappozze F, Puzenat E, Païsse O, Houas A, Guillard C. Kinetic of adsorption and of photocatalytic degradation of phenylalanine effect of pH and light intensity. *Appl. Catal. A*. 380 (2010) 142-148.

[112] Rincón A.G, Pulgarin C. Effect of pH, inorganic ions, organic matter and H_2O_2 *E. coli* K12 photocatalytic inactivation by TiO_2: Implications in solar water disinfection. *Appl. Catal. B: Environ.* 51 (2004) 283-302.

[113] Norzita N, Jamaludin S.K. Effects of pH on ethanol photocatalytic oxidation using TiO_2 and zeolite 13x as catalyst. *J. Tech.* 43 (2005) 27-38.

[114] Muradov N.Z, Raissi A.T, Muzzey D, Painter C.R, Kemme M.R. Selective photocatalytic degradation of air borne VOCs. *Sol. Energy*. 56 (1996) 445- 453.

[115] Rincon A.G, Pulgarin C. Photocatalytical inactivation of *E. coli*: effect of (continuous-intermittent) light intensity and of (suspended-fixed) TiO_2 concentration. *Appl. Catal. B: Environ*. 44 (2003) 263-284.

[116] Pin C. M, Sharon S, Daniel M. B, Zheng H, Edward J. W, William A. J. Bactericidal Activity of Photocatalytic TiO_2 Reaction: toward an Understanding of Its Killing Mechanism. *Appl. Environ. Microbio.* 65 (1999) 4094–4098.

[117] Sven M, Ann-Sofie A, Leif R, Goran L. Wild-type *Escherichia coli* Cells Regulate the Membrane Lipid Composition in a "Window" between Gel and Non-lamellar Structures. *J. Biol. Chem*. 271 (1996) 6801–6809,

[118] Ould-Mame S.M, Zahraa O, Bouchy M. Photocatalytic degradation of salicylic acid on fixed TiO_2 – kinetic studies . *Inter. J. Photochem*. 2 (2000) 59-66.

[119] Saito T, Iwase T, Morioka T. Mode of photocatalytic bactericidal action of powdered semiconductor TiO_2 on mutans streptococci. *J. Photoch. Photobio. B.* 14 (1992) 369–379.

[120] Wei C, Lin W.Y, Zaina Z, Williams N. E, Zhu K, Kruzic A. P, Smith R. L, Rajeshwar K. Bactericidal activity of TiO_2 photocatalyst in aqueous media: toward a solar-assisted water disinfection system. *Environ. Sci. Technol*. 28 (1994) 934–938.

[121] Matsunaga T, Tomada R, Nakajima T, Wake H. Photochemical sterilization of microbial cells by semiconductor powders. *FEMS Microbiol. Lett*. 29 (1985) 211–

214.

[122] Matsunaga T, Tomoda R, Nakajima Y, Nakamura N, Komine T. Continuous-sterilization system that uses photosemiconductor powders. *Appl. Environ. Microbiol.* 54 (1988) 1330–1333.

[123] Caballero L, Whitehead K.A, Allen N.S, Verran J. Inactivation of *Escherichia coli* on immobilized TiO_2 using fluorescent light. *J. Photochem. Photobiol. A.* 202 (2009) 92–98.

[124] Schindler K.M, Kunst M. Charge-carrier dynamics in titania powders. *J. Phys. Chem*. 94 (1990) 8222-8226.

[125] Agustina T.E, Ang H.M, Vareek V.K. A review of synergistic effect of photocatalysis and ozonation on wastewater treatment. *J Photochem. Photobiol. C* (2005) 264-273.

[126] Zhang Z, Wang C.C, Zakaria R, Ying J.Y, Role of particle size in nanocrystalline TiO_2-based photocatalysts. *J. Phys. Chem. B*. 102 (1998) 10871-10878.

[127] Shah S.I, Huang C.P, Chen J.G, Doren D, Barteau M. Semiconductor Metal Oxide Nanoparticles for Visible Light Photocatalysis. NSF Nanoscale Science and Engineering Grantees Conference NSF NIRT Grant No. 0210284 (2003).

[128] Kashif N, Ouyang F. Parameters effect on heterogeneous photocatalysed degradation of phenol in aqueous dispersion of TiO_2. *J. Environ. Sci*.21 (2009) 527–533.

[129] Piscopo A. Chimie solaire et traitements photocatalytiques des eaux polluées : Applications aux traitements selectifs et exemples d'utilisation de catalyseurs supportes, Thèse, Université de Metz. (2002).

[130] Junpei N, Masahiro T, Hussein T. Z, Yoshinori K. Photocatalytic decolorization of azo-dye with zinc oxide powder in an external UV light irradiation slurry photoreactor. *J. Hazard. Mater*. 138 (2006) 106–115

[131] Yu L, Yu H, Lv Z, Sihui Z, Jiangyao Y, Xinhong P, Yixuan R, Xiaoyan W.

Simulated-sunlight-activated photocatalysis of Methylene Blue using cerium-doped SiO_2/TiO_2 nanostructured fibers. *J. Environ. Sci.* 24 (2012) 1867–1875.

[132] Satterfield C.N. Mass Transfer in Heterogeneous Catalysis, *MIT Press, Cambridge, MA* (1970) 177–179.

[133] Ollis D.F. Contaminant degradation in water. *Environ. Sci.Tech.*19 (1985) 480-484.

[134] Fernández A, Lassaletta G, Jiménez V.M, Justo A, González-Elipe A.R, Herrmann J.M, Tahiri H, Ait-Ichou Y. Preparation and characterization of TiO_2 photocatalysts supported on various rigid supports (glass, quartz and stainless steel). Comparative studies of photocatalytic activity in water purification. *Appl. Catal. B*: *Environ.* 7 (1995) 49-63.

[135] Arslan I, Balcioglu I.A, Bahnemann D.W. Heterogeneous photocatalytic treatment of simulated dyehouse effluents using novel TiO_2-photocatalysts. *Appl. Catal. B*: *Environ*. 26 (2000) 193-206.

[136] Aguedach A, Brosillon S, Morvan J, Lhadi E.K. Influence of ionic strength in the adsorption and during photocatalysis of reactive black 5 azo dye on TiO_2 coated on non woven paper with SiO_2 as a binder. *J. Hazard. Mater*. 150 (2008) 250–256.

[137] Paspaltsis I, Kotta K, Lagoudaki R, Grigoriadis N, Poulios I, Sklaviadis T. Titanium dioxide photocatalytic inactivation of prions. *J. Gen. Virol.* 87 (2006) 3125–3130.

[138] Herrera J. A, Doña, J. M, Vieira A, Tello E, Valdés C, Arana J, Pérez J.The photocatalytic disinfection of urban waste waters. *Chemosphere*. 41, (2000) 323–327.

[139] Downes A, Blunt T. P. Researches on the Effect of Light Upon Bacteria and other Organisms. *Proc. R. Soc. London*. 26 (1877) 488–500.

[140] McGuigan K. G, Joyce T. M, Conroy R M. Solar disinfection: use of sunlight to decontaminate drinking water in developing countries. *J. Med. Microbiol* .48

(1999) 765–787.

[141] Acra A, Jurdi M, Mu H, Karahagopian Y, Raffoul Z. Water disinfection by solar radiation: assessment and application, international development research centre. (1990) 53-65.

[142] Reed R.H. Solar inactivation of faecal bacteria in water the critical role of oxygen. *Lett. App. Microbio*. 24 (1997) 276-280.

[143] McGuigan K.G, Joyce T.M, Conroy R.M, Gillespie J.B, Elmore-Meegan M. Solar disinfection of drinking water contained in transparent plastic bottles: characterizing the bacterial inactivation process. *J. Appl. Microbio*. 84 (1998) 1138- 1148.

[144] Black H.S, Gruijl F.R, Forbes P.D, Cleaver J.E, Ananthaswamy H.N, Fabo E.C, Ullrich S.E, Tyrrell R.M. Photocarcinogenesis: an overview. *J. Photochem. Photobiol. B.* 40 (1997) 29-47.

[145] Moan J, Peak M.J. Effects of UV radiation on cells. *J. Photochem. Photobiol. B.* 4 (1989) 21-34.

[146] Yoakum G, Ferron W, Eisenstark A, Webb R.B. Inhibition of replication gap closure in *Escherichia coli* by near-ultraviolet light photoproducts of L.tryptophan. *J. Bacteriol*. 119 (1974) 62-69.

[147] Yoakum G.H. Tryptophan photoproduct(s): sensitized induction of strand breaks (or alkali-labile bonds) in bacterial deoxyribonucleic acid during near-ultraviolet irradiation, *J. Bacteriol*. 122 (1975) 199-205.

[148] Kehoe S.C, Joyce T.M, Ibrahim P, Gillespie J.B, Shahar R.A, McGuigan K.G. Effect of agitation, turbidity, aluminium foil reflectors and volume on inactivation efficiency of batch-process solar disinfectors. *Water. Res*. 35 (2001) 1061- 1065.

[149] Gelover S, Gómez L.A, Reyes K, Teresa Leal M. A practical demonstration of water disinfection using TiO_2 films and sunlight. *Water. Res.* 40 (2006) 3274-3280.

[150] Gill L.W, McLoughlin O. A. Solar disinfection kinetic design parameters for continuous flow reactors. *J. Sol. Energy. Eng. 129* (2005) 111-118

[151] Lonnen J, Kilvington S, Kehoe S. C, Al-Touati , and McGuigan K. G. Solar and photocatalytic disinfection of protozoan, fungal and bacterial microbes in drinking water. *Water. Res*. 39 (2005) 877–833

[152] Vidal A, and Díaz A. J. High performance, low-cost of collectors for disinfection of contaminated waters. *Water. Environ. Res*. 72 (2000) 271–276

[153] Martín-Domínguez A, Alarcón-Herrera M.T, Martín-Domínguez R.R, González-Herrera A. Efficiency in the disinfection of water for human consumption in rural communities using solar radiation. *Sol. Energy*. 78 (2005) 31–40.

[154] Zhang L, Ding Y, Povey M, York D. ZnO nanofluids – a potential antibacterial agent, *Prog*. *Nat. Sci*. 18 (2008) 939–944.

[155] Jiang W, Mashayekhi H, Xing B, Bacterial toxicity comparison between nanoand micro-scaled oxide particles. *Environ. Pollut*. 157 (2009) 1619–1625.

[156] Gogniat G, Thyssen M, Denis M, Pulgarin C, Dukan S. The bactericidal effect of TiO_2 photocatalysis involves adsorption onto catalyst and the loss of membrane integrity. *FEMS. Microbiol. Lett*. 258 (2006) 18–24.

[157] Huang Z, Maness P, Blake D. M, Wolfrum E. J, Smolinski S. L, Jacoby W.A. Bactericidal mode of titanium dioxide photocatalysis. *J. Photochem. Photobiol. A*. 130 (2000) 163–170.

[158] Sunada K, Watanabe T, Hashimoto K. Studies on photokilling bacteria on TiO_2 thin film. *J. Photochem. Photobiol. A*. 6221 (2003) 1–7.

[159] Adams L, Lyon K L. Y, Alvarez P. J. Comparative ecotoxicity of nanoscale TiO_2, SiO_2, and ZnO water suspensions. *Water. Res*. 40 (2006) 3527 – 3532

[160] Cho M, Yoon J. Measurement of OH radical ct for inactivating *Cryptosporidium parvum* using photo/ferrioxalate and photo/ TiO_2 systems. *J. Appl. Microbiol*. 104 (2008) 759–766.

[161] Pulgarina C, Kiwia J, Nadtochenkob V. Mechanism of photocatalytic bacterial inactivation on TiO_2 films involving cell-wall damage and lysis. *Appl. Catal. B: Environ*, 128 (2012) 179– 183.

[162] Kashige N, Kakita Y, Nakashima Y, Miake F, Watanabe K. Mechanism of the photocatalytic inactivation of Lactobacillus casei phage PL-1 by titania thin film. *Curr. Microbiol*. 42 (2001) 184–189.

[163] Huang Z. B, Zheng X, Yan D. H, Yin G. F, Liao X.M., Kang Y. Q, Yao Y.D, Huang D, Hao B.Q. Toxicological effect of Zno nanoparticles based on bacteria. *Langmuir*. 24 (2008) 4140–4144.

[164] Brayner R, Ferrari-Iliou R, Brivois N, Djediat S, Benedetti, M. F, Fievet F. Toxicological impact studies based on *Escherichia coli* bacteria in ultrafine ZnO nanoparticles colloidal medium. *Nano. Letters*. 6 (2006) 866–870.

[165] Kikuchi Y, Sunada K, Iyoda T, Hashimoto K, Fujishima A. Photocatalytic bactericidal effect of TiO_2 thin films: dynamic view of the active oxygen species responsible for the effect. *J. Photochem. Photobiol. A*. 106 (1997) 51–56.

[166] Podporska-Carroll. J, Panaitescu E,Quilty B, Wang L, Menon L, Suresh C.P. Antimicrobial properties of highly efficient photocatalytic TiO_2 nanotubes. *Appl. Catal. B: Environ.*176–177(2015) 70-75

[167] Sunada K, Kikuchi Y, Hashimoto K, Fujishima A. Bactericidal and detoxification effects of TiO_2 thin film photocatalyst. *Environ. Sci. Technol*. 32 (1998) 726–728.

[168] Jacoby W.A, Maness P.C, Wolfrum E.J, Blake D.M, Fennell J.A. Mineralization of bacterial cell mass on a photocatalytic surface in air. *Environ. Sci. Technol*. 32 (1998) 2650–2653.

[169] Maness P.C, Smolinski S, Blake D.M, Huang Z, Wolfrum E.J, Jacoby W.A. Bactericidal activity of photocatalytic TiO_2 reaction: toward an understanding of its killing mechanism. *Appl. Environ. Microbiol*. 65 (1999) 4094– 4098.

[170] Dalrymple O.K, Stefanakos E, Trotz M.A, Goswami D.Y. A review of the mechanisms and modeling of photocatalytic disinfection. *Appl. Catal. B: Environ*.

98 (2010) 27–38.

[171] Gaëlle C, Erwann H, Saïd E, Maxime E, Marie-Claire L, Peter H, Jean-Pierre G, Valérie K, Nicolas K, Philippe A. TiO_2 Photocatalysis damages lipids and proteins in *Escherichia coli*. *Appl. Environ. Microbiol*. 80 (2014) 2573-81

[172] Kiwi J, Nadtochenko V. Evidence for the mechanism of photocatalytic degradation of the baterial wall membrane at the TiO_2 interface by ATR-FTIR and laser kinetic spectroscopy. *Langmuir*. 21 (2005) 4631– 4641.

[173] Pigeot-Rémy S, Simonet F, Errazuriz-Cerda E, Lazzaroni J.C, Atlan D, Guillard C. Photocatalysis and disinfection of water: Identification of potential bacterial targets. *Appl. Catal. B: Environ*.104 (2011) 390-398.

PARTIEII :

Synthèse et Caracterisation de Nouveaux Catalyeurs Pour Le Traitement Des Eaux Usées

CHAPITRE I: Aqueous synthesis and enhanced photocatalytic activity of ZnO/Fe_2O_3 heterostructures

Résumé

Au cours des dernières décennies, la pollution de l'eau est devenue un problème majeur dans le monde. Diverses méthodes de dépollution sont mises en œuvre, dont la photocatalyse hétérogène, et ont reçu une attention particulière parce qu'elles permettent la dégradation d'un grand panel de polluants organiques récalcitrants et de microorganismes pathogènes. Ce procédé est basé sur l'irradiation d'un semiconducteur par une source lumineuse appropriée afin de produire des espèces réactives de l'oxygène (EROs).

Actuellement, TiO_2 et le ZnO sont deux semiconducteurs les plus utilisés pour de nouvelles applications photocatalytiques, mais ils présentent l'inconvénient d'une absorbance limitée dans le domaine UV qui ne représente que 4 à 5% du spectre solaire.

Dans ce premier chapitre, nous présentons une méthode de synthèse de nanoparticules ZnO avec comme objectif l'amélioration de leur absorbance et, par conséquent, l'augmentation du rendement photocatalytique de dégradation des polluants. Nous avons synthétisé avec succès des hétérostructures ZnO/Fe_2O_3 par hydrolyse de $FeCl_3$ en présence de particules de ZnO.

Tout d'abord, les observations de microscopie optique en transmission (TEM) montrent que les particules de Fe_2O_3 sont étroitement attachées à la surface des particules de ZnO. Cette structure est avantageuse pour la création d'une hétérojonction qui améliore la séparation des charges et donc l'activité photocatalytique.

Ensuite, cette hétérostructure ZnO/Fe_2O_3 a été utilisée et caractérisée en photocatalyse sous irradiation UV proche. Les résultats expérimentaux montrent que les particules ZnO/Fe_2O_3 génèrent plus d'EROs (radicaux $^{\bullet}OH$ et $O_2^{\bullet-}$) que les particules de ZnO et que leur activité photocatalytique est donc améliorée. Cette séparation effective de la paire électron-trou dans l'hétérostructure ZnO/Fe_2O_3 permet une dégradation plus rapide de l'acide salicylique sous irradiation UV par rapport à ZnO (64% vs 44% pour ZnO et ZnO/Fe_2O_3 après 1h, respectivement). L'utilisation répétée de ZnO/Fe_2O_3 dans des expériences photocatalytiques a

également montré une faible perte d'efficacité au cours du temps. La préparation du photocatalyseur ZnO/Fe_2O_3 est simple, respectueuse de l'environnement, et de faible coût, ce qui devrait rendre son utilisation facile pour le traitement des eaux usées.

Ces résultats ont fait l'objet d'un article publié dans la revue '' *Journal of Physics and Chemistry of Solids.*

Faouzi Achouri, Serge Corbel, Abdelhay Aboulaich, Lavinia Balan , Ahmed Ghrabi, Myriam BenSaid, Raphaël Schneider. Aqueous synthesis and enhanced photocatalytic activity of ZnO/Fe_2O_3 heterostructures. ***Journal of Physics and Chemistry of Solids*** **75 (2014) 1081–1087**

CHAPITRE I: Aqueous synthesis and enhanced photocatalytic activity of ZnO/Fe_2O_3 heterostructures

I.1 Abstract

We report a facile synthesis of ZnO/Fe_2O_3 heterostructures based on the hydrolysis of $FeCl_3$ in the presence of ZnO nanoparticles. The material structure, composition, and its optical properties have been examined by means of transmission electron microscopy, scanning electron microscopy, X-ray diffraction, X-ray photoelectron spectroscopy and diffuse reflectance UV-visible spectroscopy. Results obtained show that 2.9 nm-sized Fe_2O_3 nanoparticles produced assembles with ZnO to form ZnO/Fe_2O_3 heterostructures. We have evaluated the photodegradation performances of ZnO/Fe_2O_3 materials using salicylic acid under UV-light. ZnO/Fe_2O_3 heterostructures exhibited enhanced photocatalytic capabilities than commercial ZnO due to the effective electron/hole separation at the interfaces of ZnO/Fe_2O_3 allowing the enhanced hydroxyl and superoxide radicals production from the heterostructure.

Keywords:

Oxides, Semiconductors, Nanostructures, Chemical Synthesis, Optical properties

I.2 Introduction

Zinc oxide (ZnO) is a major component of photocatalyst due to its similar bandgap energy and favourable bandgap positions compared with titanium dioxide (TiO_2) [1, 2]. Therefore, ZnO has been extensively studied for the removal of contaminants from water and air [2-11] and for microbial disinfection [12, 13]. When ZnO absorbs photons of energy equal or exceeding its bandgap, electron-hole pairs are formed that induce redox reactions at its surface. A hydroxyl radical ($^{\bullet}OH$) is created through an oxidative process when a hole reacts with a water molecule or hydroxide ion on the particle surface [2,14]. The electron can react with molecular oxygen to generate the superoxide radical ($O_2^{\bullet-}$) through a reductive process [2]. Singlet oxygen is mostly produced indirectly from aqueous solution of superoxide radicals [15]. Hydroxyl radicals and singlet oxygen are strong and non selective oxidants and can damage quite all types of organic molecules [2, 15]. However, one major bottleneck

drawback associated with semiconductor photocatalysts currently is their high charge recombination rate. In order to address this issue, the coupling of two semiconductors with suitable energetic has been proposed to enhance the charge-separation yield and thus improve the photocatalytic efficiency [16-20]. This enhanced photocatalytic activity can be explained as a result of a transfer of photo-generated electrons and holes from a semiconductor to another [21, 22].

Iron (III) oxide (Fe_2O_3), including α-, β-, ε-, and γ-Fe_2O_3, is a narrow band gap (~ 1.9-2.2 eV) semiconductor which is suitable to be coupled with ZnO to enhance the separation of photo-generated electron-hole pairs in ZnO and Fe_2O_3. Both the valence band and the conduction band of Fe_2O_3 are more negative than those of ZnO (Figure 17), thus allowing photo-generated electron transfer from the conduction band of Fe_2O_3 to the conduction band of ZnO after light activation. Recently, some combinations of ZnO with Fe_2O_3 have been investigated in order to enhance ZnO photocatalytic activity. ZnO/Fe_2O_3 nanocomposites or heterostructures have been prepared by wet chemical routes like the sol-gel method [23,24], which is generally followed by calcination [25]. Other methods like solution combustion [26] or impregnation of ZnO with Fe $(NO_3)_3$ followed by calcination [27] have also been reported.

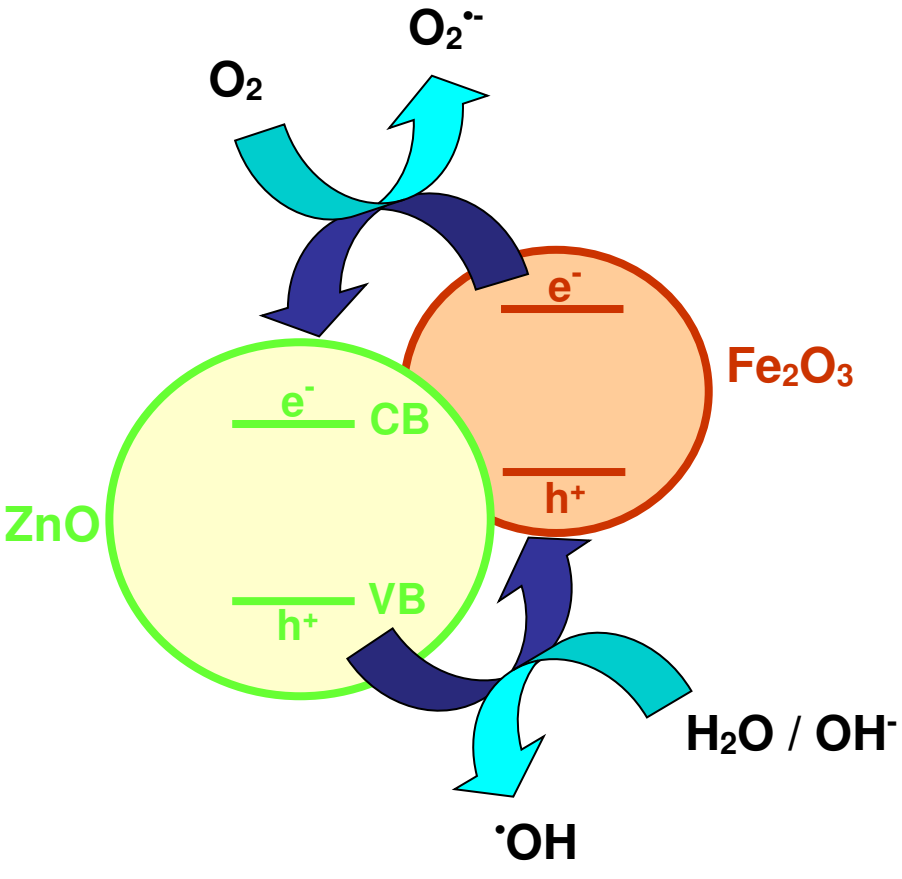

Figure 17: Schematic representation of $^{\bullet}OH$ and $O_2^{\bullet-}$ radicals production from the ZnO/Fe_2O_3 heterostructure.

Herein, a simple and cost-effective route is proposed for the preparation of ZnO/Fe_2O_3 heterostructures via a simple solution method at low temperature under mild conditions. Fe_2O_3 nanoparticles with diameters of ca. 2.9 nm were produced by hydrolysis of $FeCl_3$ in the presence of commercial ZnO nanoparticles. Terephthalic acid fluorescence and nitroblue tetrazolium adsorption probing techniques were used to observe the formation of $^{\bullet}OH$ and $O_2^{\bullet-}$ radicals, respectively. To verify the advantages of the heterojunction built between ZnO and Fe_2O_3, the catalytic activity of the material was evaluated using as test reaction the degradation of salicylic acid in aqueous solution. The ZnO/Fe_2O_3 heterostructure turned out to be superior to ZnO and TiO_2 under similar conditions.

I.3 Experimental section

I.3.1 Materials

Iron chloride hexahydrate ($FeCl_3$. $6H_2O$, 97%), salicylic acid, SA (> 99%) and DMSO (> 99.9%) were purchased from Sigma-Aldrich. Zinc oxide (ZnO, Merck) and P25 TiO_2 (Degussa) were used as received without additional purification. All solutions were prepared using Milli-Q water (18.2 MΩ.cm, Millipore) as the solvent.

I.3.2 Characterization

Transmission electron microscopy (TEM) images were taken by placing a drop of the particles in water onto a carbon film-supported copper grid. Samples were studied using a Philips CM20 instrument operating at 200 kV equipped with Energy Dispersive X-ray Spectrometer (EDS). The X-ray diffraction (XRD) data were collected from an X'Pert MPD diffractometer (Panalytical AXS) with a goniometer radius 240 mm, fixed divergence slit module (1/2° divergence slit, 0.04 rd Sollers slits) and an X'Celerator as a detector. The powder samples were placed on zero background quartz sample holders and the XRD patterns were recorded at room temperature using Cu K_α radiation (λ= 0.15418 nm). X-ray photoelectron spectroscopy (XPS) analyses were performed on a Gammadata Scienta (Uppsala, Sweden) SES 200-2 spectrometer under ultra-high vacuum ($P < 10^{-9}$ mbar). The measurements were performed at normal incidence (the sample plane is perpendicular to the emission angle). The spectrometer resolution at the Fermi level is about 0.4 eV. The depth analyzed extends up to about 8 nm.The monochromatized AlKα source (1486.6 eV) was operated at a power of 420 W (30 mA and 14 kV) and the spectra were acquired at a take-off angle of 90° (angle between the sample surface and photoemission direction). During acquisition, the pass energy was set to 500 eV for wide scans and to 100 eV for high-resolution spectra. CASAXPS software (Casa Software Ltd, Teignmouth, UK, www.casaxps.com) was used for all peak fitting procedures and the areas of each component were modified according to classical Scofield sensitivity factors.

All the optical measurements were performed at room temperature (20 ± 1°C) under ambient conditions. Absorption spectra were recorded on a Thermo Scientific Evolution 220 UV-visible spectrophotometer. Photoluminescence (PL) spectra were recorded on a Horiba Fluoromax-4 Jobin Yvon spectrofluorimeter. Diffuse reflectance UV-vis spectra of the

samples were measured using a Shimadzu UV-2101 PC spectrophotometer. $BaSO_4$ is used as a standard for baseline measurements and spectra are recorded in a range of 200-800 nm.

I.3.3 Preparation of the ZnO/Fe_2O_3 photocatalyst

For a theoretical 5 mol. % loading of Fe_2O_3 on ZnO, iron (+3) chloride (19.4 mg, 7.177 mmol) was added to ZnO particles (200 mg) dispersed in 50 mL of ultrapure water at pH = 6.5. This mixture was stirred at 100°C for 15h. After cooling to room temperature, particles were recovered by centrifugation and washed twice with ethanol and water. The yellowish-white ZnO/Fe_2O_3 nanocomposite obtained was then heated at 100°C for 12 h before use.

I.3.4 DST assays

The production of hydroxyl radicals ($^{\bullet}OH$) by ZnO and ZnO/Fe_2O_3 particles was estimated using disodium terephthalate (DST), which turns into fluorescent 2-hydroxyterephthalate, 2-OH-DST (λ_{em} = 428 nm) upon reaction with $^{\bullet}OH$ radicals. Briefly, 5 mg of particles (ZnO or ZnO/Fe_2O_3) were dispersed in 100 mL of water. 1 mL of this dispersion was mixed with 1 mL of DST (0.1 M in water) before being irradiated (P = 350 mW). The mixture was treated with 1 mL of 1M NaOH and incubated for 50 min at r.t. before filtration on 0.2 µm polyvinylidene fluoride Acrodisc Syringe Filter. The PL spectra were recorded to estimate 2-OH-DST formed.

I.3.5 NBT assays

The production of $O_2^{\bullet-}$ radicals was estimated using the nitroblue tetrazolium (NBT) assay. NBT assay is based on spectrophotometric measurements quantifying the reduction of yellowish NBT into purple formazan derivatives. This reduction into mono- and diformazan derivatives results in an increase of absorbance between 450 and 700 nm. Typically, ZnO or ZnO/Fe_2O_3 particles (5 mg) and NBT (8 mg) were mixed in a 1:1 water/DMSO mixture (100 mL) under light protection. The solution was next irradiated by a Hg-Xe lamp (P = 50 mW) for various times. The absorbance spectra were recorded to quantify formazan derivatives formed. Reference samples were (i) NBT irradiated in the absence of particles and (ii) NBT + particles without light activation.

I.3.6 Photocatalytic activity

The photoreactor is a self-constructed microreactor [28] with fluorescent lamp (365 nm, I = 2.45 mW/cm²). An aqueous dispersion of the ZnO/Fe_2O_3 catalyst was deposited in the

microreactor using a pipette and the microreactor was next heated to 70°C until water was completely evaporated. 30 mg of the photocatalyst were deposited in the microreactor in each experiment.

Salicylic acid (SA) solution (10 mg/L) was injected by means of a syringe pump through the microreactor at a constant flow rate of 10 mL/h. SA can adsorb on the photocatalyst, which may result in a decrease in the solution concentration and the optical density of the solution. To take account of this background effect, we carried out the photodegradation reaction after flowing SA in the microreactor for 1 h in the dark to reach the adsorption equilibrium. The photocatalytic degradation of SA was initiated by irradiating the microreactor at 365 nm. The SA conversion was estimated by UV-vis spectroscopy over the course of photocatalysis. For each reaction time, final results were averaged out of at least three independent experiments. Less than 2.0% SA decomposed after 4 h in the absence of either the photocatalyst or the light irradiation and, thus, could be neglected in comparison with the SA degraded via photocatalysis.

I.4 Results and discussion

I.4.1 Synthesis and characterization of ZnO/Fe_2O_3 heterostructure

The ZnO/Fe_2O_3 photocatalyst was prepared by mixing commercial ZnO particles with an aqueous solution of iron (+3) chloride, followed by heating for 15 h at 100°C. ZnO acts as a support to adsorb $FeCl_3$ at its surface and upon heating $FeCl_3$ is converted into Fe oxides. Upon centrifugation and washing, the ZnO/Fe_2O_3 material was heated at 100°C for 12 h.

The external morphology of ZnO particles and of the ZnO/Fe_2O_3 heterostructure was first investigated by SEM (Fig 18). Partially separated large grains with an average size of ca 2 µm could be observed. These grains are clusters of ZnO particles. The shapes and sizes of these clusters are well-maintained in the course of their association with Fe_2O_3 nanoparticles (Fig. 18b).

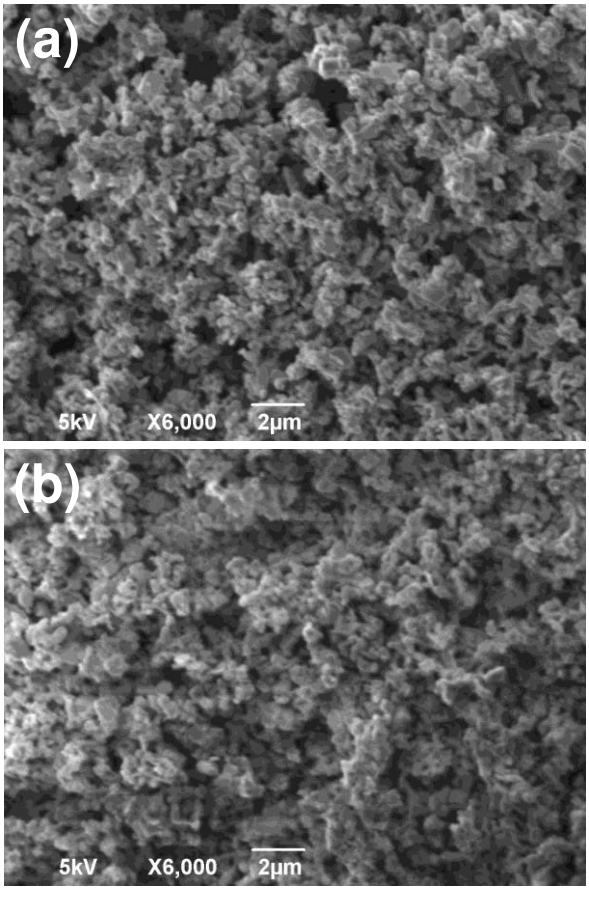

Figure 18: SEM images of (a) ZnO particles and (b) the ZnO/Fe_2O_3 photocatalyst

Representative TEM images (Fig. 19a-d) show ZnO crystals with very inhomogeneous morphologies (roughly spherical, wires, and polyhedras), including some isolated particles and particles with sharp edges. Fe_2O_3 particles produced in aqueous solution at 100°C were found to be uniform, with an average diameter of 2.9 ± 0.7 nm, and spherical in shape (Fig. 19d). These very small particles could not observed by SEM. Fe_2O_3 nanoparticles were also found to assemble at the surface of ZnO crystals to form ZnO/Fe_2O_3 heterostructures. EDX analyses were carried out in different regions of the ZnO/Fe_2O_3 composite and an average atomic ratio of Zn to Fe of 11.2 was determined (Fig. 19e).

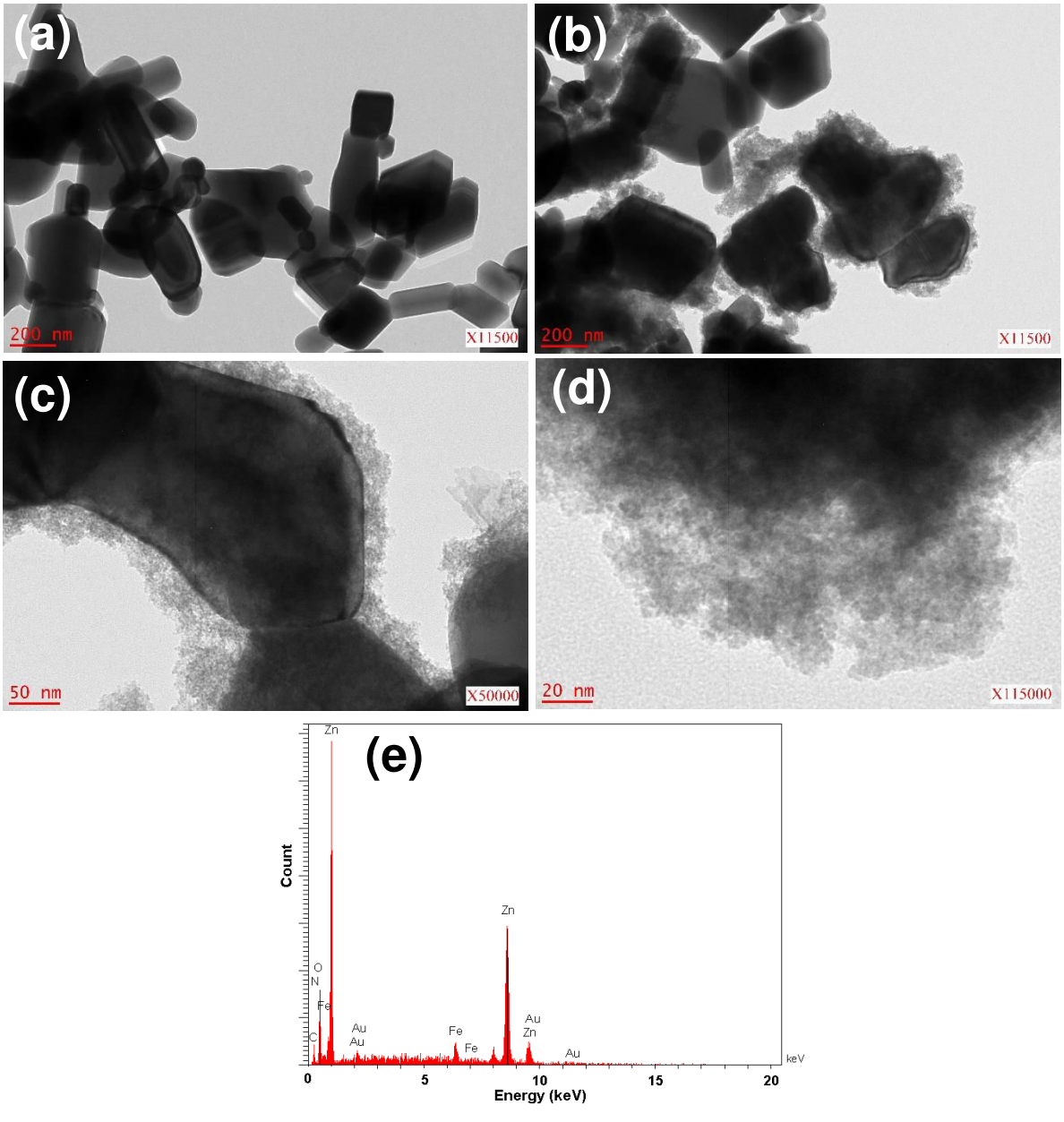

Figure 19: TEM images of (a) ZnO particles, (b), (c) and (d) the ZnO/Fe_2O_3 photocatalyst, and (e) EDX analysis of the ZnO/Fe_2O_3 photocatalyst.

Diffuse reflectance spectra of ZnO and ZnO/Fe_2O_3 samples are presented in Fig. 20. As can be seen, ZnO has no absorption response to the visible light due to its wide band gap. The photoabsorption of ZnO particles was modified due to its association with Fe_2O_3 nanoparticles. The ZnO/Fe_2O_3 heterostructure reveals extended optical absorption in the range 400-600 nm. Diffuse reflectance spectra illustrate that the association of Fe_2O_3 with ZnO

could effectively extend the light absorption range and are consistent with the fact that Fe_2O_3 has smaller energy gap that ZnO material. This result suggests that the ZnO/Fe_2O_3 (Eg=3.06 eV) particles have potential for photocatalysis using the visible part of the spectrum (*vide infra*).

Fig. 21 is the typical XPS spectra of the ZnO/Fe_2O_3 heterostructure, where panel (a) is the survey spectrum and panels (b-d) are the high resolution binding energy spectra for O, Zn, and Fe, respectively. Three binding energy peaks can be observed for the O 1s spectrum. The peaks at 530.9 and 530.0 eV correspond to oxidic O^{2-} linked to Zn and Fe, respectively. The signal observed at 532.5 eV is related to small amount of OH^- caused by non-stoechiometric surface oxygen [29]. The main peak observed for zinc is located at 1021.8 eV (Zn $2p_{3/2}$) and is related to the oxide. A weaker peak can be observed at 1022.94 eV and is associated to Zn-OH bonds located at the periphery of the crystals. The Fe $2p_{3/2}$ photoelectron peak is observed at 710.7 eV, which is consistent with typical values for ferric oxides (α- or γ-Fe_2O_3) reported in the literature [26, 30, 31]. The distinctive shake-up satellite can be observed at ca. 717.9 eV.

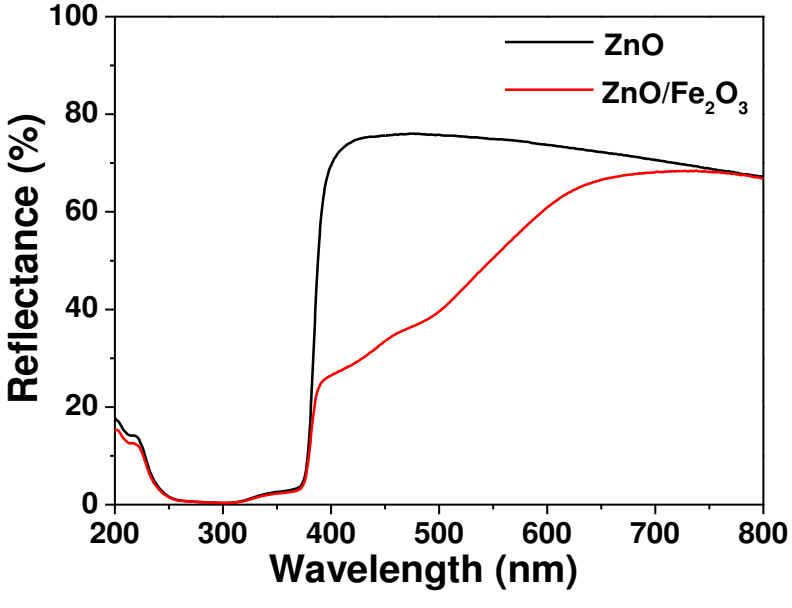

Figure 20: UV-vis diffuses reflectance spectra of ZnO and ZnO/Fe_2O_3 materials.

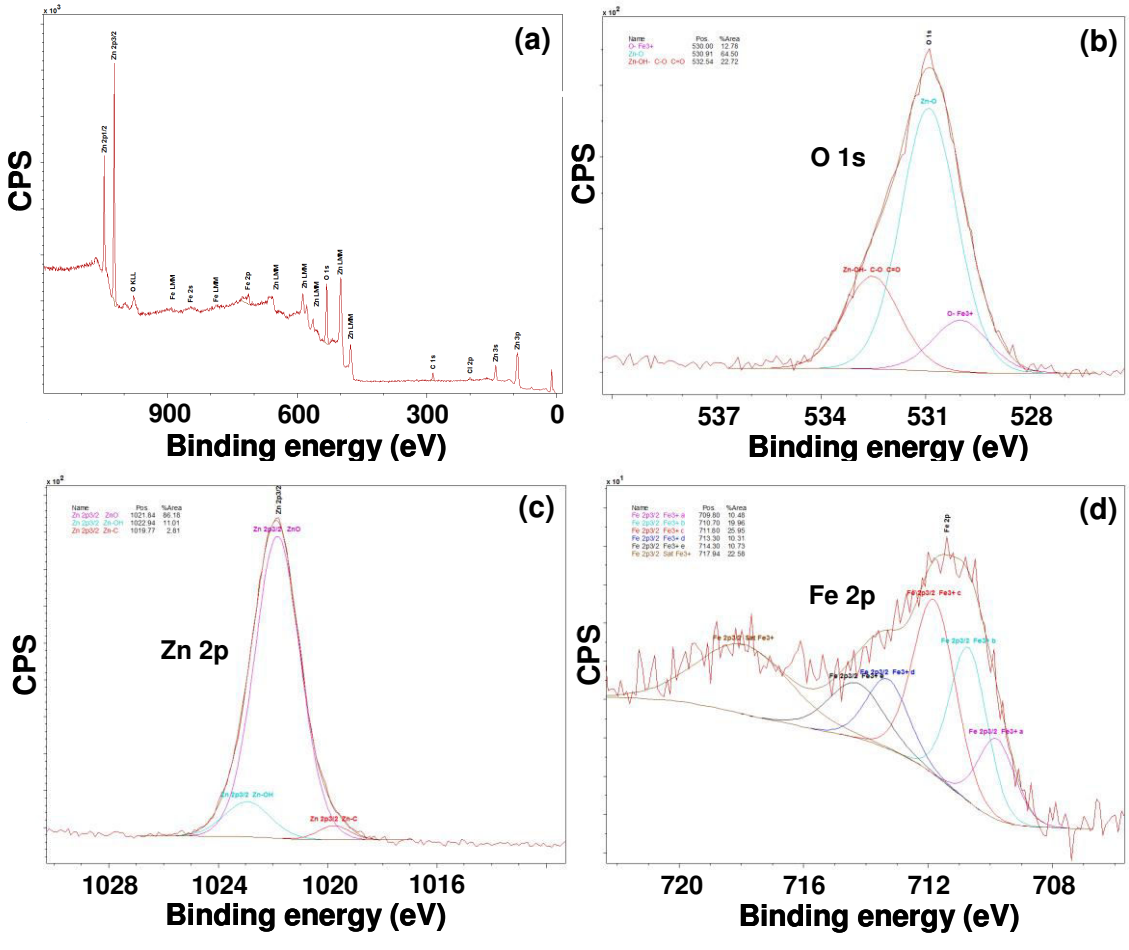

Figure 21: XPS spectra of the ZnO/Fe_2O_3 photocatalyst: (a) overview, (b), (c) and (d) are the high-energy resolution core-level spectra of O 1s, Zn 2p, and Fe 2p, respectively.

The crystallinity, phase and purity of the ZnO sample after association with Fe_2O_3 were finally examined by powder XRD as shown in Fig. 22. All the peaks can be well indexed to a pure hexagonal wurtzite structure of zinc oxide (JCPDS File No. 36-1541). All reflections associated to ZnO remained unchanged, which could indicate that Fe_2O_3 particles are well dispersed on ZnO surface. The peaks related to Fe_2O_3 could not be identified, the possible reasons are its low degree of crystallinity, its low content in the sample (XRD is unable to detect lower percentage than 5% of a crystalline phase), or the partial dehydroxylation of FeOOH to form Fe_2O_3 [32]. The Fe_2O_3 association with ZnO was however observed by TEM, XPS, and EDS analyses (*vide supra*).

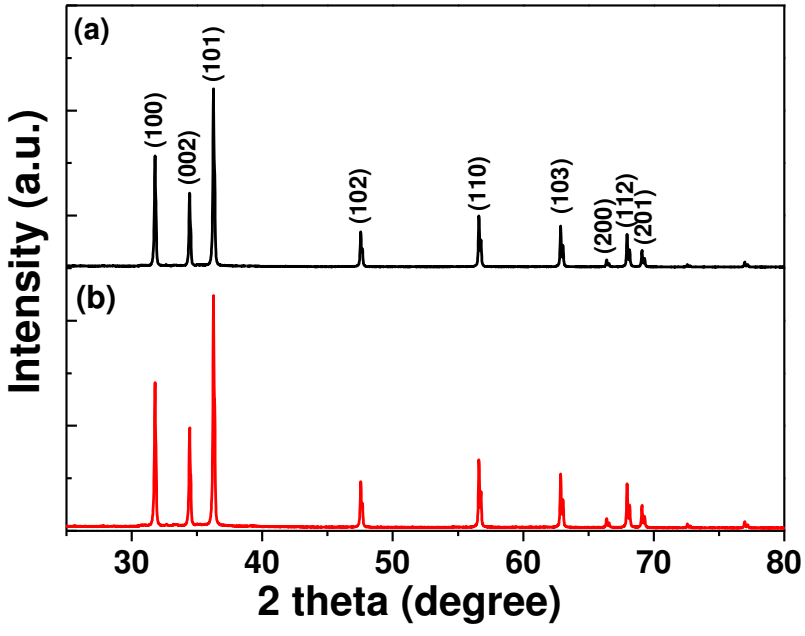

Figure 22: XRD patterns of (a) ZnO nanoparticles and (b) ZnO/Fe_2O_3 heterostructure.

I.4.2. Trapping of electrons and holes

The formation of hydroxyl radicals •OH upon irradiation of ZnO and ZnO/Fe_2O_3 particles was monitored by a •OH radical-specific fluorimetric assay. In this assay, disodium terephthalate (DST) reacts with •OH radicals to form the highly fluorescent 2-hydroxyterephthalate anion (2-OH-DST), which emits at 428 nm in basic medium [33, 34]. Fig. 23a and 23b show the typical fluorescence emission spectra recorded for dispersion of the ZnO particles and the ZnO/Fe_2O_3 heterostructure containing DST and irradiated for various times. Since the fluorescence intensity increases steadily with irradiation time, •OH radicals are continuously generated upon photo-activation. Fig. 23c depicts results obtained for ZnO and ZnO/Fe_2O_3 particles, where the relative fluorescence intensity at λ_{em} = 428 nm was plotted against the irradiation time. Results obtained show that the association of Fe_2O_3 with ZnO induces enhanced production of •OH radicals, which are formed to a smaller extent by ZnO particles.

2-OH-DST was not produced in control experiments performed without irradiation, thus confirming a photo-induced mechanism. Finally, the addition of cysteine, a •OH radical scavenger [35], caused no DST oxidation which indicates the direct production of •OH radicals by the nanocomposite (Fig. 23c).

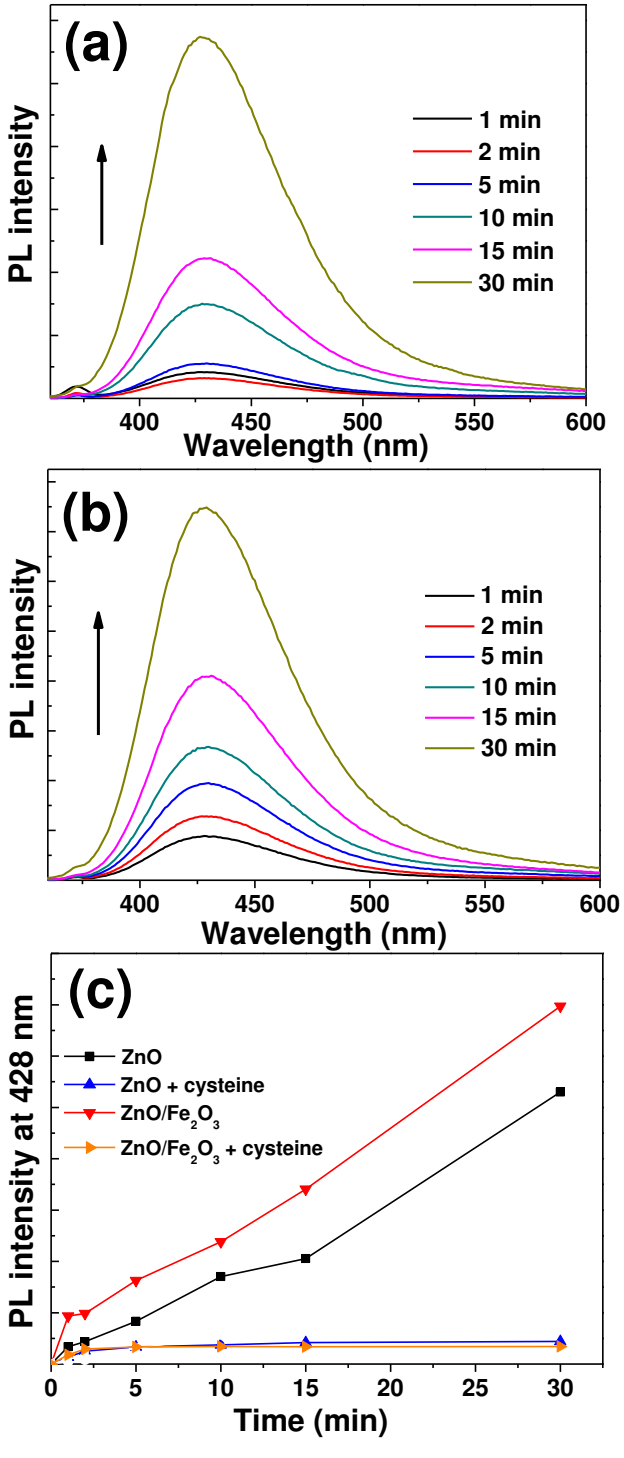

Figure 23: Changes in the fluorescence intensity of 2-OH-DST upon irradiation of DST with (a) ZnO particles, (b) the ZnO/Fe_2O_3 heterostructure, and (c) comparison 2-OH-DST production by ZnO and ZnO/Fe_2O_3 particles as a function of time.

The production of superoxide $O_2^{\bullet-}$ radicals by ZnO and ZnO/Fe_2O_3 particles was evaluated with a scavenging assay based on their ability to reduce NBT into dark blue formazan derivatives [36]. Fig. 24a and 24b show the typical absorption spectra recorded for dispersions of the ZnO particles and of the ZnO/Fe_2O_3 heterostructure containing NBT and irradiated for various times. As can be seen, the absorption intensity of formazan derivatives between 450 and 700 nm increases with time until ca. 45-60 min of irradiation, indicating that the amount of $O_2^{\bullet-}$ reaches an equilibrium after this duration under UV light irradiation. Results depicted in Fig. 24c indicate that the ZnO/Fe_2O_3 heterostructure generates $O_2^{\bullet-}$ radicals to a significantly greater extent (ca. 1.6-fold) than ZnO particles.

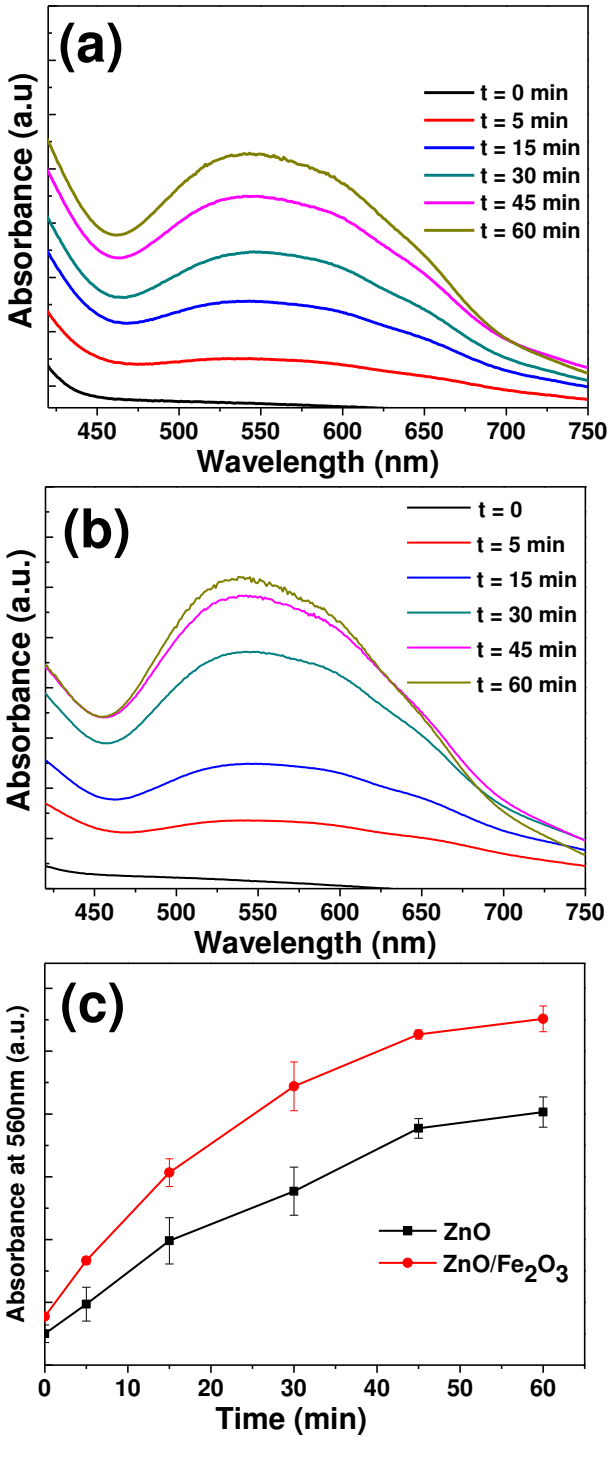

Figure 24: Typical UV-vis absorption spectra obtained during irradiation of NBT with (a) ZnO particles, (b) the ZnO/Fe_2O_3 heterostructure, and (c) comparison of superoxide radicals production by ZnO and ZnO/Fe_2O_3 particles as a function of time.

I.4.3. Photocatalytic activity

To investigate the potentiality of the ZnO/Fe_2O_3 heterostructure as photocatalyst, its catalytic performances were examined by the photodegradation of salicylic acid (SA) as followed by spectrophotometric monitoring. SA was used as a model compound with respect to the degradation of aromatic compounds in aqueous medium. Commercial ZnO and P25 TiO_2 particles were used for comparison in these experiments. Photodegradation reactions were conducted using UV light irradiation and in microreactors. After deposition of the photocatalyst, a solution of SA (10 $mg.L^{-1}$, pH = 4.5) was continuously injected in the microreactor through a syringe pump. Preliminary control experiments showed that no degradation of SA was observed in the absence of either irradiation or photocatalyst. Fig. 25a shows the time-dependent UV-vis spectra of SA during the adsorption equilibrium phase (ca. 60 min) and once the UV-light turned on. The characteristic peak at 297 nm gradually decreased with irradiation time and 64% of SA were degraded after 60 min using the ZnO/Fe_2O_3 catalyst. In the course of the reaction, no new peaks were generated suggesting the almost complete degradation of SA. During the first 40 min of irradiation, the rates of SA decomposition were found to be similar for ZnO and ZnO/Fe_2O_3 photocatalysts (Fig. 25b). However, upon further irradiation, the ZnO/Fe_2O_3 catalyst was able to remove ca. 64% of SA, while the degradation remained limited to 44 and 40% with ZnO and TiO_2 particles, respectively. The effective coupling of ZnO and Fe_2O_3 allowing the photogenerated electrons and holes to be separated and thus the inhibition of the recombination of these charge carriers is probably at the origin of the improved photocatalytic activity of the ZnO/Fe_2O_3 heterostructure. The capability of the ZnO/Fe_2O_3 nanocomposite to be reused was assessed by performing consecutive photocatalytic degradation of SA. Experiments were conducted under the continuous flow (10 mL/h) of SA in the microreactor by simply turning on or turning off near UV light. It is worth to mention that no treatment like UV-A exposition [37] was performed to cleaning active sites on the catalyst surface from degradation by-products. The results of these experiments can be seen in Fig. 26. A good conversion of SA (64%) was obtained during the first trial and the catalytic activity was preserved in the following uses (58% degradation after the 10^{th} cycle). The high photodegradation efficiencies observed throughout the recyclability test indicate that the ZnO/Fe_2O_3 photocatalyst displayed a high stability (no aggregation and maintain of its surface area).

The effect of the Fe_2O_3 loading (5 or 10 mol% relative to ZnO) on the photodegradation of SA under the same irradiation conditions was also evaluated. The sample prepared with 5 mol% Fe_2O_3 exhibited the highest activity after 1 h irradiation (64 and 47% degradation of SA for 5 and 10% loading in Fe_2O_3, respectively). This is in agreement with previous works onsemiconductors particles and confirms that the catalytic activity depends on an optimum content of both semiconductors [25, 38, 39].

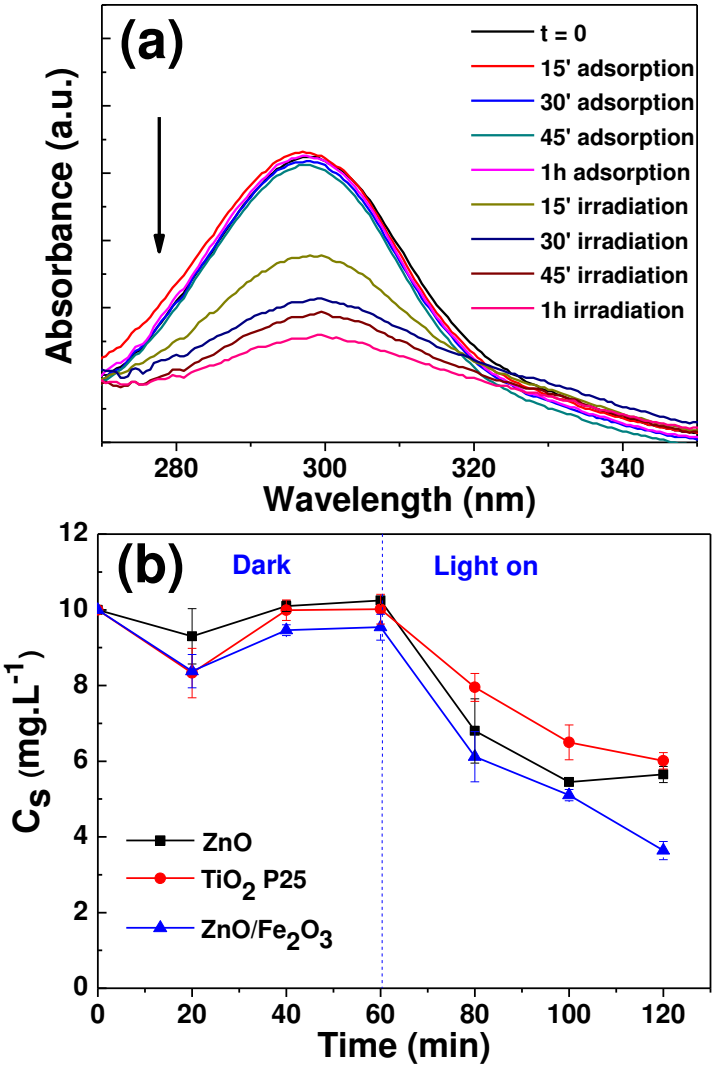

Figure 25: (a) The UV-vis spectral changes of SA upon irradiation in the presence of the ZnO/Fe_2O_3 photocatalyst, and (b) Variations of SA concentration (C_S) at the outlet of the microreactor during photocatalytic experiments using TiO_2, ZnO and ZnO/Fe_2O_3 catalysts at pH = 4.35.

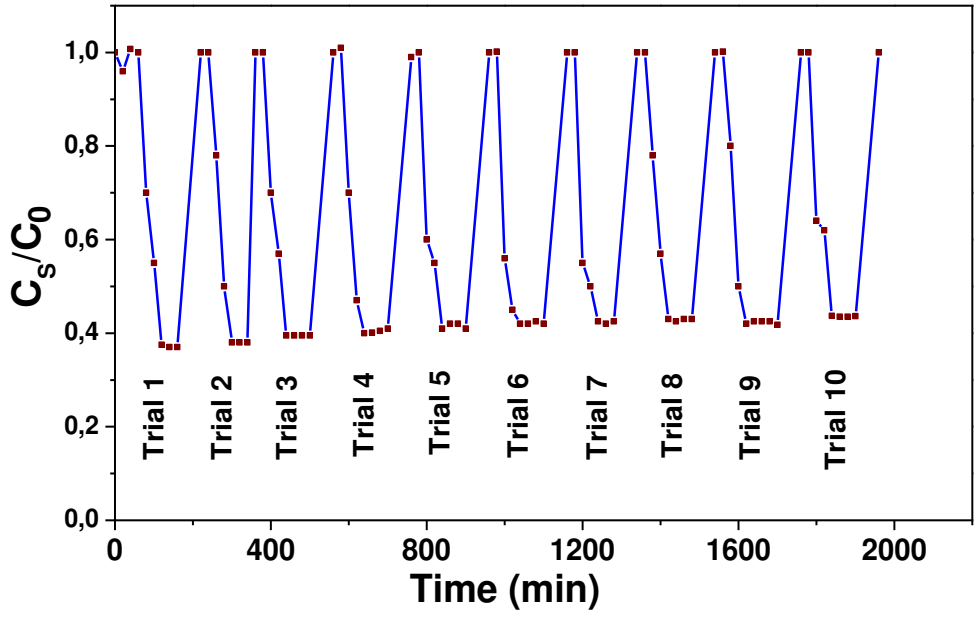

Figure 26: Recyclability study of the ZnO/Fe_2O_3 nanocomposite deposited in a microreactor. Experiments were conducted under near UV light irradiation and with a concentration C_0 in SA of 10 mg/L.

Finally, photocatalytic degradation of SA was also attempted under visible light ($\lambda > 420$ nm) irradiation. Reactions were conducted in 50 mL Pyrex beaker containing 40 mL of the SA solution. After addition ZnO/Fe_2O_3 catalyst (50 mg) and one hour in the dark to establish SA absorption/deabsorption equilibrium on the nanocomposite surface, visible light was turned on (light intensity = 30 $mW.cm^{-2}$). A gradual decrease of SA absorption at 297 nm was observed by UV-vis spectrocopy. However, even on prolonging the illumination time (2 h), the conversion was limited to ca. 30%. This result indicates that degradation of SA is a time-consuming process under visible light irradiation.

I.5 Conclusions

In summary, ZnO/Fe_2O_3 heterostructures have been successfully fabricated by hydrolysis of $FeCl_3$ in the presence of ZnO particles used as seeds. TEM experiments show that Fe_2O_3 particles are grown and closely attached on ZnO particles surface. This structure is beneficial for the creation of a heterojunction which enhances the photogenerated carrier separation and thus improves the photocatalytic activity. The ZnO/Fe_2O_3 heterostructure has been investigated for photocatalysis under near UV light irradiation. Results obtained show that

ZnO/Fe_2O_3 particles generate more ROS ($^{\bullet}OH$ and $O_2^{\bullet-}$ radicals) than ZnO particles and that its photocatalytic activity is enhanced compared to ZnO. The effective electron-hole pair separation in the ZnO/Fe_2O_3 heterostructure results a much faster degradation of salicylic acid under UV-light irradiation compared to ZnO (64% vs 44% for ZnO and ZnO/Fe_2O_3 photodegradation in 1 h, respectively). The repeated application of the ZnO/Fe_2O_3 in photocatalytic experiments has also been demonstrated. The preparation of the ZnO/Fe_2O_3 photocatalyst is simple, environmentally benign, and cost effective which should render its use easy for waste water treatment.

Acknowledgements

This work is supported by the Agence Nationale pour la Recherche (ANR CESA 2011, project NanoZnOTox). We thank Ghouti Medjahdi (IJL, Université de Lorraine) for XRD analyses.

I.6 References

[1] D. Chu, Y. Masuda, T. Ohji, K. Kato, Langmuir 26 (2009) 2811-2815.

[2] M.R. Hoffmann, S.T. Martin, W. Choi, D.W. Bahnemann, Chem. Rev. 95 (1995) 69-96.

[3] A.A. Khodja, T. Schili, J.F. Pilichowski, P. Boule, J. Photochem. Photobiol. A 141 (2001) 231-239.

[4] G. Marci, V. Augugliaro, M.J. Lopez-Munoz, C. Martin, L. Palmisano, V. Rives, M. Schiavello, R.J.D. Tilley, A.M. Venezia, J. Phys. Chem. B 105 (2001) 1033-1040.

[5] C. Hariharan, Appl. Cat. A: Gen. 304 (2006) 55-61.

[6] N. Sabana, M. Swaminathan, Sep. Purif. Technol. 56 (2007) 101-107.

[7] F. Xu, P. Zhang, A. Navrotsky, Z.-Y. Yuan, T.-Z. Rent, M. Halasa, B.-L. Su, Chem. Mater. 19 (2007) 5680-5686.

[8] H. Ezng, W. Cai, P. Liu, X. Xu, H. Zhou, C. Klingshirm, H. Kalt, ACS Nano 2 (2008) 1661-1670.

[9] D. Jassby, J.F. Budarz, M. Wiesner, Environ. Sci. Technol. 46 (2012) 6934-6941.

[10] A. Di Paola, E. Garcia-Lopez, G. Marci, L. Palmisano, J. Hazardous Mater. 211-212 (2012) 3-29.

[11] Y. Hong, C. Tian, B. Jiang, A. Wu, Q. Zhang, G. Tian, H. Fu, J. Mater. Chem. A 1 (2013) 5700-5708.

[12] R.J. Barnes, R. Molina, J. Xu, P.J. Dobson, I.P. Thompson, J. Nanopart. Res. 15 (2013) 1432-1443.

[13] K. Rekha, N. Nirmala, M.G. Nair, A. Anukaliani, Physica B 405 (2010) 3180-3185.

[14] M. Okuda, T. Tsuruta, K. Katayama, Phys. Chem. Chem. Phys. 11 (2009) 2287-2292.

[15] L. Brunet, D.Y. Lyon, E.M. Hotze, P.J.J. Alvarez, M.R. Wiesner, Environ. Sci. Technol. 43 (2009) 4355-4360.

[16] J.S. Jang, S.H. Choi, H.G. Kim, J.S. Lee, J. Phys. Chem. C 112 (2008) 17200-17205.

[17] V.V. Shvalagin, A.L. Stroyuk, I.E. Kotenko, S.Y. Kuchmii, Theor. Exp. Chem. 43 (2007) 229-234.

[18] Z. Liu, D.D. Sun, P. Guo, J.O. Leckie, Nano Lett. 7 (2007) 1081-1085.

[19] J.Y. Kim, S.B. Choi, J.H. Noh, S.H. Yoon, S. Lee, T.H. Noh, A.J. Frank, K.S. Hong, Langmuir 25 (2009) 5348-5351.

[20] H. Labiadh, T. Ben Chaabane, L. Balan, N. Becheik, S. Corbel, G. Medjahdi, R. Schneider, Appl. Cat. B: Environ. 144 (2014) 29-35.

[21] W. Ho, J.C. Yu, J. Lin, P. Li, Langmuir 20 (2004) 5865-5869.

[22] N. Serpone, Photochem. Photobiol. A: Chem. 85 (1995) 247-255.

[23] E. Redel, P. Mirtchev, C. Huai, S. Petrov, G.A. Ozin, ACS Nano 5 (2011) 2861-2869.

[24] W. Wu, S. Zhang, X. Xiao, J. Zhou, F. Ren, L. Sun, C. Jiang, ACS Appl. Mater. Interfaces 4 (2012) 3602-3609.

[25] A. Hernandez, L. Maya, E. Sanchez-Mora, E.M. Sanchez, J. Sol-Gel Sci. 42 (2007) 71-78.

[26] G.K. Pradhan, S. Martha, K.M. Perida, ACS Appl. Mater. Interfaces 4 (2012) 707-713.

[27] J. Madhavan, P.S. Sathish Kumar, S. Anandan, M. Zhou, F. Grieser, M. Ashokkumar, Chemosphere 80 (2010) 747-752.

[28] G. Charles, T. Roques-Carmes, N. Becheikh, L. Falk, J. M. Commenge, S. Corbel, J. Photochem. Photobiol. A : Chem. 223 (2011) 202-211.

[29] M. Aroniemi, J. Lahtinen, P. Hautojärvi, Surf. Interfaces Anal. 36 (2004) 1004-1006.

[30] G. Bhargaba, I. Gouzman, C.M. Chun, T.A. Ramanarayanan, S.L. Bernasek, Appl. Surf. Sci. 253 (2007) 4322-4329.

[31] T. Yamashita, P. Hayes, Appl. Surf. Sci. 254 (2008) 2441-2449.

[32] S. Bharati, D. Nataraj, D. Mangalaraj, Y. Masuda, K. Senthil, K. Yong, J. Phys. D: Appl. Phys. 43 (2010) 015501.

[33] B.I. Ipe, M. Lehning, C.M. Niemeyer, Small 1 (2005) 706-709.

[34] C. Bohne, K. Faulhaber, B. Giese, A. Hafner, A. Hofmann, H. Ihmels, A.-K. Kohler, S. Pera, F. Schneider, M.A.-L. Sheepwash, J. Am. Chem. Soc. 127 (2005) 76-85.

[35] M. L. Sagrista, A.F. Garcia, M.A. De Madariaga, M. Mora, Free Radical Res. 36 (2002) 329-340.

[36] A. Anas, H. Akita, H. Harashima, T. Itoh, M. Ishikawa, V. Biju, J. Phys. Chem. B 112 (2008) 10005-10011.

[37] S. Linley, T. Leshuk, F.X. Gu, ACS Appl. Mater. Interfaces 5 (2013) 2540-2548.

[38] S. Zhang, W. Xu, M. Zeng, J. Li, J. Xu, X. Wang, Dalton Trans. 42 (2013) 13417-13424.

[39] F. Shen, W. Que, Y. Liao, X. Yin, Ind. Eng. Chem. Res. 50 (2011) 9131-9137.

CHAPITRE II: Porous Mn-doped ZnO nanoparticles for enhanced solar and visible light photocatalysis.

Résumé

Dans la continuité du travail précédent, l'objectif de cette recherche était l'amélioration des performances des semiconducteurs en vue de la dépollution de l'eau par photocatalyse.

Tout d'abord, nous avons recherché une solution au phénomène de recombinaison des charges (e^-/h^+). Cette recombinaison reste l'inconvénient principal qui diminue l'efficacité de l'activité photocatalytique. Pour cela, notre contribution a consisté au dopage de ZnO par des métaux de transitions comme Mn pour améliorer son activité photocatalytique.

Dans ce travail de recherche, nous avons développé avec succès une nouvelle voie de synthèse donnant accès à des nanoparticules poreuses ZnO et ZnO dopé Mn, qui ne nécessite pas de recuit post-synthétique ni d'attaque chimique. L'influence du pourcentage de dopant Mn^{2+} sur les propriétés structurales, optiques et photocatalytiques des particules de ZnO:Mn a été étudiée. L'hétérostructure ZnO:Mn (3%) présente la meilleure activité photocatalytique pour la dégradation de l'Orange II sous irradiation solaire. Ce matériau présente également une surface spécifique plus élevée que celle de ZnO seul. Cette surface spécifique élevée, associée à la capacité du dopant Mn^{2+} d'agir comme un piège d'électrons, permet de diminuer la recombinaison électrons/trous. Ceci entraîne une augmentation de la production des radicaux $^{\bullet}OH$ par ZnO:Mn (3%) et donc l'efficacité photocatalytique. De plus, le photocatalyseur ZnO:Mn peut être réutilisé jusqu'à dix fois sans aucun traitement particulier. Cette hétérostructure présente un grand intérêt pour de nouvelles applications et, en particulier, pour son utilisation dans l'assainissement de l'eau.

Ces résultats ont fait l'objet d'un article publié dans la revue '*Materials and Design'* :

Faouzi Achouri, Serge Corbel, Lavinia Balan, Kevin Mozet, Emilien Girot, Ghouti Medjahdi, Myriam Ben Said, Ahmed Ghrabi, Raphaël Schneider. Porous Mn-doped ZnO nanoparticles for enhanced solar and visible light photocatalysis. ***Materials and Design*** **101 (2016) 309–316.**

CHAPITRE II: Porous Mn-doped ZnO nanoparticles for enhanced solar and visible light photocatalysis.

II.1 Abstract

Porous Mn-doped ZnO (ZnO:Mn) nanoparticles with an average diameter of ca. 21 nm were prepared by a simple and cheap solvothermal process involving no templates, post-synthetic annealing or etching. The particles produced were characterized by XRD, Raman spectroscopy, SEM, TEM, XPS, diffuse reflectance spectroscopy and BET surface area measurements and the effects of Mn^{2+} doping on the structural, optical and photocatalytic properties of ZnO particles were investigated. The particles doped with 3mol% Mn^{2+} were found to exhibit the highest catalytic activity toward the photodegradation of the Orange II dye under solar light irradiation. Our results demonstrate that Mn^{2+} doping shifts the optical absorption to the visible region, increases the specific surface area of the photocatalyst and reduces the recombination of electron-hole pairs. The influence of various operational parameters (amount of catalyst, concentration of dye and pH) on the photodegradation and the photocatalytic mechanism were studied. Finally, we demonstrated that the ZnO:Mn photocatalyst is stable and can be easily recycled up to ten times without any significant decrease in photocatalytic activity.

Keywords: Mn-doped ZnO; Porous nanoparticles; Photocatalysis; Oxidation

II.2 Introduction

The photocatalytic degradation of organic pollutants like dyes or pesticides from water using semiconductor materials has recently attracted a lot of attention [1-3]. Among photocatalysts, zinc oxide ZnO is a promising material either for the generation of hydrogen or for decomposition of organics owing to its large exciton binding energy (60 meV) at room temperature, high photosensitivity, low cost, high chemical stability and weak toxicity [4-7]. However, the wide bandgap of ZnO (3.37 eV) limits its response to the UV light only, leaving 95-97% energy of the whole solar spectrum unusable. Moreover, due to the very fast recombination of photogenerated electron (e^-)/hole (h^+) pairs, surface reactions that generate

the reactive oxygen species (ROS) like hydroxyl $^{\bullet}OH$ or superoxide $O_2^{\bullet-}$ radicals and H_2O_2 responsible for the catalytic photodegradation cannot optimally occur.

In recent years, a variety of effective approaches like semiconductor coupling [6, 8, 9] or doping [10-13] have been developed to modify ZnO in order to improve its photoresponse capability. Doping, which consists in the intentional incorporation of impurities into the host lattices, is the most commonly used method to tune the optical and chemical properties of nanomaterials [14, 15]. Because Mn^{2+} doping generates new energy states within the bandgap of ZnO [16-22], Mn-doped ZnO (ZnO: Mn) particles were recently found to be efficient for solar or visible-light driven photocatalysis for two reasons. First, because this doping enhances the absorption in the visible region. Second, because the new energy states act as intermediate steps for e^- in their transitions between the valence and the conduction bands and thus efficiently promote the separation of photogenerated e^- and h^+. All studies clearly demonstrated that ZnO:Mn particles exhibit a higher photocatalytic activity than ZnO under UV or visible light irradiation and that the morphology, the size, the defect concentrations and the level of doping play crucial roles on the photodegradation efficiency of various organic dyes like methyl orange or methylene blue [16-22].

Porous ZnO materials have also gained much attention recently owing to their superior photocatalytic properties compared to ZnO particles [23-27]. Since the contaminant molecules need to be adsorbed on the photocatalyst surface for the redox reactions to occur, a high effective surface area associated to the high diffusivity of contaminants will give enhanced photocatalytic activity [28]. Up to now, several methods such as hydrolysis of $Zn(OAc)_2$ followed by high temperature annealing [29, 30], hydrothermal synthesis followed by etching [31], aminoacid-assisted synthesis [32] or hydrolysis of $Zn(OAc)_2$ in the presence of templates (starch, polystyrene, gelatin,…) followed by calcination [33-37] have been developed to obtain porous ZnO particles. However, most of these preparation methods are often faced with problems such as high temperature or tedious procedures. In this paper, we report a facile method for the preparation of porous Mn-doped ZnO particles via a solvothermal process. The high photocatalytic activity of ZnO:Mn particles for the degradation of Orange II under solar light irradiation was further demonstrated.

II.3 Experimental section

II.3.1 Materials

Zn $(OAc)_2$. $2H_2O$ (> 98%, Sigma), Mn $(OAc)_2$. $4H_2O$ (99.99%, Sigma), Orange II sodium salt (> 85%, Sigma), sodium hydroxide (> 97%, Sigma), and anhydrous ethanol were used as received without further purification. All solutions were prepared using Milli-Q water (18.2 MΩ.cm, Millipore) as solvent.

II.3.2 Preparation of ZnO and Mn-doped ZnO particles.

ZnO particles were synthesized by a solvothermal method based on the hydrolysis of Zn$(OAc)_2$. Typically, in a three-necked flask equipped with a condenser and a dropping funnel, Zn $(OAc)_2$.2 H_2O (511 mg, 2.33 mmol) was dissolved in 35 mL ethanol. To this solution, NaOH (96 mg, 2.33 mmol) in 35 mL ethanol was added dropwise and the mixture stirred for 30 min at room temperature. Then, the solution was transferred into a 140 mL Teflon-sealed autoclave and was heated at 160 °C for 24 h. After cooling to room temperature, the ZnO particles were collected by centrifugation, washed three times with water, one time with ethanol, and dried at 70 °C overnight.

Mn-doped ZnO particles were prepared using a similar synthetic procedure. For the particles doped with 3% Mn, Zn $(OAc)_2$.2 H_2O (496 mg, 2.259mmol) and Mn$(OAc)_2$. $4H_2O$ (17 mg, 0.069 mmol) were used. The purification and drying procedures are similar to those previously described for ZnO particles.

II.3.3 Photocatalytic degradation of Orange II

The photocatalytic activity was evaluated by the degradation of an aqueous solution of Orange II (10 mg/L) at room temperature under solar light irradiation. In a typical experiment, the ZnO:Mn nanoparticles (60 mg) were dispersed in 30 mL Orange II aqueous solution (10 mg/L) and the suspension was magnetically stirred under ambient conditions for 60 min in the dark to reach an adsorption-desorption equilibrium. Under stirring, the suspension was exposed to simulated solar light irradiation produced by Sylvania LuxLine FHO T5 neon tubes. The light intensity was estimated to be 5.5mW/cm^2. At certain time intervals, 1 mL of the suspension was extracted and centrifuged (15000 rpm for 2 min) to remove the photocatalyst. The degradation process was monitored by measuring the absorption of Orange II at 485 nm using a UV-visible absorption spectrometer. The visible light irradiation was

carried out using the neon tubes previously described and a polycarbonate film was used as the UV cutoff filter.

II.3.4 Quantification of hydroxyl radicals production, DST assays

The production of •OH radicals by ZnO and ZnO: Mn particles was estimated using disodium terephthalate (DST), which turns into fluorescent 2-hydroxyterephthalate, 2-OH-DST (λ_{em} = 428 nm) upon reaction with •OH radicals [38-40]. Briefly, 5 mg of ZnO or ZnO:Mn particles were dispersed by magnetic stirring in 100 mL water. Next, 1 mL of this dispersion was mixed with 1 mL of DST (0.1 M in water) before being irradiated with a Hg-Xe lamp (light intensity = 200 $mW.cm^{-2}$) for various times. The mixture was then treated with 1 mL of 1M NaOH and incubated for 50 min at room temperature before filtration on 0.2 μm polyvinylidene fluoride Acrodisc Syringe Filter. The photoluminescence spectra were recorded to estimate 2-OH-DST formed (λ_{ex} = 300 nm). Control samples were (i) DST irradiated in the absence of particles and (ii) DST and particles but without light activation. PL intensities measured after these control experiments were substracted from those measured when the particles were irradiated in the presence of DST.

II.3.5 Characterization

Transmission electron microscopy (TEM) images were taken by placing a drop of the particles dispersed in methanol onto a carbon film-supported copper grid. Samples were studied using a Philips CM200 instrument operating at 200 kV. Scanning electron microscopy (SEM) pictures were prepared using JEOL Scanning Electron Microscope JSM-6490 LV. The X-ray powder diffraction (XRD) diagrams of all samples were measured using PanalyticalX'Pert Pro MPD diffractometer using Cu Kα radiation. The X-ray powder diffraction data were collected from an X'Pert MPD diffractometer (Panalytical AXS) with a goniometer radius 240 mm; fixed divergence slit module (1/2° divergence slit, 0.04 rdSollers slits) and an X'Celerator as a detector. The powder samples were placed on a silicon zero-background sample holder and the XRD patterns were recorded at room temperature using Cu K_α radiation (λ = 0.15418 nm). X-ray photoelectron spectroscopy (XPS) analyses were performed on a GammadataScienta (Uppsala, Sweden) SES 200-2 spectrometer under ultra-high vacuum ($P < 10^{-9}$ mbar). The measurements were performed at normal incidence (the sample plane is perpendicular to the emission angle). The spectrometer resolution at the Fermi level is about 0.4 eV. The depth analyzed extends up to about 8 nm.The

monochromatizedAlKα source (1486.6 eV) was operated at a power of 420 W (30 mA and 14 kV) and the spectra were acquired at a take-off angle of 90° (angle between the sample surface and photoemission direction). During acquisition, the pass energy was set to 500 eV for wide scans and to 100 eV for high-resolution spectra. CASAXPS software (Casa Software Ltd, Teignmouth, UK, www.casaxps.com) was used for all peak fitting procedures and the areas of each component were modified according to classical Scofield sensitivity factors.

The textural properties of the materials were investigated with a Micromeritics 3Flex Surface Characterization Analyzer instrument using liquid nitrogen (-196 °C). Prior to the analyses, the samples were out-gassed overnight under primary vacuum at 40°C on the ports of the Micromeritics Vac Prep 061 degasser followed by 4 h out-gassing under high vacuum on the analyse ports. The resulting isotherms were analysed using the BET (Brunauer-Emmett-Teller) method.

All the optical measurements were performed at room temperature (20 ± 1°C) under ambient conditions. Absorption spectra of liquid samples were recorded on a Thermo Scientific Evolution 220 UV-visible spectrophotometer. The diffuse reflectance absorption spectra (DRS) were recorded on a Shimadzu 2600 UV-visible spectrophotometer. $BaSO_4$ powder was used as a standard for baseline measurements and spectra were recorded in a range of 250-1400 nm. Raman spectra were recorded using aXplora spectrometer from Horiba Scientific with 532 nm wavelength incident YAG laser light.

II.4 Results and discussion

II.4 .1 Synthesis and characterization of photocatalysts

Fig. 27 shows the powder XRD patterns of ZnO particles when varying the molar dopant percentage in Mn^{2+} from 0 to 7. All diffraction peaks could be indexed to the standard hexagonal wurtzite structure of ZnO (space group $P6_3mc$, JCPDS No 36-1451, a = 3.250 Å, c = 5.207 Å). The diffraction peaks were sharp, indicating the high crystallinity of the materials produced. Although the ionic radius of Mn^{2+} (0.80 Å) is larger than that of Zn^{2+} (0.74 Å), no significant distortion in the lattice structure was observed. No impurity phase attributed to manganese oxides could be detected, indicating that Mn^{2+} was completely doped into the ZnO crystal lattice.

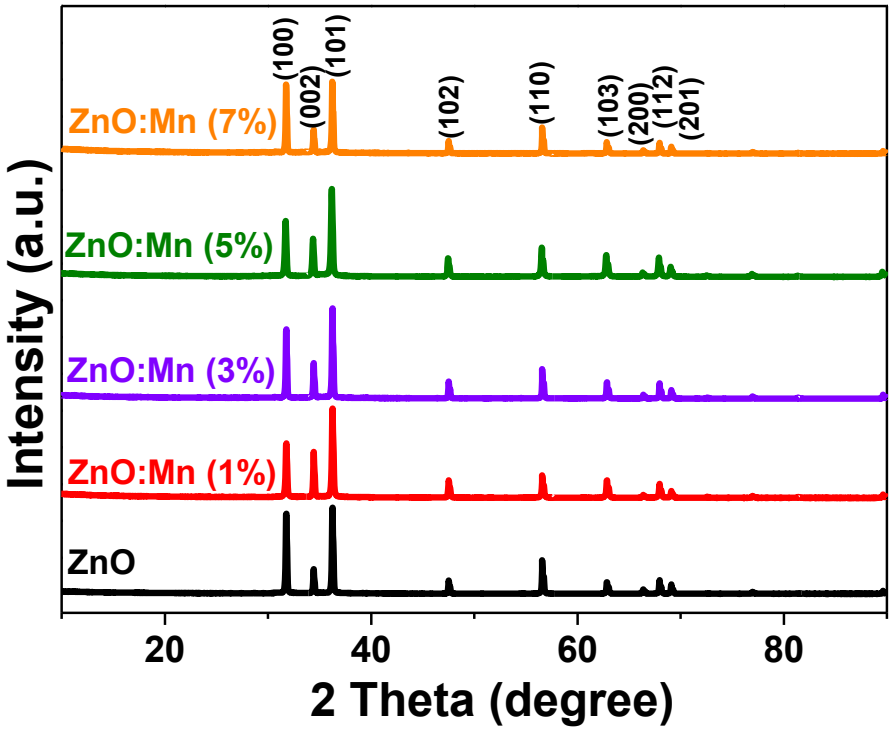

Figure 27: XRD patterns of ZnO and Mn-doped ZnO particles.

The wurtzite crystal structure of ZnO particles was further confirmed by Raman spectroscopy (Fig. 28). The peaks located at 330, 378, 410 and 436 cm^{-1} can be assigned to E_2, A_{1TO}, E_1, and $E_2(high)$ vibration modes of ZnO with $P6_3mc$ symmetry, respectively [41]. Well-resolved peaks originating from multiphon on processes could also be observed at 206 and between 1030 and 1200 cm^{-1}. XRD and Raman analyses demonstrate that ZnO: Mn particles produced are composed of hexagonal ZnO with good crystal quality.

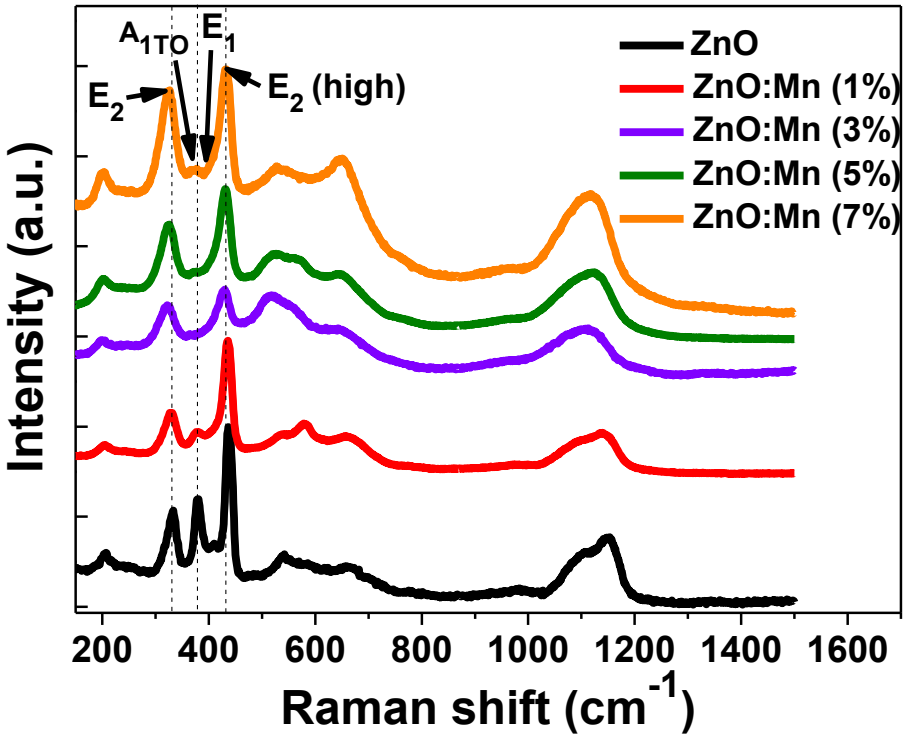

Figure 28: Room temperature Raman spectra of ZnO and Mn-doped ZnO nanoparticles.

Fig. 38 (supporting information) shows SEM images of ZnO nanoparticles and of the ZnO sample doped with 3% Mn^{2+}. Both samples assemble into microparticles of globular morphology that are more homogeneous in size for the doped nanoparticles. Numerous pores can be seen in the ZnO and ZnO: Mn materials which should be beneficial to increase the contact area for reactant diffusivity and for enhanced photocatalytic activity [42]. The energy dispersive X-ray (EDX) spectrum of the ZnO: Mn (3%) sample only show peaks corresponding to Zn, O, and Mn and no trace amount of impurities could be seen in the detection limit of the EDX analysis (Fig. 39supporting information). Quantitative analysis shows that the concentration of Mn^{2+} in the 3% atomic Mn-doped ZnO particles is 2.2%, indicating that the amount of Mn incorporated into the ZnO lattice is slightly lower than the nominal amount of Mn used during the synthesis. To obtain more details about the structures of these materials, TEM and HR-TEM experiments were conducted (Fig. 29). The ZnO sample is mainly composed of spherical/ellipsoidal nanoparticles with an average diameter of 28 nm (Fig. 29a). A few particles with hexagonal morphology can also be observed. A

decrease in nanoparticles size to ca. 21 nm was observed for ZnO: Mn (3%) particles (Fig. 29b). This decrease may be attributed to the growth inhibition of the nanocrystals originating from the presence of dopant ions in the reaction medium [43, 44]. The smaller size of ZnO: Mn particles should be beneficial for photocatalytic activity. The selected area electron diffraction (SAED) patterns (insets of Fig. 29a-b) show a set of concentric reflexes, indicating the hexagonal structure of the ZnO particles prepared. This was further confirmed by a HR-TEM image of ZnO: Mn particles which show clear lattice fringes with d-spacing of 0.55 nm, value consistent with the distance between two (001) crystal planes of hexagonal ZnO (Fig. 29c).

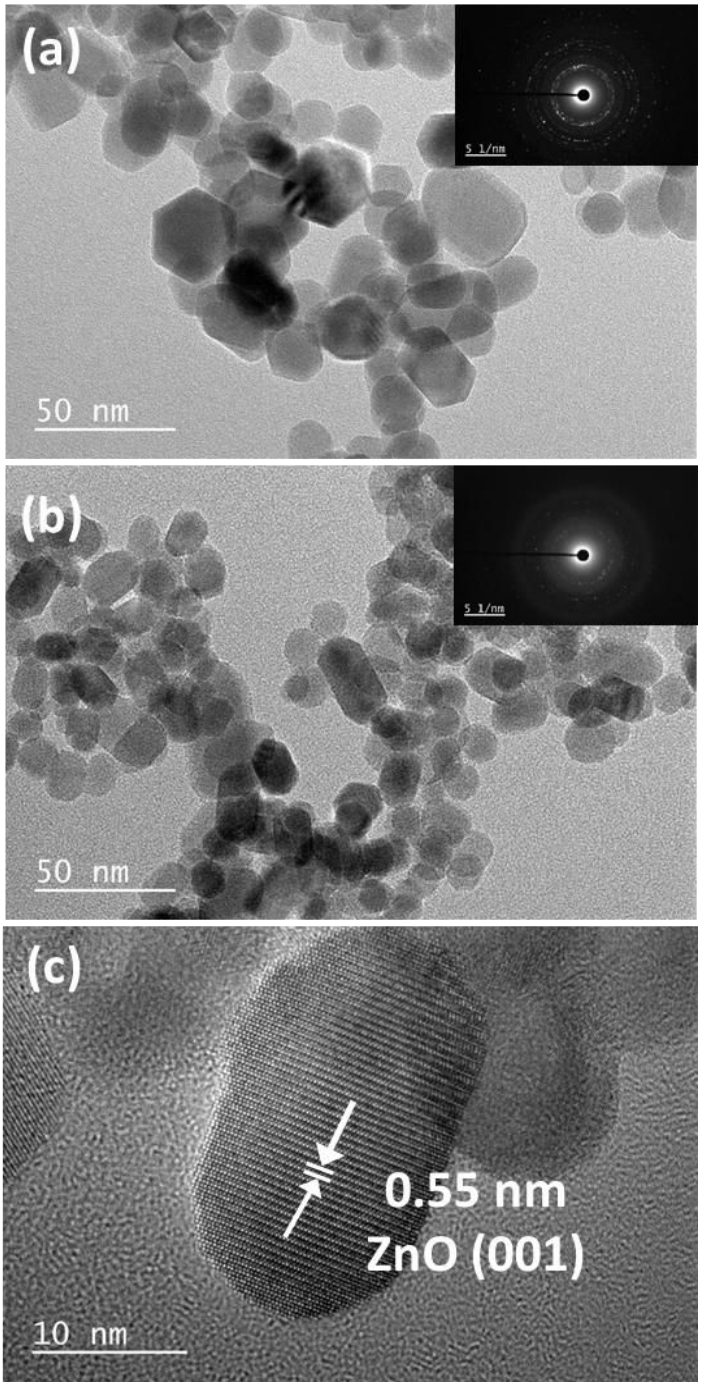

Figure 29: TEM images of (a) ZnO and (b) ZnO: Mn (3%) nanoparticles (the inserts are the SAED patterns). (c) HR-TEM micrograph of ZnO: Mn (3%) particles.

Further characterization studies using XPS provided evidences for the surface states and composition and the results obtained with ZnO doped with 3% Mn^{2+} are shown in Fig. 30. Fig. 30a shows the survey scan of the sample where the presence of Zn, O and Mn is evident. The spectrum also shows the signal of Na which originates from NaOH used for the synthesis.

The fine XPS spectra show that the Zn $2p_{3/2}$ signal appears at 1021.46 eV, which corresponds to Zn-O bonds in the ZnO lattice (Fig. 30b). For Mn $2p_{3/2}$, the energy of the signal located at 640.54 eV is close to Mn^{2+} in MnO (Mn $2p_{3/2}$: 640.7 eV). The signals observed at 641.51 and 642.44 eV could be assigned to Mn_2O_3 and MnO_2, respectively; indicating the presence of Mn oxides associated Mn-doped ZnO and/or the incorporation of Mn ions in the ZnO lattice in the +3 or +4 oxidation states. The latter hypothesis is supported by recent reports [45, 46]. Finally, Fig. 4d shows the high resolution signal for the O 1s orbital. The broad peak is due to the surface-adsorbed OH^- ions on ZnO particles. The high intensity peak located at the lower binding energy side is associated to Zn-O or Mn-O bonds.

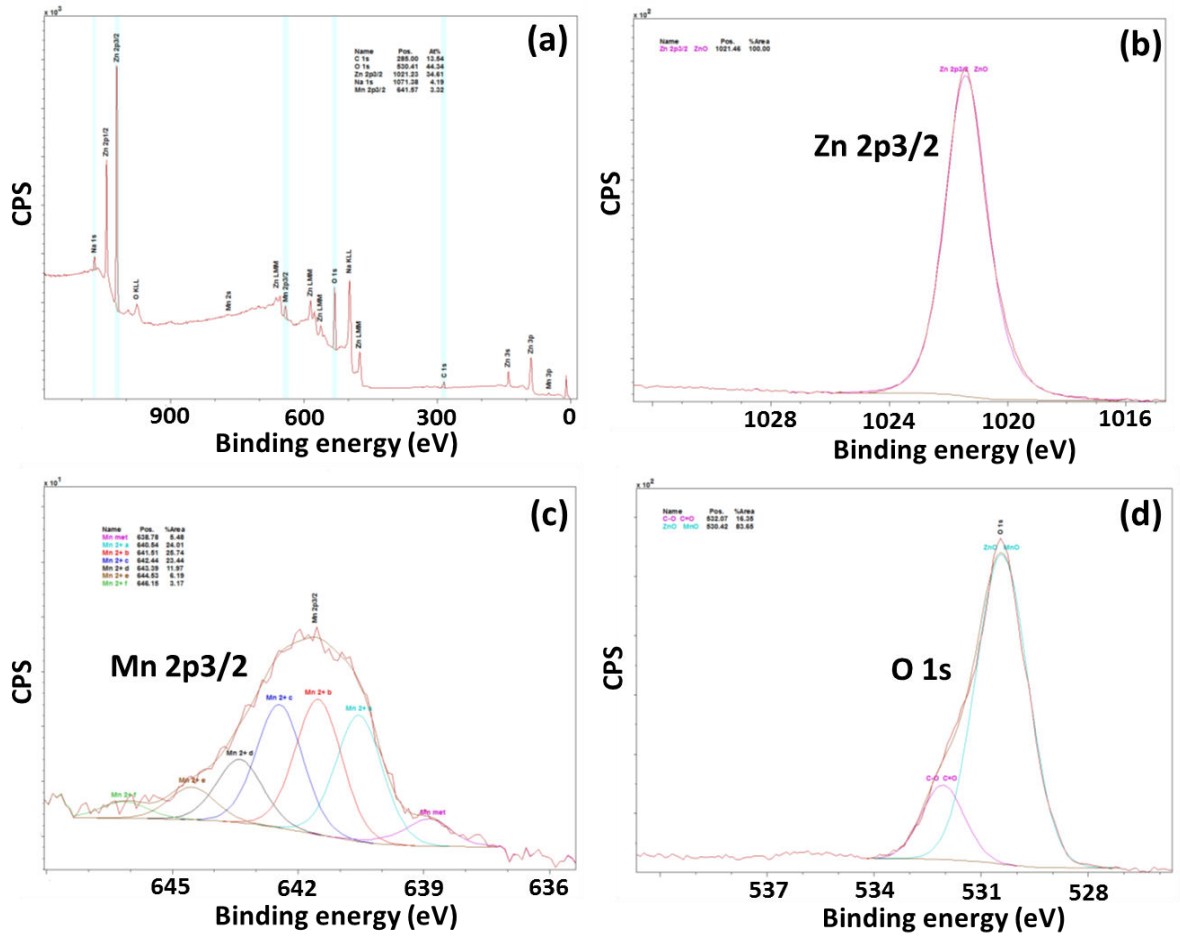

Figure 30: (a) XPS survey scan for ZnO: Mn (3%) particles. (b-d) High resolution peaks for Zn 2p, Mn 2p, and O 1s, respectively.

The optical properties of undoped and Mn-doped ZnO samples were further analyzed by UV-visible absorption and diffuse reflectance spectroscopy (DRS). ZnO shows a sharp near band edge absorption at ca. 380 nm due to its bandgap of 3.3 eV. After Mn^{2+} doping, the absorption markedly increases in the visible region (Fig. 40 supporting information). ZnO particles exhibit the highest reflectance throughout the whole visible region while the reflectance decreases with the increase of Mn^{2+} doping in the visible region (Fig. 31), indicating that ZnO:Mn particles should be better photocatalysts under solar and visible light irradiation. The bandgap values were determined from DRS spectra by converting the absolute reflection to the Kubelka-Munck function (F_{KM}) and were found to gradually decrease from 3.06 for ZnO to 2.83 eV for ZnO:Mn (7%) (Fig. 41 supporting information). This decrease originates from the formation of various optically active sub-levels through the bandgap of ZnO, resulting in a decrease in its optical bandgap. Finally, no fluorescence signal was observed for all Mn-doped samples after excitation at 300 nm. This indicates that the electron-hole recombination is completely inhibited through the Mn^{2+} doping and the presence of a large number of carrier traps within the nanoparticles.

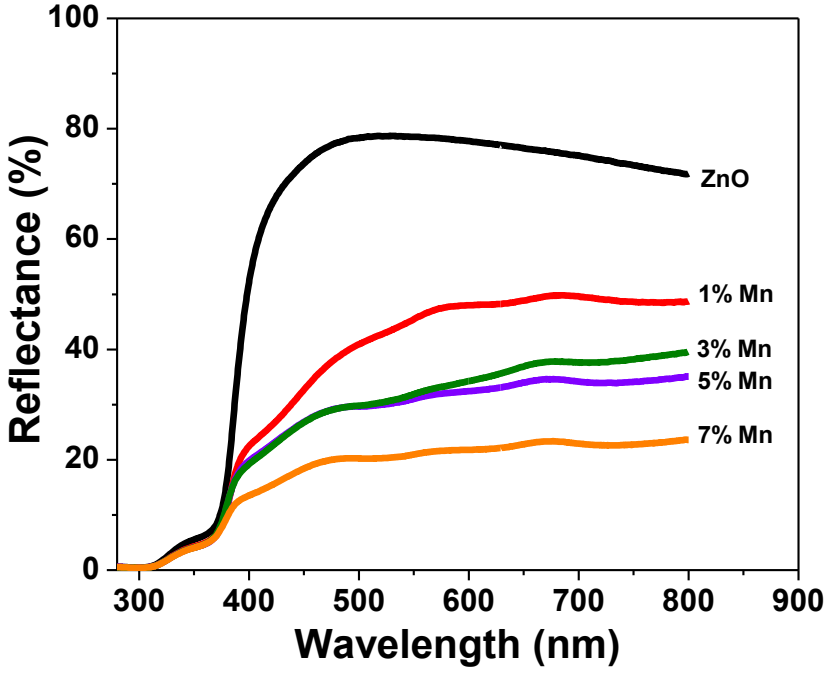

Figure 31: Room temperature UV-visible diffuse reflectance spectra of ZnO and Mn^{2+}-doped ZnO particles.

II.4.2 Photocatalytic activity

The photocatalytic performances of ZnO: Mn particles have been evaluated for the degradation of Orange II (10 mg/L) and compared with ZnO particles under solar light irradiation (5.5 mW/cm^2). In preliminary experiments conducted in the absence of the photocatalyst, no significant photolysis of the dye was observed during 6 h of irradiation. Once the catalyst added, the photodegradation was monitored by the time dependent UV-visible spectral changes of Orange II in the presence of ZnO and ZnO: Mn catalysts (Fig. 32). Using the ZnO: Mn (3%) catalyst, the characteristic peak at 485 nm gradually decreases with irradiation time and disappears completely after 210 min, suggesting the complete photodegradation (Fig. 32b). All other photocatalysts exhibited a weaker activity. The results described in Fig. 32a also demonstrate that when the doping in Mn^{2+} is higher that the optimal value (3%), Mn^{2+} ions probably act as electron and holes recombination centers and hence decrease the photocatalytic activity.

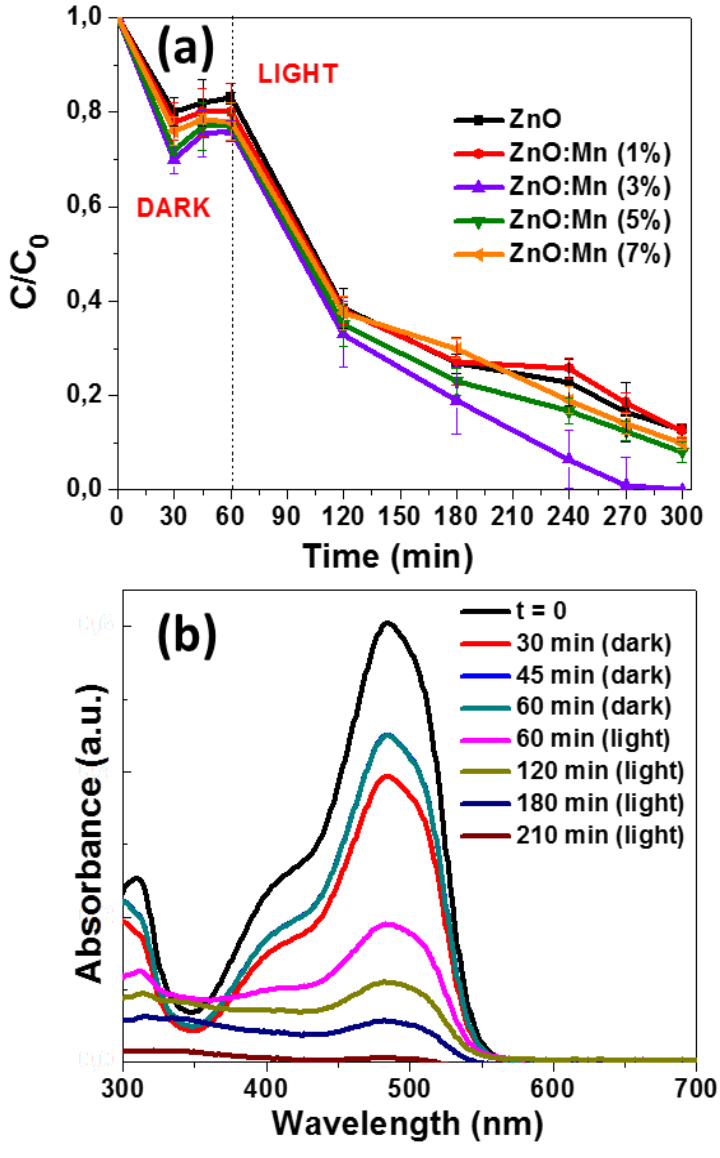

Figure 32: (a) Influence of the Mn doping of ZnO nanoparticles for the degradation of Orange II in aqueous solution (C is the Orange II concentration at time t, and C_0 is the concentration of the dye at t = 0; Volume of solution, 30 mL; Mass of photocatalyst, 60 mg; Orange II concentration, 10 mg/L). (b) Variation of Orange II concentration as a function of irradiation time using the ZnO: Mn (3%) photocatalyst.

We also evaluated the photodegradation of Orange II under visible irradiation using a light intensity of 15 mW/cm^2 (Fig. 42 supporting information). Results obtained showed that the mineralization of the dye could be achieved (ca. 75% of degradation after 240 min) but

required a longer time than under solar irradiation (near complete photodegradation after 210 min illumination).

II.4.3 Effect of catalyst dosage, of Orange II concentration and of pH

The effect of the catalyst amount on the photodegradation of Orange II under simulated solar light was studied by varying the ZnO:Mn (3%) catalyst concentration from 0.5 to 3.0 g/L (Fig. 33a). From 0.5 to 2.0 g/L of catalyst, the photodegradation rates increase with the catalyst amount. The initial rate constants given by the slope at the initial time of irradiation are 0.004, 0.005, 0.007, 0.017 and 0.006min^{-1} for 0.5, 1.0, 1.5, 2.0 g/L and 3 g/L of catalyst, respectively. Since the adsorption phase is not markedly influenced by the amount of catalyst used, the increase of the photodegradation rate when increasing the amount of catalyst probably originates from the increase of the surface illuminated during photocatalytic experiments. A decrease of the reaction rate was observed when using 3 g/L of the catalyst. This probably originates from light scattering by the ZnO: Mn particles, as previously observed for ZnO materials [47].

The effect of the initial Orange II concentration (5, 10, or 20 mg/L) on the photocatalytic efficiency was also investigated (Fig. 33b). As can be seen, the photodecomposition rate was found to decrease with the increase of the dye concentration (k = 0.025, 0.024, and 0.003 min^{-1} for Orange II concentrations of 5, 10 and 20 mg/L, respectively). Since no marked differences were observed during the adsorption phase, the decrease in light penetration by Orange II molecules (filter effect) is probably the cause of this phenomenon.

The adsorption of the dye at the surface of the catalyst is well-known to depend on the pH of the solution used [48]. We varied the pH of the Orange II solution from 4.5 to 9.0 before the adsorption phase and the results are shown in Fig. 33c. No significant differences were observed on the adsorption of the dye. Results obtained show that the optimum pH for Orange II photodegradation is 9.0 but the photocatalytic activity is not markedly altered at pH 6.5 and 4.5. The later results are of interest since ZnO is known to exhibit a lower catalytic efficiency at acidic pH due to its slow dissolution at such pH values. The initial pseudo-first order rate constants of the ZnO:Mn photocatalyst at pH 4.5, 6.5, and 9.0 are 0.014, 0.017, and 0.019 min^{-1}, respectively. We attribute the high catalytic activity at pH = 9 to the excess of OH^- anions that facilitate the photogeneration of $^{\bullet}OH$, which are well-established as the primary oxidizing species during photocatalytic experiments.

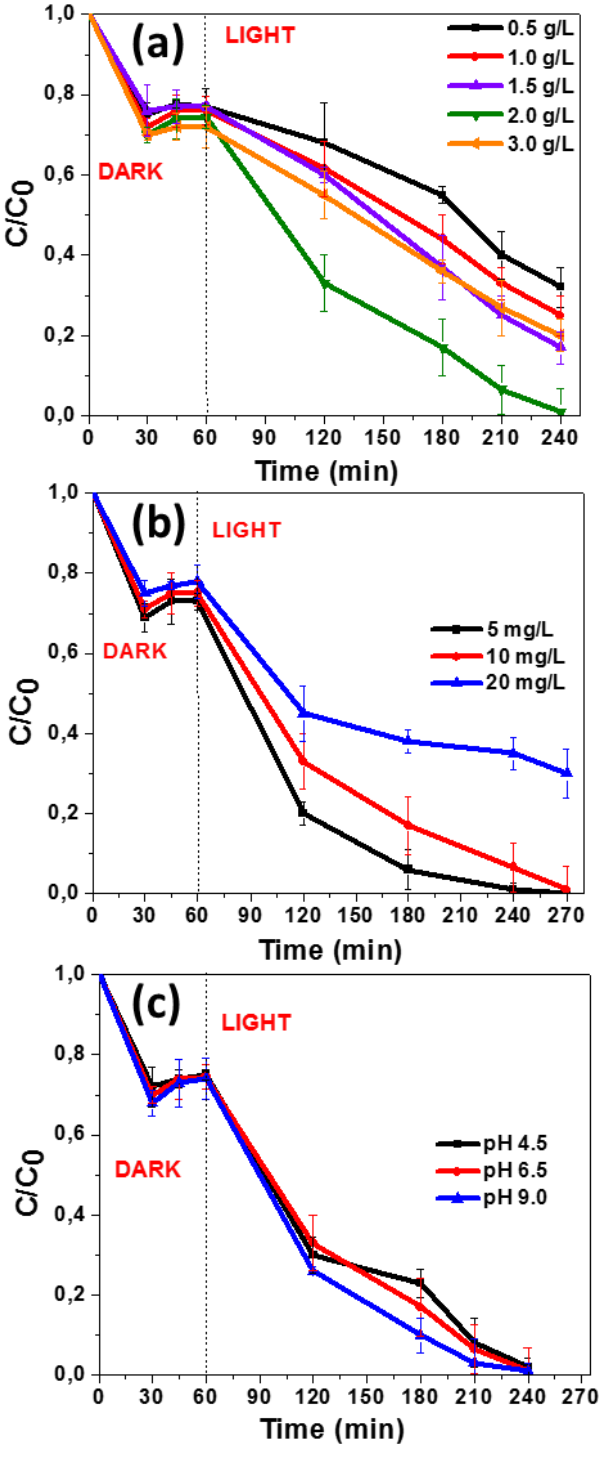

Figure 33: Influence of (a) the amount of catalyst, (b) the dye concentration and (c) the pH of the Orange II solution on the photocatalytic activity of ZnO:Mn (3%) particles.

II.4.4 Mechanism

It is well-known that the photocatalytic efficiency of semiconductor oxides like ZnO is mainly governed by surface area, defects and surface hydroxyl groups [4-7].To gain some informations on the mechanism of the photocatalytic degradation, we first measured the specific surface areas and the microporosityof ZnO and of the 3% Mn^{2+}-doped ZnO sample by nitrogen sorption performed at 77 K (Fig. 34). For both materials, the N_2-adsorption-desorption isotherms are of type II, according to the Brunauer-Dening-Dening-Teller (BDDT) classification [49]. A H3-type hysteresis loop can be observed at high relative pressures, characteristic of an adsorbent composed of aggregates, having a non-rigid texture, and indicating the existence of an undefined mesoporosity, which is in good agreement with SEM observations (Fig. 43 supporting information). ZnO: Mn particles were found to exhibit a higher specific surface area than ZnO (41.46 and 54.03 m^2/g for ZnO and ZnO:Mn, respectively). The pore size distributions were determined using the Barrett-Joyner-Halenda (BJH) method and are shown in Fig. 43 (supporting information). ZnO: Mn particles have a smaller pore size (23.2 nm) than ZnO particles (29.1 nm). These data suggest that the high specific surface area of ZnO: Mn particles may explain the enhancement of the solar-light driven photocatalytic oxidation of Orange II.

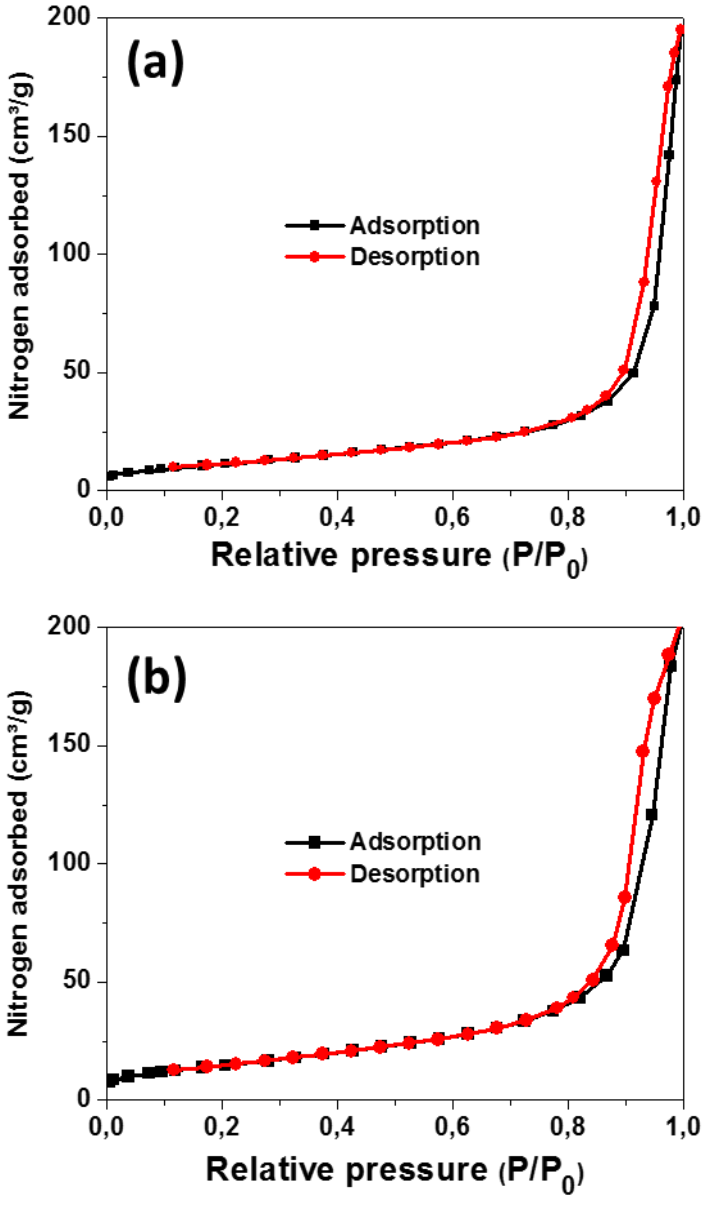

Figure 34: N_2 adsorption-desorption isotherms at 77 K of ZnO and 3% Mn^{2+}-doped ZnO particles.

For the mineralization of organic dyes by photocatalysis, •OH radicals are generally considered to have a prominent role as the active species in photodegradation. We therefore compared the production of •OH radicals upon irradiation of ZnO and ZnO: Mn particles using a fluorescence technique. Hydroxyl radicals are well-known to react with disodium terephthalate (DST) to generate 2-OH-DST which strongly emits fluorescence centered at 428 nm upon excitation at 312 nm (Fig. 35a) [6, 38-40]. As can be seen on Fig. 35b, a gradual

increase in fluorescence intensity at 428 nm was observed with increasing the irradiation time. The production of •OH radicals was markedly enhanced when irradiating ZnO: Mn particles. For example, a ca. 3.7-fold increased formation of •OH radicals was observed for ZnO: Mn after 15 min of irradiation compared to the experiment conducted with ZnO (Fig. 35b). Finally, it is worth to mention that 2-OH-DST was not produced in control experiments performed without light irradiation thus confirming a photo-induced mechanism.

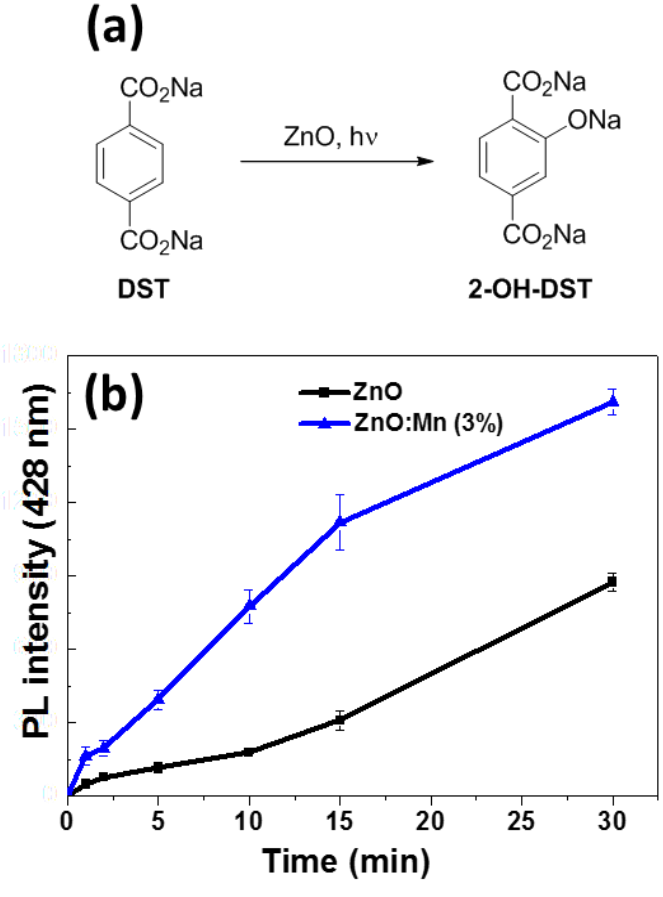

Figure 35: (a) 2-OH-DST production upon irradiation of DST in the presence of the ZnO photocatalyst. (b) Variations of the PL intensity at 428 nm of 2-OH-DST upon irradiation of DST with ZnO and ZnO:Mn (3%) nanoparticles. Results are the average of three experiments.

The key role played by •OH radicals during the photocatalytic degradation of Orange II was further confirmed with the use of *tert*-butyl alcohol (*t*-BuOH), a chemical scavenger of these radicals [50]. A strong decrease of the photocatalytic degradation rate was observed in the presence of *t*-BuOH (Fig. 44 supporting information). The previous results demonstrate that

the higher specific surface of ZnO: Mn particles associated to the ability of Mn^{2+} ions to reduce charge recombinations and thus increase $^{\bullet}OH$ radicals productions are beneficial for enhancing the photocatalytic activity.

The following mechanism can be proposed for the solar light-driven photodegradation of Orange II using ZnO: Mn particles (Fig. 36). Under solar light irradiation, the photogenerated e^- can be transferred either to the conduction band (CB) of ZnO or to Mn^{2+} energy levels localized within the bandgap of ZnO. Note that electrons promoted to the CB of ZnO can also be trapped by the Mn^{2+} dopant sites. This process inhibits e^-/h^+ recombinations and allows an enhanced production of ROS. Next, e^- react with adsorbed molecular oxygen to yield $O_2^{\bullet-}$ radicals. Meanwhile, h^+ react with surface-bound water to produce $^{\bullet}OH$ radicals. $O_2^{\bullet-}$ and $^{\bullet}OH$ free radicals, and the reactive species like $HO_2^{\bullet}$ and H_2O_2 obtained after association with H^+, oxidize Orange II into carbon dioxide and water.

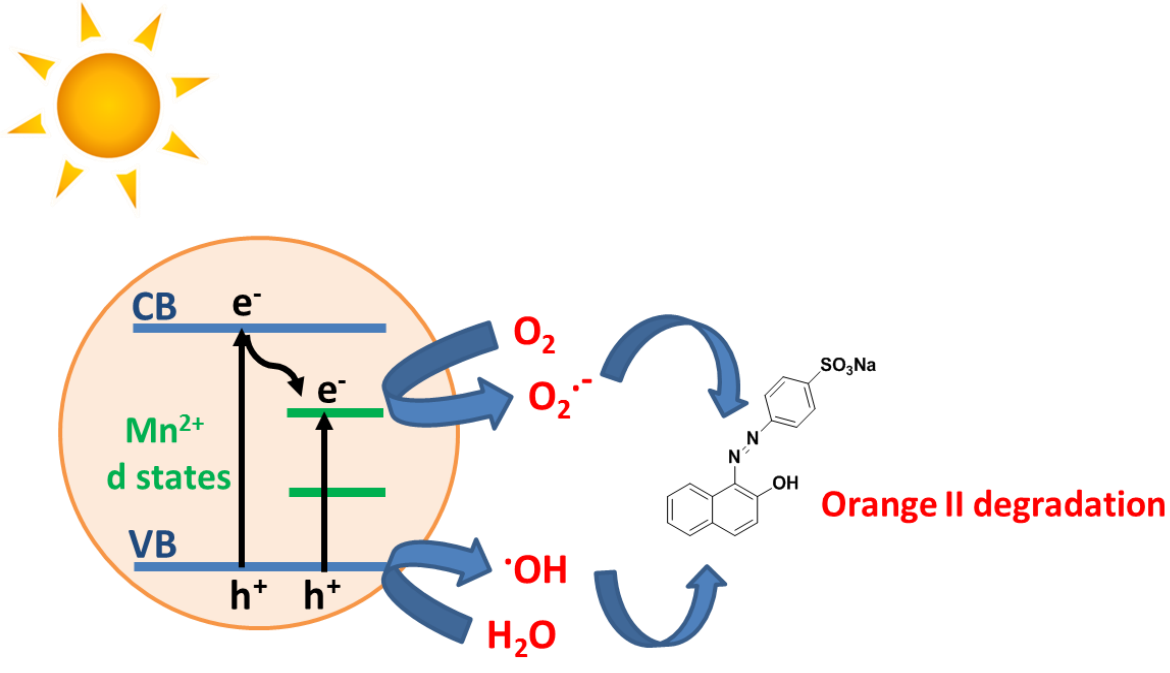

Figure 36: Schematic illustration of the photocatalytic mechanism of ZnO: Mn nanoparticles under solar light irradiation.

II.4.5 Stability

The stability and the reusability of the ZnO: Mn photocatalyst are important parameters in practical applications and were evaluated in ten successive cycles for the degradation of Orange II (10 mg/L) under solar light irradiation (5 mW/cm^2). After each run, the photocatalyst was recovered by centrifugation (4000 rpm for 15 min) and redispersed in an Orange II solution without any washing or drying. As shown in Fig. 37, after ten cycles, the photocatalytic efficiency decreased only slightly compared to the as-synthesized ZnO: Mn particles, thus indicating that the photocatalyst exhibits high stability.

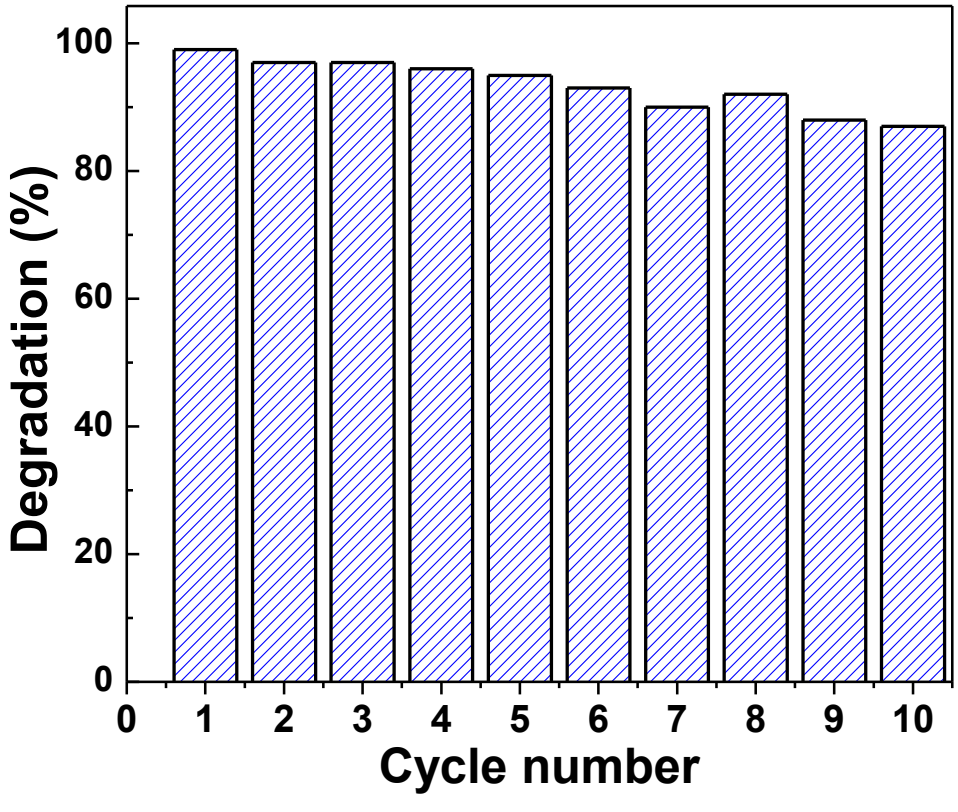

Figure 37: Plot of photodegradation percent of Orange II using the ZnO:Mn catalyst at optimized conditions versus cycle number.

II.5 Conclusions

In summary, we successfully developed a new synthetic route giving access to porous ZnO and Mn-doped ZnO particles and which does not require post-synthetic annealing, etching or the use of templates. The influence of the Mn^{2+} dopant percentage on the structural, optical and photocatalytic properties of ZnO: Mn particles were investigated. ZnO: Mn (3%) exhibits the highest photocatalytic activity for the degradation of Orange II under solar light irradiation. This material exhibits also a higher specific surface compared to pure ZnO. This high specific surface associated to the ability of the Mn^{2+} dopant to act as an electron trap and to decrease the photogenerated electron/hole pair recombination results in an increase of the $^{\bullet}OH$ radicals by the ZnO:Mn (3%) sample and thus of its photocatalytic performances. Moreover, the ZnO: Mn catalyst can be reused up to ten times with at least 85% of activity. The synthetic method developed gives an easy and fast access to porous Mn-doped ZnO particles displaying high interest for new technological applications and especially for environmental remediation.

Acknowledgements

This work is partially supported by the French-Tunisian project PHC Utique CMCU 14G0821.

II.6 References

[1] S. Dong, J. Feng, M. Fan, Y. Pi, L. Hu, X. Han, M. Liu, J. Sun, J. Sun, Recent developments in heterogeneous photocatalytic water treatment using visible light-responsive photocatalysts: a review, RSC Adv. 5 (2015) 14610-14630.

[2]S. Girish Kumar, K.S.R. Koteswara Rao, Zinc oxide based photocatalysis: tailoring surface-bulk structure and related interfacial charge carrier dynamics for better environmental applications, RSC Adv. 5 (2015) 3306-3351.

[3] N. Shaham-Waldmann, Y. Paz, Photocatalytic reduction of Cr(VI) by titanium dioxide coupled to functionalized CNTs: An example of counterproductive charge separation,Mat. Sci. Semicon. Proc. 42 (2016) 72-80.

[4] C. Hariharan, Photocatalytic degradation of organic contaminants in water by ZnO nanoparticles, Appl. Catal. A: Gen. 304 (2006) 55-61.

[5] C. Tian, Q. Zhang, A. Wu, M. Jiang, Z. Liang, B. Jiang, H. Fu, Cost-effective large-scale synthesis of ZnOphotocatalyst with excellent performance for dye photodegradation, Chem. Commun. 48 (2012) 2858-2860.

[6] F. Achouri, S. Corbel, A. Aboulaich, L. Balan, A. Ghrabi, M. Ben Said, R. Schneider, Aqueous synthesis and enhanced photocatalytic activity of ZnO/Fe_2O_3 heterostructures, J. Phys. Chem. Solids 75 (2014) 1081-1087.

[7] H. Moussa, E. Girot, K. Mozet, H. Alem, G. Medjahdi, R. Schneider, ZnO rods/reduced graphene oxide composites prepared via a solvothermal reaction for efficient sunlight-driven photocatalysis, Appl. Catal. B: Environ. 185 (2016) 11-21.

[8] V. Jeena, R.S. Robinson, Convenient photooxidation of alcohols using dye sensitised zinc oxide in combination with silver nitrate and TEMPO, Chem. Commun. 48 (2012) 299-301.

[9] F. Wang, L. Liang, L. Shi, M. Liu, J. Sun, CO_2-assisted synthesis of mesoporous carbon/C-doped ZnO composites for enhanced photocatalytic performance under visible light,Dalton Trans. 43 (2014) 16441-16449.

[10] S. Anandan, M. Miyauchi, Ce-doped ZnO ($Ce_xZn_{1-x}O$) becomes an efficient visible-light-sensitive photocatalyst by co-catalyst (Cu^{2+}) grafting, Phys. Chem. Chem. Phys. 13 (2011) 14937-14945.

[11] M. Ahmad, E. Ahmed, Y. Zhang, N.R. Khalid, J. Xu, M. Ullah, Z. Hong, Curr, Preparation of highly efficient Al-doped ZnOphotocatalyst by combustion synthesis, Appl. Phys. 13 (2013) 697-704.

[12] R. Mohan, K. Krishnamoorthy, S.-J. Kim, Enhanced photocatalytic activity of Cu-doped ZnOnanorods, Solid State Commun. 152 (2012) 375-380.

[13] J.Z. Bloh, R. Dillert, D.W. Bahnemann,Transition metal-modified zinc oxides for UV and visible light photocatalysis, Environ. Sci. Pollut. Res. 19 (2012) 3688-3695.

[14] S.C. erwin, L. Zu, M.I. Haftel, A.L. Efros, T.A. Kennedy. D.J. Norris, Doping semiconductor nanocrystals, Nature 436 (2005) 91-94.

[15] D.J. Norris, A.L. Efros, Doped nanocrystals, S.C. Erwin, Science 319 (2008) 1776-1779.

[16] R. Ullah, J. Dutta, Photocatalytic degradation of organic dyes with manganese-doped ZnO nanoparticles, J. Hazard. Mater. 156 (2008) 194-200.

[17] K. Rekha, M. Nirmala, M.G. Nair, A. Anukaliani, Structural, optical, photocatalytic and antibacterial activity of zinc oxide and manganese doped zinc oxide nanoparticles, Physica B 405 (2010) 3180-3185.

[18] M. Abbas Mahmood, S. Baruah, J. Dutta, Enhanced visible light photocatalysis by manganese doping or rapid crystallization with ZnO nanoparticles, Mater. Chem. Phys. 130 (2011) 531-535.

[19] D. Zhang,Structural, optical, electrical, and photocatalytic properties of manganese doped zinc oxide nanocrystals,Russian J. Phys. Chem. A 86 (2012) 93-99.

[20] Y. Yang, Y. Li, L. Zhu, H. He, L. Hu, J. Huang, F. Hu, B. He, Z. Ye, Shape control of colloidal Mn doped ZnO nanocrystals and their visible light photocatalytic properties, Nanoscale 5 (2013) 10461-10471.

[21] R. Saleh, N.F. Djaja, Transition-metal-doped ZnO nanoparticles: Synthesis, characterization and photocatalytic activity under UV light, Spectrochim. Acta A 130 (2014) 581-590.

[22] K. Umar, A. Aris, T. Parveen, J. Jaafar, Z.A. Majid, A.V. Bhaskar Reddy, J. Talib, Synthesis, characterization of Mo and Mn doped ZnO and their photocatalytic activity for the decolorization of two different chromophoric dyes, Appl. Catal. A: Gen. 505 (2015) 507-514.

[23] X. Wu, K.W. Li, H. Wang, Facile fabrication of porous ZnO microspheres by thermal treatment of ZnS microspheres, J. Hazard. Mater. 174 (2010) 573-580.

[24] Y. Du, R.Z. Chen, J.F. Yao, H.T. Wang, Facile fabrication of porous ZnO by thermal treatment of zeoliticimidazolate framework-8 and its photocatalytic activity, J. Alloys Compds 551 (2013) 125-130.

[25] Z.D. Li, Y. Zhou, G.G. Xue, T. Yu, J.G. Liu, Fabrication of hierarchically assembled microspheres consisting of nanoporousZnOnanosheets for high-efficiency dye-sensitized solar cells, J. Mater. Chem. 22 (2012) 14341-14345.

[26] W.L. Ong, S. Natarajan, B. Kloostra, G.W. Ho, Metal nanoparticle-loaded hierarchically assembled ZnOnanoflakes for enhanced photocatalytic performance, Nanoscale 5 (2013) 5568-5575.

[27] Z.J. Xing, B.Y. Geng, X.L. Li, H. Jiang, C.X. Feng, Self-assembly fabrication of 3D porous quasi-flower-like ZnO nanostrip clusters for photodegradation of an organic dye with high performance, CrystEngComm. 13 (2011) 2137-2142.

[28] T. Kimuro, Y. Yamauchi, N. Miyamoto, Condensation-and crystallinity-controlled synthesis of titanium oxide films with assessed mesopores, Chem. -Eur. J. 16 (2010) 12069-12073.

[29] Z. Jing, J. Zhan, Fabrication and gas-sensing properties of porous ZnOnanoplates, Adv. Mater. 20 (2008) 4547-4551.

[30] M. Chen, Z. wang, D. Han, F. Gu, G. Guo, Porous ZnO polygonal nanoflakes: synthesis, use in high-sensitivity NO_2 gas sensor, and proposed mechanism of gas sensing, J. Phys. Chem. C 115 (2011) 12763-12773.

[31] H. Wang, G. Li, L. Jia, G. Wang, C. Tang, Controllable preferential-etching synthesis and photocatalytic activity of porous ZnO nanotubes, J. Phys. Chem. C 112 (2008) 11738-11743.

[32] X. Liu, J. Zhang, L. Wang, T. Yang, X. Guo, S. Wu, S. Wang, 3D hierarchically porous ZnO structures and their functionalization by Au nanoparticles for gas sensors, J. Mater.Chem. 21 (2011) 349-356.

[33] F. Xu, P. Zhang, A. Navrotsky, Z.-Y. Yuan, T.-Z. Ren, M. Halasa, B.-L. Su, Hierarchically assembled porous ZnO nanoparticles: synthesis, surface energy, and photocatalytic activity, Chem. Mater. 19 (2007) 5680-5686.

[34] Z. Deng, M. Chen, G. Gu, L. Wu, A facile method to fabricate ZnO hollow spheres and their photocatalytic property, J. Phys. Chem. B 112 (2008) 16-22.

[35] M. Chen, L. Hu, J. Xu, M. Liao, L. Wu, X. Fang, ZnO hollow-sphere nanofilm-based high-performance and low-cost photodetector, Small 7 (2011) 2449-2453.

[36] X. Wu, K. Li, H. Wang, Facile fabrication of porous ZnO microspheres by thermal treatment of ZnS microspheres, J. Hazard. Mater. 174 (2010) 573-580.

[37] G. Zhang, Y. Shen, Y. Yang, Facile synthesis of monodisperse porous ZnO spheres by a soluble starch-assisted method and their photocatalytic activity, J. Phys. Chem. C 115 (2011) 7145-7152.

[38] C. Bohne, K. Faulhaber, B. Giese, A. Hafner, A. Hofmann, H. Ihmels, A.-K. Kohler, S. Pera, F. Schneider, M.A.L. Sheepwash, Studies on the mechanism of the photo-induced dan damage in the presence of acridizinium salts involvement of singlet oxygen and an unusual source for hydroxyl radicals, J. Am. Chem. Soc. 127 (2005) 76-85.

[39] Y. Iida, K. Yasui, T. Tuziuti, M. Sivakumar, Y. Endo, Ultrasonic cavitation in microspace, Chem. Commun. (2004) 2280-2281.

[40] H. Sies, Oxidative stress: oxidants and antioxydants, Experimental Physiol. 82 (1997) 291-295.

[41] K.A. Alim, V.A. Fonobarov, M. Shamsa, A.A. Balandin, Micro-Raman investigation of optical phonons in ZnO nanocrystals, J. Appl. Phys. 97 (2005) 124313.

[42] L.F. Koao, F.B. Dejene, H.C. Swart, J.R. Botha, The effect of Ce^{3+} on structure, morphology and optical properties of flower-like ZnO synthesized using the chemical bath method, J. Lumin. 143 (2013) 12-17.

[43] M.I. Dar, N. Arora, N.P. Singh, S. Sampath, S.A. Shivashankar, Role of spectator ions in influencing the properties of dopant-free ZnO nanocrystals, New J. Chem. 38 (2014) 4783-4790.

[44] H. Moussa, C. Merlin, C. Dezanet, L. Balan, G. Medjahdi, M. Ben-Attia, R. Schneider, Trace amounts of Cu^{2+} ions influence ROS production and cytotoxicity of ZnO quantum dots, J. Hazard. Mater. 304 (2016) 532–542.

[45] X. Yan, D. Hu, H. Li, L. Li, X. Chong, Y. Wang, Nanostructure and optical properties of M doped ZnO (M= Ni, Mn) thin films prepared by sol–gel process,Physica B 406 (2011) 3956-3962.

[46] S. Yilmaz, S. Garry, E. Mc Glynn, E. Bacaksiz, Synthesis and characterization of Mn-doped ZnO nanorods grown in an ordered periodic honeycomb pattern using nanosphere lithography, Ceram. Int. 40 (2014) 7753-7759.

[47] B. Subash, B. Krishnakumar, R. Velmurungen, M. Swiminathan, M. Shanti, Synthesis of Ce co-doped Ag–ZnO photocatalyst with excellent performance for NBB dye degradation under natural sunlight illumination, Catal. Sci. Technol. 2 (2012) 2319-2326.

[48] R. Velmuragan, M. Swaminathan, An efficient nanostructured ZnO for dye sensitized degradation of Reactive Red 120 dye under solar light, Sol. Energy Mater. Sol. Cells 95 (2011) 942-950.

[49] K. Singh, D. Everett, R. Paul, L. Moscou, R. Pierotti, J. Rouquerol, T. Siemieniewska, Reporting physisorption data for gas/solid systems with special reference to the determination of surface area and porosity, Pure Appl. Chem. 57 (1985) 603-619.

[50] Y. Ou, J.D. Lin, H.M. Zou, D.W. Liao, Effects of surface modification of TiO_2 with ascorbic acid on photocatalytic decolorization of an azo dye reactions and mechanisms, J. Mol. Catal. A: Chem. 241 (2005) 59–64.

Supporting Information: Synthesis and enhanced photocatalytic activity of porous Mn-doped ZnO nanoparticles

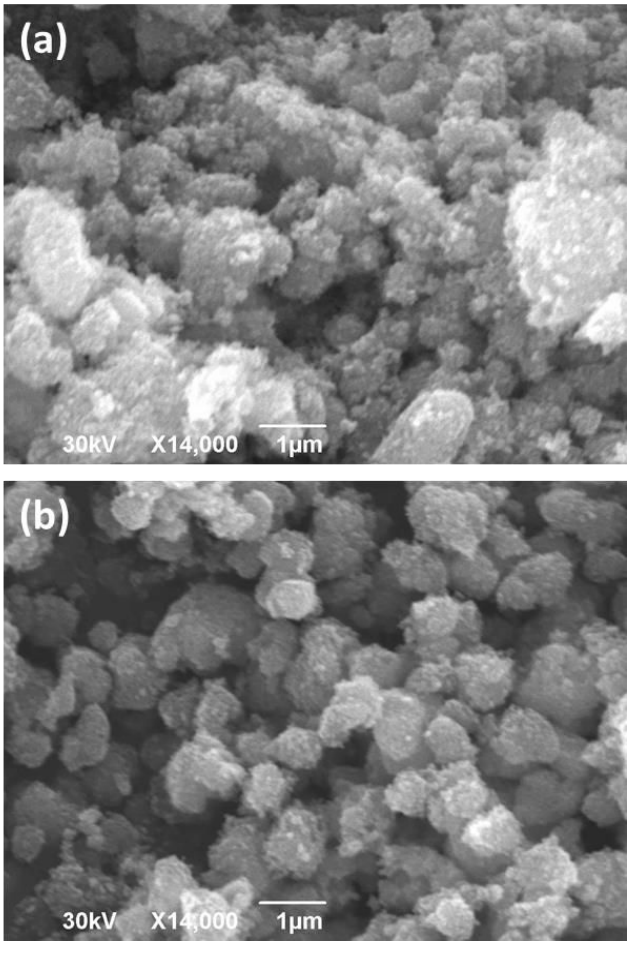

Figure 38: SEM images of (a) ZnO and (b) 3% Mn^{2+}- doped ZnO particles.

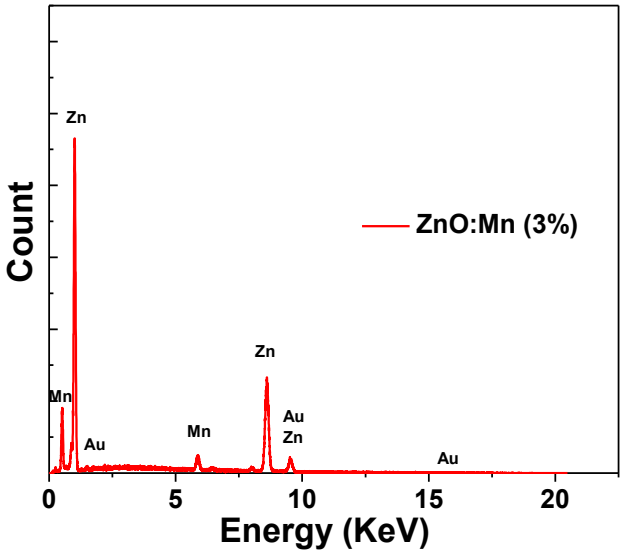

Figure 39: Energy dispersive X-ray spectrum of the 3% Mn^{2+}-doped ZnO particles.

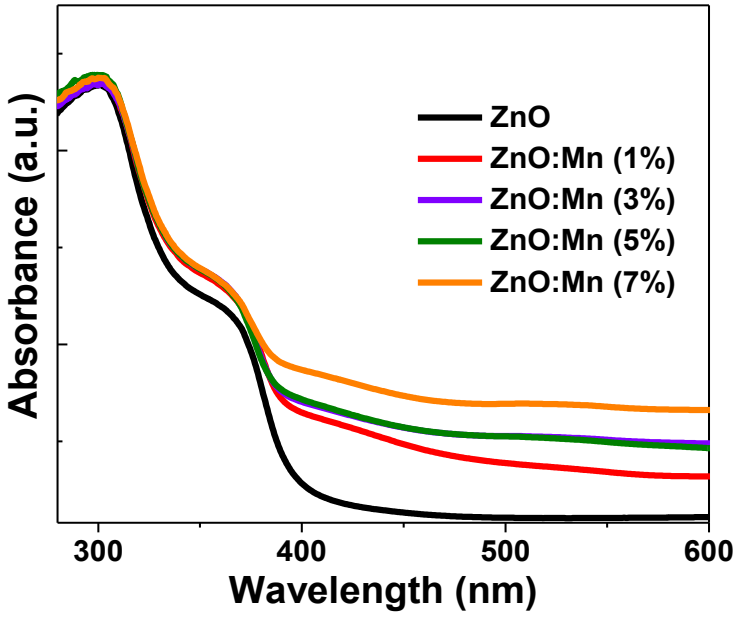

Figure 40: UV-visible absorption spectra of ZnO and Mn^{2+}- doped ZnO particles.

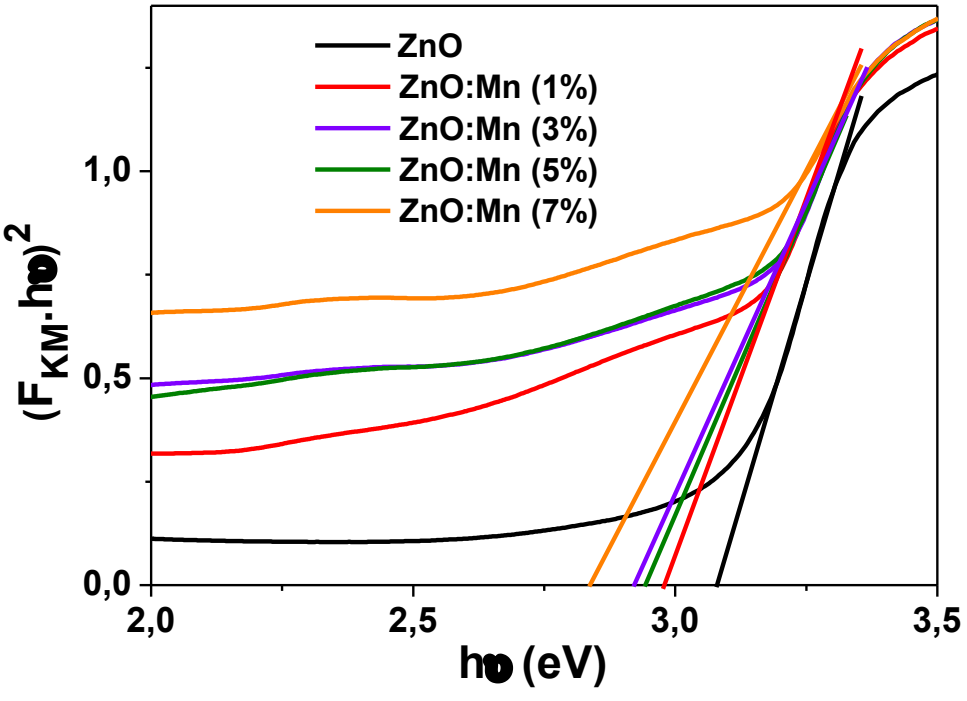

Figure 41: Kubelka-Munk plots of ZnO and Mn^{2+}- doped ZnO particles.

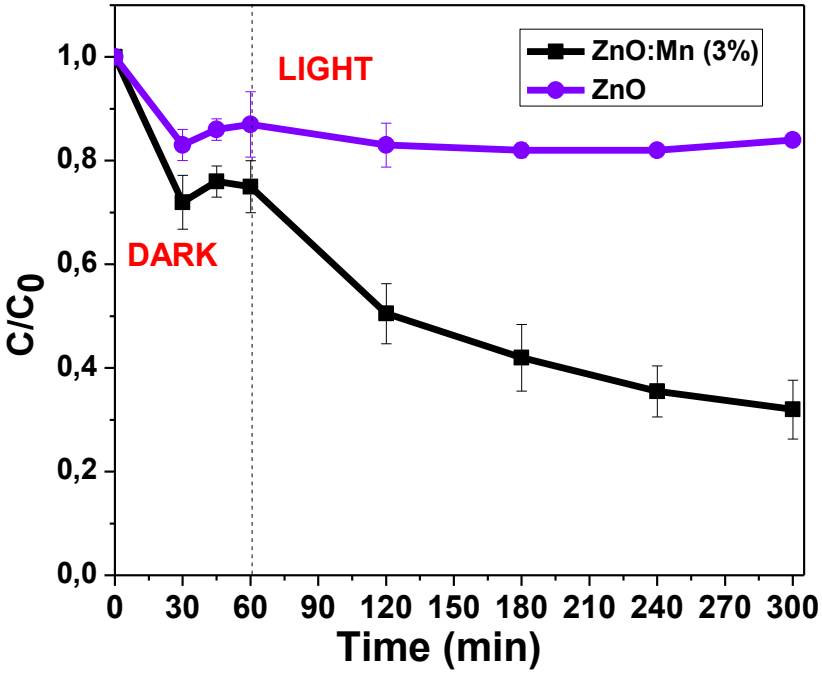

Figure 42: Photodegradation of Orange II under visible light irradiation (light fluence = 15 mW/ cm^2). C is the Orange II concentration at time t, and C_0 is the concentration of the dye at t = 0; Volume of solution, 30 mL; Mass of photocatalyst, 60 mg; Orange II concentration, 10 mg/L.

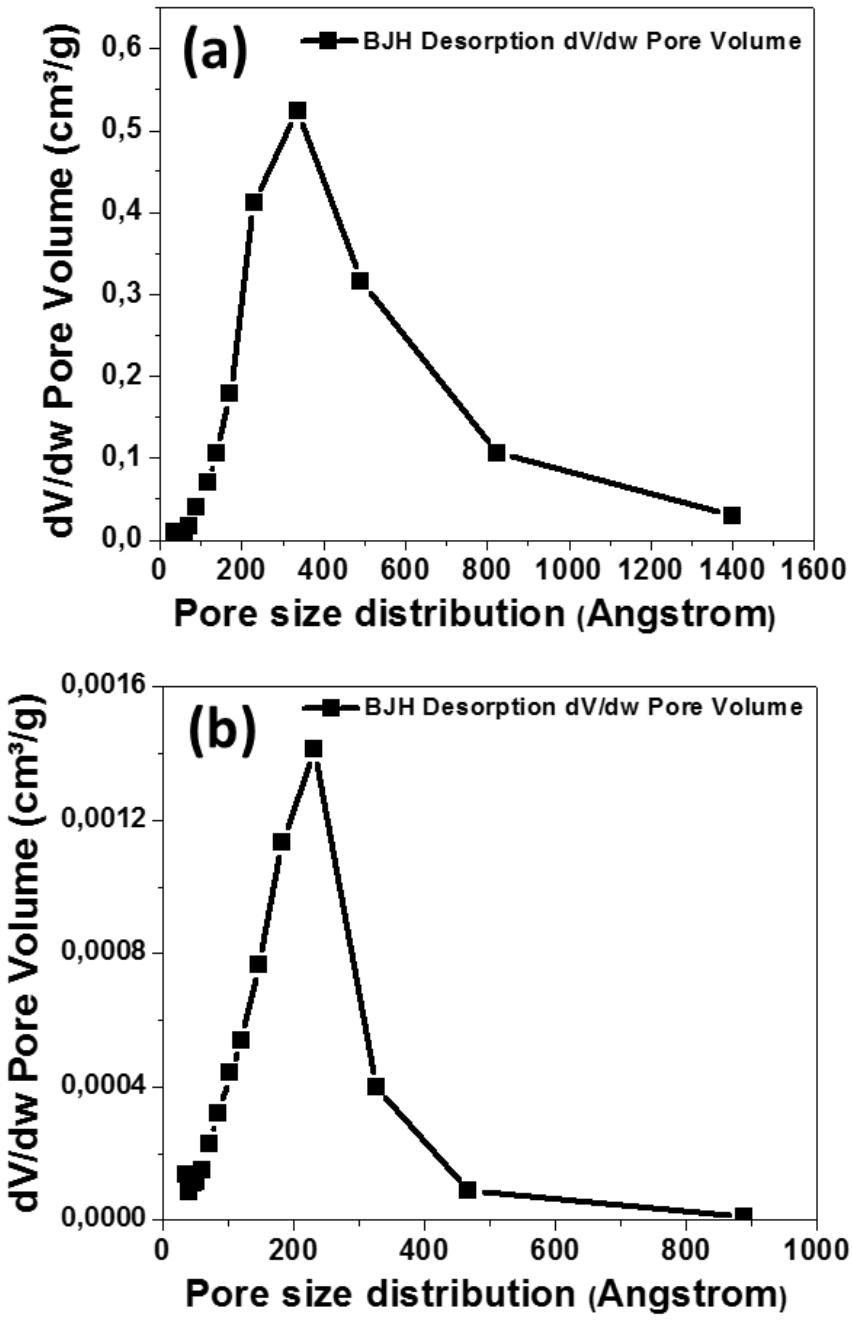

Figure 43: Pore size distribution of (a) ZnO and (b) ZnO: Mn (3%) particles during the adsorption phase.

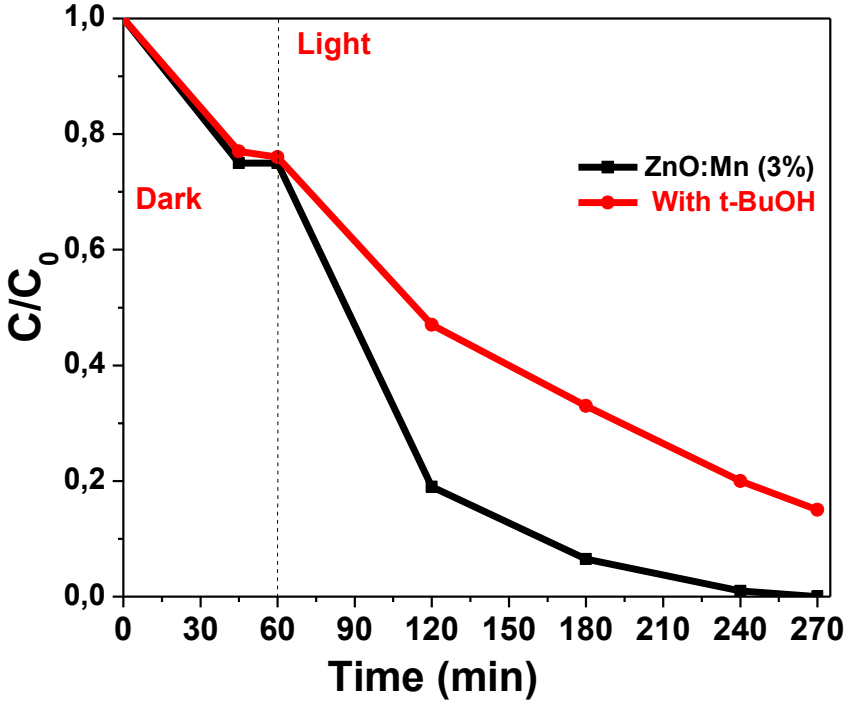

Figure 44: Influence of *t*-BuOH used as •OH scavenger on the photocalytic activity of the ZnO: Mn particles.

CHAPITRE III: *ZnO nanorods with high photocatalytic and antibacterial activity under solar light irradiation.*

Résumé

Dans ce chapitre, nous avons focalisé nos travaux sur la synthèse d'un nouveau catalyseur constitués de nanobâtonnets ZnO. Dans une première partie, la dégradation photocatalytique d'un polluant chimique « l'Orange II » et d'une souche bactérienne de référence *E. coli* MG 1655 a été réalisée avec un catalyseur en suspension ou immobilisé sous irradiation solaire.

Les résultats expérimentaux montrent un bon rendement de dégradation de l'Orange II lorsque le catalyseur est en suspenson ou immobilisé. L'utilisation du catalyseur dans plusieurs cycles de dégradation sans aucun traitement montre sa stabilité avec une faible perte d'efficacité.

L'inactivation photocatalytique d'*E. coli* MG 1655 montre une perte de cultivabilité assez importante avec le catalyseur en suspension ou immobilisé. La concentration du catalyseur immobilisé joue un rôle important dans l'inactivation bactérienne.

Dans une seconde partie, le mécanisme d'action des EROs générées par photocatalyse sur cette bactérie a été étudié par des analyses microscopiques en utilisant la microscope électronique à balayage (MEB), la microscopie à épifluorescence, la microscopie à force atomique AFM et la photoluminescence. Ces analyses montrent des dommages affectant la perméabilité membranaire ainsi que les protéines bactériennes. La cytométrie en flux montre que le matériel génétique n'est pas affecté lors du traitement photocatalytique.

Ces résultats font l'objet d'une publication en cours de soumission :

'Faouzi Achouri, Christophe Merlin, Serge Corbel, Halima Alem-Marchand, Laurence Mathieu, Lavinia Balan, Ghouti Medjahdi, Myriam Ben Said, Ahmed Ghrabi, Raphaël

Schneider. **ZnO nanorods with high photocatalytic and antibacterial activity under solar light irradiation.'**

CHAPITRE III: ZnO nanorods with high photocatalytic and antibacterial activity under solar light irradiation.

III.1 Introduction.

According to the World Health Organization, about 884 million people lack access to clean water and use sources microbiologically unsafe sources, which promotes a higher damage of exposures to waterborne diseases, including typhoid, hepatitis and cholera [1, 2]. With the growing demand in water, various strategies and solutions have been adopted to solve the problems of water pollution. Absorption and coagulation only concentrate the pollutants but provide no solution for their elimination [3]. Oxidation processes like ozonization and chlorination present limitations. Ozonization requires technical skills to install, is of high cost and induces the formation of harmful by-products for humans [4, 5]. Recent studies have demonstrated that chlorination induces the formation of potentially dangerous products such as trihalomethanes (THMs) and haloacetic acids (HAAs) that have mutagenic and carcinogenic effects on animals and humans [6, 7]. Moreover, some microorganisms are able to develop resistance to chlorine, thus requiring doses higher than those classically used [8, 9].

Heterogeneous photocatalysis is currently regarded as the most emerging advanced oxidation process (AOP). Once the semiconductor photocatalyst irradiated with light of energy equal or greater than its bandgap, electron/hole pairs are formed. These electrons and holes react respectively with oxygen and water molecules absorbed at the surface of the photocatalyst to generate reactive oxygen species (ROS) like superoxide ($O_2^{\bullet-}$) or hydroxyl ($^{\bullet}OH$) radicals, hydrogen peroxide (H_2O_2) or singlet oxygen ($^1O_2$) responsible of the oxidation of pollutants or for microorganisms disinfection. Zinc oxide (ZnO) is a wide bandgap semiconductor (Eg = 3.37 eV) with a large exciton binding energy (60 meV). Due to its highly attractive optical and electronic properties, ZnO has not only found applications in solar cells, optical coating, gas sensors or electrical devices [10-13] but also in photocatalysis both for the degradation of pollutants and for the damaging or disrupting of microorganisms like bacteria [14-16]. Another interest of ZnO, especially for photocatalytic applications, is that various nanostructures with different morphologies (spheres, rods, tubes, needles,…) can be engineered using relatively simple and mild methods (sol/gel, hydrothermal, solvothermal)

without any templates or surfactants. Among these nanostructures, ZnO nanorods (NRs) are of high interest for photocatalytic applications due to their high surface area [17-19]. Moreover, ZnO NRs prepared at low temperature exhibit higher photocatalytic activity than large ones due to the presence of defect sites that favor light absorption and hinder the electron/hole recombination. However, because such small particles are subject to agglomeration and/or difficult to recover from the reaction medium after photocatalysis but also to avoid the release of ZnO particles in water, immobilization of ZnO photocatalysts has recently gained interest [20-25].

In this paper, we report the preparation of ZnO NRs with an average length and a diameter of ca. 186 and 20 nm, respectively, and their successful immobilization on glass slides by a mild thermal treatment at 70 °C. The ability of ZnO NRs to produce reactive oxygen species (ROS), both in dispersed and immobilized forms, was first demonstrated for the photocatalytic degradation of the Orange II organic dye under simulated solar light irradiation. Moreover, the photocatalysts can be reused up to ten times without significant loss in catalytic activity. ZnO NRs also exhibited excellent activity toward the photo-inactivation of *Escherichia coli* cells (complete bacterial inhibition using dispersed ZnO NRs and 10-fold decrease of cell viability using immobilized ZnO NRs). The fluorescence of the Tryptophan aminoacid contained in *E. coli* proteins, epifluorescence microscopy, scanning electron microscopy (SEM) and atomic force microscopy (AFM) were used to monitor the damages caused by the photocatalytic treatment to *E. coli* cells. The results described in this paper demonstrate that ZnO NRs are a highly active and low cost photocatalyst with a real potential for water treatment.

III.2 Experimental section.

III.2.1 Materials.

$Zn(OAc)_2$. $2H_2O$ (> 98%, Sigma), Orange II sodium salt (> 85%, Sigma), sodium hydroxide (> 97%, Sigma), anhydrous methanol (Sigma) and absolute ethanol (HPLC Grade) were used as received without further purification. All solutions were prepared using Milli-Q water (18.2 MΩ.cm, Millipore) as solvent.

III.2.2 Synthesis of ZnO NRs and immobilization onto glass slides.

A sol-gel solvothermal processusing $Zn(OAc)_2$ as starting materialwas used to prepare ZnO NRs [26]. In a typical synthesis, $Zn(OAc)_2$. $2H_2O$ (7.37g, 3.35 mmol) was dissolved in 16

mL methanol, and NaOH (3.7 g, 9.25 mmol) was dispersed in 16 mL ethanol. Next, the NaOH solution was added dropwiseto the Zn $(OAc)_2.2\ H_2O$ solution and the mixture was stirred for 72 h at 60 °C. After cooling to room temperature, the ZnO NRs were collected by centrifugation, washed three times with water, two times with ethanol, and dried at 50°C overnight.

To fix ZnO NRs onto microscope glass slides, 200 mg of the photocatalyst were dispersed in 50 mL of demineralized water and drops of this dispersion were deposited onto glass slides followed by drying at 70°C. This operation was repeated until the appropriate mass of catalyst and homogeneous layers were obtained. For photocatalytic experiments conducted with the Orange II dye, 148.5 mg of ZnO NRs were deposited onto 10 glass slides of a total area of 87.5 cm^2.

For experiments conducted with the bacteria *E. coli*, 260 mg ZnO NRs were deposited onto 10 microscope glass slides (5 of these slides were used for photocatalytic experiments and the other 5 for control experiments conducted in the dark).

III.2.3 Characterizations

Transmission electron microscopy (TEM) images were taken by placing a drop of the particles dispersed in methanol onto a carbon film-supported copper grid. Samples were studied using a Philips CM200 instrument operating at 200 kV. Scanning electron microscopy (SEM) pictures were prepared using JEOL Scanning Electron Microscope JSM-6490 LV. The X-ray powder diffraction (XRD) diagrams of all samples were measured using PanalyticalX'Pert Pro MPD diffractometer using Cu Kα radiation. The X-ray powder diffraction data were collected from an X'Pert MPD diffractometer (Panalytical AXS) with a goniometer radius 240 mm; fixed divergence slit module (1/2° divergence slit, 0.04 rdSollers slits) and an X'Celerator as a detector. The powder samples were placed on a silicon zero-background sample holder and the XRD patterns were recorded at room temperature using Cu K_α radiation (λ = 0.15418 nm). All the optical measurements were performed at room temperature (20 ± 1°C) under ambient conditions. Absorption spectra of liquid samples were recorded on a Thermo Scientific Evolution 220 UV-visible spectrophotometer.Photoluminescence (PL) spectra were recorded on a Horiba Fluoromax-4 Jobin Yvon spectrofluorimeter. The diffuse reflectance absorption spectra (DRS) were recorded on a Shimadzu 2600 UV-visible spectrophotometer. $BaSO_4$ powder was used as a standard for baseline measurements and spectra were recorded in a range of 250-1400 nm.

III.2.4 Photocatalytic degradation of Orange II.

The photocatalytic activity of ZnO NRs was evaluated by the degradation of an aqueous solution of the Orange II dye (10 mg/L) at room temperature under simulated solar light irradiation produced by Sylvania LuxLine FHO T5 neon tubes. The irradiation intensity was estimated to be 5.5 mW/cm^2.

In the case of dispersed ZnO NRs, the photocatalyst (40 mg) were dispersed in 40 mL Orange II aqueous solution (10 mg/L) and the suspension was magnetically stirred under ambient conditions for 30 min in the dark to achieve an adsorption-desorption equilibrium. Under stirring, the suspension was exposed to light irradiation. At certain time intervals, 1 mL of the suspension was extracted and centrifuged (15000 rpm for 2 min) to remove the photocatalyst. The degradation process was monitored by measuring the absorption of Orange II at 485 nm using a UV-visible absorption spectrometer.

For experiments conducted with fixed ZnO NRs, 10 glass slides covered by 148.5 mg of photocatalyst fixed on 10 glass slides is introduced in a petri glass dish and covered by 60 mL of the Orange II aqueous solution (10 mg/L). The Orange II photodegradation was monitored as previously described for dispersed ZnO NRs.

III.2.5 Preparation of bacterial strains and growth media

The *E. coli* strain MG 1655 was used as model for all photocatalytic inactivation tests. This laboratory strain is non-pathogenic and extensively studied for laboratory research. The bacteria was routinely cultured in Lysogenic Broth (LB) (LB Broth Miller, Difco™),at 37°C under aerobic conditions with constant stirring at 160 rpm. Bacterial growth was monitored by measuring the optical density of the cultures at 600 nm (OD_{600}). For NRs toxicity testing, bacteria were cultured up to early stationary phase (DO_{600} = 0.4, CFU/mL = 10^9), collected by centrifugation at 9000g for 4 min and washed twice with sterile demineralized water. Finally, cell pellets were re-suspended insaline buffer (0.85%) and cell density was adjusted to 10^6 and 5.10^5 units forming colony per mL (CFU/mL) per photocatalytic experiments conducted with dispersed and immobilized ZnO NRs, respectively.

III.2.6 Photocatalytic inactivation process

Before each experiment, materials and water were autoclaved at 121°C for 15 min. The experiments were conducted under sterile hood and in sterile beaker of 100 mL. For each

experiment, four conditions were used: with and without photocatalyst, and with and without light irradiation.

For the dispersed photocalyst: 20 mL of *E. coli* MG1655 cells suspension (CFU/mL = 10^6) were mixed with 20 mg of ZnO NRs (concentration 1g/L). For photocatalytic experiments, the bacteria and ZnO NRs mixture was irradiated for 3h with constant magnetic stirring. Serial dilutions were performed in demineralized water and aliquots were plated on LB agar for 24h at 37°C for an estimation viable cultivable cells. Each experiment was repeated three times to confirm the reproducibility.

For the immobilized photocatalyst: 260 mg of ZnO NRs are dispersed in 60 mL of demineralized water and immobilized on ten glass slides by drying at 70°C. Five of these slides were used for the control experiments conducted in the dark and five for photocatalytic experiments. In each experiment, 50 mL of the bacterial suspension (CFU/mL = 5 x 10^5) were introduced into a petri dish (ID = 120mm) containing the glass slides, which was illuminated as previously described.

III.2.7 Fluorescence spectroscopy measurements

To estimate the damages on bacteria proteins during photocatalytic experiments, the tryptophan (Trp) fluorescence emission at 331 nm was measured after an excitation at 295 nm. Bacteria samples were taken during the photocatalytic reaction and the fluorescence was measured directly after vortexing.

III.2.8 Counting of cells and study of damage on bacterial permeability

Bacterial cell counts were determined microscopically after Sybr Green and propidium iodide (PI) staining. Cell suspensions (2 mL) were stained (Sybr-II 10x and 0.6 mM PI) for 15 min in the dark before being filtered through a 25 mm diameter, 0.2 µm pore-size black polycarbonate membrane (Nucleopore), air dried, and mounted in mounting oil (Citifluor). Cell counts were carried out with an epifluorescence microscope (BX40, Olympus) equipped with a ×100 immersion objective lens, a 470–490 nm excitation filter, and a 520 nm barrier filter. Undamaged cells ($Sybr^+$green-stained cells) and membrane-damaged cells (PI^+red-stained cells) were enumerated using 60 randomly chosen fields.

III.2.9 Flow Cytometry

Cells suspensions were washed and resuspended as before but in a 0.85% NaCl saline buffer filtered before hand (0.2 µm) to limit contaminating particles. Cells were subsequently stained

(or not) with SybrII (10x for 15 min) and analyzed by flow cytometry (BD Accuri™) equipped with a 50 mW laser emitting at a fixed wavelength of 488 nm. Fluorescence intensity was collected at FL2 channel (λ_{em}: 510±15 nm), as well as sideward (SSC) and forward (FSC) scattered light intensities. The FCM is equipped with volumetric counting hardware and measurements were performed at pre-set flow rate of 35 mL/min. A threshold value of 2000 was applied on the FSC. The signal was narrowed to fluorescent cells by an electronic gating to separate positive signals (stained cells) from background thus limiting the SSC to the signal provided by a pure cell suspension and excluding the parasite signal obtained NaCl buffer alone (with or without ZnO NRs exposure; Supporting information).Unless stated otherwise, the instrument settings and electronic gates were kept the same for all samples in order to achieve comparable data. Event counts provide an estimation of the total cell amount (dead or alive) while the stability of the mean fluorescence reflects the integrity of the intracellular DNA.

III.2.10 SEM experiments on *E. coli* cells

During the photocatalytic inactivation test of *E. coli* strain MG 1655, samples of the cell suspension were centrifuged to remove NaCl and then fixed with 2.5% glutaraldehyde (2h) after what, washed the cells were subsequently dehydrated through a graded series of ethanol solutions (37%, 67%, 95% and 100%) for 15 min. Scanning electron microscopy (SEM) pictures were prepared using JEOL Scanning Electron Microscope JSM-6490 LV.

III.2.11 AFM experiments on *E. coli* cells

The *E. coli* MG 1655 cell morphology was characterized by atomic force microscopy (AFM) in intermittent-contact mode (Tapping mode) on Asylum Research MFP-3D Infinity™ equipped with a 100 µm close-loop scanner. Pointprobes robes (Asylum Research) were used. The cantilevers had a resonance frequency around 270 kHz and spring constant values around 26 $N.m^{-1}$. Images were acquired in air at ambient temperature with drive amplitude of 15 mV and an attenuation set-point of 0.8 to 0.7. At least five different zones were scanned on each sample and images at different magnification were acquired (we only show the5 x 5 µm² and 1 x 1 µm² images). The images were treated and analyzed using procedures developed under Igor Pro (Wavemetrics) by Asylum software.

III.3 Results and discussion

III.3.1 Synthesis and characterization of ZnO NRs

ZnO NRs were prepared via a sol-gel process by treatment of $Zn(OAc)_2$ with NaOH in ethanol [26]. Fig. 45a shows the X-ray diffraction pattern of the NRs obtained after 72 h heating at 60°C.All diffraction peaks are intense and narrow which indicates that the NRs are highly crystalline. All peaks correspond to the hexagonal wurtzite structure of ZnO with cell constants of a = 3.251 Åand c = 5.208 Å (JCPDS Card No. 36-1451) and no impurities were detected. SEM and TEM data collected for the same nanocrystals are shown in Figure 45b-c. Analysis of ca. 100 particles indicates that the ZnO NRs have an average length of 186 nm and a diameter of ca. 20 nm and that their size distribution is relatively narrow. The high crystallinity of the particles is further evidenced from the selected area electron diffraction (SAED) pattern shown in the inset of Fig. 45c and from the HR-TEM image which shows continuous lattice fringes through the whole particle (Fig. 45d). The interplanar spacing is 0.26 nm and corresponds well to the (002) plane of wurtzite ZnO.

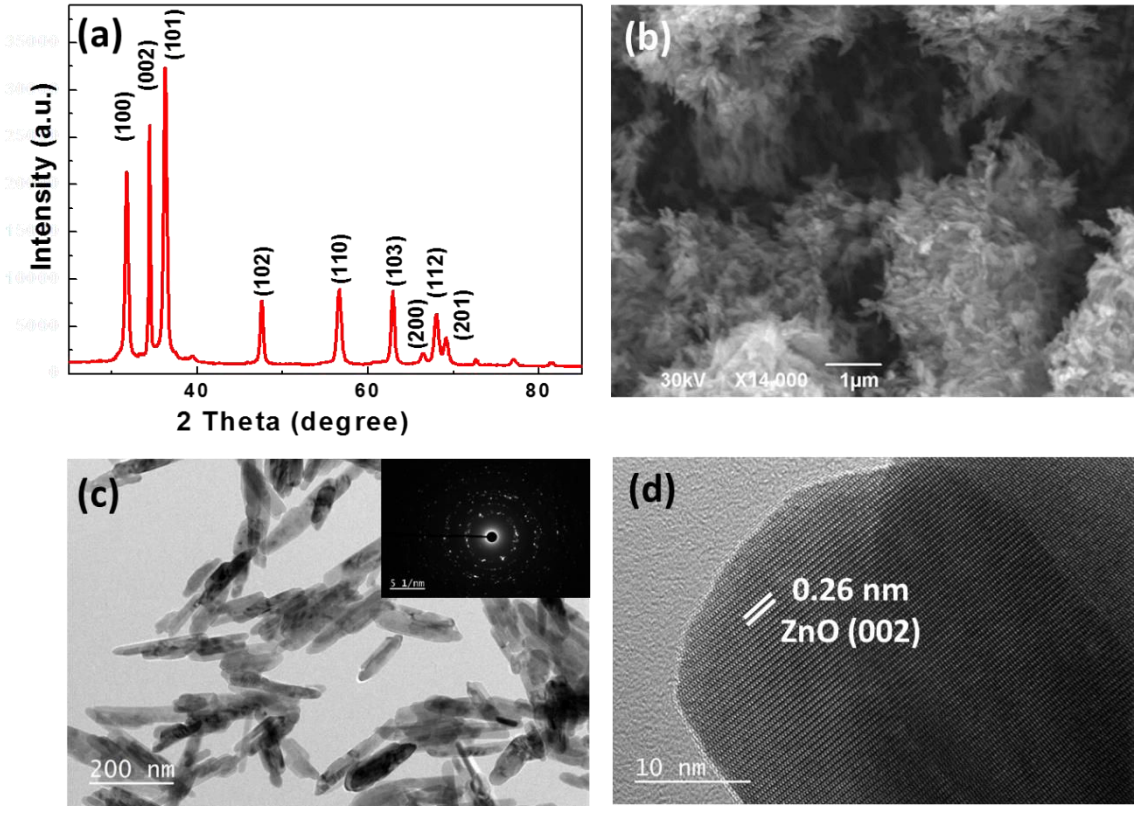

Figure 45: (a) X-ray diffraction pattern, (b) SEM and (c-d) TEM images of the ZnO NRs (the inset of Fig. 1c is the SAED pattern of ZnO NRs).

For practical photocatalytic applications and to easily reuse the photocatalyst without separation via centrifugation or filtration, the ZnO material was immobilized on microscope glass slides. For that purpose, an aqueous solution of the ZnO NRs was deposited on glass slides followed by thermal treatment at 70°C for 12 h. The SEM images of the immobilized catalyst demonstrate the size and morphology of the NRs were not altered by that treatment (Fig. 46a). The thickness of the ZnO NRs layer deposited was estimated of be of ca. 650 µm (Fig. 46b).

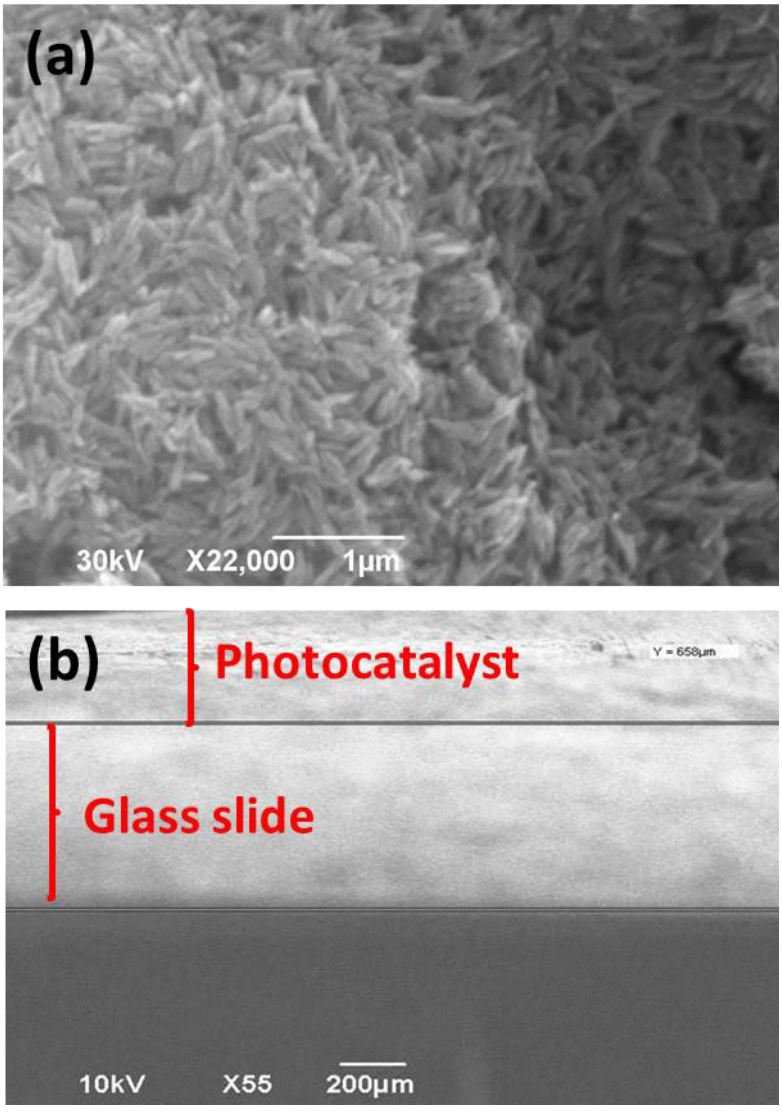

Figure 46: SEM images of the immobilized ZnO photocatalyst (a) top view and (b) cross sectional view.

III.3.2 Photocatalytic degradation of Orange II

The photocatalytic efficiency of the ZnO NRs used either as powder or as films was first evaluated in the degradation of the 10 mg/L solution of Orange II dye under sunlight irradiation (5.5 mW/cm^2). For experiments conducted with the ZnO NRs as powder, the photocatalyst (40 mg) was dispersed in 40 mL of the Orange II aqueous solution. For the

immobilized catalyst, 148.5 mg of the ZnO NRs were deposited on glass slides (with a surface of 87.5 cm^2) and the slides immersed into 60 mL of the Orange II solution.

Preliminary blank experiments demonstrated that in the absence of the catalyst, no bleaching of the dye was observed after 5 h of irradiation. Once the photocatalyst is added and after reaching of the adsorption-desorption equilibrium (ca. 30 min), a gradual decrease in the dye absorption at 484 nm was observed as a function of the irradiation time (Fig. 57). The complete disappearance of Orange II was obtained after 150 min with the ZnO NRs used as powder and in 210 min with the immobilized photocatalyst (Fig. 47a). The efficiencies of Orange II degradation by ZnO NRs were determined quantitatively using the pseudo-first-order model $\ln(C/C_0) = -kt$, where k is the apparent rate constant (min^{-1}) and C_0 and C are the concentrations of Orange II at time 0 and t, respectively (Fig. 47b). The rate constants k determined for the bleaching of the 10 mg/L dye solution were found to be 0.016 and 0.004 min^{-1} for ZnO NRs used as powder and immobilized, respectively (results were normalized relative to the mass of ZnO NRs and to the volume of the Orange II solution). The highest photocatalytic activity observed for the dispersed catalyst originates from the decreased specific surface of the immobilized ZnO NRs and thus from thereduced probability of contact between the dye and the photocatalyst as previously observed in other studies [27.28].

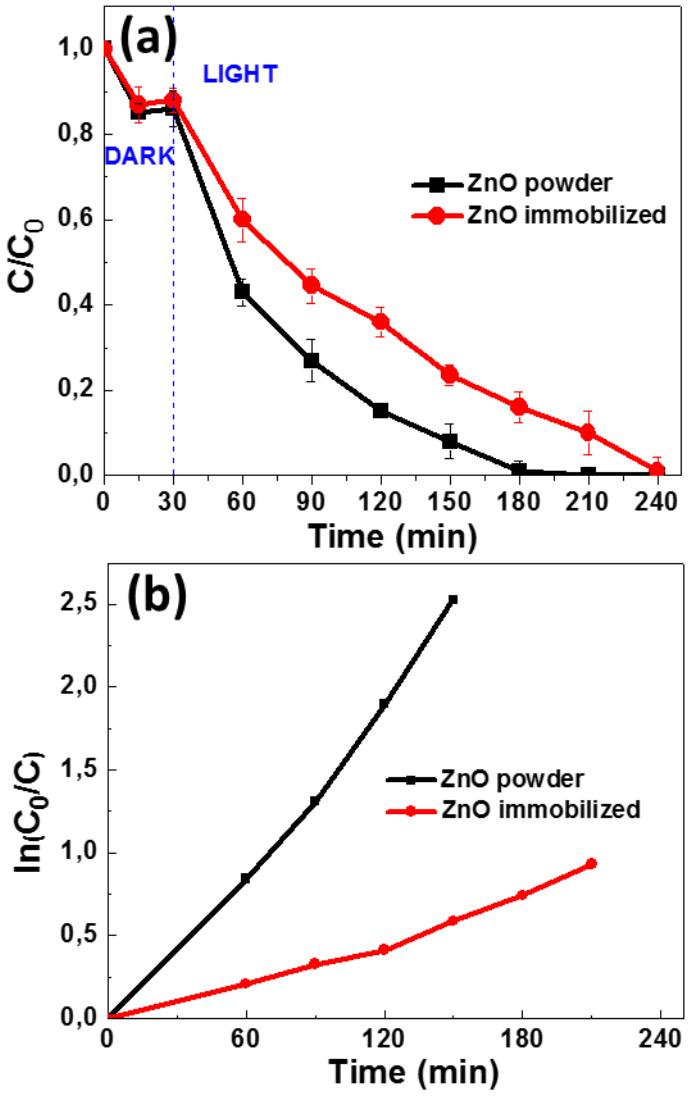

Figure 47: (a) Variation of Orange II concentration as a function of irradiation time (C is the Orange II concentration at time t, and C_0 is the concentration of the dye at t = 0). (b) Plots of ln (C_0/C) of Orange II versus reaction time for the ZnO photocatalyst used as powder or deposited on glass slides (results were normalized relative to the mass of ZnO NRs and to the volume of the Orange II solution used in photocatalytic experiments).

The stability and the reusability of the photocatalyst were investigated using the immobilized ZnO NRs without anyof washing or drying treatment between two runs (Fig. 48). As can be seen, no significant decrease of catalytic activity could be observed during the ten successive cycles of Orange II degradation under light irradiation (5.5 mW/cm^2). Moreover, XRD and

SEM experiments demonstrate that the crystallinity and the morphology of deposited particles were not altered during the repeated photocatalytic experiments (Fig. 58 and 59).

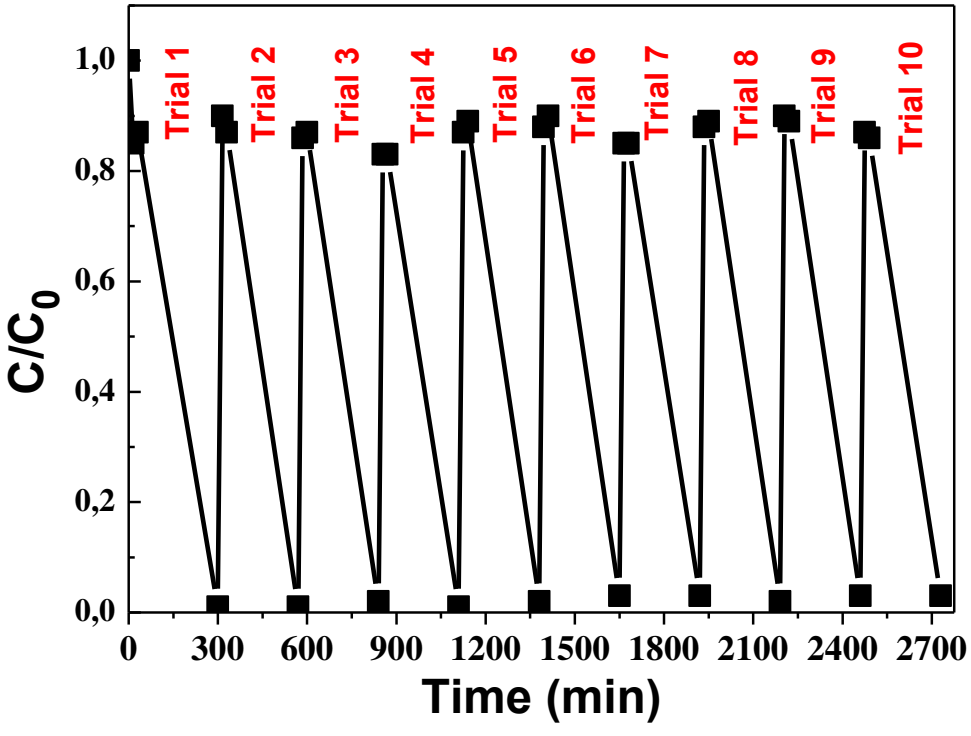

Figure 48: Recyclability of ZnO NRs fixed on glass slides. Experiments were performed under light irradiation (5.5 mW/cm^2) and with an initial Orange II concentration of 10 mg/L.

III.3.3 Photocatalytic inactivation of *E. coli* MG 1655.

Fig. 49 shows the bacterial inactivation of *E. coli* MG1655 under light irradiation (5.5 mW/cm^2) using dispersed and fixed photocatalysts. Control experiments (light irradiation in the absence of the photocatalyst and the photocatalyst used in the dark) are also provided for comparison. Simulated solar light irradiation has no effect on the *E. coli* MG1655 inactivation in the absence of photocatalyst despite the artificial sunlight contains 4-5% of UV that may induce cellular damages.

Dispersed and immobilized ZnO NRs used in the dark induce a 10-fold and 3-fold decrease of cell viability after 3 h, respectively, thus indicating that these particles were toxic to bacterial

cells even without light activation. These results are in good agreement with previous reports that demonstrated that ZnO particles are toxic to bacterial cells in the dark. This toxicity may originate from the electrostatic interaction between the positively charged ZnO NRs with the negatively charged bacterial surface components (at neutral pH) [29-31].

The rates of bacterial inactivation were markedly improved when ZnO NRs were used under light irradiation and when increasing the irradiation time (Fig. 49). For example, after 2 h photocatalysis, the bacterial survival kinetics shows a decrease in the number of cells from 1 x 10^6 CFU/mL to 1 x 10^2 CFU/mL. After 3 h irradiation, the bacterial inhibition was complete with dispersed ZnO rods and decrease ca. 25-fold with fixed ZnO NRs. As previously observed with the Orange II dye, the photocatalytic activity of the fixed catalyst is lower than that of the dispersed ZnO NRs. Several studies have demonstrated that the bacterial inactivation by photocatalysis originates from the oxidative stress generated by the production of ROS like hydroxyl $OH^{\bullet}$ and superoxide $O_2^{\bullet-}$ radicals, H_2O_2 and $^1O_2$ during the irradiation of ZnO with light [32, 33]. These ROS are responsible for the oxidation of several cellular components [34], like lipids [27], proteins [35] and DNA [36]. The stability of the fixed photocatalyst during repeated bacterial inactivation was also evaluated. The same catalyst was successfully reused for five photocatalytic cycles after a simple washing with demineralized water (Fig. 60 supporting information).

We also evaluated the influence of the amount of ZnO NRs fixed onto the glass slides on the photocatalytic activity (Fig. 61 supporting information). Actually, the amount of catalyst used is a key parameter in photocatalytic experiments because the pollutants or microorganisms have to adsorb on the surface of the photocatalyst to be degraded. When two glass slides (covered by 52 mg ZnO NRs) were used instead of five slides (covered by ca. 130 mg ZnO NRs), the bacterial inactivation was reduced by ca. 10-fold, thus highlighting the key role played by the active surface of the catalyst.

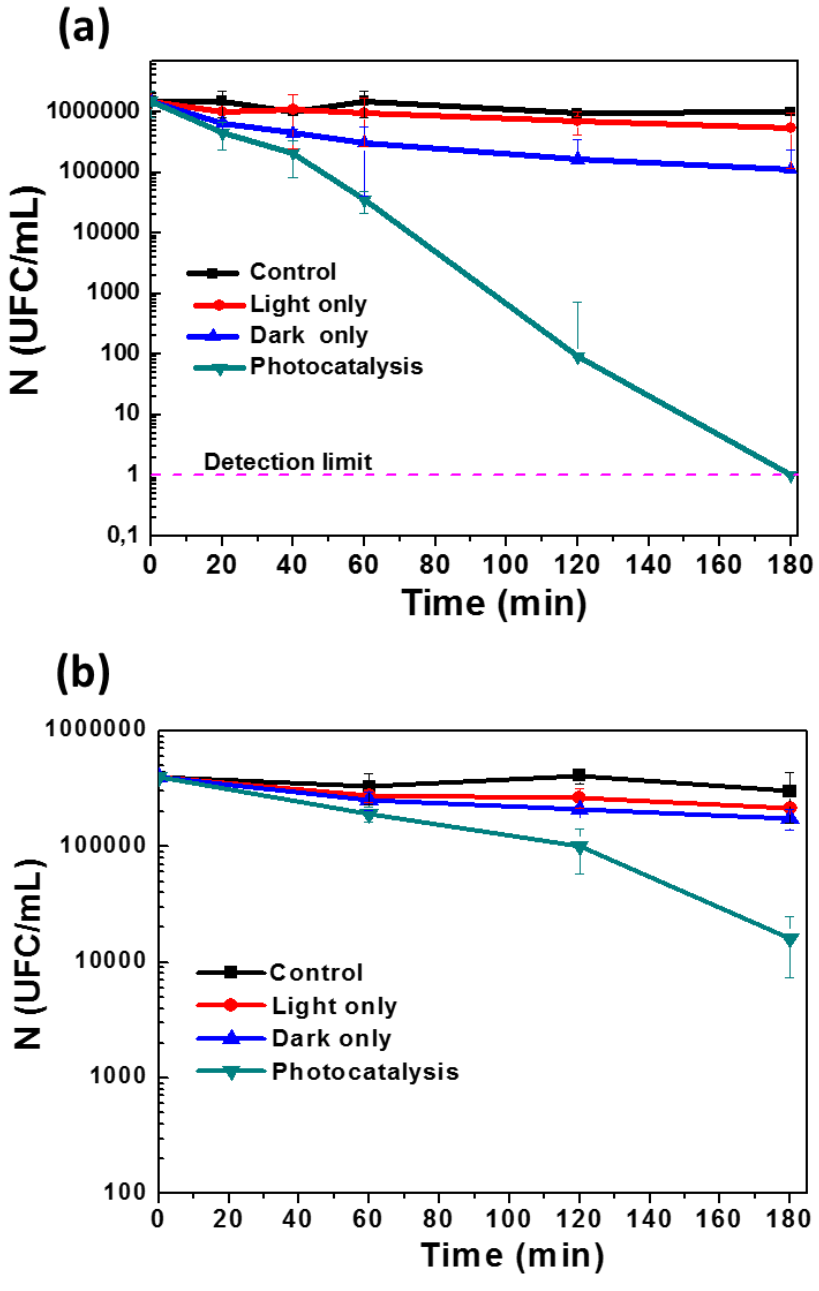

Figure 49: *E. coli* MG1655 inactivation by photocatalysis using (a) dispersed and (b) fixed ZnO NRs.

III.3.4 Bacterial damages induced by the photocatalytic treatment

To understand the photocatalytic effects on the loss of bacterial cultivability/viability, we first conducted fluorescence experiments to monitor the evolution of tryptophan (Trp) unit of the bacteria proteins (located at ca. 331 nm after excitation at 295 nm) during photocatalytic

experiments [37]. As can be seen, the fluorescence intensity of Trp decreases by ca. 3.5-fold and 2-fold during photocatalytic experiments conducted with dispersed and fixed ZnO NRs, respectively, indicating damages/denaturation to the proteins containing the Trp amino acid. The time evolution of Trp fluorescence and of the bacterial cultivability observed after the photocatalytic experiments demonstrate that the damages caused to bacterial proteins are, at least partly, responsible of their inactivation (Fig. 50 b and 50d). These results are in good accordance with those obtained using the 2D SDS–PAGE technique, which demonstrated that during the photocatalytic treatment, bacterial proteins in whole cells or in the membranes are damaged, thus leading to the inactivation of cells and consequently to their death [38].

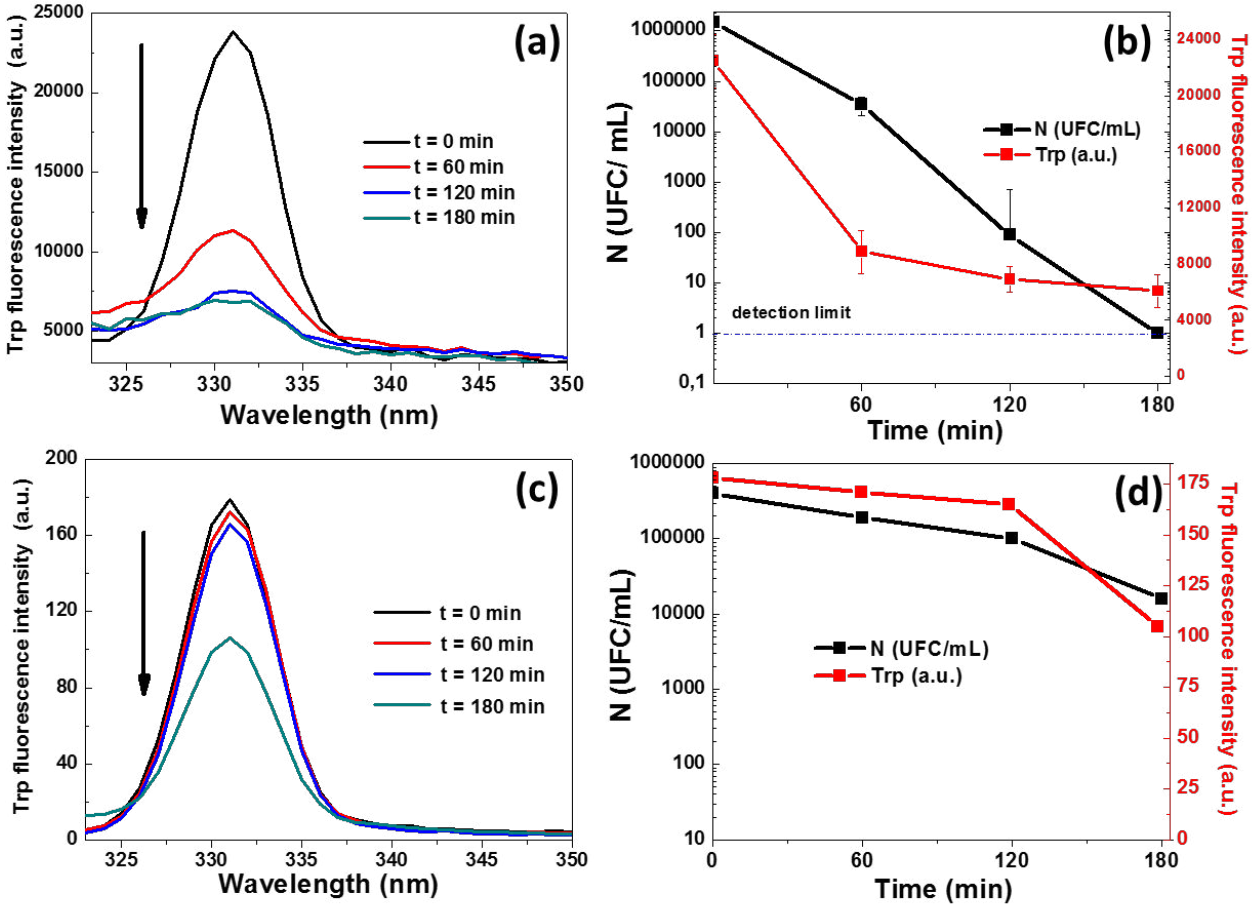

Figure 50: (a, c) Trp fluorescence spectraduring photocatalytic experiments and (b,d) time evolution of Trp fluorescence and bacterial cultivability during photocatalytic experiments with (a,b) dispersed and (c,d) fixed ZnO NRs.

Next, a series of experiments using epifluorescence microscopy was performed to analyze the changes induced on the bacterial cell membrane permeability during the photocatalytic treatment. These experiences are based on the dual labeling of bacterial DNA with Sybr-II and propidium iodide (PI) fluorochromes that differ both in their spectral characteristics and their ability to cross cell membranes (PI can enter the cell only when the membrane has been damaged). Membrane damages where estimated on cell suspensions in saline buffer, bacteria, with and without exposure to light, and with and without exposure to ZnO NRs (Fig. 51).

First, no significant effects on membrane integrity could be detected in control experiments (bacteria in saline buffer (Fig. 62b-c, supporting information) and 1 or 3 h exposition of the bacterial suspensions to artificial sunlight (Fig. 62 d-e, supporting information). The red labelled cells observed on epifluorescence microscopy images may originate from the preparation of the suspensions by centrifugation. No significant damages to bacterial permeability were observed when exposing the bacteria to the fixed ZnO NRs in the darkness (Fig. 62f-g, supporting information). However, after 1h and especially after 3 h of photocatalytic treatment, a marked decrease of bacterial membrane permeability was detected. These results are in good accordance with bacterial cultivability monitoring and with the degradation of proteins previously described (Fig. 49 and 50). Several studies have shown that the outer membrane is the first target of ROS generated in the surface of the illuminated photocatalyst [39, 40]. ROS can attack the fatty acids and polyunsaturated lipids in the cell membrane through the lipid peroxidation process, thus inducing a decrease of the membrane fluidity and of its integrity [41].

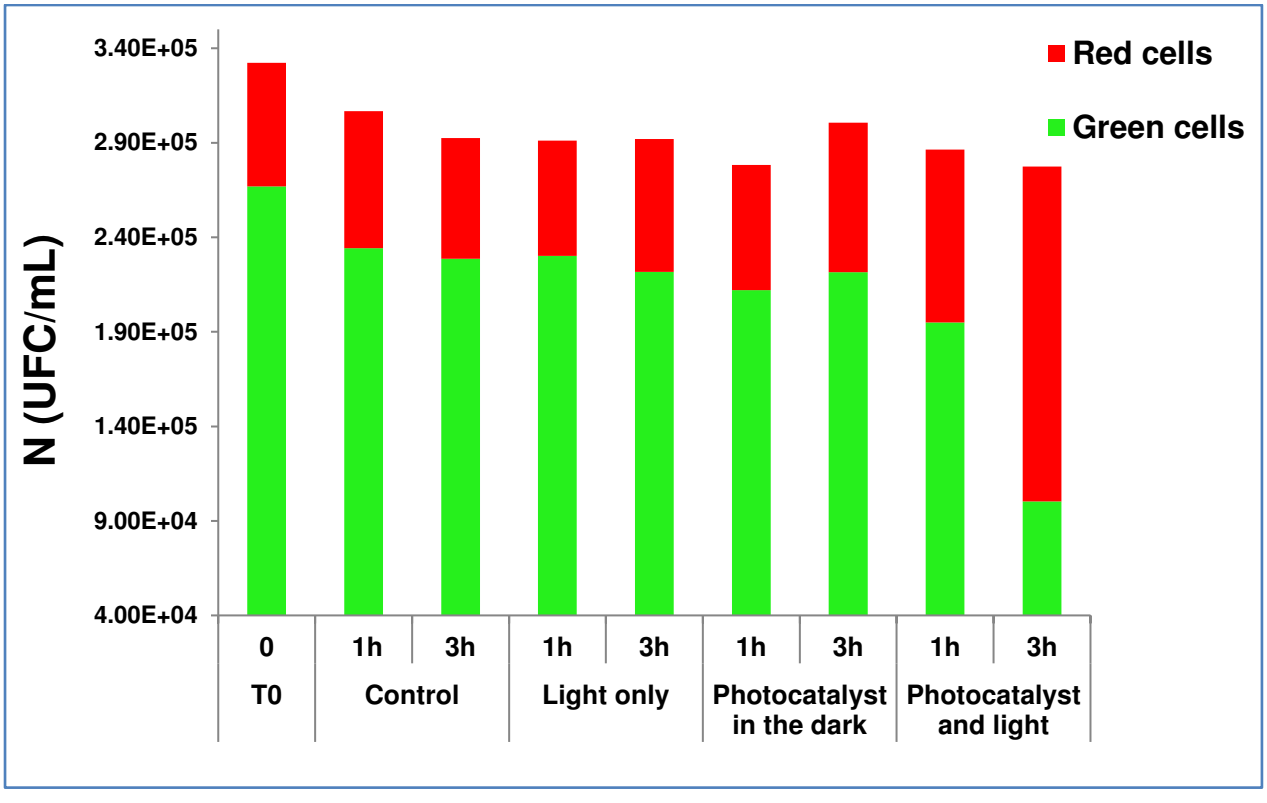

Figure 51: (a) Number of bacterial cells detected by epifluorescence microscopy after Sybr-II and PI staining.

III.3.5 Flow Cytometry Results

E. coli cell suspensions were analyzed by flow cytometry after exposure (or not) to ZnO NRs, and with or without light irradiation (Fig. 52 and 63 supporting information). Cell counts indicated that the loss of cultivability is not accompanied by a reduction of the total cell number, therefore suggesting that the photocatalysis-generated damages are not severe enough to disrupt the bacterial cells. Moreover, the analysis of the mean fluorescence intensity obtained on the FL2 channel showed a relatively stable DNA staining, which signify that the intracellular nucleic acid were not altered enough to limit the binding of the stain. All together, these results demonstrate that the photocatalysis mostly injured surface structures on *E. coli* cell, which results in fragile cells that progressively lost their viability while inner biomolecule such as DNA kept their staining properties therefore limiting the ZnO NRs effect to outer cell component at this level of photocatalysis.

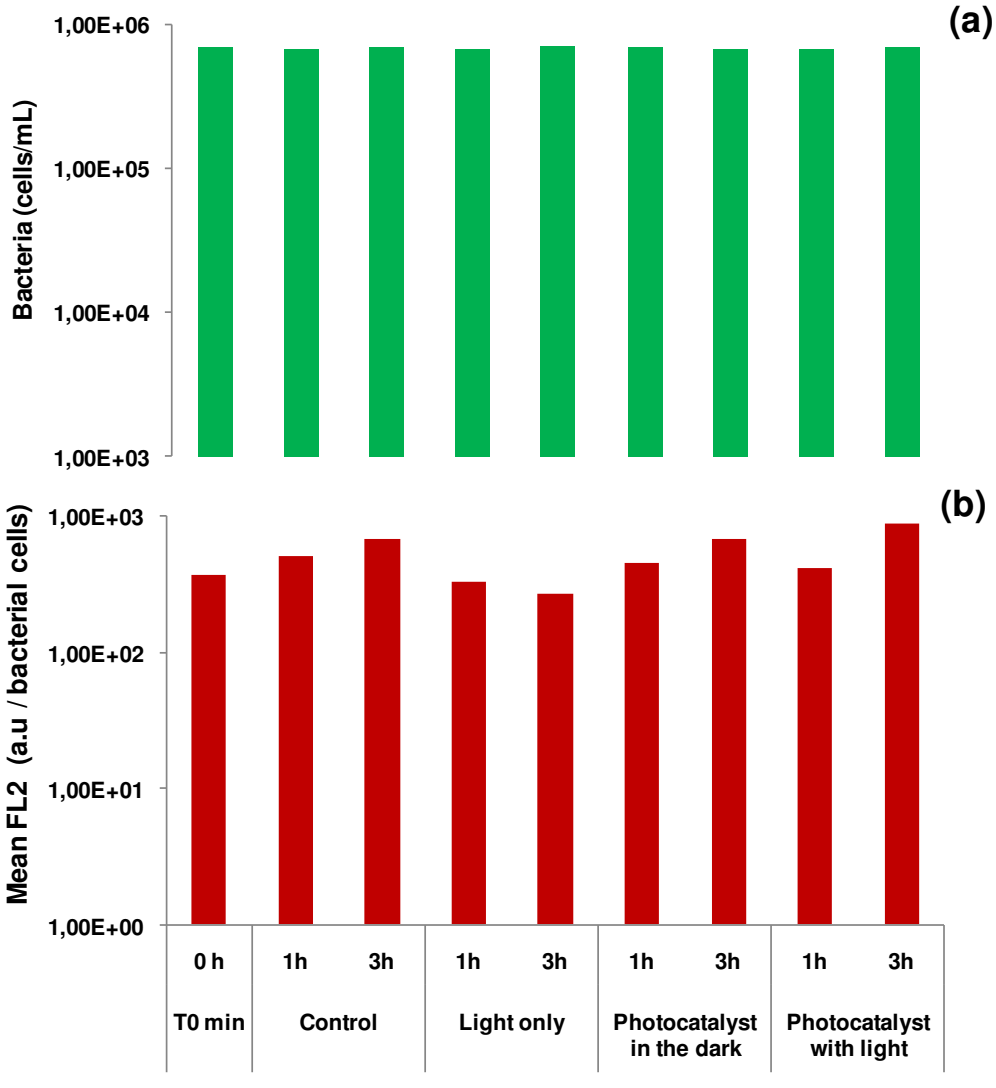

Figure 52: (a) Number of bacterial cells detected by flow cytometry after Sybr-II staining and (b) mean fluorescence intensity (FL2) of the Sybr-II fluorochrom per cells.

III.3.6 SEM and AFM results.

Next, the morphological alterations of *E. Coli* cells (10^8 CFU/mL) exposed to ZnO NRs and to light irradiation wereexamined by SEM. Control *E. coli* cells are rod-shaped cells with anaverage size varying between 1 and 2 µm and their surfaces are continuous and damage-free (data not shown). After 1.5 or 3 h of contact with the ZnO NRs in the dark, it can be observed that the outer membrane of numerous *E. coli* cells was damaged and that rumples appear (Fig. 53a-b). After 1.5 h of photocatalytic treatment (Fig. 53c) and especially after 3 h (Fig. 53d), the outer membrane of the cell is clearly damaged and cells alterations are

pronounced. After 3 h of photocatalytic treatment, all cells are affected, pits and holes appear in the cell walls and the cell sizes decrease. These results are in accordance with previous reports and confirm that the attack of ROS on the cell wall and/or cell membrane occurs in the primary step of the photocatalytic treatment.

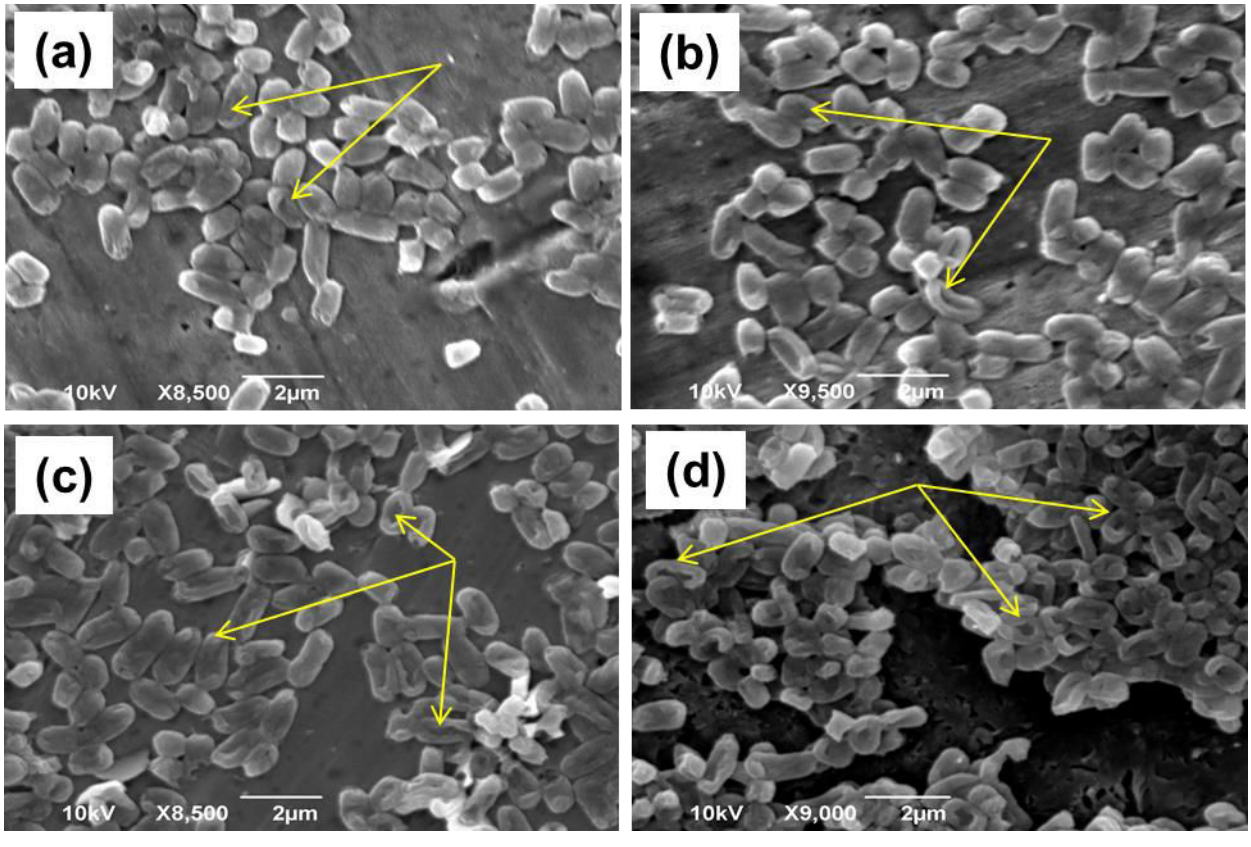

Figure 53: SEM images of *E. coli* MG1655 bacteria (a-b) exposed to the photocatalyst in the darkness for 1.5 and 3 h, respectively, and (c-d) exposed to the photocatalyst under light irradiation (5.5 mW/cm^2) for 1.5 and 3 h, respectively.

AFM microscopy was also carried out to get more information on the damages caused by ZnO NRs on *E. coli* cells both in the dark and under light irradiation. Noteworthy is that these experiments were conducted using a cell concentration of 5 x 10^5 CFU/mL (10^8 CFU/mL was used in SEM experiments). Fig.54 shows AFM topography images of *E. coli* cells before photocatalysis (Fig. 54a and 54d) at different magnifications. The bacteria are surrounded by their flagellum (Fig.54a) and the surface of the bacteria does not display any defect (Fig. 54d). The length of the bacteria is of ca. 1µm; their width is ca. 400 nm and their height of ca. 85

nm. After 1.5 h photocalysis using ZnO NRs, the rod-shape of *E. coli* cells started to disappear and the dimensions of the bacteria decreased as showed in Fig. 54 (i.e. 800 nm length, 200 nm width, and 40 nm height). Finally, after 3 h photocatalysis (Fig. 54c and 54f), a complete lysis of the cells was observed only thin bacterial fragments (200 nm of length and width and 2 nm thickness) could be detected (Fig. 55).

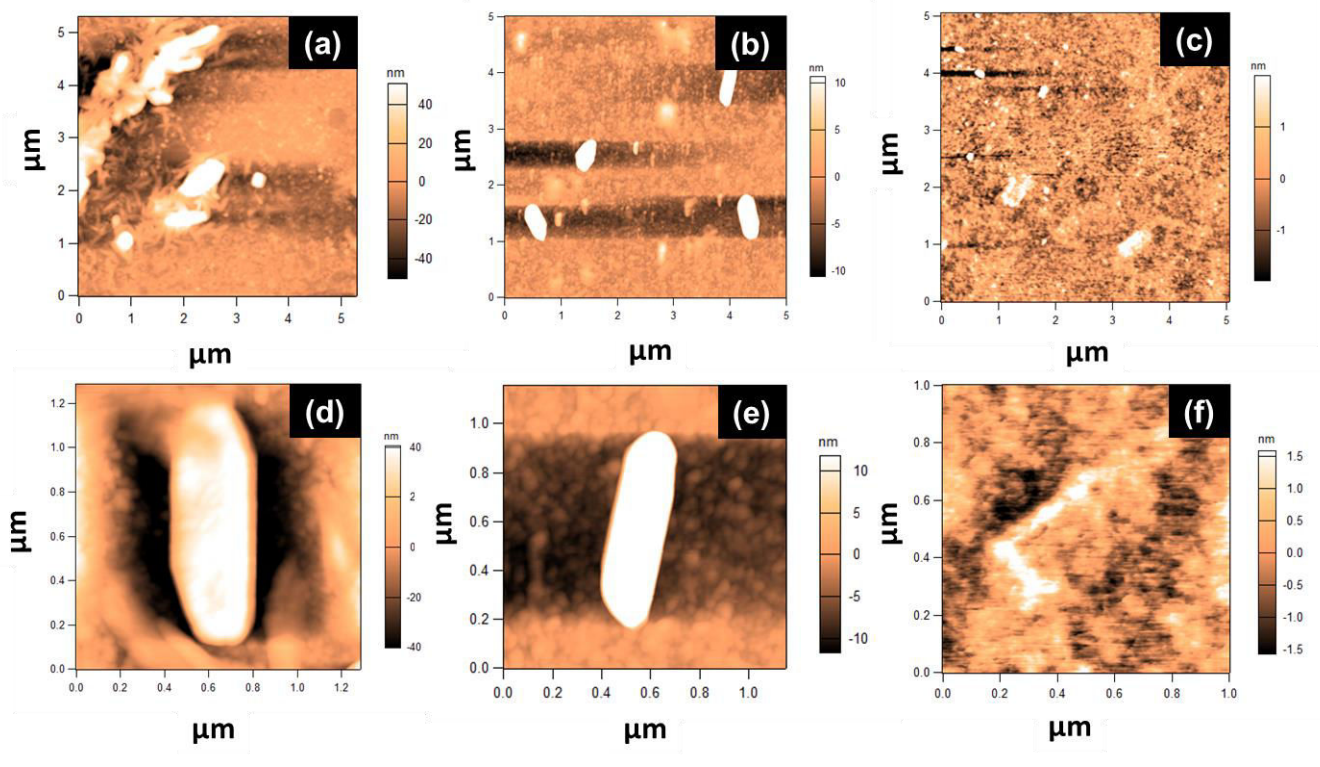

Figure 54: AFM images of *E. coli* MG 1655. (a, b, c) Height images at large scan and (d, e, f) Height images at small scan. (a and d) before photocatalysis, (b and e) after 1.5 h of photocatalysis, and (c and f) after 3 h of photocatalysis.

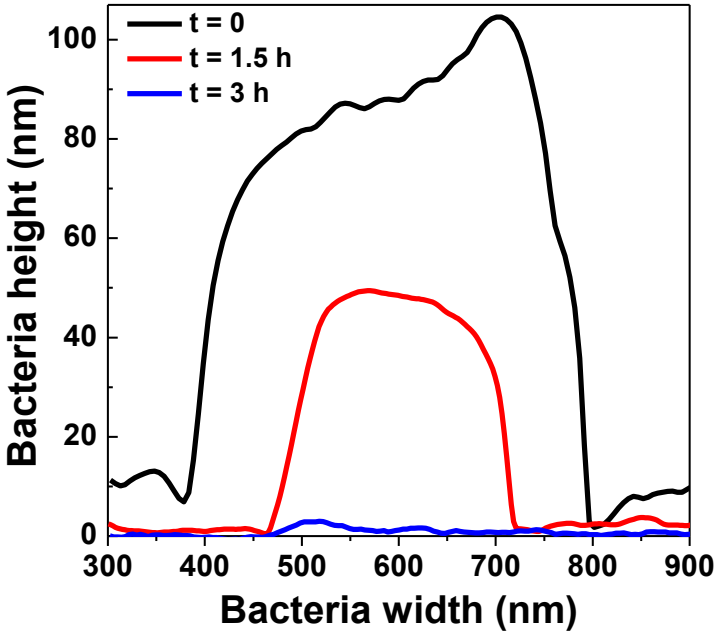

Figure 55: *E. coli* MG 1655 dimensions determined by AFM during the photocatalysis process.

The continuous drastic reduction of the bacteria volume with the duration of photocatalysis is in good agreement with previous studies [27,42- 43]. It is known that the cell walls implosion occurs as soon as small amount of damages are created at the surface of the bacteria during the photocatalytic process [44]. Sunada *et al.* showed that the first damages created on the bacteria wall by photocatalysis started with the release of lipo-polysaccharides which are the amphipatic molecules that constitute the external bilayer membrane [45]. By destabilizing this layer, the solute concentration within the bacteria increased, which leads to a pressure increase within the cell [44]. The consequence of this disequilibrium is the burst of the solution inside the bacteria and its flow out, in other word, the solution run out from the bacteria, and only remains the envelop of the cell. This result is confirmed in our experiments as the volume of the bacteria decreases with the photocatalysis duration. Fig. 54c and f and Fig. 55 demonstrate that the bacteria are completely empty and disrupted and that only flat cell and/or fragments of about 2 nm thickness remain after 3 h of photocatalysis.

III.4 Conclusion

ZnO NRs with average lengths and diameters of 186 and 20 nm, respectively, were easily prepared via a low temperature sol-gel process. ZnO NRs were found to exhibit high solar photocatalytic activity both in dispersed form and immobilized on glass for the photodegradation of the Orange II organic dye and for the *E. coli* bacteria decontamination. Although less photocatalytically active than the dispersed ZnO NRs, the immobilized rods can be easily reused at least five times without significant decrease in activity. Fluorescence spectroscopy, epifluorescence microscopy, SEM and AFM demonstrate that the ROS generated during the photocatalytic treatment alter *E. coli* bacteria proteins and membranes, thus resulting in the inactivation of the bacteria. Our results demonstrate that the photocatalytic activity of ZnO NRs constitutes an alternative to classical oxidation treatments like chlorination and ozonization, especially in isolated areas, and that ZnO NRs have the potential to be used within real environmental applications.

III.5 References

[1] S. Malato, P.Fernandez-Ibanez, M.I. Maldonado, J. Blanco, Gernjak.W, Decontamination and disinfection of water by solar photocatalysis: Recent overview and trends, *Catal. Today*. 147 (2009) 1–59.

[2] WHO, Economic and health effects of increasing coverage of low cost household drinking-water supply and sanitation interventions to countries off-track to meet MDG target 10 (2007).

[3] P.V.A. Padmanabhan, K.P. Sreekumar, T.K. Thiyagarajan, R.U. Satpute, K. Bhanumurthy, P. Sengupta, G.K. Dey, K.G.K. Warrier, Nano-crystalline titanium dioxide formed by reactive plasma synthesis, *In.A.Sc*. 80 (2006) 11-12.

[4] W.J. Huang, G.C. Fang, C.C. Wang. The determination and fate of disinfection by-products from ozonation of polluted raw water, *Sci. Total. Environ***.** 345 (2005) 261-272.

[5] R. Sadiq, M.J. Rodriguez, Disinfection by-products (DBPs) in drinking water and the predictive models for their occurrence: a review, *Sci. Total. Environ*. 321, 1-3, (2004) 21-46.

[6] H. Gallard, G.U. Von, Chlorination of natural organic matter: kinetics of chlorination and of THM formation, *Water. Res*. 36 (2002) 65-74.

[7] W. J. Chen, C. P. Weisel, Halogenated DBP concentrations in a distribution system, J. Am. Water. Works. Ass. 90 (1998) 151-163.

[8] E.W Rice, J.C Hoff, F.W. Schaefer, *3rd* Inactivation of Giardia cysts by chlorine, *Appl. Environ. Microbiol*. 43 (1982) 250–251.

[9] Q. Walter, J. Betancourt, B. Rose, Drinking water treatment processes for removal of Cryptosporidium and Giardia, *Vet. Parasitol*. 126 (2004) 219–234.

[10] P.V. Kamat, B. Shangavi, Interparticle electron transfer in metal/semiconductor composites. Picosecond dynamics of CdS-capped gold nanoclusters, *J. Phys. Chem. B*. 101 (1997) 7675-7679.

[11] T. Mokari, C.G. Sztrum, A. Salant, E. Rabani, U. Banin, Formation of asymmetric one-sided metal tipped semiconductor nanocrystal dots and rods, *Nat. Mater*. 4 (2005) 855-863.

[12] J. Phillips, W. Bowen, E. Cagin, W, Wang, Electronic and optoelectronic devices based on semiconducting zinc oxide, *Semicond. Sci. Technol*. 6 (2011) 101-127.

[13] Z.L. Wang, ZnO nanowire and nanobelt platform for nanotechnology, *Mater. Sci. Eng. R.* 64 (2009) 33-71.

[14] M. Quintana, E, Ricra, J, Rodriguez, W, Estrada, Spray pyrolysis deposited zinc oxide film for photo-electrocatalytic degradation of Methyl Orange: Influence of the pH, *Catal. Today*. 76 (2002) 141-148

[15] S. Singh, K.C. Barick, D, Bahadur, Shape-controlled hierarchical ZnO architectures: photocatalytic and antibacterial activities, *Cryst.Eng.Comm*. 15 (2013) 4631-4639.

[16] J. Das, D. Khushalani, Nonhydrolytic route for synthesis of ZnO and its use as a recyclable photocatalyst, *J. Phys. Chem. C*. 114 (2010) 2544-2550.

[17] S. Baruah, M. Jaisai, J. Dutta, Development of a visible light active photocatalytic portable water purification unit using ZnO nanorods, *Catal. Sci. Technol*. 2 (2012) 918-921.

[18] J. Rodríguez, F. P.D, A. López, J. Alarcón, W. Estrada, Synthesis and characterization of ZnO nanorod films for photocatalytic disinfection of contaminated water. *Thin. Solid. Films*, 519 (2010) 729-735

[19] O. Akhavan, M. Mehrabian, K. Mirabbaszadeh, R. Azimirad, Hydrothermal synthesis of ZnO nanorod arrays for photocatalytic inactivation of bacteria, J. Phys. D: Appl. Phys. 42 (2009) 225-305.

[20] A.R. Khataee, M. Zarei. Photocatalysis of a dye solution using immobilized ZnO nanoparticles combined with photoelectrochemical process, *Desalination*. 273 (2011) 453-460.

[21] M. A. Behnajady, S. G. Moghaddam, N. Modirshahla, M. Shokri, Investigation of the effect of heat attachment method parameters at photocatalytic activity of immobilized ZnO nanoparticles on glass plate, *Desalination*. 249 (2009) 1371-1376.

[22] C. Li, J. Zhang, J. Yang, T. Wang, X. Lv, Z. Tang, Methods to improve the photocatalytic activity of immobilized ZnO/Bi_2O_3 composite, *Appl. Catal. A: Gen*. 402 (2011) 80-86.

[23] S.S.Mehdi, F. Mehrdad, D. C. S.Reza,K. Alireza , S. Tajassosi, Photocatalytic reduction of hexavalent chromium over ZnO nanorods immobilized on kaolin, *Ind. Eng. Chem. Res*.53 (2014) 1079-1087.

[24] S. Balachandran, M. Swaminathan, Facile fabrication of heterostructured Bi_2O_3-ZnO photocatalyst and its enhanced photocatalytic activity, J. Phys. Chem. C. 116 (2012) 26306-26312.

[25] Y. Zhi, Y. Li, Q. Zhang, H. Wang, ZnO nanoparticles immobilized on flaky layered double hydroxides as photocatalysts with enhanced adsorptivity for removal of acid red G, *Langmuir*. 26 (2010) 15546-15553.

[26] Y. Guo, H. Wang, C. He, L. Qiu, X.Cao, Uniform carbon-coated ZnO nanorods: microwave-assisted preparation, cytotoxicity, and photocatalytic activity, Langmuir. 25 (2009) 4678-4684.

[27] C. Pulgarina, J. Kiwia, V. Nadtochenkob, Mechanism of photocatalytic bacterial inactivation on TiO_2 films involving cell-wall damage and lysis, *Appl. Catal. B: Environ*. 128 (2012) 179– 183.

[28] A. Fernández, G. Lassaletta, V.M. Jiménez, A. Justo, A.R. González-Elipe, J.M. Herrmann, H. Tahiri, Y. Ait-Ichou, Preparation and characterization of TiO_2 photocatalysts supported on various rigid supports (glass, quartz and stainless steel). Comparative studies of photocatalytic activity in water purification, *Appl. Catal. B: Environ*. 7 (1995) 49–63

[29] S. Parra, S.E. Stanca, I. Guasaquillo, K.R. Thampi, Photocatalytic degradation of atrazine using suspended and supported TiO_2, *Appl. Catal. B: Environ*. 51 (2004) 107-116

[30] L. Zhang, Y. Ding, M. Povey, D .York, ZnO nanofluids – a potential antibacterial agent, *Prog. Nat. Sci*. 18 (2008) 939–944.

[31] W. Jiang, H. Mashayekhi, B. Xing, Bacterial toxicity comparison between nanoand micro-scaled oxide particles, *Environ. Pollut*. 157 (2009) 1619–1625.

[32] D. Gumy, C. Morais, P. Bowen, C. Pulgarin, S. Giraldo, R. Hajdu, J. Kiwi, Catalytic activity of commercial of TiO_2 powders for the abatementof the bacteria (*E. coli*) under solar simulated light: influence of the isoelectricpoint, *Appl. Catal. B : Environ*. 63 (2006) 76- 84.

[33] C. Vacaroiu, M. Enache, M. Gartner, G. Popescu, M. Anastasescu, A. Brezeanu, N. Todorova, T. Giannakopoulou, C. Trapalis, L. Dumitru, The effect of thermal treatment on antibacterial properties of nanostructured TiO_2 (N) films illuminated with visible light, World. *J. Microbiol. Biotechnol*. 25 (2009)27–31

[34] S. Pigeot-Rémy, F. Simonet, E. Errazuriz-Cerda, J.C. Lazzaroni, D. Atlan, C. Guillard, Photocatalysis and disinfection of water: identification of potential bacterial targets, *Appl. Catal. B : Environ*. 104 (2011) 390–398.

[35] M. Cho, J. Yoon, Measurement of OH radical CT for inactivating Cryptosporidium parvum using photo/ferrioxalate and photo/TiO_2 systems, *J. Appl. Microbiol*. 104 (2008) 759–766.

[36] P.C. Maness, S. Smolinski, D.M. Blake, Z. Huang, E.J. Wolfrum, W.A. Jacoby, Bactericidal activity of photocatalytic TiO_2 reaction: toward an understandingof its killing mechanism, *Appl. Environ. Microb*. 65(1999) 4094–4098.

[37] J.R. Lakowicx, Principle of Fluorescence spectroscopy, Spring Science & Business Media, New York, 3rd edn. (2006).

[38] G-C. Florence, J. Sebastien, K. Nicolas, K. Valerie, L. Marie-Claire. Monitoring the bactericidal effect of UV-A photocatalysis: A first approach through 1D and 2D protein electrophoresis, *Catal. Today*. 147 (2009) 169–172.

[39] G. Gogniat, S. Dukan, TiO_2 photocatalysis causes DNA damage via Fenton reaction-generated hydroxyl radicals during the recovery period, *Appl. Environ. Microb*. 73 (2007)7740–7743

[40] T. Saito, T. Iwase, J. Horie, T. Morioka, Mode of photocatalytic bactericidal action of powdered semiconductor TiO_2 on mutans streptococci, *J. Photoch. Photobio. B*. 14 (1992) 369-379.

[41] K. Sunada, Y. Kikuchi, K. Hashimoto, A. Fujishima. Bactericidal and detoxification effects of TiO_2 thin film photocatalysts, *Environ. Sci.Technol*. 32 (1998) 726-728.

[42] C.S. Laspidou, B.E. Rittmann, Non-steady state modeling of extracellular polymeric substances, soluble microbial products, and active and inert biomass, *Water. Res*. 36 (2002) 1983-1992.

[43] W. Wang, G. Huang, J. C. Yu, P. K. Wong, Advances in photocatalytic disinfection of bacteria: development of photocatalysts and mechanisms, *J. Environ. Sci*. 34 (2015) 232–247.

[44] V. A. Nadtochenko, A. G. Rincon, S. E. Stanca., J. Kiwi, Dynamics of E. coli membrane cell peroxidation during tio_2 photocatalysis studied by ATR-FTIR spectroscopy and AFM microscopy, *J. Photoch. Photobio.* 169 (2005)131–137.

[45] K.Sunada, Watanabe. T, K. Hashimoto. Studies on photokilling of bacteria on TiO_2 thin film, *J. Photoch. Photobio*. 156 (2003) 227–233.

Supporting Information: ZnO nanorods with high photocatalytic and antibacterial activity under solar light irradiation.

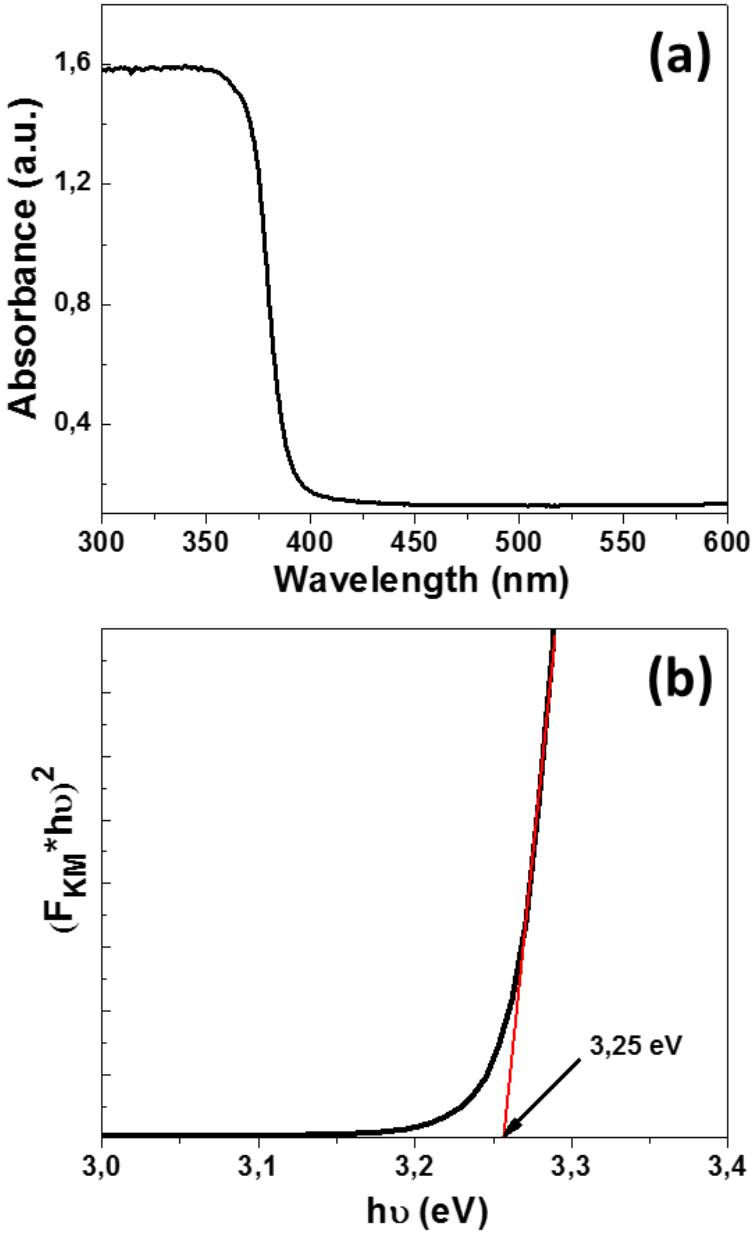

Figure 56: (a) Room temperature UV-visible diffuse reflectance spectra of ZnO NRs. (b) Tauc plot of ZnO NRs for the determination of the bandgap energy value.

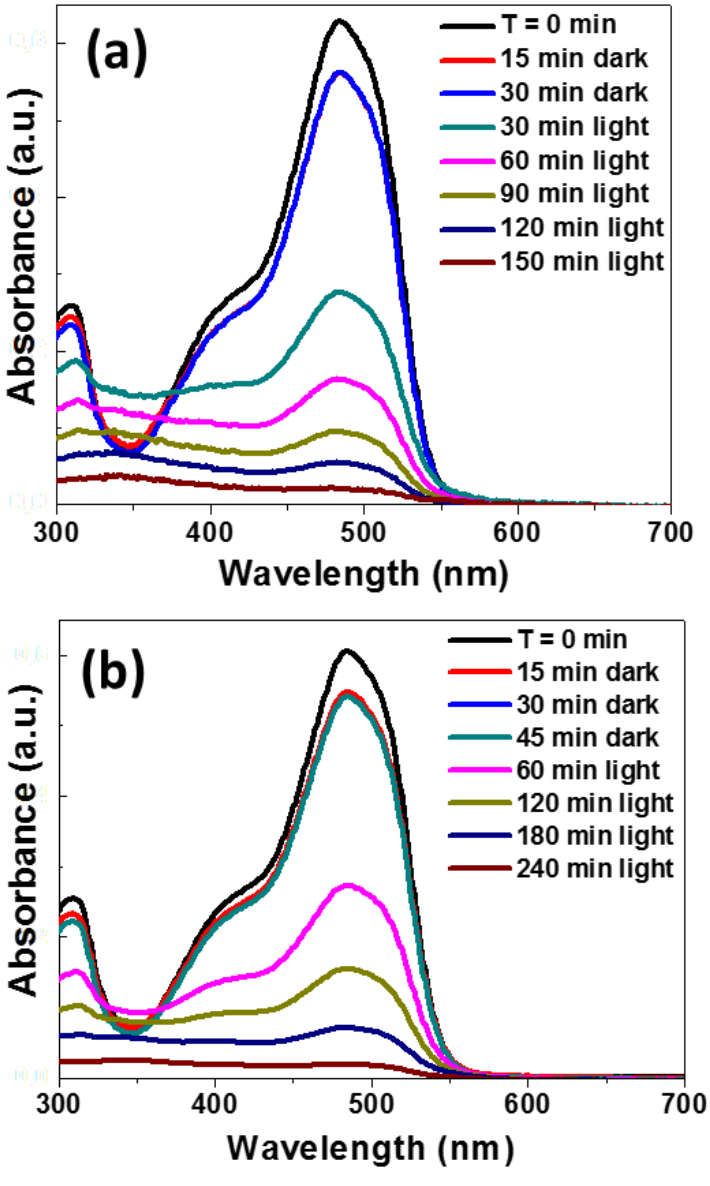

Figure 57: UV-visible spectra used to monitor the variation of the Orange II concentration as a function of irradiation time using ZnO NRs as (a) powder and (b) fixed on glass slides.

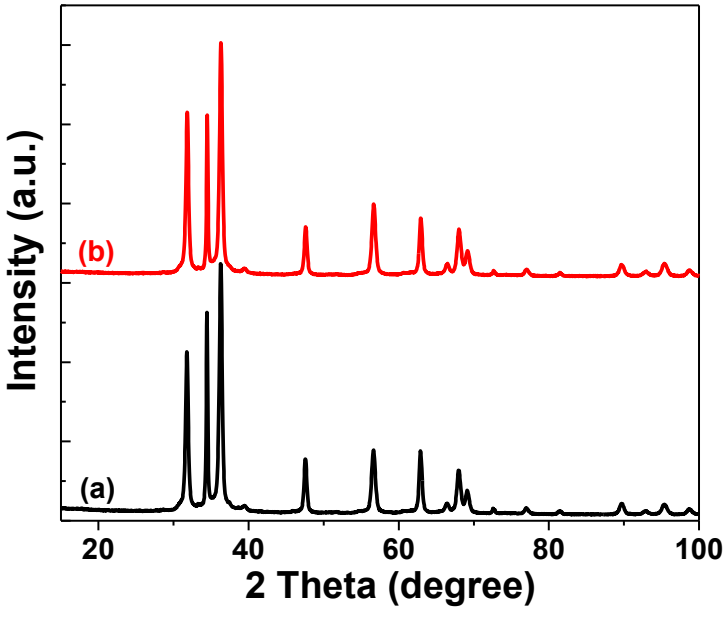

Figure 58: XRD patterns of the immobilized ZnO NRs (a) before and (b) after ten successive photocatalytic cycles.

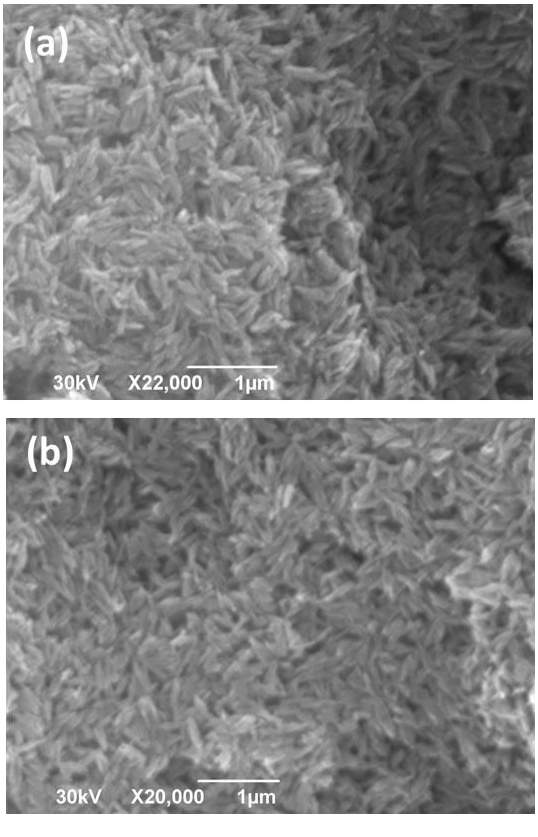

Figure 59: SEM images of the immobilized ZnO NRs (a) before and (b) after ten successive photocatalytic cycles.

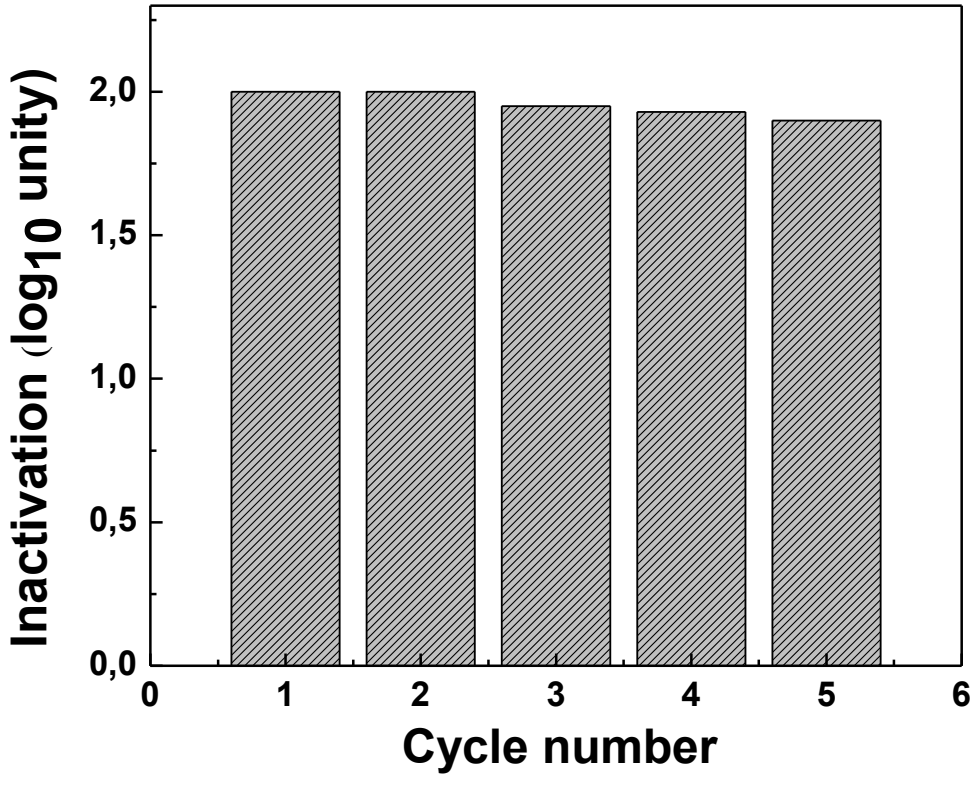

Figure 60: Recyclability of fixed ZnO NRs in photocatalytic bacterial inactivation.

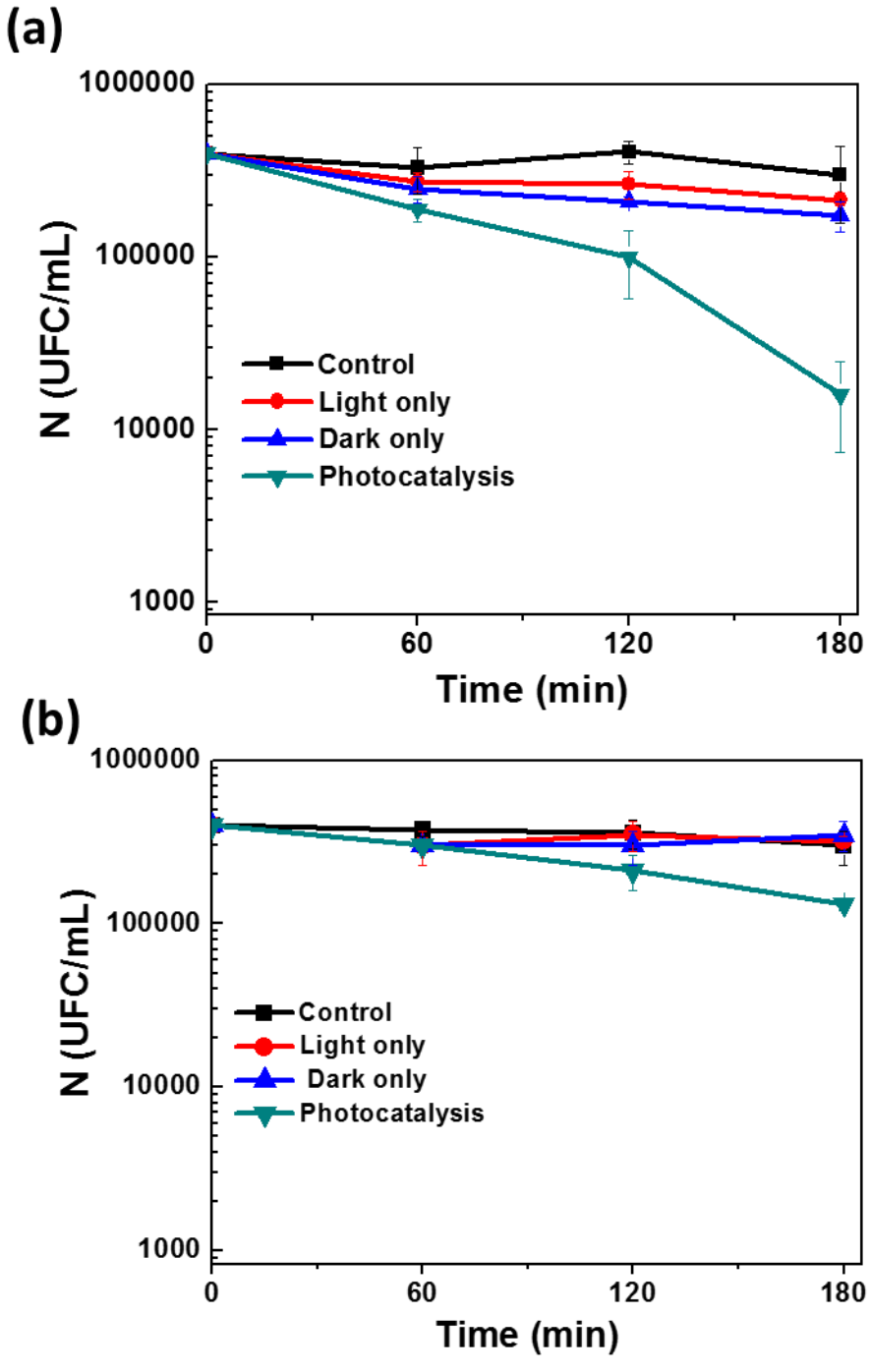

Figure 61: Influence of the amount of ZnO NRs used on the inactivation of *E. coli* MG1655 (a) 130 and (b) 52 mg of the photocatalyst were used, respectively.

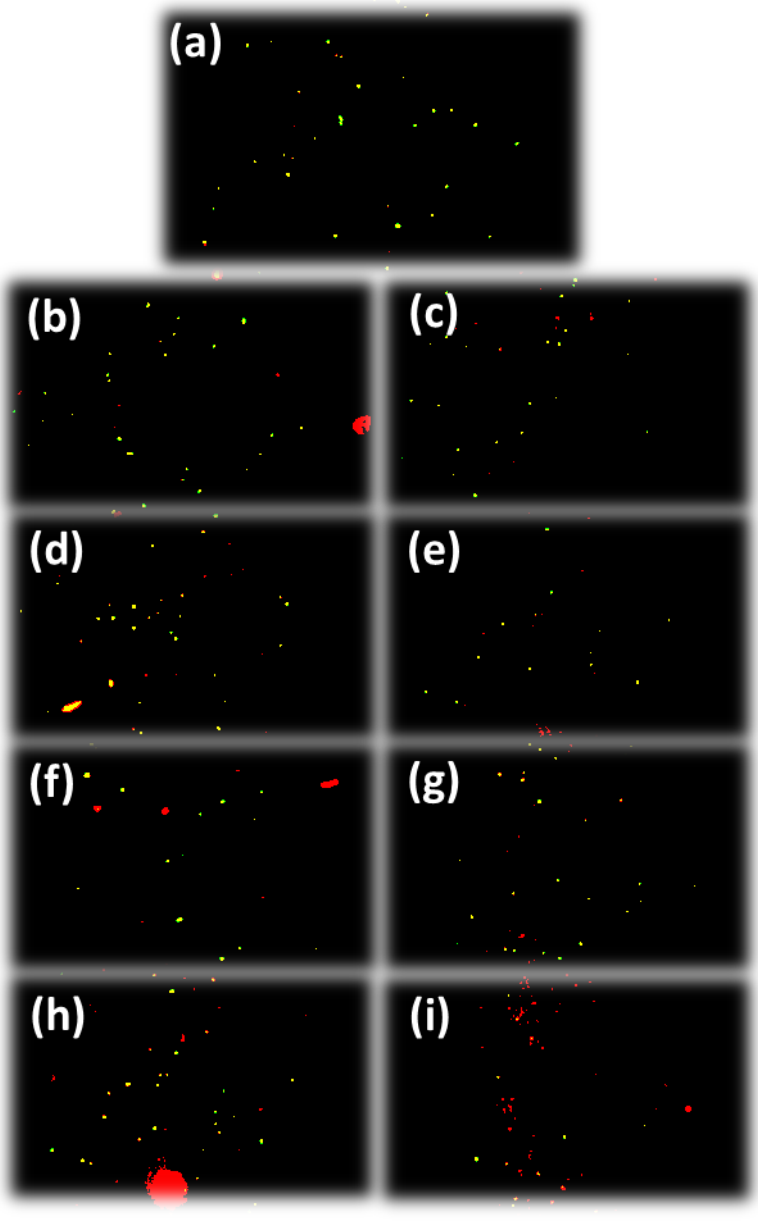

Figure 62: Evaluation of the photocatalytic effect of ZnO NRs on *E. coli* MG 1655 bacterial membrane by detection of viable versus nonviable cells using the LIVE/DEAD®BacLight™ bacterial viability kit. (a) starting bacteria, (b-c) control after 1 and 3 h respectively, (d-e) bacteria exposed to light after 1 and 3 h, respectively, (f-g) bacteria exposed to ZnO NRs in the dark after 1 and 3 h, respectively, and (g-h) bacteria exposed to fixed ZnO NRs and to light irradiation after 1 and 3 h, respectively.

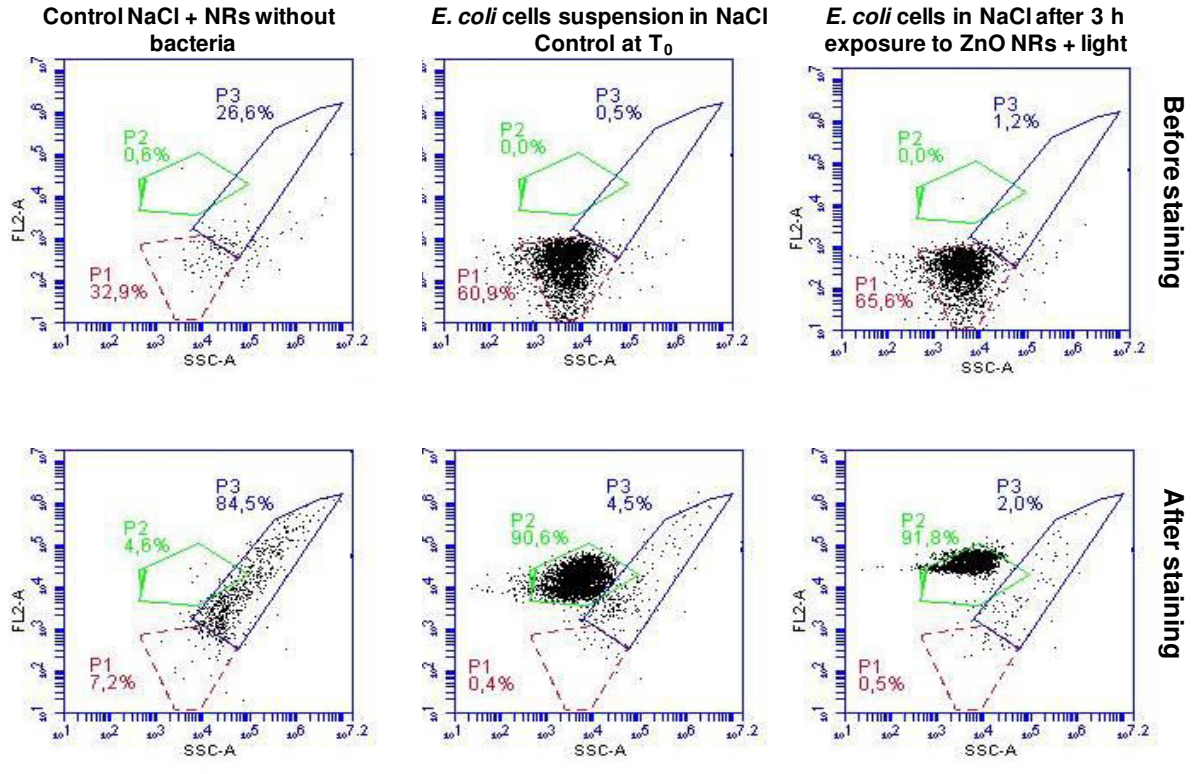

Figure 63: Representative cytograms of *E. coli* populations exposed or not to ZnO NRs before and after staining the bacterial cells with SYBR fluorochrom. P1, P2 and P3 represent the gating zones illustrative of: bacterial signal before and after staining and signal parasite of control NaCl + ZnO NRs without bacteria, respectively.

PARTIE III :

Effet Bactéricide de la Photocatalyse à Base de TiO_2 sur les Bactéries

CHAPITRE I: Solar photocatalytic bacterial inactivation with titanium dioxide immobilized in a fixed-bed reactor.

Résumé

Dans ce chapitre, nous nous sommes intéressés à l'étude de l'effet photacatalytique du dioxyde de titane (TiO_2- P25) fixé sur un support inerte (plaque de verre) et irradié par la lumière solaire. Cette étude a été réalisée pour quantifier la cinétique de l'inactivation (désinfection) sur trois souches bactériennes à savoir: *Escherichia coli, Pseudomonas aeruginosa et Salmonella enterica* Typhi. La cinétique d'inactivation bactérienne est déterminée selon le modèle de premier ordre de Chick–Watson et le modèle de *series-events* modifiés. Pour ces trois types de bactéries, une comparaison des différents paramètres cinétiques (k, A) déterminés à travers les modèles est analysée et discutée.

Les résultats obtenus montrent une différence dans la réponse des bactéries testées à l'effet photocatalytique. Cette différence peut être liée soit à la concentration du nanocatalyseur ou à la dose UV, soit aux propriétés morphologiques métaboliques et génétiques des bactéries (relation dose/réponse).

En se basant sur l'étude de la relation dose/repose et afin d'optimiser l'étape de désinfection par photocatalyse et de minimiser le risque de re-contamination de l'eau après traitement, nous avons déterminé le coefficient de la réactivition bactérienne déterminé selon le modèle modifié de Lindauer *et al.* (1994).

L'étude de la réactivation des bactéries post-traitées nous a montré la capacité de certaines souches bactérienne comme *E. coli* et *P. aeruginosa,* à se réactiver après traitement photocatalytique. Ce résultat nous a conduit à améliorer cette étape de traitement de l'eau par l'ajustement des paramètres de fonctionnement tel que le temps d'exposition à la lumière solaire et la concentration en nanoparticules. Par la suite, cette base de données nous a servi pour établir des recommandations de traitement de l'eau par photocatalyse et à assurer une production d'une eau de bonne qualité.

Les résultats de cette étude sont publiés dans la revue '***African Journal of Microbiology Research***'

Achouri F, Ben Said M , Bousselmi L and Ghrabi A.Solar photocatalytic bacterial inactivation with titanium dioxide immobilized in a fixed-bed reactor. ***African Journal of Microbiology Research.*** **Accepted (in press).**

CHAPITRE I: Solar photocatalytic bacterial inactivation with titanium dioxide immobilized in a fixed-bed reactor

I.1 Abstract

Solar photocatalytic bacterial inactivation with titanium dioxide TiO_2 (Degussa P-25) immobilized in a fixed-bed reactor has been modeled with simplified kinetic equations. Kinetic parameters: the photocatalytic inactivation coefficient ($k_{d,QUV}$), the initial bacterial reduction rate in the contact with the disinfecting agent (A), and the threshold level of damage (n) were determined to report the effect of Q_{UV}/TiO_2-P25 on bacterial cultivability and viability and to compare the response of bacterial strains to photocatalytic treatment. In addition, the integration of the coefficient of reactivation (Cr) in the photocatalytic inactivation equation allowed the determination of potential bacteria rate able to resuscitate after photocatalytic treatment.

Key words: Photocatalysis, TiO_2-P25, Solar UV radiation, Inactivation kinetic, Reactivation.

I.2 Introduction

In arid countries, re-use of domestic wastewater for agricultural and industrial activities has been proposed as a strategy for suitable water use and conservation of resources. However, the use of these effluents must be carefully considered, as they could contain high levels of pathogenic agents and harmful chemical compounds (Rengifo-Herrera et al. 2010). Over the last 20 years environmental remediation has emerged as a high national and international priority for disinfection of contaminated water from hazardous wastes.

Chlorine-based technologies have long been used as disinfection processes for drinking water supplies and also for the tertiary treatment of wastewater effluents. However, this technology is becoming of increasing concern due to recent studies about the formation of potentially harmful chloro-organic disinfection by-products (DBPs) (Gallard and Von Gunten 2002). For that reason, new disinfection technologies are currently in development.

Methods such as ozone and ultraviolet light are equally effective and less toxic. However, these techniques are expensive and often technically difficult to apply in less favorable conditions. In this context, a semiconductor photocatalysis has emerged as a very attractive,

environmentally friendly technology for water disinfection, especially considering the possibility of using solar light to drive the process photocatalysis.

Titanium dioxide (TiO_2) nanoparticles have been of interest in a wide range of applications such as photocatalyst, dye-sensitized solar cells, gas sensor and nanomedicine (Sapizah et al. 2012). It is also well known that TiO_2 is one of the most superior semiconductor materials for decomposing organic materials due to its strong photocatalytic property. TiO_2 semiconductor becomes a photocatalyst when exposed to ultraviolet or near-visible light ($E \geq E$ band gap) with wavelengths shorter than 390 nm. If this light is absorbed by the semiconductor surface, it will have enough energy to overcome the energy barrier and excite an electron to transfer the electron from the filled valence band (Vb) to the empty conduction band (cb), leaving an electron deficiency (hole) in the valence band. Once the charge carriers are generated across the band gap, they may transfer to the semiconductor surface and be absorbed by the reactants (Ni et al. 2007).

The photo-generated holes and electrons react with water molecules attached to TiO_2 surfaces in the presence of oxygen to form hydroxyl radicals (•OH). These are highly reactive for both the oxidation of organic substances and the inactivation of bacteria and viruses (Sinha et al. 2001). The TiO_2 particle may also directly penetrate the cell. Other reactive oxygen species (ROS), such as superoxide ions ($O_2•-$) or ($HO_2•$) are less effective against bacteria, due to the negative charge which prevents them from penetrating bacteria cell membranes (Rengifo-Herreraet al. 2010; Caballero et al. 2009).

The photocatalytic sterilization property of Titanium dioxide (TiO_2) has been documented. The first research on the bactericidal effect of TiO_2 photocatalytic reactions was carried out with *Escherichia coli* (Matsunaga et al. 1985) and subsequently has been intensively conducted on a wide spectrum of organisms including viruses, bacteria, fungi, algae and cancer cells. In the last decade, TiO_2 has been widely utilized as a self-cleaning and self-sterilizing material for coating many clinical tools including sanitary ware, food tableware and cooking ware and items for use in hospitals (Sikong et al. 2010).

Commercial TiO_2 Degussa P-25 has been used in most previous studies (Chong et al. 2009). Most of the reports about photocatalytic disinfection of water sources use TiO_2 slurries (Pablos et al. 2011). However, the difficulty of separation and reuse of nanostructured TiO_2 (10–30 nm) from treated water often limits its application in practice (Caballero et al. 2009).

Numerous material engineering solutions have been investigated in order to resolve this problem. One of the more prominent solutions is the immobilization the TiO_2 nanoparticles onto an inert carrier to retain its quantum effects in the form of a thin film, while allowing ease of separation from the treated water (Chonga et al. 2011). The thin-film fixed-bed reactor (TFFBR) is one of the most used solar photoreactor which has received an increasing interest as a suitable commercial application. Therefore, these reactors can employ both direct and diffuse portions of solar radiation as a light source and do not require the separation of the photocatalysts from the purified water (Caballero et al. 2009). Indeed, the real application of this technology has to avoid the separation step for a feasible continuous water treatment. Indeed, employing the photocatalyst as a suspension or slurry makes the scaling-up of the process difficult, as the TiO_2 has to be removed from the decontaminated water to be reused several times. This problem presented a significant hurdle to commercial application.

The objective of this research was to develop a modeling approach to describe the kinetics of photocatalytic inactivation for solar photocatalytic reactor utilizing immobilized TiO_2-P25. The overall goal was to build simple equations which could report the influence of the synergic effects of solar light radiation and TiO_2-P25 on bacterial inactivation. The model will serve as a predictive tool to design disinfection systems, so that water can be disinfected quickly, efficiently and inexpensively and without risk of recontamination with pathogenic bacteria.

I.3 Materials and methods

I.3.1 Photocatalyst

The standard TiO_2 Degussa P-25 powder was used as photocatalyst (Degussa, Germany). Degussa P25 TiO2 has set the standard for photoreactivity in environmental applications. It is a non-porous 80% to 20% anatase to rutile mixture. P25 is available as high surface area (50±15 m2g-1) nanoparticles with an average individual particle size of 20-30 nm (Bhatkhande et al. 2002).

I.3.2 Bacterial strains

The tested bacteria: *E. coli*, *P. aeruginosa* and *S. typhi* were grown on LB media overnight at 37°C in a shaking incubator in Luria–Bertani (LB) broth. The overnight culture was harvested by centrifugation, washed, and diluted in 0.8% saline. The cell suspension concentration was approximately about 10^6colony-forming units (CFU)/ml (optical density at 0.6).

I.3.3 Solar photocatalytic reactor

All the experiments were carried out under natural sunlight. The supported photocatalyst tests have been carried out with TiO_2 immobilized on an inert matrix; glass plate of $0.8m^2$inclinedat 30° (Bouselmi 2002). The Degussa P-25 (10 g/l) was coated as a thin film on glass plate by spry. The TiO_2 thin film was dried afterwards in air at room temperature then heated in an oven at 100°C for 10 h. The adsorption experiments were carried out in the darkness condition at pH 7. The surface of TiO_2 (isoelectric point, 6.3) at this initial pH is predominantly negatively charged (Cho et al. 2005).

A wastewater stream was pumped up to the reactor using a dispenser. The system can operate in recirculation mode or continuously (Figure 64). The system operates in a closed loop driven by a centrifugal pump with a reservoir tank.

I.3.4 Radiation evaluation

The incident solar irradiance in the photo-reactor was measured with a Dr.Hoenle pyranometer. Since those experiments were done in different days where solar intensity change from day to other, bacterial inactivation was represented as a function of the accumulated UV (Q_{UV}) in the photoreactor per unit of treated water volume for given periods of time during the experiment: Q_{UV} (KJ/L).

Incident UV energy (Q_{UV}) is calculated according by Malato et al. (2000)

$$\mathbf{Q_{UV,n} = Q_{UV,\,n-1} + \Delta t_n\, UV_n\, S_r/V_t;\ \Delta t_n = t_n - t_{n-1}}$$

where, $\boldsymbol{Q_{UV}}$**,** Accumulated energy received by the reactor per litre of solution for each sample taken during the experiment; $\boldsymbol{t_n}$, experimental time for each sample; $\boldsymbol{UV_n}$, average solar ultraviolet radiation measured during $\boldsymbol{\Delta t_n}$; $\boldsymbol{S_r}$, surface area ($1m^2$); $\boldsymbol{V_t}$, total volume of the reactor (1L). During experiments the average of global accumulated incident UV radiation energy$\boldsymbol{Q_{UV}}$was equal to 134 KJ/L for 60 min of solar irradiation.

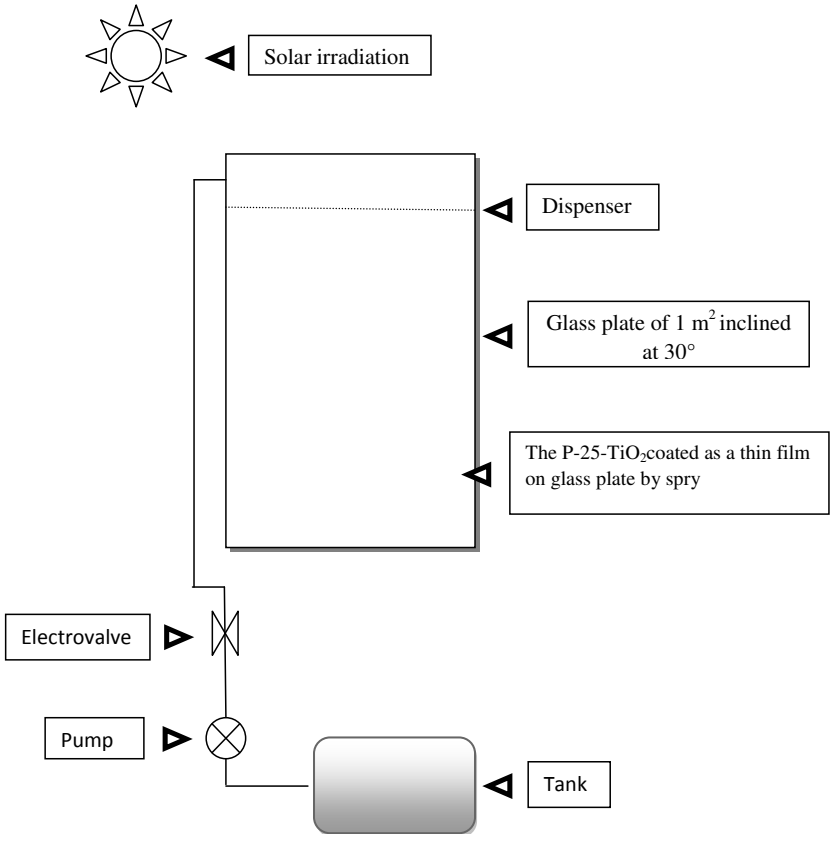

Figure 64: Solar photocatalytic reactor with immobilized TiO_2 (recycling mode)

I.3.5 Irradiation procedure

Tested bacteria suspended in sterile 0.8% (w/v) NaCl aqueous solution was used as a synthetic wastewater. Bacteria were inoculated into Luria Bertani (LB) broth, and incubated for 18 h at 159 rpm in a shaker at 37°C. Cells were harvested by centrifugation at 4000 rpm for 5 min before washing twice with sterile 0.85% sodium chloride (NaCl). Following washing, the aqueous phase was discarded and the bacterial pellet was re-suspended in 0.85% NaCl to prevent carryover of nutrient from the original culture medium, and hence any unintentional increase in cell numbers or effect on cell physiology. A 10-fold dilution was prepared using saline solution as diluents (ensuring cells were well suspended by vortex mixing each dilution before transfer). The required cell density corresponded to approximately 10^{-6} (cfu)/ml. A volume of 1L of bacterial suspension was used to investigate the photocatalytic inactivation of tested bacterial strains using immobilized TiO_2 on glass surface (Figure 1) with solar UV light. A control test was conducted in the dark with TiO_2-P25 in the darkness condition.

I.3.6 Determination of viable and cultivable bacterial cells

Samples of bacterial suspension were taken at regular times of the photocatalytic experiments. Serial dilution were performed in saline water and then spread onto LB agar plate to calculate the concentration of viable and cultivable bacteria. After incubation for 24h at 37°C, bacterial colonies were numbered. Three replicate plates were used at each sampling time.

I.3.7 Bacterial reactivation in dark conditions

Photo-irradiated samples were transferred into separate sterile Petri dishes covered with foil to examine the bacterial potential to dark repair at room temperature. This part of experiment was carried out to verify the ability of post-photo-irradiated bacteria in presence of fixed TiO_2 to restore their UV/TiO_2- P25 induced lesions by molecular mechanisms and especially with dark repair systems such as excision-repair mechanisms, SOS system, etc.

I.4 Results and discussion

I.4.1 Kinetics of photo-disinfection reactions

A series of experiments were carried out to highlight the effects of solar photocatalytic treatment on bacterial cultivability and viability. The number of surviving bacteria was expressed as the ratio (survival ratio) of the number of viable and cultivable bacteria remaining after exposure to experimental conditions (N) to the number of the initial viable bacteria (N_0) (log N/N_0). Figure 65 shows the photocatalytic Gram-negative bacilli: *E. coli*, *P. aeruginosa* and *S. typhi* inactivation with immobilized TiO_2-P25. This figure shows that the bactericidal rates were enhanced when we combine the effect of TiO_2-P25 with solar UV and were increased by increasing UV-irradiation. The synergic effect of TiO_2 and solar UV radiation had a remarkable effect on bacterial cultivability. However, we cannot neglect the bactericidal effect of TiO_2 without solar UV illumination

The experiments conducted with TiO_2-P25 in the darkness condition (non UV germicidal activity) did not show an important bacterial inactivation (0.7 to 1-$\log_{10}$) but, we cannot avoid the germicidal effect of pure TiO_2-P25. Lifen et al (2009) were reported that pure TiO_2 had a high germicidal activity. Indeed, from microscopy observations, it is found that Yeast cells on fresh TiO_2 were deformed under specific experimental condition of pH and TiO_2 concentration, suspended TiO_2.

The bactericidal effect of this semiconductor was highlighted only in the presence of solar UV irradiation after 60 min (Q_{UV}= 134 KJ/L) of a contact time with solar UV/ TiO_2-P25, the bacterial strains*: E. coli*, *P. aeruginosa* and *S. typhi* showed a cultivability inactivation superior to 5-log $_{10}$.

The antimicrobial photo-biological activity of TiO_2 on bacterial cells using solar-UV irradiation has been attributed to the generation of very active free radical species called ROS (reactive oxygen species) (Acevedo et al. 2011). In fact, hydroxyl radicals (HO•) and superoxide anions ($O_2^{\bullet-}$) are considered the main generated species in the anodic and cathodic pathways, respectively, of photocatalytic processes in the presence of oxygen (Fujishima et al. 2000), both species known to be highly reactive with biological samples. Other oxygen reactive species have been also proposed, including hydro- gen peroxide (H_2O_2), hydroperoxyl radical ($HO_2^{\bullet}$) and singlet oxygen ($^1O_2$) (Fujishima et al. 2000). Chromosomal aberration by DNA lesion caused by photoexcited TiO_2 was also reported.

Moreover, during solar UV radiation, the combination of indirect effect of UV-A (320-450 nm) radiation with direct germicidal action of UV-B (290–320 nm) can be lethal to cells respectively through the photosensitization of endogenous chromophores such as co-enzymes or cytochromes, which could damage enzymes essential to bacteria growth and the blockage of DNA replication and RNA transcription (Pigeot-Rémy et al. 2012). However, low solar irradiation can easily affect solar disinfection causing bacterial regrowth by photorepair mechanisms (Schuch et al. 2009).

In particular, some studies have demonstrated that the decrease of cultivability results from alteration in the bacterial metabolism due to the deleterious action of Sun-UV light in combination with TiO_2. Indeed, the cell membrane is the primary site of reactive photogenerated oxygen species attack, leading to lipid peroxidation (Kiwi and Nadtochenko. 2005). The combination of cell membrane damage and further oxidative attack of intracellular components ultimately results in cell death (Rincon et al. 2004). Other studies have suggest that the mode of action is the photooxidation of coenzyme A, leading to the inhibition of cell respiration and thus to cell death (Bonetta et al. 2013).

Knowing that the surface of TiO_2 is amphoteric and consequently, the charge of surface is pH-dependant (Piscopo et al. 2009). For the TiO_2-P25, the pHzpc is close to 6.3. Degussa P-25 that has a negative charge at pH =7.0. Thus, the photocatalytic inactivation of the

observed inactivation behaviour of tested bacteria is hypothesized to be mediated by the bulk phase free hydroxyl radical, not by the surface-bound one. This can be rationalized based on the electrostatic interaction between the TiO_2 surface and the cell surface. Since the surface of TiO_2 (isoelectric point, 6.3) at pH 7 is predominantly negatively charged, and the outer membrane of bacteria is negatively charged (Cho et al. 2005). Thus, it was expected that electrostatic repulsion between the TiO_2 surface and bacteria at pH 7 would be higher due to their both having the same negative charge. Consequently, adsorption of bacteria onto the surfaces of the TiO_2 particles is not favoured, and the direct contact between the cells and the illuminated TiO_2 surface should be minimal. Cho et al. (2005) reported that photochemical removal of coliform bacteria was unaffected by the pH of the solution in the range of 6–8 pH units. Rahmani et al. (2009) were reported that the electrostatic interaction at the TiO_2/water interface could be important in many cases of photocatalytic degradation of charged substrates; it is a relatively weak force, which can be dominated by other factors (Robertson et al. 2005). Thus, the initial pH of the water did not play an important role within a range of 5.5–8.5 pH units (Dheaya et al. 2009)

The performance of a disinfection system is directly relied on the knowledge of the inactivation rate of a target or indicator organism by the disinfectant. For photocatalysis, the synergistic effect of catalyst concentration and solar light intensity on the rate of the process determines the most efficient combination of contact time and dose to employ. Currently, most of this information is obtained from bench-scale studies and extrapolated with a series of empirical models which do not adequately describe photocatalytic disinfection.

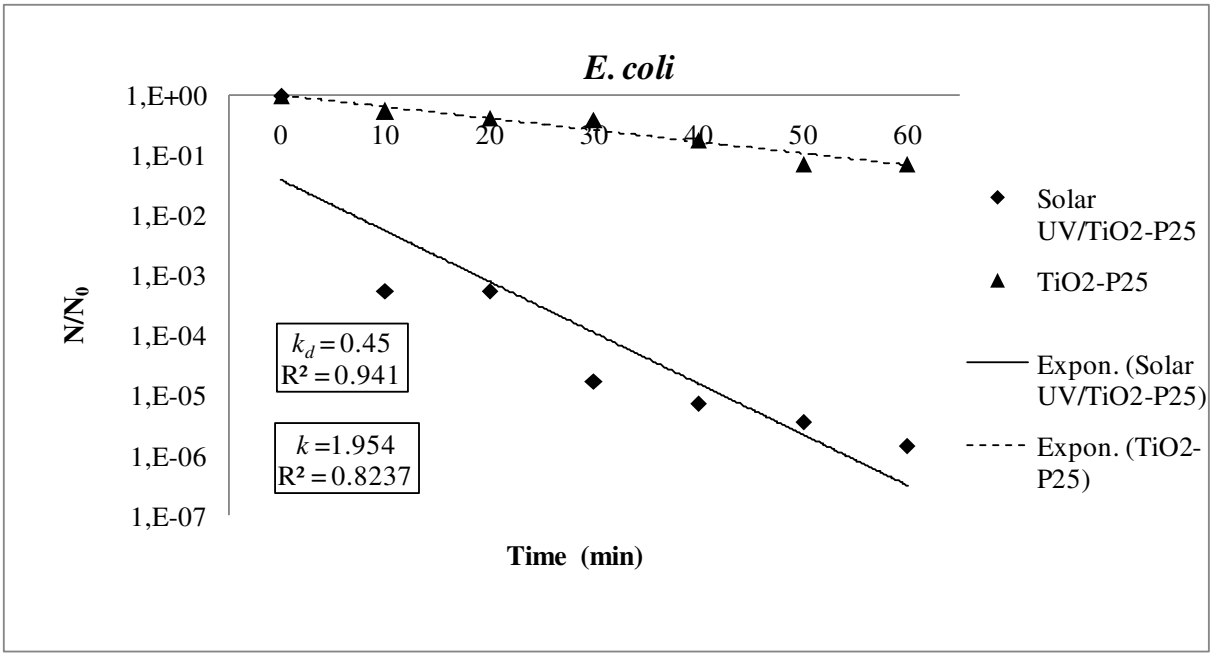

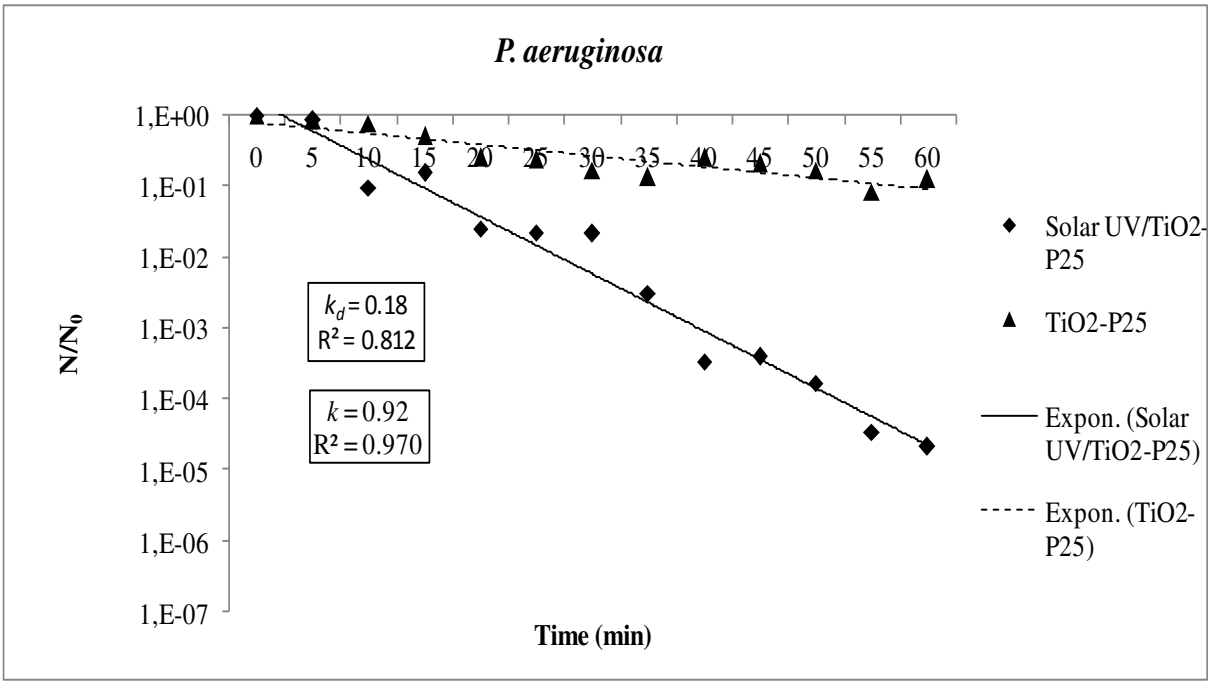

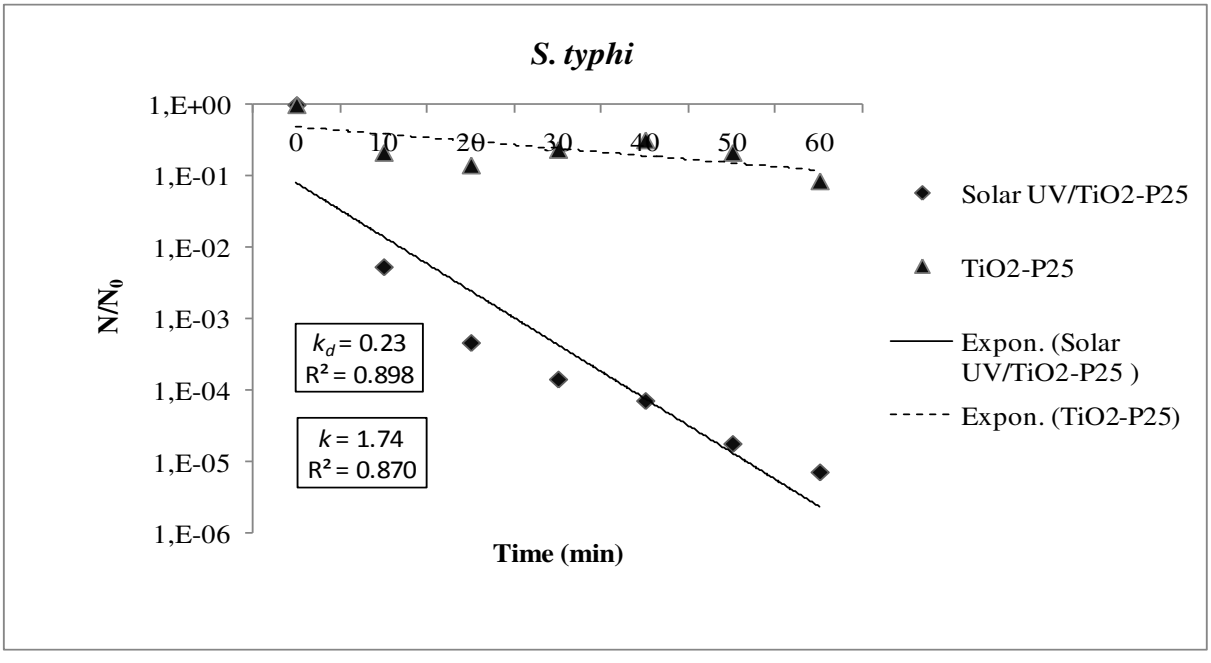

Figure 65: Monitoring of bacterial cultivability in contact with with immobilized TiO_2 in the darkness condition and with solar UV radiation/TiO_2-P25. Where, k_d: is the disinfection kinetic constant related to the catalytic action of TiO_2-P25.

The most common application is the Chick-Watson (C-W) model used primarily to fit inactivation data with first order decay or modified for data with an initial lag, and whose general expression is given by this equation (Watson. 1908):

$$N/N_0 = \text{Exp}\,(-k\,C^n\,t) \qquad (1)$$

Where, N/N_0: is the reduction in the bacterial concentration, k: is the disinfection kinetic constant, C**:** is the disinfectant concentration with, $C = d \times Q_{UV}$; d**:** is the catalyst concentration (g/L); for our experimental condition (fixed bed reactor), the disinfectant concentration (TiO_2-P25) during photocatalysis was supposed to be constant) and Q_{UV}: the accumulated UV energy (KJ/L), t: time (min) and n**:** is the threshold level of series-event model; n is equal to 1 for the first order CW model.

The C-W model was modified to consider the initial reduction in the contact with the disinfecting agent (A):

$$N/N_0 = A\ \text{Exp}\,(-k\,C^n t) \quad (2)$$

Where, ***A*****:** the initial bacterial reduction rate in the contact with the synergic action between cumulate solar UV radiation (Q_{UV}) and the catalyst TiO_2-P25.

$$\mathbf{A= (N_C+ N_d)/\mu} \quad \mathbf{(3)}$$

Where, $N_{C,}$: is the number of CFUs after the first contact with solar UV radiation and catalyst TiO_2-P25, N_d is the initial number of CFUs in the dark condition in the presence of semiconductor, and μ_t: is the adsorption coefficient in the fixed bed of TiO_2 that is assumed to be negligent due to the negative charge of TiO_2-P25 at pH=7.

In this C-W model, the reduction in enumerated bacteria was proportional to the contact time. This correlation, however, cannot be applicable for every instance, as various factors such as the reactor configuration, solar intensity change from day to other, bacterial response (dose/response), inactivation mode and the bacterial resistance to disinfectant used might also cause severe non-linearity characteristics. Thereby, the incorporation of an additional empirical parameter was made to accurately account the photocatalytic inactivation mechanism.

$$N/N_0= A \ \mathbf{Exp}\ (-k\, C^n\, t^m) \quad \mathbf{(4)}$$

m: is empirical parameter that controls the deflection of the inactivation rate. If (***m***) is greater than 1, there is an increase in the inactivation rate and vice versa. This variation depends essentially of water quality and the photoreactor configuration.

$$\mathbf{k = k_{(d,Quv)}\ (k_d+ k_{QUV})} \quad \mathbf{(5)}$$

Where,

k: is the disinfection kinetic constant, $k_{(d,QUV)}$: is the global photocatalytic inactivation coefficient, k_d and k_{QUV} is the disinfection kinetic constant related separately to the catalytic action and solar UV effects, ***d***: is catalytic concentration (g/L), Q_{UV}**:** the accumulated UV energy (KJ/L).

In the studied strains, the time required for bacterial inactivation by photocatalysis, depends of the type of microorganism, Indeed, the time required for the inactivation of nearly 99.99% of cultivable bacteria bacterial was estimated at 30 min of irradiation for the indicator of biological contamination bacteria, *E. coli* and it's equal to 40 min of contact time for

pathogenic bacteria, *S. typhi* against 45 min of exposure time for nosocomial bacteria, *P. aeruginosa*.

Based on the kinetics parameters determined according to CW model (Figure 66; Table III.1), the photocatalytic inactivation coefficient (k) that represents the slope of inactivation curve is more important for *E. coli* (k = 1.95) strain than for *S. typhi* (k = 1.57) and *P. aeruginosa* (k = 1.157). According to Pagan (1999), the greater the coefficient k, the lower is the bacterial resistance to the applied disinfectant. Thus, we can deduce the photocatalytic sensibility of *E. coli* followed by *S. typhi* and we can estimate *P. aeruginosa* as the most tolerant to a solar UV-disinfection with fixed TiO_2-P25.

The results represented in the table III.1, show that the reduction of bacterial cultivability rate in the initial contact with the disinfecting agent (A) is more significant for *P. aeruginosa*. Thus, this strain was estimated to be the more sensitive bacteria in the retention of cultivability in the initial contact with the disinfectant. However, *E. coli* was qualified the more resistant bacteria in the retention of cultivability, followed by *S. typhi*.

Although, when we based on the comparison of the photocatalytic inactivation coefficient (k), we can deduce that *P. aeruginosa* was the more resistant or tolerant strain to the photocatalytic activities. This difference in bacterial behavior or response was probably due to an inter-specific difference concerning the cell growth strategy, the response to the environmental stress, the metabolism activity, the genetic regulation and flexibility, etc.

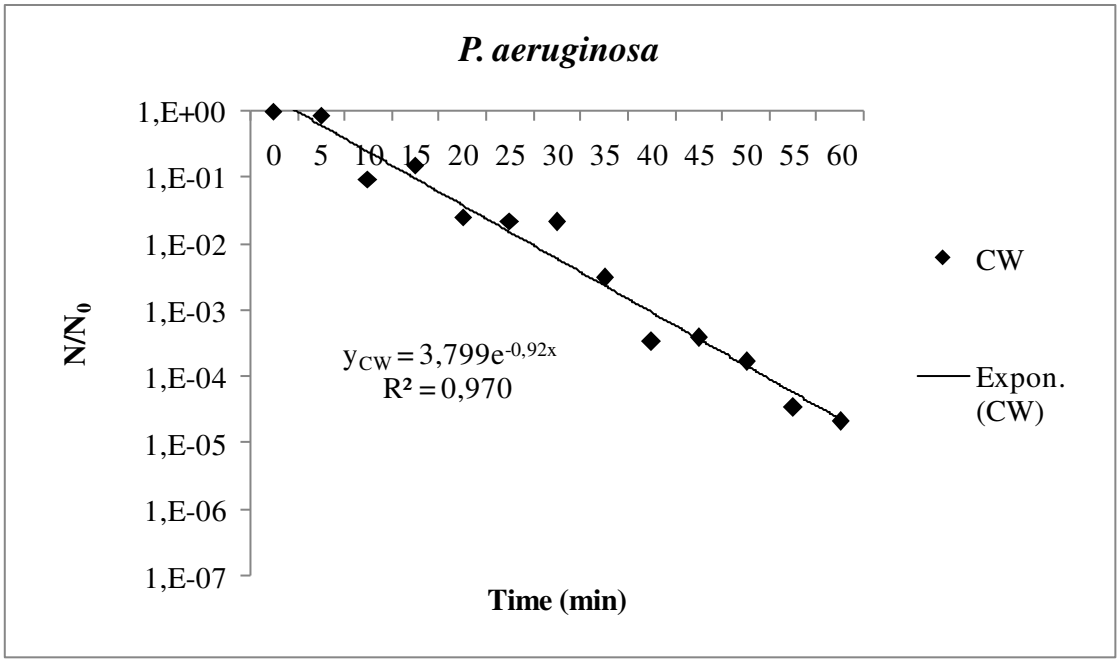
P. aeruginosa
1,E+00
1,E-01
1,E-02
1,E-03
1,E-04
1,E-05
1,E-06
1,E-07
0 5 10 15 20 25 30 35 40 45 50 55 60
N/N0
yCW = 3,799e-0,92x
R² = 0,970
CW
Expon. (CW)
Time (min)

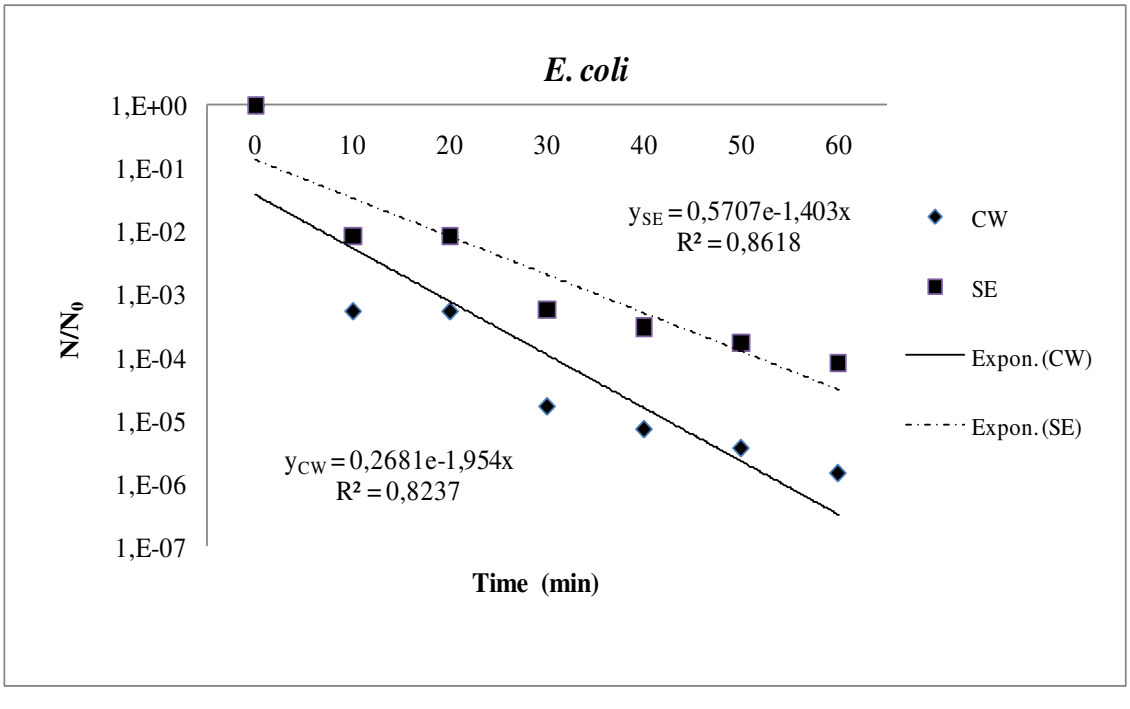
E. coli
1,E+00
1,E-01
1,E-02
1,E-03
1,E-04
1,E-05
1,E-06
1,E-07
0 10 20 30 40 50 60
N/N0
ySE = 0,5707e-1,403x
R² = 0,8618
yCW = 0,2681e-1,954x
R² = 0,8237
CW
SE
Expon. (CW)
Expon. (SE)
Time (min)

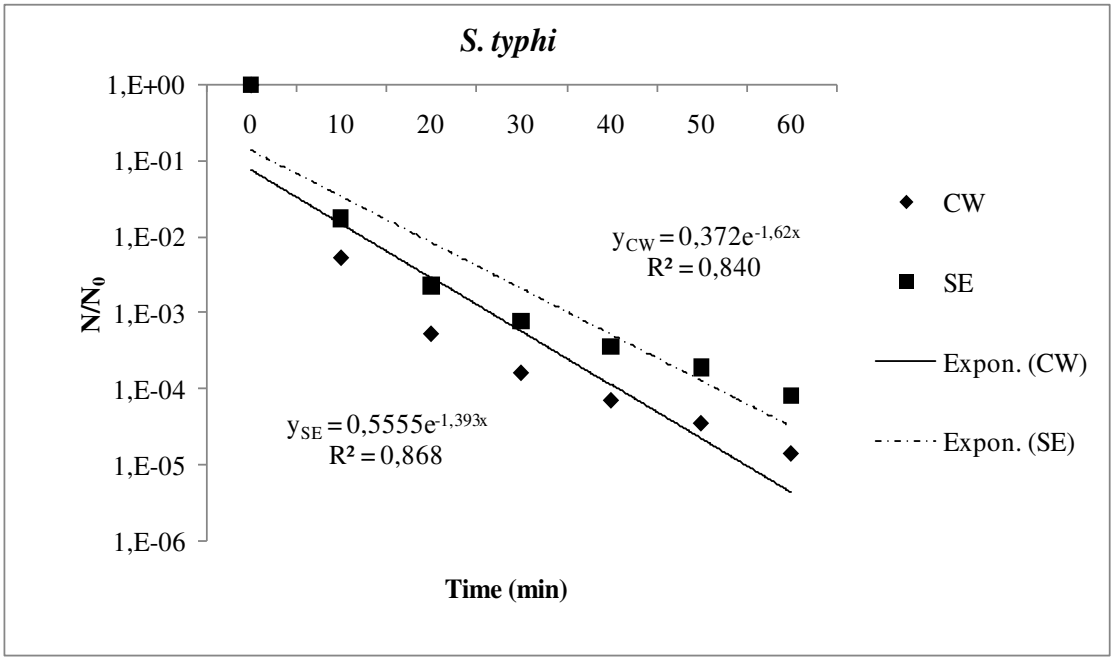

Figure 66: Response of tested bacteria to solar-photocatalytic treatment with immobilized TiO_2, and monitoring of bacterial cultivability according to Chick-Watson model (CW) and series-event model (SE).

Table III.1: Kinetic parameter for tested bacterial strain according to the first order Chick-Watson model (CW) with modification.

Bacterial strain	***A***	***k***
E. coli	0.268	1.95
P. aeruginosa	3.79	0.928
S. typhi	0.372	1.62

To describe bacterial inactivation behaviour we were used in addition to Chick Watson model with modification; series-event (SE) kinetic model with modification. The inactivation process is modelled as a progression of discrete damage levels. The microorganism is assumed to be inactivated at a threshold level of damage (Figure 66; Table III.2).

Each step is characterized by first order kinetics. Each damage level D_i has a kinetic constant k_i and n is the threshold level of damage.

$$D_0 \xrightarrow{k_1} D_1 \xrightarrow{k_2} D_2 \xrightarrow{k_i} D_i \dots D_{n-1} \xrightarrow{k_n} D_n$$

By assuming that the kinetic constant is the same at each level, the following generalized expression can be derived for the series-event model (Severin et al. 1984).

$$\frac{N}{N0} = A\exp(-K \times C^n t^m) + \ln \frac{(1+\Sigma_{i=0}^{n-1} \times C^n t^m)^i}{i!} \quad (6)$$

Table III.2 illustrates the ability of the series-event model to report bacterial response behavior. We can note no change in the kinetic constants (k and A) but, the use of this model can report the series-events undergone by tested bacteria.

Table III.2: Kinetic parameter for tested bacterial strain according to series-events model (SE) with modification

Bacterial strain	***n***	***A***	***k***
E. coli	4	0.57	1.4
P. aeruginosa	1	3.79	0.928
S. typhi	2	0.555	1.393

For example, *E. coli* underwent series of damages D_4. The accumulation of damages was directly related by the keep of cultivability in initial contact with disinfectant. Thus, to response to solar UV-disinfection with fixed TiO_2, *E. coli* was chosen to keep cultivability and therefore this bacterial strain has passed through different damage level (D_1 to D_4). However, *P. aeruginosa* has adapted another strategy. This bacteria strain was decreased in the bacterial cultivability at the initial contact with the disinfectant as a response to stress. Thereby, the damage level determined for this bacteria was $n = 1$ (D_1).

We can conclude that, the keep or the loss of bacterial cultivability can be related to a bacterial adapted to overcome the stress effects. Thus the loss of cultivability is not constantly the synonym of sensibility and vulnerability and, in the same means, the retention of cultivability cannot reveal the resistance or tolerance of bacteria. The bacterial growth modality is directly related by the response of each species bacteria to stress.

I.4.2 Post irradiation events after the photocatalytic treatment

To investigate the durability of UV-disinfection process using TiO_2 (Degussa P-25) on a glass plate we were studied the post irradiation events after the photocatalytic treatment.

To semi-quantify the reactivation level of post-irradiated bacteria in dark condition, a log ratio was determined according to a modified version of the Lindauer and Darby (1994) equation with modification:

$$\mathbf{C_r = Log\ N_r / N_{QUV/TiO2}} \qquad \mathbf{(7)}$$

Where: ***Cr***: is the coefficient of reactivation; N_r= Number of viable and cultivable bacteria after a rest time in the darkness; **UV** radiation and $N_{UV/TiO2}$: Number of viable and cultivable bacteria after photo-disinfection process with immobilized TiO_2.

According to Lindauer and Darby (1994), the reported log values range from 1 to 3.4. When the ***Cr*** is inferior to 1, there is no reactivation; if ***Cr*** ranged between 1 and 3.4, we can conclude that reactivation occurs in the darkness or/and in visible light; when *Cr* is superior to 3.4, there are no disinfectant effects and the cells grow naturally without any environmental stress. In effluents from the studied photoreactor and according to the result of, *E. coli* and *P. aeruginosa* showed slight recovery after photocatalytic treatment during the subsequent 24 h in dark conditions. Indeed, ***Cr*** is equal to 1.07 for *E. coli* and 1.22 for *P. aeruginosa* (Figure 67).

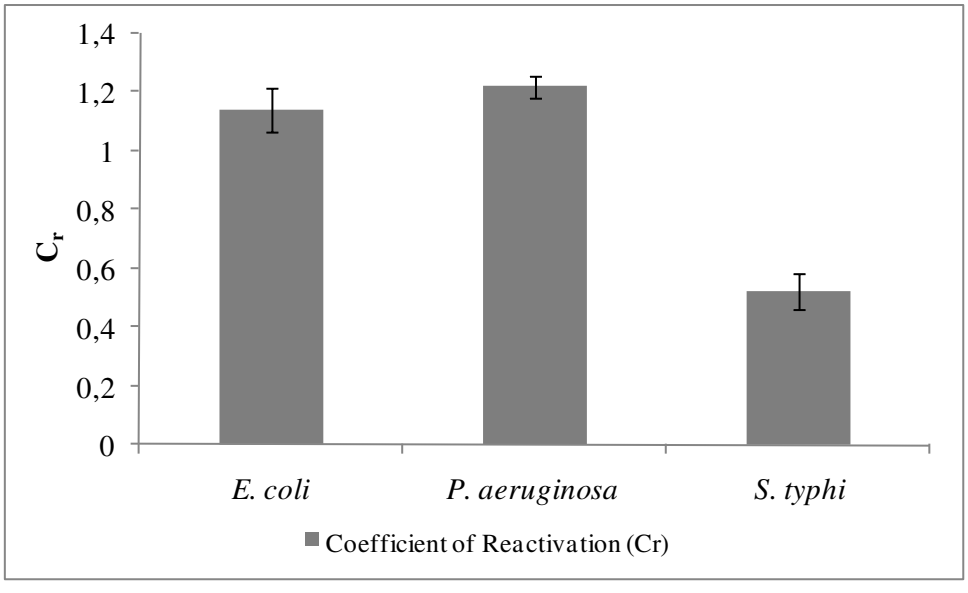

Figure 67: Coefficient of bacterial reactivation (C_r) determined after a rest time in dark condition

Where, C_r is the coefficient of reactivation, Cr = Log N_r/ $N_{UV/TiO2}$; N_r = Number of viable and cultivable bacteria after a rest time in the darkness; UV radiation and $N_{UV/TiO2}$: Number of viable and cultivable bacteria after photo-disinfection process with immobilizedTiO_2.

After solar-UV/TiO_2 treatment, the density of cultivable bacteria (*E. coli* and *P. aeruginosa*) was increased. This enhancement can be related by a biological systems have evolved mechanisms to appropriately respond to environmental stresses that can damage proteins and DNA (Marugán et al. 2008). In this case, to response to UV damage, bacteria generally possess molecular mechanisms to restore DNA lesions. Indeed, bacteria can evolve four main mechanisms in the repair or damage tolerance of UV radiation-damaged DNA, including photoreactivation, nucleotide excision repair (NER), mutagenic DNA repair (MDR), and recombinational DNA repair (Friedberg et al. 1995). These results can affect the effectiveness and the durability of solar photocatalytic treatment with fixed titanium dioxide device.

Bacterial resuscitation after the photocatalytic treatment could be explained by the fact that, under oxidative stress, their cells can enter a viable but non cultivable (VBNC) state.

The result of no cultivability after TiO_2 photocatalytic treatment under solar light does not always represent total bacterial death. The ROS produced during the photocatalytic process can induce oxidative stress on the microorganisms, causing the cells to enter a viable but non cultivable (VBNC) state.

Solar-UV irradiation and attacks by oxidative species generate changes in the permeability of the lipid membrane and/or modify the bacterial DNA, leading the loss of cultivability while viability remains unaltered (Ben Said et al. 2010). When the oxidative stress ends (dark conditions), the microorganisms recover their cultivability. In addition, the growth state of bacteria (exponential or stationary) varies in time. Depending on this parameter, some bacteria could persist under photocatalytic conditions and consequently, their recovery rate in the dark could also be influenced. This hypothesis can explain the recovery of *E. coli* and *P. aeruginosa* after a rest time in the darkness.

In addition, the decrease in the accumulated UV energy (Q_{UV}) and the fluctuation of the visible spectral composition of sunlight during exposed day can affect directly the solar photo-inactivation, and photoreactivation as well as the bacterial behavior in the subsequent dark period.

We can also observe a reactivation of bacteria even during photocatalytic treatment. Indeed, between t = 20 min and t = 30 min, *P. aeruginosa* present a reactivation (Figure 66). This bacterial resicilience during this period can be explained by the cells' ability to restore their UV-induced lesions by molecular photo-dependant mechanism called photoreactivation. This mechanism repair is thought to be an important component of the bacterial arsenal in the repair or reversal of UV-mediated DNA damage (Ben Said et al. 2012). Photoreactivation in bacteria involves a single enzyme called photolyase which binds CPDs and, in a light-dependent step, monomerizes the CPD and dissociates from the repaired lesion (Ben Said et al. 2013). Indeed, UV-A is essential for photoreactivation, although it also has lethal and sublethal effects on microorganisms (Oguma et al. 2002). Thus, when the value of log ratio (Cr) is inferior to 1, we can deduce that the lethal effects of Q_{UV} radiation take over its beneficial effects but when (Cr) is superior to 1, the inactivation effect of photocatalytic can be slowed down and thereby, we can integrate this log ratio in the inactivation equation as well:

$$N/N_0 = A\ (1-1/C_r)\ [\mathrm{Exp}\ (-k\ (C^n\ t^m)] \qquad (8)$$

Figure 68 shows the bacterial kinetic of *P. aeruginosa* and *E. coli* after integration of Cr in the kinetic model. We can note a modification of the initial bacterial reduction rate in the contact with solar UV radiation and TiO_2-P25 for both tested bacteria that shown a reactivation after photocatalytic treatment where, for *E. coli*, *A'* is equal to 0.082 instead of 0.57 determined with SE model and for *P. aeruginosa*, *A'* is equal to 0.38 instead of 3.79 determined with CW model. The difference between the two kinetic values (*A* - *A'*) represent the potential bacteria rate able to resuscitate after photocatalytic treatment.

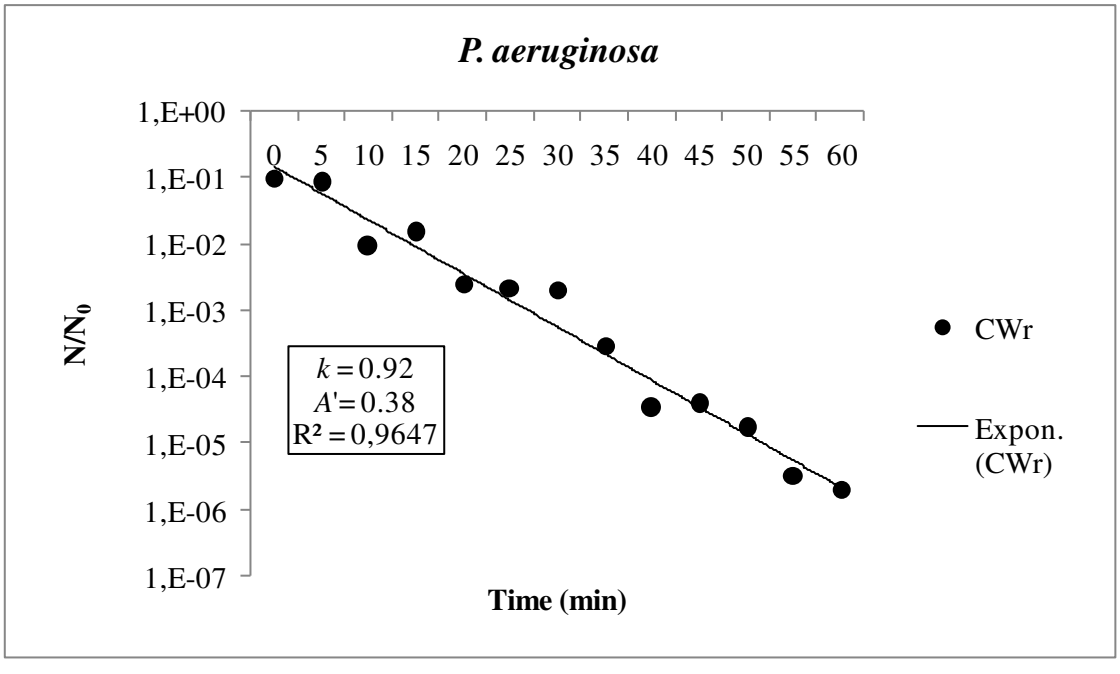

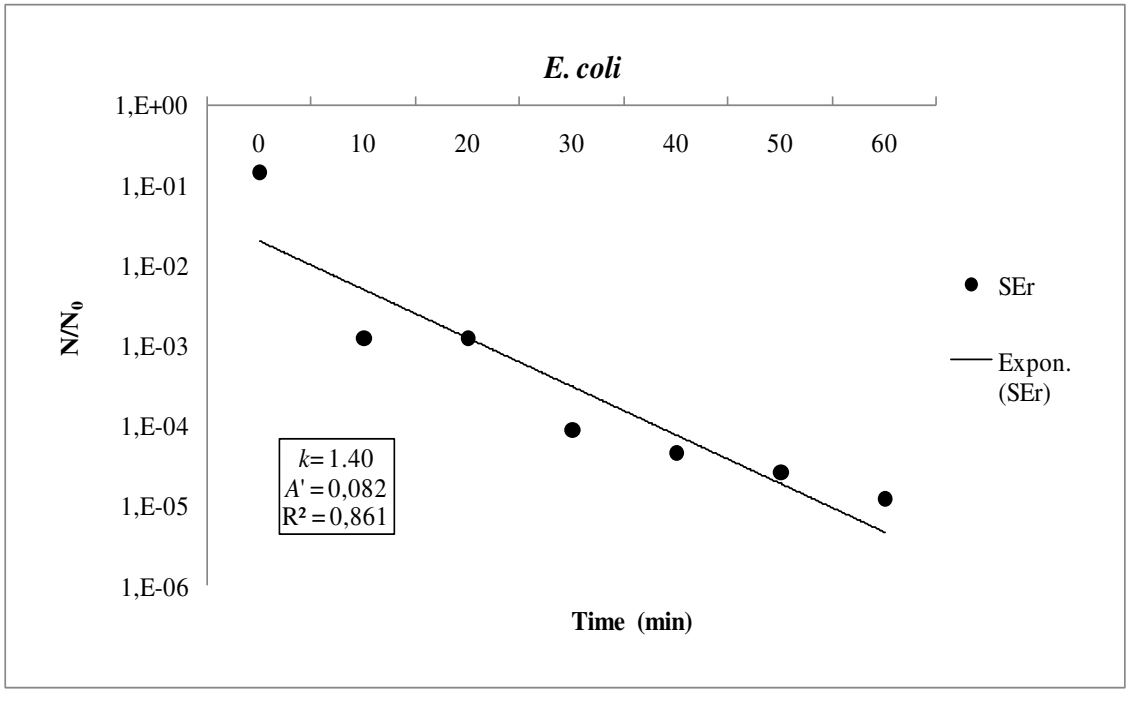

Figure 68: Bacterial kinetic of *P. aeruginosa* and *E. coli* after integration of coefficient of reactivation (*Cr*) in the kinetic models: Chick-Watson model (C-W) and Series-events model (SE).

The integration of *Cr* rate in the photocatalytic inactivation equation has as goal to consider an eventual reactivation after photocatalytic treatment in real scale and to find a solution to overcome the inconvenient related to this interesting technology.

Figure 67 shows no recovery was observed for tested *S. typhi* after 24 h in the darkness (*Cr* equal to 0.52). In this case, only *S. typhi* complete loss of viability and cultivability; other tested bacteria were not affected**.** Thus, the behavior in the dark of *S. typhi* suggest that during photocatalytic disinfection radicals and other oxidative species produced by illuminated TiO_2-P25 induce damage that can in certain cases get worse in the dark, generating a ‘‘residual effect’’ of the photocatalytic treatment. For this reason in post- treated *S. typhi* suspension, bacterial cells continue to decrease in the dark. In this case, the DNA repair mechanism becomes less active rendering the *S. typhi* inactivation irreversible. In other words, the bacterial injury generated by photocatalytic treatment continuous to enhance in the dark.

For this delayed process we apply the term of ‘‘residual effect’’ but it is not necessarily induced by the residual presence of any active oxidative compound. In a previous article we

reported that that this ‘‘residual effect’’ in the dark is dependent on the light intensity previously applied (Marugán et al. 2008).

I.5 Conclusion

The photocatalytic solar UV/TiO_2 system was tested for its bactericide action against three bacterial strains: *E. coli*, *P. aeruginosa* and *S. typhi*. The comparison of different kinetics parameters determined according to C-W model and Series-events model (k, A) for studied bacteria shown a difference in each tested bacterial response to a disinfectant agent. This difference in bacterial behavior or response was probably due to an inter-specific difference concerning the cell growth strategy, the response to the environmental stress, the metabolism activity, the genetic regulation and flexibility, etc.

After solar-UV/TiO_2 treatment, the density of cultivable bacteria (*E. coli* and *P. aeruginosa*) was increased. This enhancement can be related by a biological systems have evolved mechanisms to appropriately respond to environmental stresses. These results can affect the effectiveness and the durability of solar photocatalytic treatment with fixed titanium dioxide device. However, no recovery was observed for tested *S. typhi* after 24 h in the darkness. In this case, only *S. typhi* complete loss of viability and cultivability**.** Thus, the behavior in the dark of *S. typhi* suggest that during photocatalytic disinfection radicals and other oxidative species produced by illuminated TiO_2 induce damage that can in certain cases get worse in the dark, generating a ‘‘residual effect’’ of the photocatalytic treatment.

Enhancing the photocatalytic process efficiency remains a challenge and a subject of extensive research. In the end of this paper, we can propose many solutions such as: (i) the increase of retention time, (ii) the change of photoreactor conception, (iii) the addition of supplement step applied before or after solar UV-TiO_2.

I.6 References

Acevedo A. E.A, Rodríguez J, Manzano M.A. (2011). Disinfection of Natural Water by Solar Photocatalysis Using Immobilized TiO_2 Devices: Efficiency in Eliminating Indicator Bacteria and Operating Life of the System. *J. Sol. Energy. Eng.* 134(1): 011008

Ben Said M, Masahiro O .(2013). Enhancement of ultraviolet water disinfection process. *Afr. J. Biotechnol.* 12(20): 2932-2938,

Ben Said M, Masahiro O, Hassen A. (2010). Detection of viable but non cultivable *Escherichia coli* after UV irradiation using a lytic Qβ phage. *Ann. Microbial*. 60:121-127.

Ben Said M, Otaki M. (2012). Development of a DNA-dosimeter system for monitoring the effects of pulsed ultraviolet radiation. *Ann. Microbial*. 62: 1339-1344

Bhatkhande DS, Pangarkar VG, Beenackers AACM (2002). Photocatalytic degradation for environmental applications. a review. *J. Chem. Technol. Biotechnol.* 77:102-116.

Bonetta S, Bonetta S, Motta F, Strini A, and Carraro E. (2013). Photocatalytic bacterial inactivation by TiO_2-coated surfaces. *AMB. Express*. 3:59

Bousselmi L, Ghrabi A, Ghozzi K, Zayani G, Ennabli M. (2002). Traitement photo catalytique solaire des eaux usées textiles: Possibilités et limitations dans le contexte tunisien Solar photo catalytic treatment of textile waste water: *Proceedings of International Symposium on Environmental Pollution Control and Waste Management* (EPCOWM'2002), 804-812.

Caballero L, Whitehead K.A, Allen N.S, Verran J. (2009). Inactivation of *Escherichia coli* on immobilized TiO_2 using fluorescent light. *J. Photoch. Photobio.A*. 202: 92–98

Cho M, Chung H, Choi W, Yoon J (2005). Different inactivation behaviors of MS-2 phage and *Escherichia coli* in TiO_2 photocatalytic disinfection. *Appl. Environ. Microbiol*. 71(1): 270-75

Chong M.N, Lei S, Jin B, Saint C, Chow C.W.K. (2009) Optimisation of an annular photoreactor process for degradation of Congo Red using a newly synthesized titania impregnated kaolinite nano-photocatalyst. *Sep. Purif .Technol*. 67: 355–363).

Chonga M.N, Jinb B, Saint C.P. (2011). Bacterial inactivation kinetics of a photo-disinfection system using novel titania-impregnated kaolinite photocatalyst. *Chem. Eng. J* 171: 16–23

Alrousan D.M, Dunlop P.S, McMurray T.A, Byrne J.A. (2009). Photocatalytic inactivation of *E. coli* in surface water using immobilised nanoparticle TiO_2 films. *Water.Res* 43:47–54.

Friedberg E.C, Walker G.C, Siede W. (1995). DNA Repair and Mutagenesis. *ASM. Press, Washington DC.*

Fujishima A, Rao T.N, Tryk D.A. (2000). Titanium dioxide photocatalysis. *J. Photoch. Photobio. C*. 1:1–21

Gallard H, Von Gunten U (2002). Chlorination of Natural Organic Matter: Kinetics of Chlorination and of THM Formation. *Water.Res*. 36(1): 65-74.

Kiwi J, Nadtochenko V. (2005). Evidence for the mechanism of photocatalyticdegradation of the bacterial wall membrane at the TiO_2 interface by atr-ftir and laser kinetic spectroscopy. *Langmuir.* 21:4631–4641

Lifen L, Barford J, King Lun Y. (2009). Non-UV germicidal activity of fresh TiO_2 and Ag/TiO_2. *J. Environ. Sci*. 21: 700–706.

Lindauer K.G, Darby J. (1994). Ultraviolet disinfection of waste water: effect of dose on subsequent photoreactivation. *Water.Res*. 28:805–817.

Malato S, Blanco J, Richter, C, Fernández P, Maldonado M.I. (2000). Solar photocatalytic mineralization of commercial pesticides: oxamyl. *Sol. Energ. Mat. Sol. C*. 64: 1–14.

Marugán JO, Grieken RV, Sordo C, Cruz C (2008). Kinetics of the photocatalytic disinfection of *Escherichia coli* suspensions. *Appl. Catal. B : Environ*. 82: 27–36.

Matsunaga R, Tomodam T, Wake N.H. (1985). Photoelectrochemical sterilization of microbial cells by semiconductor powders. *FEMS. Microbiol. Lett*. 29:211–214

Ni M, Leung M.K.H, Leung D.Y, Sumathy K. (2007). A review and recent developments in photocatalytic water-splitting using TiO_2 for hydrogen production. *Renew. Sust. Energ. Rev.* 11:401–425.

Oguma K, Katayama H, Ohgaki S. (2001). Photoreactivation of escherichia coli after low- or medium-pressure uv disinfection determined by an endonuclease sensitive site assay. *Appl. Environ. Microb.* 68 (12): 6029–6035

Pablos C, Van Grieken R, Marugán J, Moreno B. (2011) . Photocatalytic inactivation of bacteria in a fixed-bed reactor: mechanistic insights by epifluorescence microscopy. *Catal. Today*. 161: 133-139.

Pagan R, Manas P, Raso J, Condon S. (1999). Bacterial resistance to ultrasonic waves under pressure at nonlethal (manosonication) and lethal (manothermosonication) temperatures. *Appl. Environ. Microb*. 65 (1): 297–300

Pigeot-Rémy S, Simonet F, Atlan D, Lazzaroni J.C, Guillard C. (2012). Bactericidal efficiency and mode of action: a comparative study of photochemistry and photocatalysis. *Water. Res*. 46 (10): 3208-18.

Piscopo A, Robert D , Weber J.V. (2001). Influence of pH and chloride anion on the photocatalytic degradation of organic compounds Part I. Effect on the benzamide and para-hydroxybenzoic acid in TiO_2 aqueous solution. *Appl. Catal. B : Environ*. 35: 117–124

Rahmani A.R, Samarghandi M.R, Samadi M.T, Nazemi F. (2009). Photocatalytic Disinfection of Coliform Bacteria Using UV/TiO_2. *J. Res. Health. Sci*. 9 (1): 1-6.

Rengifo-Herrera J.A, Pulgarin C, Machuca F, Sanabria J. (2010). TiO_2 photocatalytic inactivation under simulated solar light of bacterial consortia in domestic wastewaters previously treated by uasb, duckweed and facultative ponds. *Quim. Nova*, 33(8): 1636-1639

Rengifo-Herrera J.A, Pulgarin C. (2010). TiO_2 photocatalytic inactivation under simulated solar light of bacterial consortia in domestic wastewaters previously treated by UASB, duckweed and facultative ponds. *Quim. Nova*, 33 (8): 1636-1639, 2010.

Rincon A.G, Pulgarin C. (2004). Field solar *E. coli* inactivation in the absence and presence of TiO_2: is UV solar dose an appropriate parameter for standardization of water solar disinfection. *Sol. Energy*. 77: 635–648)

Robertson J.M.C, Robertson P.K.J, Lawton L.A. (2005). A comparison of the effectiveness of TiO_2 photocatalysis and UVA photolysis for the destruction of three pathogenic micro-organisms. *J. Photoch. Photobio. A*. 175: 51-56.

Sapizah R, Shahidan R, Ainon H. (2012). Inactivation of *Escherichia coli* Under Fluorescent Lamp using TiO_2 Nanoparticles Synthesized Via Sol Gel Method. *Sains. Malays.* 41(2): 219–224

Schuch A.P, Galhardo R.S, Lima-Bessa K.M, Schuch N.J, Menck C.F.M. (2009). Development of a DNA-dosimeter system for monitoring the effects of solar-ultraviolet radiation. *Photochem. Photobiol. Sci*. 8: 111-120.

Severin B.F, Suidan M.T, Engelbrecht R.S. (1984). Series-event kinetic model for chemical disinfection. *J. Environ. Eng*.110: 430-439.

Sikong L, Kongreong B, Kantachote D, Sutthisripok W. (2010). Photocatalytic Activity and Antibacterial Behavior of Fe^{3+}- Doped TiO_2 /SnO_2 Nanoparticles. *Energy. Rec. J.* 1 (2): 120-125

Watson H.E .(1908). A note on the variation of the rate of disinfection with change in the concentration of the disinfectant. *J. Hyg. (Lond)*.8: 536-542.

CHAPITRE II: Impact of photocatalysis-TiO_2 on Pseudomonas aeruginosa: cells viability and biofilm formation

Résumé

Dans ce chapitre, nous présentons l'impact de la photocatalyse sous irradiations UV sur l'inactivation et l'atténuation des caractères de virulence pour une souche de référence *Pseudomonas aeruginosa (*ATCC 4114). Cette étude se situe en perspective pour optimiser le processus de désinfection photocatalytique de l'eau, et elle est basée sur l'exploration de l'expression et de la rétention des facteurs de virulence par un indicateur bactérien.

Nos travaux se sont focalisés sur l'effet photocatalytique du dioxyde de titane (TiO_2– P25) irradié par la lumière de la bande A (UV-A) sur la rétention de l'expression des caractères de virulences d'une souche bactérienne; *Pseudomonas aeruginosa* (ATCC4114).

Comme première étape, nous avons étudié l'effet de TiO_2/UV-Asur la morphologie bactérienne. Les observations par microscopie à force atomique (AFM) ont montré des dommages significatifs sur la membrane bactérienne, causés par l'effet photocatalytique.

Vue la discordance des résultats entre la perte de cultivabilité sur milieu usuel et rétention des caractères de virulences après traitement, nous avons évalué l'efficacité du système de traitement photocatalytique en terme de virulence (mobilité bactérienne, production de biofilm, production de protéases, etc.), appuyé par une évaluation classique sur l'abattement bactérien en amont et en aval du système épuratoire. En effet, le risque sanitaire n'est pas seulement fonction de l'abondance des contaminants mais aussi de leur capacité à survivre dans le milieu récepteur et à maintenir leur virulence.

Les expériences ont été menées sur la souche bactérienne, *P. aeruginosa* (ATCC 4114), pris comme modèle indicateur de l'expression de facteur de virulence après le traitement, et la détermination des conditions optimales de traitement d'eau permettant l'inactivation des bactéries et l'atténuation des facteurs de virulence.

Ces résultats ont fait l'objet d'un article soumis dans la revue '*Journal of environmental sciences*'

Faouzi Achouri, Myriam Ben said, Latifa Bousselmi, Serge Corbel, Raphaël Schneider, Ahmed Ghrabi. Impact of photocatalysis-TiO_2 on *Pseudomonas aeruginosa*: cells viability and biofilm formation. *Journal of environmental sciences.*

CHAPITRE II: Impact of photocatalysis-TiO_2 on Pseudomonas aeruginosa: cells viability and biofilm formation

II.1 Abstract

Photocatalytic treatment by TiO_2 (P-25), could be a way to prevent bacterial proliferation or, at least, to significantly reduce the amount of microorganisms that grow on resistant structure; biofilm. Previous works involving TiO_2 have already shown the inactivation of bacteria by the photocatalysis process. This paper studies the inactivation of *Pseudomonas aeruginosa* bacteria by photocatalysis involving TiO_2 nanoparticles. The antibacterial activity including viable and cultivable bacteria counts which was confirmed by the Colony-forming unit (CFU), reactivation mechanisms, and biofilm formation of TiO_2 was evaluated through experiments under UV-A irradiation. The results contribute to the understanding of the bactericidal mechanism and kinetics of photocatalytic disinfection that are essential for to enhance the performances of the water disinfection processes via photocatalysis by an establishment of new recommendations taking into consideration the potential recovery of post-treated bacteria and retention of the expression of virulence factors by *Pseudomonas aeruginosa* after photocatalytic treatment.

Key words: biofilm, kinetic, Photocatalysis, *Pseudomonas aeruginosa*, Wastewater treatment.

II.2 Introduction

Waterborne diseases are the leading cause of death in the world before malnutrition.According to the WHO in 2008, 88% of cases of diarrhea worldwide are attributed to unsafe water resulting in the deaths of more than 1.5 million people annually, most of which are children [1]. Among bacterial pathogens, *Pseudomonas aeruginosa* (*P. aeruginosa*) is responsible for 10–15% of the nosocomial infections worldwide [2]. Recognized as opportunistic pathogen, it is the main responsible of nosocomial infections in immunocompromised patients, and its presence in water facilitates the spread of diseases and

epidemics [3, 4]. Nevertheless virulence of *P. aeruginosa* is multifactorial and has been attributed to cell associated factors like alginate, lipopolysaccharide (LPS), flagellum, pilus and non-pilus adhesins as well as with exoenzymes or secretory virulence factors like protease, elastase, phospholipase, pyocyanin, exotoxin A, exoenzyme S, hemolysins (rhamnolipids) and siderophores [5,6].These factors provide a crucial role in the pathogenesis of *P. aeruginosa* induced infections such as respiratory tract infections; burn wound infections and keratitis [7,8]. All microbes like Gram positive and Gram negative bacteria have capacity to synthesized biofilm. Indeed, biofilm formation is a resistance strategy adopted by several types of bacteria. Further,greater than 99% of all bacteria are found in biofilms [9] and 80% of bacterial infections are caused by bacteria living in biofilms [10]. Indeed, the water disinfection by chlorination and ozonation, widely used, has proven that it can generate carcinogenic and mutagenic byproducts [11, 12]. During the recent decades, photocatalysis generally mediated by (TiO_2) appears as an interesting alternative for the inactivation of pathogenic microorganisms. When TiO_2 absorbs photons of energy equal or exceeding its band gap, electron–hole pairs are formed that induce redox reactions at its surface. A hydroxyl radical ($^{\cdot}OH$) is created through an oxidative process when a hole reacts with a water molecule or hydroxide ion on the particle surface [13, 14]. The electron can react with molecular oxygen to generate the superoxide radical ($O_2^{\cdot-}$) through a reductive process [13]. The photocatalytic inactivation of bacteria with TiO_2 -P25 as a photocatalyst has been studied for the first time in 1985 by Matsunaga *et al* [15]. Since thenmore research is oriented towards the application of photocatalytic disinfection of water which is the most widespread, demonstrating the effectiveness of TiO_2 illuminated by UV light to inactivate a wide range of microorganisms including bacteria[16,17] virus [18], yeast and fungi[19,20]. Matsunaga *et al* concluded that cell death was induced by inhibition its respiratory activity via the reduction of coenzyme A.They also reported that no destruction of the cell wall caused by the semiconductor [21].Saito and al [22] reported that the destruction of the walls causes destruction of bacterial cells following a rapid leakage of potassium ions from the bacteria and slow release of protein and RNA.However, the photocatalytic action gradually increases cell permeability and subsequently allows the release of intracellular contents ultimately leading to death [23].

The main objective of this study was to investigate the effect of TiO_2 aqueous suspension illuminated with UV-A on: (i) bacterial viability and cultivability; (ii) bacterial physiology and ecology as well as morphology, biofilm production and other virulence factors required

for biofilm formation such bacterial motilities (Swimming, swarming and twitching). Taken together, these experiments can provide data that helps us to understand bacterial responses to photocatalytic treatment and to determine the optimal treatment conditions (exposure time, UV-A dose, TiO_2-P25 concentration, etc.) to reduce and/or prevent possible biofilm formation by post-treated bacteria.

II.3 Methods and Materials

II.3.1 Catalyst

The used photocatalyst was TiO_2 Degussa P-25, which is made of anatase (80%) and rutile (20%). The non-porous TiO_2 particles have a surface area of 50 m^2/g and mean crystallite size of 30 nm.

II.3.2 Preparation of Bacterial strains and growth media

P aeruginosa (ATCC 4114) bacteria were maintained on Nutrient agar (GN) and stored at 4°C. For the experiments, they were grown overnight at 37°C in nutrient broth NB medium overnight under aerobic conditions, with constant shaking. The bacterial growth was monitored by measurement of optical density at 600 nm. Then, samples of culture were taken at a stationary growth phase. Bacteria cells were then collected by centrifugation at 1400 rpm for 10 min and washed twice with sterile demineralized water. Finally, they were re-suspended in buffered saline (0.85%). The required cell density corresponded to approximately 5. 10^6 cfu/ml.

II.3.3 Bacterial viability assessing after photocatalytic treatment

The experiments were conducted in the beaker 100 mL. Before each experiment, glass containers were autoclaved at 121°C for 15 min. Then 20 ml of a suspension of *P aeruginosa* (ATCC 4114) was mixed with 20 mg of TiO_2 (concentration $1g.L^{-1}$). The reaction was irradiated with a UV-A lamp (**Philips Actinic BL 15W/10 SLV** under intensity of 1.7 mW / cm^2) with constant magnetic stirring during 1h.

Ten microliters of *P. aeruginosa* bacterial suspension was taken from bacteria suspension after photocatalytic treatment for CFU (colony forming unit) counting. A dilution series was performed to achieve a suitable amount of bacteria on LB agar plates for counting.

The LB agar plates were cultured at 37°C overnight and the resulting CFUs on the agar plates were counting. The number of surviving bacteria was expressed as the ratio (survival ratio) of

the number of viable and cultivable bacteria remaining after exposure to experimental conditions (N) to the number of the initial viable bacteria (N_0) (log N/N_0).

II.3.4 Bacterial Reactivation after photocatalytic treatment

Photo-irradiated samples were transferred into 2 separate sterile Petri dishes. One petri dishes was covered with foil and, another one was placed under visible light at room temperature. This part of experiment was carried out to verify the ability of post-photo-irradiated bacteria in presence of TiO_2 to restore their UV-A/TiO_2-induced lesions by molecular mechanisms in darkness condition and under visible light.

II.3.5 Atomic force microscopy

Post treatment *P aeruginosa* with the UV-A/TiO_2 was dropped on the glass and dried for the AFM measurements by nanoscope multimode scanning probe microscope (SPM, Digital Instruments Inc., USA).

II.3.6 Biofilm formation by *P. aeruginosa*

Biofilm disinfecting susceptibility was studied into their free-cells or planktonic form and with biofilm community. Biofilms formation was quantified as described [24]. An overnight culture of *P. aeruginosa* was diluted 100-fold in fresh TSB both and 200 µl was added to each well of a 96 wells of Microtiter plate. Cells were grown for 3days at 30°C (preformed biofilm) before treatment by disinfectant agents (UV-Airradiation TiO_2-P25 and UV-A/TiO_2). Then, they were stained with crystal violet (CV) and quantified. Biofilm formation for different samples was determined by an increase or decrease in optical density at 600 nm, compared to the control test (media only).

II.4. Results and discussion

II.4.1 Batch photocatalytic inactivation

A series of experiments were carried out to highlight the effects of UV-A photocatalytic treatment on bacterial cultivability and viability. Figure 69 presents the kinetics inactivation of *P. aeruginosa* (ATCC 4114) under different conditions. This figure shows that the bactericidal rates were enhanced when TiO_2-P25 and UV-A irradiation were combined and by increasing the power of UV-illumination. The synergic effect of TiO_2 and UV-A radiation had a remarkable effect on bacterial cultivability. However, we cannot neglect the bactericidal effect of TiO_2 without UV-A irradiation. In 1985, Matsunaga et al., [25] reported that

TiO_2 suspensions inactivate bacteria. After Matsunaga many studies have reported on the TiO_2 photocatalytic bacterial cell wall damage [26,27].

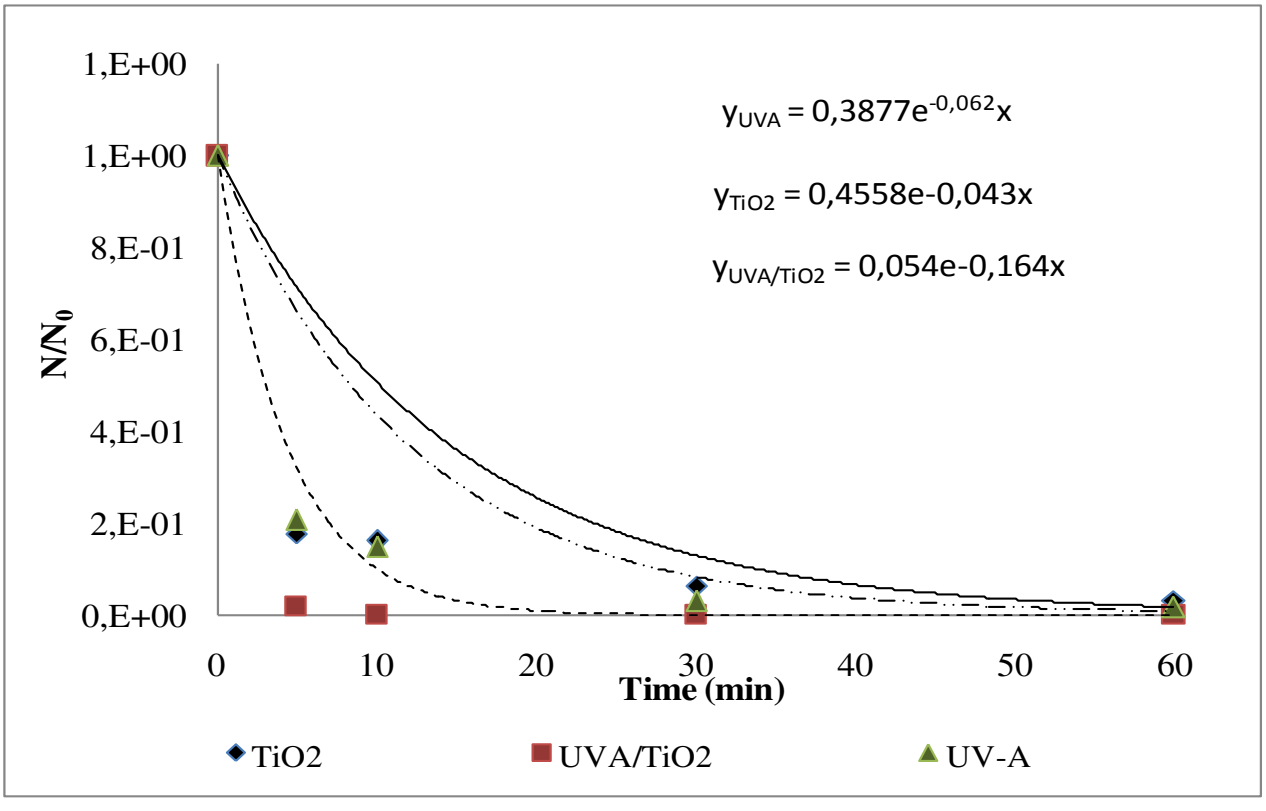

Figure 69: Kinetics of inactivation of *P. aeruginosa* (ATCC 4114) under different conditions (UV-A without TiO_2, TiO_2 without UV-A and UV-A with TiO_2). Data are averages of three experiments

P. aeruginosa outer cell wall damages due to TiO_2 photocatalysis have been reported recently by P. Amezaga-Madrid et al. [16] The TiO_2 interaction with the bacteria was reported to cause damages/disorganization in the cell wall morphology modifying its permeability and the capacity to regulate the outer layers osmotic pressures.

The inactivation of *P. aeruginosa* is compared to the Chick-Watson model was used [28]. The inactivation efficiency followed 1st order kinetics with respect to bacterial colony count (N_t), which is shown by Equation (1):

$$N/N_0 = \text{Exp}\,(-k\,C^n\,t)$$

where, N/N_0: is the reduction in the bacterial concentration, *k:* is the disinfection kinetic constant, *C*: is the disinfectant concentration, in our case (*C*) is the combination between two disinfectant agent {*d* , D_{UV-A}}with, *d*: is the catalyst concentration (mg/L) and, D_{UV-A}: UV-A dose ($mW.s^{-1}$), *t*: time (min), and *n*: is the threshold level; *n* is equal to 1 for the first order Chick-Watson model.

$$\mathbf{k = k_{(d,DUV-A)}\ (k_d + k_{DUV-A})}$$

where, *k*: is the disinfection kinetic constant, $k_{(d,DUV-A)}$: is the global photocatalytic inactivation coefficient, k_d and $k_{DUV-A}$is the disinfection kinetic constant related separately to the catalytic action and UV-A irradiation effects, *d*: is catalytic concentration (1g/L), D_{UV-A}: UV-A dose (1.7 $mW.s^{-1}$).

Chick-Watson model was modified to consider the retention of viability and cultivability rate in the contact with disinfectant agent according to the following equation (2):

$$\boldsymbol{N/N_0 = A\ Exp\ (-k\ C^n t)}$$

Based on the kinetics parameters determined according to CW model (Figure 1), the photocatalytic inactivation coefficient (*k*) that represents the slope of inactivation curve is more important after phtocatalytic treatment ($k = 0.164$) than after UV-A irradiation or TiO_2 treatment in the darkness; *k* is equal to 0.062 and 0.043 respectively.

The antimicrobial photo-biological activity of TiO_2 on bacterial cells using UV-A irradiation is expected because under irradiation of UV-A, TiO_2 can generate a large amount of ·OH, which is a potential biocide with strong oxidation potential and nonselective reactivity [29]. This may agree with Cho et al. (2004) [30] , who derived a linear correlation between the amount of ·OH and the extent of *E. coli* inactivation Their results demonstrated an excellent linear correlation between steady-state concentrations of ·OH radicals and the inactivation rates of *E. coli* indicating that ·OH radical is the primary oxidant species responsible for inactivating *E. coli*.

II.4.2 Post irradiation events after the photocatalytic treatment

To investigate the durability of UV-disinfection process using TiO_2 (Degussa P-25) on a glass plate we were studied the post irradiation events after the photocatalytic treatment.

To semi-quantify the reactivation level of post-irradiated bacteria in dark condition, a log ratio was determined according to a modified version of the Lindauer and Darby (1994) [31] equation with modification:

$$C_r = Log\ N_r / N_{UV/TiO2}$$

Where: ***Cr***: is the coefficient of reactivation; N_r= Number of viable and cultivable bacteria after a rest time in the darkness; UV-A radiation and $N_{UV\text{-}A/TiO2}$: Number of viable and cultivable bacteria after photo-disinfection process with immobilized TiO_2.

According to Lindauer and Darby (1994) [31] the reported log values range from 1 to 3.4. When the ***Cr*** is inferior to 1, there is no reactivation; if ***Cr*** ranged between 1 and 3.4, we can conclude that reactivation occurs in the darkness or/and in visible light; when ***Cr*** is superior to 3.4, there are no disinfectant effects and the cells grow naturally without any environmental stress.

In effluents from the studied photoreactor and according to the result, *P. aeruginosa* showed a bacterial recovery after photocatalytic treatment during the subsequent 24 h in dark and visible conditions. Indeed, ***Cr*** is equal to 1.41 and 2.1 (Data are averages of three experiments) respectively in darkness and under visible light.

This bacterial recovery can be related by a biological systems have evolved mechanisms to appropriately respond to environmental stresses that can damage proteins and DNA [32].

In their response to stress, bacteria generally possess molecular mechanisms to restore DNA lesions. Indeed, bacteria can evolve four main mechanisms in the repair or damage tolerance of UV radiation-damaged DNA, including photoreactivation, nucleotide excision repair (NER), mutagenic DNA repair (MDR), and recombinational DNA repair [33].

These results can affect the effectiveness and the durability of UV-A photocatalytic treatment. Bacterial resuscitation after the photocatalytic treatment could be explained by the fact that, under oxidative stress, a part of stressed cells can enter in a viable but non cultivable (VBNC) state. The result of no cultivability after TiO_2 photocatalytic treatment under UV-A light does not always represent total bacterial death. The ROS produced during the photocatalytic process can induce oxidative stress on the microorganisms, causing the cells to enter a viable but non cultivable (VBNC) state.

UV-A irradiation and attacks by oxidative species generate changes in the permeability of the lipid membrane and/or modify the bacterial DNA, leading the loss of cultivability while viability remains unaltered [34] When the oxidative stress ends (dark conditions), the microorganisms recover their cultivability. In addition, the growth state of bacteria (exponential or stationary) varies in time. Depending on this parameter, some bacteria could persist under photocatalytic conditions and consequently, their recovery rate in the dark could also be influenced. This hypothesis can explain the recovery of *P. aeruginosa* after a rest time in the darkness.

Photoreactivation in bacteria involves a single enzyme called photolyase which binds CPDs and, in a light-dependent step, monomerizes the CPD and dissociates from the repaired lesion [33] Indeed, UV-A is essential for photoreactivation, although it also has lethal and sublethal effects on microorganisms [35]. Thus, when the value of log ratio (*Cr*) is inferior to 1, we can deduce that the lethal effects of UV-A radiation take over its beneficial effects but when (*Cr*) is superior to 1, the inactivation effect of photocatalytic can be slowed down and thereby, we can integrate this log ratio in the inactivation equation as well:

$$N/N_0 = A\,(1-1/C_r)\,[Exp\,(-k\,(C^n\,t)]$$

The integration of *Cr* rate in the photocatalytic inactivation equation has as goal to consider an eventual reactivation after photocatalytic treatment in real scale and to find a solution to overcome the inconvenient related to this interesting technology.

II.4.3 Investigatingchanges in bacterial cell morphologyafter TiO_2-P25 photocatalysis treatment using AFM

Figure 70 shows AFM photographs of *P. aeruginosa* cells after different UV-A illumination times with TiO_2.

Before irradiation, the cells have a cylindrical shape (Figure; 70a). After irradiation for 10 min (Figure; 70b), obvious morphological changes were recognized presented by an increase in the membrane curvature. Under stress, the morphological change in bacterial shape is considered as a bacterial strategy to protect against stress and to escape, or to minimize the bactericidal effect of photocatalytic treatment to survive [36].

After 60 min of photocatalytic treatment, the observation reflects the change in concentration of the cell wall components, and a disorganization in the outermost layer of the cell with grooves on the cell surface owing probably to the change in the concentrations of extracellular polymeric substances (EPS) or the release of cytoplasm (Figure; 70c).

The presence and variability of capsular EPS on the three *P. aeruginosa* strains strongly impacts the extent of membrane damage sustained during exposure to the photoactive TiO_2 nanoparticles [37]. While structural features of the cell membrane may contribute to oxidant resistance prior to lethal damage, capsular EPS provides an additional barrier against TiO_2 nanoparticles toxicity. Capsular EPS may play dual roles in minimizing nanoparticles toxicity, it may provide a physical barrier between the cell and particle at the cell surface, but also provides an alternative oxidation and consumption site for ROS. This observation can strongly approve the recovery of a part of post treated bacteria in darkness and under rest time in visible light.

The cell damages were more apparent and severe after 90 min. Indeed, Figure; 70d shown that the cylindrical shape of the cells disappeared completely, suggesting the complete decomposition of dead cells.

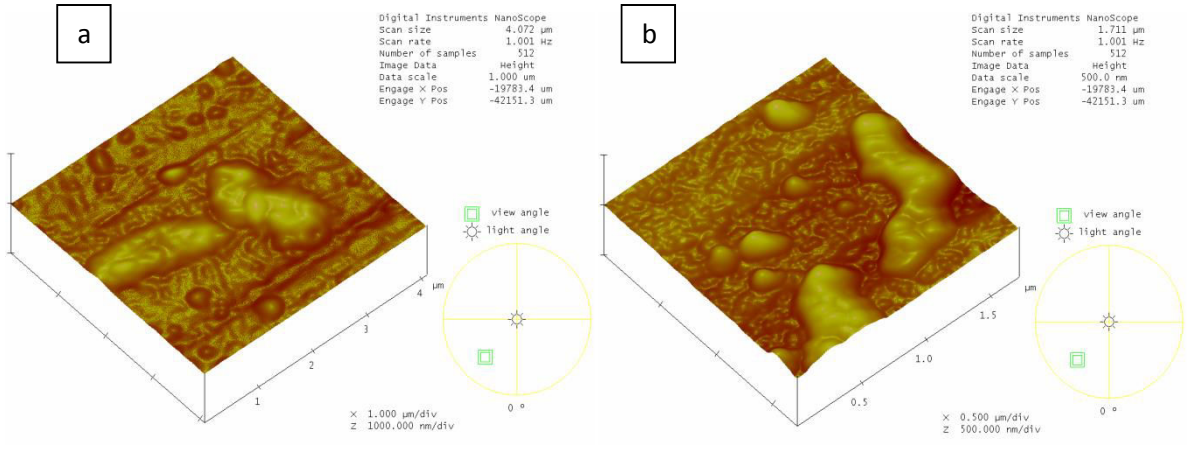

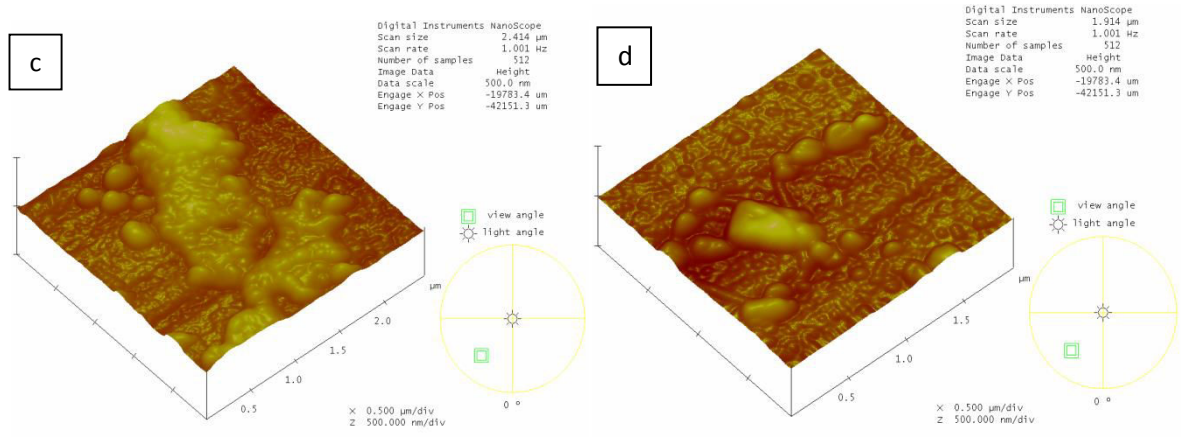

Figure 70: AFM amplitude images of *P. aeruginosa* (ATCC 4114) following photocatalytic treatment (a) before treatment, (b) after 10 min of UV-A/TiO_2 treatment, (c) after 60 min .of photocatalytic treatment, and (d) after 90 min of treatment.

II.4.4 Monitoring of biofilm production by *P. aeruginosa* strain under different treatment conditions

P. aeruginosa is a ubiquitous bacteria recognized by its genetic and metabolic flexibility. In addition, this strain of bacteria can expressed many virulence factors. These factors are either related or secreted by bacteria and they are involved in various stages of host infection (human, animal or plant).

The aim of this study was to evaluate the impact of photocatalytic treatment on biofilm formation by *P. aeruginosa* studied strain.

Practically, we have treated *P. aeruginosa* under different cells' forms; planktonic cells (Figure 71,a) and sessile cells (biofilm-associated) (Figure 71,b) to demonstrate respectively, the effectiveness of photocatalytic treatment to inhibit the biofilm initiation by a planktonic cells and also to demonstrate the capacity of this disinfection process to disorganize this bio-structure already bent.

The modeling of biofilm production in relationship with physical (UV-A) and chemical (TiO_2) effects were determined according the model employed by Chick-Watson with modifications [28] as following equation (3):

$$M_t/M_b = A \exp(-k\, C^n)$$

with; M_b: The total biomass of the biofilm continues to grow for the control test (before treatment); M_t: The biomass of the biofilm at time t, after treatment; A: Biofilm weakness rate; k: Biofilm inactivation rate; C: is the disinfectant concentration, and n: is the threshold level; n is equal to 1 for the first order CW model is equal to 1.

Then, The biofilm growth constants, mainly: *A:* Biofilm stability rate and, *k*: Biofilm inactivation rate; were determined and compared to the control test; Biofilm production at time *t* under different treatment conditions (Figure. 3).

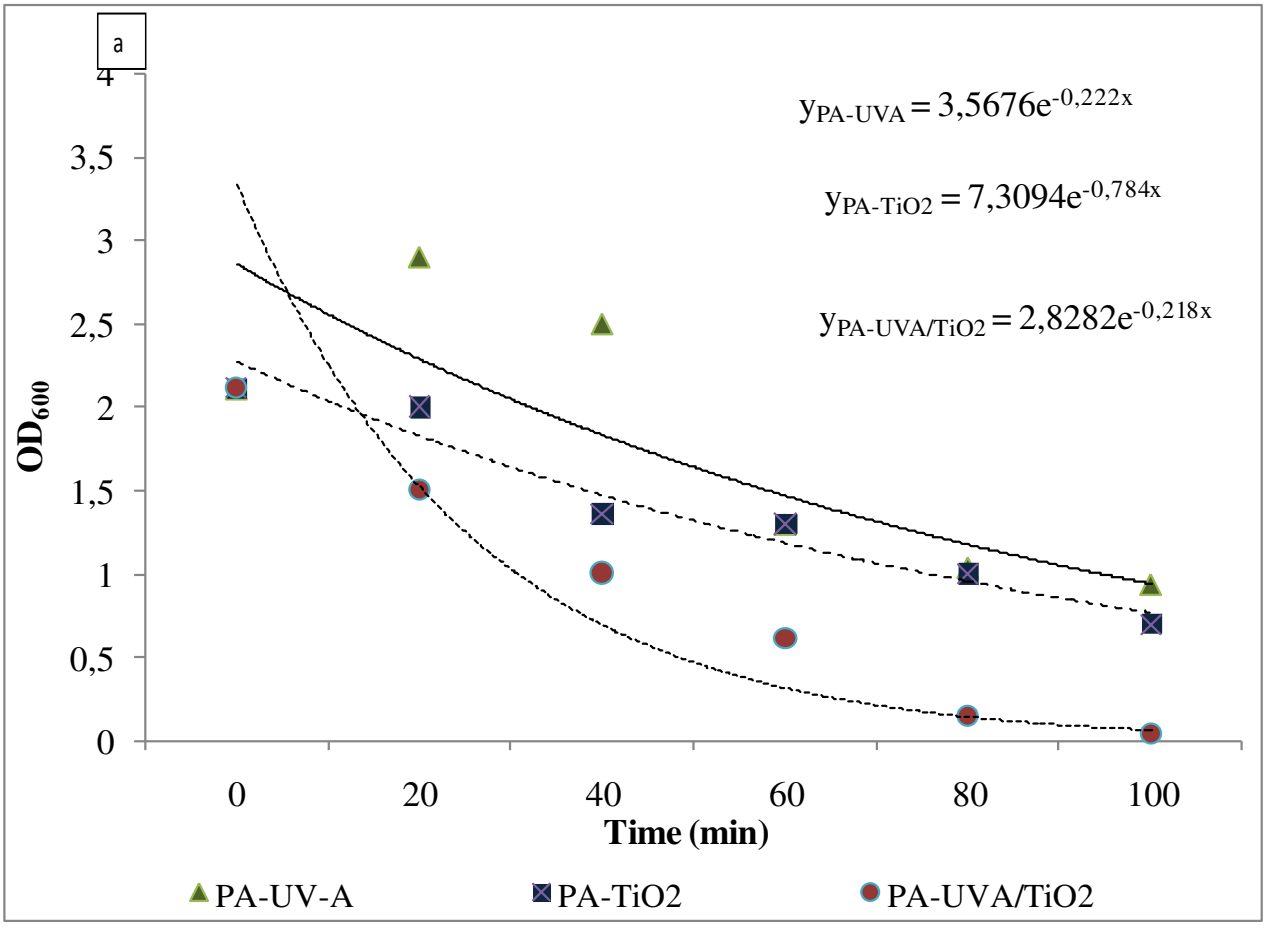

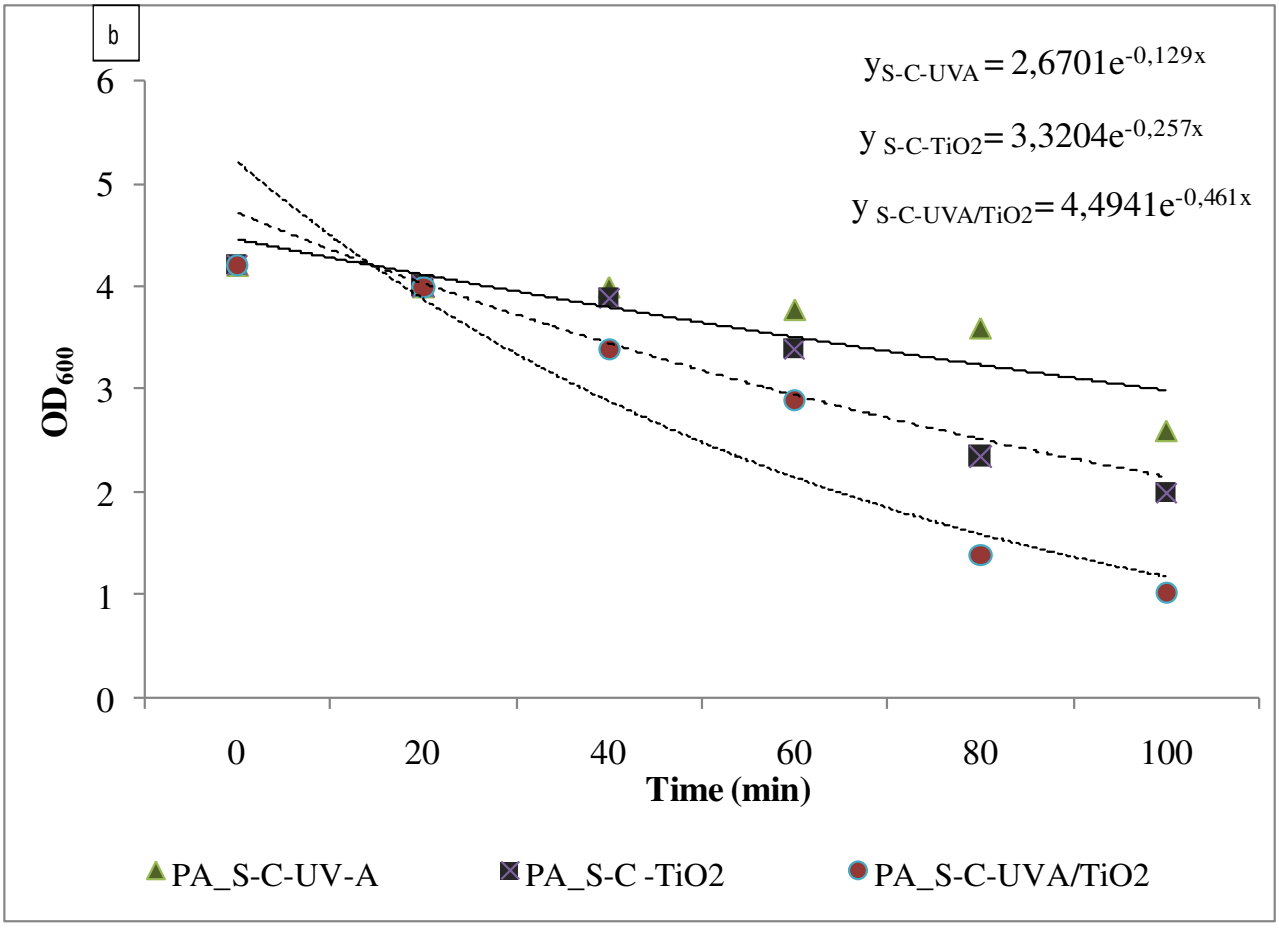

Figure 71: Monitoring of biofilm production by *P. aeruginosa* under different treatment conditions With: S-C: Sessil cell and, PA: planktonic form of *P. aeruginosa.* Data are averages of three experiments.

A figure 71a show that, for the tested *Pseudomonas aeruginosa*, biofilm production exhibits a progressive increase with increasing UV-A exposure until the threshold UV-A dose noted (***Hs***). To model this response, we propose a model that associates biofilm kinetic growth with UV-A dose (***Hs***):

$$dM_b/dH_s = \mu . dM_a/dH_s$$

Where M_b is the total biomass of the biofilm, which continues to grow for the control test (before exposure to UV-A light); M_a is active bacteria responsible for production and maturation of biofilm; μ is biofilm growth rate; and H_s the threshold UV-A dose.

After irradiation of bacteria with a UV-A dose higher than threshold dose (***Hs***), we noted a progressive decrease in the production of biofilm correlated with increased UV-A dose.

We can model this observation as following:

$$(dM_b/dH_t) = \mu . M_a . [1- (dM_d/dH_t)]$$

With, H_t is UV-A dose over than H_s dose.

After photocatalytic treatment of *P. aeruginosa* in the planktonic form allows an inhibition of biofilm production independently of H_s UV-A dose. Indeed, when we compare the biofilm kinetic constants determined after UV-A/TiO_2 treatment, we can note an increasing of the biofilm inhibition coefficient; (k= 0.784) and in biofilm weakness rate (A = 7.31) compared to the kinetic constants determined after UV-A irradiation and TiO_2 in the darkness (Figure 71,a). Consequently, we can conclude that the photocatalytic treatment allows a decrease the active bacterial density including VBNC bacteria and recoverable Bactria after treatment (M_a) and the increase in defective bacteria (M_d), and consequently, the UV-A/TiO_2 treatment can limit the production and maturation of biofilm.

M_a = Viable and Cultibale bacteria + VBNC bacteria+ Viable bacteria not yet Resuscitate

M_d = Death bacteria + Viable bacteria cannot resuscitate.

We can modelthis observation using biofilm growth model as follow:

$$(dM_b/dH_t) = \mu . M_a . [1- (dM_d/dC_t)]$$

Where, M_b is the total biomass of the biofilm as it continues to grow for the control test (before photocatalytic treatment); M_a is active bacteria responsible for production and maturation of biofilm; M_d is inactive bacteria no longer involved in the construction of biofilm; μ is biofilm growth rate; and C_t is the disinfectant concentration (UV-A/TiO_2).

For the second studied case; the monitoring of biofilm inhibition by sessile cells under different disinfection conditions (Figure 71, b), we can note also an increase of the biofilm inactivation rate, and in the biofilm weakness rate after photocatalytic treatment similar to the previous relationship. By this analysis, we can conclude that the combination action of UV-Airradiation and TiO_2 was able to disorganize the biofilm structure but not at the same performance for the first case of study. We have to increase the contact time UV-A/TiO_2 and a formed biofilm to allow the destruction of this resistant structure.

Additionally, in bacteria, the regulation of many important changes in gene expression is mediated by systems of signaling between cells known as Quorum Sensing (QS) cells [38]. Cells in a population will sense their density and number through the presence of signals that diffuse freely across cell membranes and between cells. Via an auto-induced positive feedback mechanism, a population of cells can quickly induce the appropriate phenotypes required for responding to a particular environmental condition or for proceeding with the differentiation process of the population [39]**.** The diverse small signal molecules used for QS transform independent cells into specialized cell communities. These small molecules are used to regulate biofilm formation [40]. *P. aeruginosa* possesses two QS systems, *las* and *rhl*. Each system has its own signal synthase, signal receptor and distinct acylhomoserine lactone (AHL) signal. Quorum sensing regulated functions is known to be critical for acute virulence [41]. Consequently, these QS systems regulate virulence factors mainly the biofilm formation [42].

Given that QS is defined as the cell-density-dependent control of gene expression, photocatalitic treatment has an inhibitory effect on cell-to-cell communication via diffusible signal molecules due to the decrease in density of active bacteria ($\boldsymbol{M_a}$) and the increase in defective bacteria ($\boldsymbol{M_d}$). Thus, the photocatalytic treatment of plonctonic bacterial leads to a decrease in bacterial density and, consequently, limits the establishment of intercellular communication (QS), thus preventing biofilm formation and inhibiting the expression of other virulence factors.

The Toxicological evaluation of TiO_2 Nanoparticles in *P.aeruginosa* cell after photocatalytic treatment was done on slide through one drop of treated or non treated sample, and was examined under optical microscope (x 40 magnification).

After 10 min (Figure 72, b) of photocatalytic treatment, we can observe a cell aggregation. This bacterial behavior can reflect the induction of biofilm formation as bio-protection structure against the photo-bactericidal effects. In contrast, the illumination of *P. aeruginosa* strain with TiO_2 have an inhibitor effect on cell aggregation and thus on cell-to-cell communication via Quorum Sensing communication due probably to the decrease of active bacteria density ($\boldsymbol{M_a}$) and the increase of defectives ones ($\boldsymbol{M_d}$) (Figure 72,c).

However, we can observe a cell aggregation under 60 min of photocatalytic treatment. This result can explain by a partially return of cells to cells communication of resuscitate bacteria.

This result can explain a discrepancy between CFU counting and planktonic forming biofilm results after TiO_2/ UV-A treatment. Indeed, CFU counting can provide an underestimation of viability if the bacterial cells aggregate, and this was a reason *P. aeruginosa* was well not assessed with CFU counting after 10 min of treatment.

We can therefore change the kinetic model of bacterial inactivation according to the following equation:

$$N/N_0 = A' \text{ Exp } (-k\ C^n t)$$

$$\text{With, } A' = A + \gamma$$

Where,*A*: the retention of viability and cultivability rate in the contact with disinfectant agent and γ*:* error estimation due to the putative presence of cells aggregation.

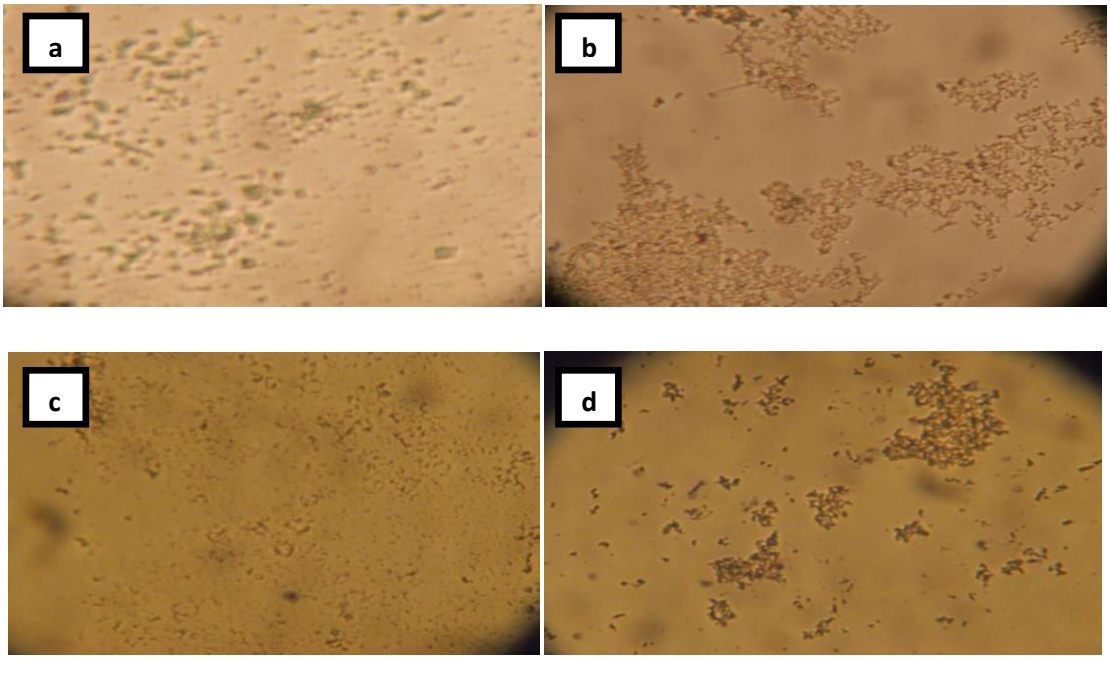

Figure 72: Toxicological evaluation of TiO_2 Nanoparticles in stained *Pseudomonas aeruginosa* cell under photocatalytic treatment by optical microscopy observation (x 40) with; a: before treatment (t_0); b, c and d: observed slide at time 10, 30 and 60 min respectively.

The study of bacterium *Pseudomonas aeruginosa* mobility: swimming, twitching and swarming.

As shown in Figure 73, the bacterium has lost its mobility for both types twitching and swarming after 60 min of treatment with a progressive increase in the swimming motility up to 60 min of photocatalytic treatment. This result can explain in part the return to cell aggregation after 60 min of TiO_2/UV-A treatment

The retention of swimming motility cells after 60 min of photocatalytic treatment could represent a survival bacterial strategy which *P. aeruginosa* can disperse from the weakened biofilm to seed new surfaces via flagellum motility.

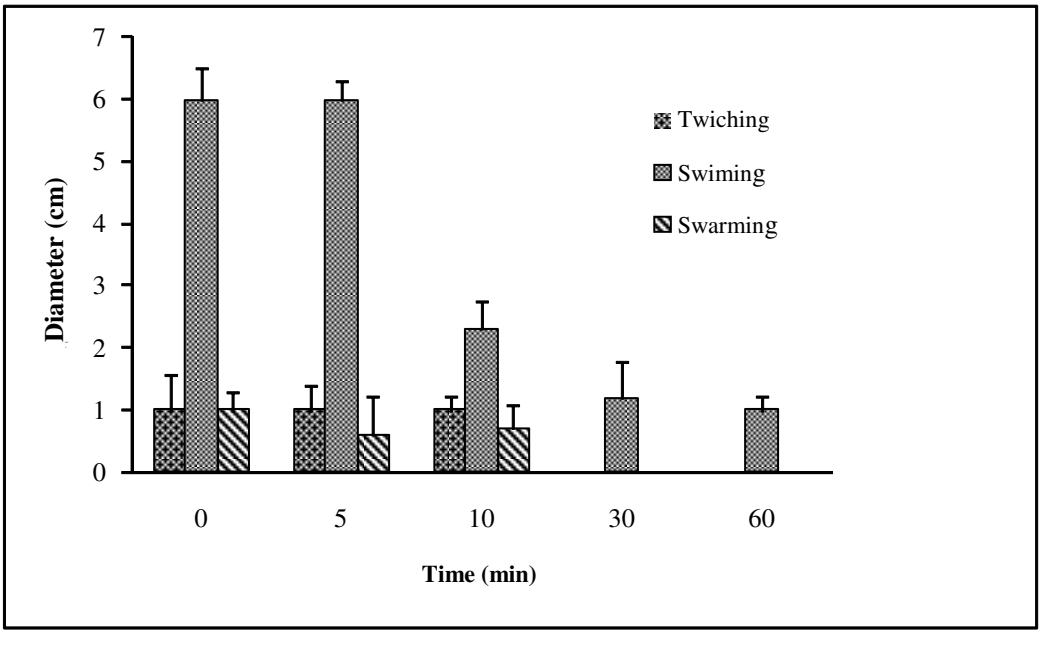

Figure 73: Monitoring of *P. aeruginosa* motility of swimming, swarming and twitching under photocatalytic treatment.

By this observation, we can modify the modelbiofilm growth taking account of a possible reactivation of bacteria during processing as follow:

$$(dM_b/dH_t) = \mu. (M_a\text{-}ln (M_r/M_a))[1- (dM_d/dC_t)]$$

With, Where M_b is the total biomass of the biofilm as it continues to grow for the control test (before photocatalytic treatment); M_a is active bacteria responsible for production and maturation of biofilm; M_d is inactive bacteria no longer involved in the construction of

biofilm; $\boldsymbol{\mu}$ is biofilm growth rate; and $\boldsymbol{C_t}$ is the disinfectant concentration (UV-A/TiO_2), $\boldsymbol{M_r}$ is a part of resuscitate bacteria.

II.5. Conclusions

P. aeruginosa has proved to be a very interesting biological model for the (i) estimation of the expression of virulence factor after water treatment, and (ii) the determination of the optimum conditions of water treatment allowing bacterial inactivation and attenuation of virulence factors.

The broad-spectrum action of photocatalytic treatment (bacterial viability, cells recovery, biofilm production...) allows an investigation of the most significant properties of the photocatalytic disinfection process: universality (i.e., the absence of weakness against any type of microorganisms), and irreversibility (i.e., avoiding cell reparation opportunities and slowing down regulatory/signalling networks).

In addition, the optimization of water photocatalytic disinfection process based on the exploration of the expression and the retention of virulence factors by indicator bacteria make as thought to introduce new recommendation to valid wastewater treatment systems by photocatalytic process and also to set up this technology in another applications such as disinfection of hospital tools and furniture, food preservation and, mainly to prevent biofilm formation. Indeed, the colony forming unit (CFU) counting can underestimate the bacterial viability if bacteria can aggregate as a response to a photocatalytic stress. So we have to integrate other tests to estimate the viability of treated cells to avoid a dysfunction of water treatment process.

As a perspective of this study, the use of photocatalytic treatment as an alternative technology to control biofilm growth can be optimized to limit and/or prevent biofilm formation by adjusting UV exposure time, nanoparticules concentration, etc.

ACKNOWLEDGMENT

This work is supported by PHC-Utique program managed by the CMCU (code 14G0821), and CERTE contract programs funded by Ministry of Higher Education and Scientific Research of Tunisia

II.5. References

[1] Moles J. 2007. Eau de distribution, désinfection. In : Les techniques de l'ingénieur . Vol. W 5500.

[2] Blanc D, Petigna S, Janin CB, Bille J, Francioli P. 1998. Frequency and molecular diversity of *Pseudomonas aeruginosa* upon admission and during hospitalization: a prospective epidemiologic study. *Clin. Microbiol. Infect*. 4: 242–247.

[3] Anaissie E.J, Penzak S.R, Dignani M.C. 2002. The hospital water supply as a source of nosocomial infections: a plea for action. *Arch. Intern. Med*. 162: 1483–1492.

[4] Exner M, Kramer A, Lajoie L, Gebel J, Engelhart S, Hartemann P. 2005. Prevention and control of health care-associated waterborne infections in health carefacilities. *Am. J. Infect. Control*. 33: S26-S40.

[5] Matheson N.R, Potempa J, Travis J. 2006. Interaction of a novel form of *Pseudomonas aeruginosa* alkaline protease (aeruginolysin) with interleukin-6 and interleukin-8. *Biol. Chem*. 5: 387-911.

[6] Veesenmeyer J.L, Hauser A.R, Lisboa T, Rello J. 2009. *Pseudomonas aeruginosa* virulence and therapy: evolving translational strategies. *Crit. Care. Med*. 37:1777-86.

[7] Lysczak J.B, Cannon C.L, Pier G.B. 2000. Establishment of *Pseudomonas aeruginosa* infection: lessons from a versatile opportunist. *Microbes. Infect*. 2: 1051-60.

[8] Woods D.E, Schaffer M.S, Rabin H.R, Campbell G.D, Sokol P.A. 1986. Phenotypic comparison of *Pseudomonas aeruginosa* strains isolated from a variety of clinical sites. *J. Clin. Microbiol*. 24: 260- 4.

[9] Costerton B, 2004. Microbial ecology comes of age and joins the general ecology community. *Proc. Natl. Acad. Sci .USA*.101: 16983–16984.

[10] Sauer K, Cullen M.C, Rickard A.H, Zeef L.A, Davies D.G, Gilbert P. 2004. Characterization of nutrient.induced dispersion in *Pseudomonas aeruginosa* PAO1 biofilm. *J. Bacteriol*. 186:7312–7326.

[11] Chen W.J, Weisel C.P. 1998. Halogenated DBP concentrations in a distribution system. *J Am. Water. Works. Ass*. 90, 4: 151-163.

[12] Krasner S.W, Weinberg H.S, Richardson Pastor S.J, Chinn R, Sclimenti M.J, Onstad G.D, Thruston A.D. 2006. Occurrence of a new generation of disinfection by-products. *Environ. Sci. T*. 40: 7175-7185.

[13] Hoffmann M.R, Martin S.T, Choi W, Bahnemann D.W. 1995. Environmental Applications of Semiconductor Photocatalysis. *Chem. Rev*. 95: 69–96.

[14] Okuda M, Tsuruta T, Katayama K. 2009. Lifetime and diffusion coefficient of active oxygen species generated in TiO_2 sol solutions. *Phys. Chem. Chem. Phys*.11: 2287–2292.

[15] Matsunaga T, Tomoda R, Nakajima T, Wake H. 1985. Photoelectrochemical sterilization of microbial cells by semiconductor powders: *FEMS. Microbiol. Lett*. 29: 211-214.

[16] Amézaga M.P, Silveyra M. R, Cordoba F.L, Nevarez M.G.V, MikiYoshida M, Orrantia B.E, Solıs F.J. 2003. TEM evidence of ultrastructural alteration on *Pseudomonas aeruginosa* by photocatalytic TiO_2 thin films. *J. Photoch. Photobio. B*. 4: 45-50.

[17] Benabbou A, Derriche Z, Felix C, Lejeune P, Guillard C. 2007. Photocatalytic inactivation of Escherischia coli: effect of concentration of TiO_2 and microorganism, nature, and intensity of UV irradiation. *Appl. Catal. B: Environ*. 76: 257–263.

[18] Vohra A, Goswami D.Y, Deshpande D.A, Block S.S. 2006. Enhanced photocatalytic disinfection of indoor air. *Appl. Catal. B: Environ*. 64, 57-65.

[19] Kilvington L.S, Keho S.C, Al-Touati F, McGuigan K.G. 2005. Solar and photocatalytic disinfection of protozoan, fungal and bacterial microbes in drinking water. *Water. Res*. 39: 877- 883.

[20] Maneerat C, Hayata Y. 2006. Antifungal activity of TiO_2 photocatalysis against Penicillium expansum in vitro and in fruit tests. *Int. J. Food. Microbiol*. 107: 99-103.

[21] Matsunaga T, Tomoda R, Nakajima T, Nakamura N, Komine T. 1988. Continuous-Sterilization System That Uses Photosemiconductor Powders. *Appl. Environ. Microb*. 54:1330-1333

[22] Saito T, Iwase T, Horie J, Morioka T. 1992. Mode of photocatalytic bactericidal action of powdered semiconductor TiO_2 on mutans streptococci. *J. Photoch. Photobio. B*. 14: 369-379.

[23] Huan Z, Maness P.C, Blake D.M, Wolfrum E.J, Smolinski S.L, Jacoby W.A. 2000. Bactericidal mode of titanium dioxide photocatalysis. *J. Photoch. Photobio.A*. 130:163-170.

[24] Toole G.O, Kaplan H.B, Kolter R. 2000. Biofilm formation as microbial development. *Ann. Rev. Microbiol*. 54: 49-79.

[25] Matsunaga T, Tomoda R, Nakajima T, Wake H. 1985. Photoelectrochemical sterilization of microbial cells by semiconductor powders. *FEMS. Microbiol. Lett*. 29: 211–214.

[26] Maness P.C, Smolinski S, Blake D.M, Huang Z, Wolfrum E.J, Jacoby W.A. 1999. Bactericidal activity of photocatalytic TiO_2 reaction: toward an understanding of its killing mechanism. *Appl. Environ. Microbiol*. 65: 4094–4098.

[27] Bacsa R., Kiwi J, Ohno T, Albers P, Nadtochenko V. 2005. Preparation, testing and characterization of doped TiO_2 active in the peroxidation of biomolecules under visible light. *J. Phys. Chem. B*. 109: 5994–6003.

[28] Haas CN, Joffe J, Hornberger JC, Anmangandla U, Heath M, Jacangelo J., 1996. The Effect of Water Quality on Disinfection Kinetics. *J. Am. Water. Works. Ass*. 88: 95-103.

[29] Pal A, Pehkonen S.O, Yu L.E, Ray M.B. 2007. Photocatalytic Inactivation of Gram-positive and Gram-negative Bacteria using Fluorescent Light. *J. Photoch. Photobio. A*. 186: 335-341.

[30] Cho M, Chung H, Won yong C, Yoon J. 2004. Linear correlation between inactivation of *E. coli* and $^{\cdot}OH$ radical concentration in TiO_2 photocatalytic disinfection. *Water. Res*. 38: 1069-1077.

[31] Lindauer KG, Darby J., 1994. Ultraviolet disinfection of waste water: effect of dose on subsequent photoreactivation. *Water. Res*. 28: 805-817.

[32] Marugán J, Grieken RV, Sordo C, Cruz C., 2008. Kinetics of the photocatalytic disinfection of *Escherichia coli* suspensions. *Appl. Catal. B: Environ*. 82: 27–36.

[33]Ben Said M, Masahiro O. 2013. Enhancement of ultraviolet water disinfection process. *Afr. J. Biotechnol*. 12: 2932-2938.

[34] Ben Said M, Masahiro O, Hassen. A.2010. Detection of viable but non cultivable *Escherichia coli* after UV irradiation using a lytic Qβ phage. *Ann. Microbial*. 60: 121-127.

[35] Oguma K, Katayama H, Ohgaki S. 2002. Photoreactivation of *Escherichia coli* after low- or medium-pressure UV disinfection determined by an endonuclease sensitive site assay. *Appl Environ. Microbiol*. 68: 6029–6035.

[36] Laspidou C.S, Rittmann B.E. 2002. Non-steady state modeling of extracellular polymeric substances, soluble microbial products, and active and inert biomass. *Water. Res*.36:1983-1992.

[37] Norton C.D, LeChevalier M.W. 2000. A pilot study of bacterial population changes through potable water treatment and distribution. *Appl. Environ. Microbiol*. 66: 268-276

[38] Girard G, Bloemberg G.V. 2008. Central role of quorum sensing in regulating the production of pathogenicity factors in Pseudomonas aeruginosa. *Future. Microbiol*. 3: 97-106.

[39] Kjelleberg S, Molin S. 2002. Is there a role for quorum sensing signals in bacterial biofilms? *Curr. Opin. Microbiol* . 5:254–258.

[40] Ueda A, Attila C, Whiteley M, Wood T.K. 2009. Uracil influences quorum sensing and biofilm formation in *Pseudomonas aeruginosa* and fluorouracil is an antagonist. *Microbial Biotechnology*. 2: 62–74.

[41] Shrout J.D, Chopp D.L, Just C.L, Hentzer M, Givsko M, Parsek M.R. 2006. The impact of quorum sensing and swarming motility on *Pseudomonas aeruginosa* biofilm formation is nutritionally conditional. *Mol. Microbiol*. 62: 1264-1277.

[42] Hammer B.K, Bassler B.L., 2003. Quorum sensing controls biofilm formation in Vibrio cholerae. *Mol. Microbiol*. 50:101- 4.

Conclusion Générale et Perspectives

Le maintien de la qualité des eaux est un défi pour l'humanité face à la complexité de la vie moderne et de la diversification des sources de pollution. Des législations de plus en plus strictes ont été adoptéespar plusieurs pays concernant la dépollution des eaux et de nouvelles normes très strictes doivent être respectées pour la mise au point de nouvelles techniques de traitement.

Parmi les solutions envisagées, plusieurs techniques ont été proposées dont la photocatalyse hétérogène, qui est une technique peu coûteuse, basée sur l'irradiation d'un semiconducteur par une source lumineuse. Les travaux publiés montrent que ce procédé permet la dégradation de plusieurs types de polluants (organiques, inorganiques voire même des microorganismes pathogènes).

L'objectif principal de ce travail était l'amélioration des procédés photocatalytiques par la synthèse de nouveaux catalyseurs actifs sous irradiation solaire. Afin de démontrer l'efficacité des nouveaux catalyseurs développés, nous avons étudié la dégradation de quelques polluants modèles chimiques et biologiques de l'eau.

Dans la première partie de notre travail, nous avons synthétisé des hétérostructures ZnO/Fe_2O_3 par hydrolyse de $FeCl_3$ en présence de particules de ZnO. La caractérisation de ce nouveau système catalytique par microscopie à transmission (MET) a montré un bon couplage entre ZnO et Fe_2O_3. Le composite ZnO/Fe_2O_3 présente une hétérojonction permettant une séparation efficace des charges (e^-/h^+) qui favorise la production d'EROs (radicaux $^{\bullet}OH$ et $O_2^{\bullet-}$) par rapport à ZnO seul. Les expériences photocatalytiques à l'aide de ZnO/Fe_2O_3 ont permis d'améliorer l'efficacité de la dégradation de l'acide salicylique. Finalement, la recyclabilité de ce nouveau catalyseur a été démontrée.

Afin d'améliorer les propriétés du catalyseur ZnO, nous avons exploré une nouvelle voie de synthèse par dopage avec le manganèse. Une synthèse solvothermale a été développée afin de préparer des nanoparticules poreuses ZnO et ZnO dopé Mn. L'influence du pourcentage de dopant Mn^{2+} sur les propriétés structurales, optiques et photocatalytiques des particules de ZnO:Mn a été étudiée. Le matériau ZnO dopé par 3% molaire de Mn^{2+} permet la photodégradation optimale du colorant Orange II sous irradiation solaire. Ce nanomatériau présente une surface spécifique plus élevée que le ZnO seul, ce qui améliore l'efficacité

photocatalytique. De plus, la capacité du dopant Mn^{2+} de piéger les électrons, assure la diminution de la recombinaison des charges et, par conséquent, améliore l'activité photocatalytique.

Afin d'élargir les applications photocatalytiques à différents types de polluants, nous avons étudié la dégradation de l'Orange II ainsi que d'une souche bactérienne de référence (*E. coli* MG 1655) par un nouveau catalyseur constitué de nanobâtonnets de ZnO. Nos résultats expérimentaux montrent un bon rendement de dégradation photocatalytique de l'Orange II avec le catalyseur en suspension ou immobilisé sur des plaques de verre ainsi qu'une excellente stabilité du semiconducteur ZnO après plusieurs utilisations sans aucun traitement chimique ou autre. L'inactivation photocatalytique d'*E. coli* MG 1655 par les nanobâtonnets de ZnO a également été prouvée. La cultivabilité bactérienne est affectée que le catalyseur soit dispersé ou immobilisé. Afin de mieux comprendre le mécanisme d'action des EROs générées lors de la photocatalyse sur cette bactérie, nous avons utilisé plusieurs techniques spectroscopiques et microscopiques. L'analyse des dommages engendrés lors de la photocatalyse a été réalisée par microscope électronique à balayage (MEB), microscope à épifluorescence, microscope à force atomique et spectroscopie de fluorescence. Les résultats montrent que les dommages photocatalytiques ont principalement touché la membrane ainsi que les protéines bactériennes. Des analyses complémentaires par cytométrie de flux ont montré que le matériel génétique bactérien n'est pas affecté par le traitement photocatalytique.

La réponse à un stress, par exemple oxydant comme dans le cas de la photocatalyse, est dépendant de la souche bactérienne et cette thématique a fait l'objet de la deuxième partie de nos recherches.

Afin de mieux comprendrel'action des EROs générées par photocatalyse sur les bactéries, nous avons étudié l'inactivation de trois souches bactériennes (*Escherichia coli, Pseudomonas aeruginosa et Salmonella enterica* Typhi) par photocatalyse à l'aide de TiO_2 P25 fixé sur lame de verre et irradié par la lumière solaire naturelle. Les résultats confirment que la réponse bactérienne au stress photocatalytique est souche-dépendant. Cette différence peut être liée soit au système photocatalytique (concentration du nanocatalyseur, dose UV solaire) soit aux propriétés morphologiques, métaboliques et génétiques des bactéries (relation dose/réponse). De plus, nous avons observé l'aptitude de quelques souches à se réactiver après traitement photocatalytique. Ce phénomène de réactivation nous contraint à chercher une optimisation du processus photocatalytique par une étape de traitement complémentaire.

Une étude basée sur l'exploration de l'expression et de la rétention des facteurs de virulence par un indicateur bactérien *Pseudomonas aeruginosa* (*ATCC* 4114) a également été réalisée. TiO_2-P25 en suspension sous irradiation UV_A a été utilisé comme photocatalyseur. Les résultats montrent une perte de la cultivabilité avec des dommages membranaires observés par microscopie à force atomique. Cependant, la bactérie a conservé sa capacité de réactivation et sa virulence n'est pas totalement atténuée.

La discordance des résultats entre la perte de cultivabilité sur milieu usuel d'une part et la rétention des caractères de virulence après traitement d'autre part, exige d'évaluer l'efficacité du système de traitement photocatalytique en terme de virulence (la mobilité bactérienne, la production de biofilm, …), appuyé par une évaluation classique sur l'abattement bactérien en amont et en aval du système épuratoire.

Les perspectives envisagées pour ce travail concernent les points suivants :

- La synthèse de nanoparticules semiconductrices activables dans le visible pour améliorer l'activité photocatalytique.
- L'optimisation de la technique de photocatalyse et du procédé (concentration en catalyseur, dose UV, géométrie du réacteur, …).
- L'étude de la réactivation bactérienne après traitement et l'ajout d'une méthode de désinfection complémentaire.
- La mise en œuvre d'une méthode efficace de détection des bactéries viables mais non cultivables (par exemple, en utilisant une sonde fluorescente ou l'utilisation des bactériophages).
- L'élargissement de l'application photocatalytique à un grand panel de microorganismes et protozoaires.
- Enfin, ce travail pourrait être une base utile à d'autres applications dans les domaines suivants : agroalimentaire, médecine (destruction des biofilms bactériens) et le nettoyage de surfaces contaminées.

Résumé

Détoxification des eaux usées urbaines par photocatalyse solaire

Mots clefs : Détoxification, Eau usée, Photocatalyse solaire, Semiconducteur, Bactérie.

Ces dernières décennies, la pollution de l'eau est devenue un problème se posant avec insistance dans le monde entier. En effet, la forte croissance des besoins en eau due à l'accroissement démographique ainsi qu'aux évolutions industrielles, agricoles et urbaines, engendre des quantités énormes de rejets d'eaux usées. Ces derniers sont déversés dans la nature avec ou sans traitement et peuvent constituer un danger via la transmission de maladies ainsi que pour l'irrigation des terres se trouvant aux alentours du site de rejet.

L'objectif de cette étude est le traitement des rejets aqueux par l'utilisation d'une nouvelle technologie appelée « photocatalyse hétérogène ». Ce procédé est basé sur l'utilisation d'un semiconducteur et d'une source lumineuse de longueur d'onde appropriée et est simple à mettre en œuvre et peu coûteux.

Des semiconducteurs ZnO couplé à Fe_2O_3, ZnO de morphologie « bâtonnets » et ZnO dopé Mn^{2+} ont été synthétisés et testés dans diverses applications photocatalytiques. Les résultats obtenus ont montré une amélioration de l'efficacité catalytique par rapport à ZnO. Les matériaux développés permettent de réduire la recombinaison des charges et, par conséquent, d'améliorer l'activité photocatalytique lors de la dégradation des polluants chimiques (acide salicylique, Orange II) et biologiques (bactéries) sous irradiation solaire. De plus, nous avons démontré la recyclabilité de ces catalyseurs sans traitement particulier.

Dans la seconde partie de notre travail, nous avons étudié le mécanisme de la photocatalyse solaire sur une souche de référence *E. coli* MG 1655 en utilisant les bâtonnets ZnO soit en suspension soit immobilisés sur un support inerte. Les résultats montrent une perte de cultivabilité de la bactérie *E. coli* avec des dommages essentiellement localisés au niveau membranaire et des protéines, le matériel génétique restant intact.

La réponse de trois souches bactériennes (*Escherichia coli, Pseudomonas aeruginosa et Salmonella enterica* Typhi) au stress oxydant de la photocatalyse a montré des différences pouvant être attribués aux différences morphologiques, métaboliques et génétiques des souches (certaines souches peuvent se réactiver après traitement). Des études réalisées sur la

souche *Pseudomonas aeruginosa* (ATCC 4114) montrent qu'il y a une perte de cultivabilité mais que la bactérie conserve sa capacité de se réactiver ainsi que ses caractères de virulence après traitement.

Summary

Detoxification of wastewater by solar photocalalysis

Keywords: Detoxification, wastewater, solar photocatalysis, Semiconductor, bacteria.

In recent decades, the water pollution has become a problem worldwide. Indeed, the strong growth in water demand due to population growth as well as industrial developments, agricultural and urban, generates huge amounts of waste water discharges. These are released into nature with or without treatment and may constitute a danger via the transmission of diseases as well as for irrigation of lands that are surrounding the site of release. The objective of this study is the treatment of aqueous waste through the use of a new technology "heterogeneous photocatalysis." This method is based on the use of a semiconductor irradiated by a light source of appropriate wavelength and is simple to implement and inexpensive.

ZnO / Fe_2O_3 semiconductors, ZnO morphology "nanorods" and Mn^{2+} doped ZnO were synthesized and tested in various photocatalytic applications. The results showed an improvement in catalytic efficiency compared to the commercial ZnO. The developed materials can reduce the recombination of charges and, therefore, improve the photocatalytic activity when the degradation of chemical pollutants (salicylic acid, Orange II) and biological (bacteria) under solar irradiation. Furthermore, we have demonstrated recyclability of these catalysts without specific treatment. In the second part of our work, we studied the solar photocatalysis mechanism on a reference strain *E. coli* MG1655 using ZnO nanorods either in suspension or immobilized on an inert support. The results show a loss of cultivability of *E. coli* with damage essentially localized in cell membranes and proteins. The genetic material remaining intact. The response of three bacterial strains (*Escherichia coli, Pseudomonas aeruginosa and Salmonella enterica* Typhi) to oxidative stress of photocatalysis showed differences can be attributed to morphology, metabolism and genetics of each strain. (Some strains can be reactivated after treatment). Studies performed on the strain *Pseudomonas aeruginosa* (ATCC 4114) show that there is a loss of cultivability but that the bacterium retains its ability to activate its virulence and characters after treatment.